20 April 2012 | $10

# Science

AAAS

## EDITORIAL



## NEWS OF THE WEEK



## NEWS & ANALYSIS



## NEWS FOCUS



## LETTERS



## BOOKS *ET AL.*



## POLICY FORUM



## PERSPECTIVES



CONTENTS continued >>

page 288

page 297


## COVER

A young polar bear (*Ursus maritimus*) on a piece of ice that is drifting in the Barents Sea, northeast of Svalbard, Norway. Polar bears depend on sea ice as a platform for hunting seals, but current melting and retreat of sea ice is increasingly forcing them onto land. A recent study has found polar bears to be evolutionarily older and genetically more distinct than was previously thought. See page 344.

***Photo: Florian Schulz, www.visionsofthewild.com***

## DEPARTMENTS

page 301

page 310

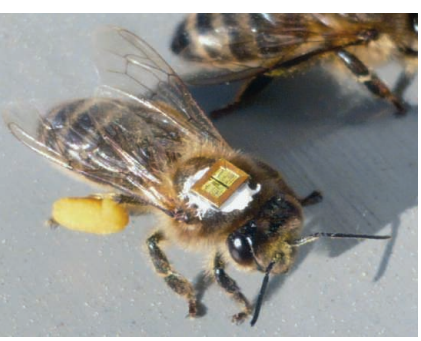

pages 348 & 351

## REVIEW



## RESEARCH ARTICLE



## REPORTS



CREDIT: (MIDDLE) KOJI FUJITA/NAGOYA UNIVERSITY



Published by AAAS

# SCIENCEONLINE

## SCIENCEXPRESS

www.sciencexpress.org

The Ancient Drug Salicylate Directly Activates AMP-Activated Protein Kinase
*S. A. Hawley* et al.
A possible molecular mechanism of action for a metabolite of aspirin is described.
10.1126/science.1215327

Don't Look Back in Anger! Responsiveness to Missed Chances in Successful and Nonsuccessful Aging
*S. Brassen* et al.
Emotionally healthy older adults show a reduced responsiveness to regret when performing a sequential decision task.
10.1126/science.1217516

Strongly Interacting Rydberg Excitations of a Cold Atomic Gas
*Y. O. Dudin and A. Kuzmich*
Illumination of an ensemble of cold rubidium atoms ultimately leads to high-level excitation of just a single atom.
10.1126/science.1217901

The Active Site of Methanol Synthesis over $Cu/ZnO/Al_2O_3$ Industrial Catalysts
*M. Behrens* et al.
Catalysis is favored by stepped copper nanoparticles decorated with zinc oxide, which promotes stronger intermediate binding.
10.1126/science.1219831

## TECHNICALCOMMENTS

Comment on "Detection of Emerging Sunspot Regions in the Solar Interior"
*D. C. Braun*
Full text at www.sciencemag.org/cgi/content/full/336/6079/296-c

Response to Comment on "Detection of Emerging Sunspot Regions in the Solar Interior"
*S. Ilonidis* et al.
Full text at www.sciencemag.org/cgi/content/full/336/6079/296-d

## SCIENCENOW

www.sciencenow.org
Highlights From Our Daily News Coverage

Drugged Honeybees Do the Time Warp
General anesthesia disrupts the insect's circadian rhythm.
http://scim.ag/Drugged_Honeybees

Unhappiness Is in the Eye of the Beholder
Facial expressions not universal, as scientists once thought.
http://scim.ag/Facial_Expressions

Dangers of Chinese Medicine Brought to Light by DNA Studies
Sequencing pinpoints origins and helps reveal unknown ingredients.
http://scim.ag/Chinese_Medicine

## SCIENCECAREERS

www.sciencecareers.org/career_magazine
Free Career Resources for Scientists

CAREER Q&A: From Science to Fiction
*E. Pain*
Spanish pharmacologist Amàlia Lafuente has written a novel about the personal and professional conflicts faced by early-career researchers.
http://scim.ag/AmaliaLafuente

Tooling Up: You Will Never Be Appreciated
*D. Jensen*
Scientists and other professionals can increase their job satisfaction by kicking their addiction to praise.
http://scim.ag/PraiseAddiction

## SCIENCESIGNALING

www.sciencesignaling.org
The Signal Transduction Knowledge Environment
**17 April issue: http://scim.ag/ss041712**

EDITORIAL GUIDE: Focus Issue—Adding Math to the Signaling Toolkit
*W. Wong and J. F. Foley*
Computational approaches can reveal how cells interpret, process, and respond to signals.

RESEARCH ARTICLE: Synthetic Signal Propagation Through Direct Cell-Cell Interaction
*M. Matsuda* et al.

PERSPECTIVE: Understanding Signaling Dynamics Through Synthesis
*A. L. Slusarczyk and R. Weiss*
An engineered system based on Notch and Delta in mammalian cultured cells recapitulates signal propagation, a phenomenon that occurs in development.

RESEARCH ARTICLE: Quantifying Crosstalk Among Interferon-γ, Interleukin-12, and Tumor Necrosis Factor Signaling Pathways Within a $T_H1$ Cell Model
*D. J. Klinke II* et al.
Combining experiments with mathematical modeling provides insights into the responses of T cells to cytokines.

PERSPECTIVE: Unmasking Functional Motifs Within Disordered Regions of Proteins
*R. K. Das* et al.
The application of a computational approach to identify short linear motifs may enable the engineering of signaling networks.

REVIEW: Computational Approaches for Analyzing Information Flow in Biological Networks
*B. Kholodenko* et al.
Signaling network construction and analysis provide insights into biology and medicine.

PROTOCOL: A Systematic Approach for Analysis of Peptide Array Kinome Data
*Y. Li* et al.
A new method of analysis of kinome data takes account of the differences between peptide arrays and DNA microarrays.

ST NETWATCH: Plant Metabolic Network (PMN)
An integrated network of researchers and data provide plant metabolic pathway models.

ST NETWATCH: Systems Biology Experiment Analysis Management System (SBEAMS)
Integrate microarray and proteomics data with a database manager and analysis package.

## SCIENCETRANSLATIONAL MEDICINE

www.sciencetranslationalmedicine.org
Integrating Medicine and Science
**18 April issue: http://scim.ag/stm041812**

FOCUS: The Power of One
*D. Louvard* et al.
A single mouse Lgr5-positive colon stem cell can be expanded into a 3D organoid that, after transplant, contributes to the repair of injured colon epithelia in a mouse model of colitis.

RESEARCH ARTICLE: Dendrimer-Based Postnatal Therapy for Neuroinflammation and Cerebral Palsy in a Rabbit Model
*S. Kannan* et al.

FOCUS: A Baby Step for Nano
*S. Tan*
A dendrimer-drug conjugate attenuates neuroinflammation and improves motor function in a rabbit model of cerebral palsy.
*>> News story p. 286*

RESEARCH ARTICLE: Patient-Specific Induced Pluripotent Stem Cells as a Model for Familial Dilated Cardiomyopathy
*N. Sun* et al.
Cardiomyocytes derived from iPS cells from patients with familial dilated cardiomyopathy can be used to model this disease.

RESEARCH ARTICLE: Targeted Delivery of PLK1-siRNA by ScFv Suppresses $Her2^+$ Breast Cancer Growth and Metastasis
*Y. Yao* et al.
Antibody-mediated delivery of anticancer small interfering RNAs suppresses $Her2^+$ breast cancer growth and metastasis.

## SCIENCEPODCAST

www.sciencemag.org/multimedia/podcast
Free Weekly Show

On the 20 April *Science* Podcast: synthetic genetics, confidence in decision-making, California's citrus crisis, and more.

**SCIENCE (ISSN 0036-8075) is published weekly on Friday, except the last week in December, by the American Association for the Advancement of Science, 1200 New York Avenue, NW, Washington, DC 20005.** Periodicals Mail postage (publication No. 484460) paid at Washington, DC, and additional mailing offices.  The title SCIENCE is a registered trademark of the AAAS. Domestic individual membership and subscription (51 issues): $149 ($74 allocated to subscription). Domestic institutional subscription (51 issues): $990; Foreign postage extra: Mexico, Caribbean (surface mail) $55; other countries (air assist delivery) $85. First class, airmail, student, and emeritus rates on request. Canadian rates with GST available upon request, GST #1254 88122. Publications Mail Agreement Number 1069624. **Printed in the U.S.A.**

**Change of address:** Allow 4 weeks, giving old and new addresses and 8-digit account number. **Postmaster:** Send change of address to AAAS, P.O. Box 96178, Washington, DC 20090–6178. **Single-copy sales:** $10.00 current issue, $15.00 back issue prepaid includes surface postage; bulk rates on request.  The identification code for *Science* is 0036-8075. *Science* is indexed in the *Reader's Guide to Periodical Literature* and in several specialized indexes.

AAAS
ADVANCING SCIENCE, SERVING SOCIETY



*Published by AAAS*

EDITED BY CAROLINE ASH AND STELLA HURTLEY

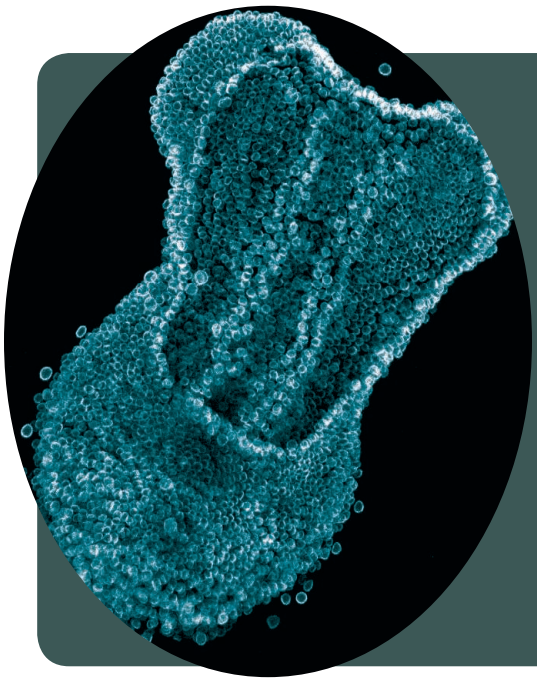

## << Tic-Toc Segmentation Clock

Molecular oscillators are an essential component of vertebrate segmentation, but whether they exist in segmented animals in general has been controversial for almost a decade. **Sarrazin *et al.*** (p. 338, published online 8 March; see the Perspective by **Roth and Panfilio**) demonstrate the existence of a segmentation clock in the growth zone of insects. Microsurgical manipulation and embryo culture revealed cyclic expression of the segmentation gene *Tc-odd* in the beetle *Tribolium castaneum*, which suggests that segmentation clocks are a widely shared mechanism that mediates animal segmentation.

## Going More Slowly

Himalayan glaciers sometimes are called the "Third Pole" because of the amount of snow and ice they contain. Despite their importance as a global water reservoir and their essential role in Asian hydrology, how their mass is changing in response to global warming is not well known. **Bolch *et al.*** (p. 310) review the contemporary evolution of glaciers in the Himalayan region, including those of the less well sampled region of the Karakoram to the Northwest, in order to provide a current, comprehensive picture of how they are changing. Most Himalayan glaciers are retreating at rates comparable to glaciers elsewhere in the world. In the Karakorum, on the other hand, advancing glaciers are more common.

## Unnatural Bases

The genetic basis of all life on the planet is comprised of deoxyribonucleic acid (DNA) with four nitrogenous nucleotide bases, abbreviated to A, G, C, and T. But there are variations on this theme, and **Pinheiro *et al.*** (p. 341; see the Perspective by **Joyce**) describe the directed evolution of unnatural nucleic acid–like genetic polymers. Variant enzymes were developed that efficiently transcribed DNA to anhydrohexitol (HNA), cyclohexenyl (CeNA), locked (LNA), and threofuranosyl (TNA) nuceic acid analogs. Further variant enzymes were developed to reverse-transcribe these analogs back to DNA. Thus, man-made nucleic acid analogs can be designed and selected that have the potential to operate in a way analogous to the natural process of heredity and evolution.

## Old Plates and the Sea

Estimates for the area and age of the ocean floor are at odds with assumptions for mantle convection, which imply that an older sea floor—rather than a new one—would be preferentially subducted over time. Previous efforts to explain these relationships have been based on geologic evidence and simple models. **Coltice *et al.*** (p. 335) created numerical three-dimensional convection models representing more realistic physical boundaries, including a spherical Earth, the existence of continents and supercontinents over time, and realistic rheologies. A combination of continents and plate-like behavior of the ocean floor sufficed to produce the observed relationship between plate area and plate age, which explains why some old oceanic crust still remains.

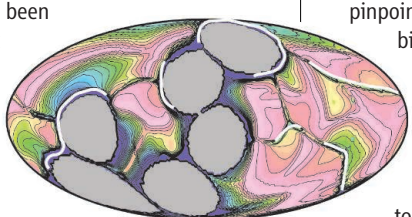

## A Specific Oxidative Catastrophe

Three different classes of antibiotics induce bacterial cell death by the production of hydroxyl radicals. Hydroxyl radicals are powerful oxidizing agents in living cells and will oxidize the nucleic acid base, guanine, to form 8-oxo-guanine, which is potentially mutagenic because it can pair with both cytosine and adenine and form lethal double-strand DNA breaks. **Foti *et al.*** (p. 315) discovered that overproduction of the nucleotide sanitizer MutT, which hydrolyzes 8-oxo-dGTP to 8-oxo-dGMP, gives striking protection against cell death.

## Bonded at the Source

Asymmetric catalysis is a relatively mature field in the laboratory, with a diverse array of techniques available for the selective transformation of organic compounds. However, scaling up these techniques for industrial application remains challenging, in part because many catalysts act best on reagents that have been expensively modified, although this process often generates copious waste. **Zbieg *et al.*** (p. 324, published online 22 March) combat this challenge with a ruthenium-based catalyst that couples an unmodified bulk commodity feedstock (butadiene) with alcohols, forming carbon-carbon bonds to generate complex products with high selectivity.

## Hydrated in a Hurry

Water has a major influence on the conformation of proteins and related biomolecules. However, so many water molecules participate in the hydrogen bonding networks that it can be difficult to pinpoint which specific interactions play the biggest role. **Nagornova *et al.*** (p. 320) sought to answer this question for the case of a 10–amino acid ring—the antibiotic compound Gramicidin S—by probing the conformational impact of successive additions of one to 50 water molecules to the naked gas-phase structure. The primary changes in the overall ring geometry came from the addition of just the first two waters.

## A Sturdy Electrode Coating

To operate efficiently, organic devices—such as light-emitting diodes—require electrodes that emit or take up electrons at low applied voltages (that is, have low work functions). Often these electrodes are metals, such as calcium, that are not stable in air or water vapor and have to be protected from environmental damage. **Zhou *et al.*** (p. 327; see the Perspective by **Helander**) report that a coating polymer containing aliphatic amine groups can lower the work functions of various types of electrodes by up to 1.7 electron volts and can be used in a variety of devices.

CREDITS (TOP TO BOTTOM): ANDREW D. PEEL, COLTICE *ET AL.*





Published by AAAS

## Ancient Bears

Polar bears are well known for adapting to their cold Arctic climate. Some recent studies, based on mitochondrial DNA, concluded that they are a relatively young species and that these adaptations occurred quite quickly. Although mitochondrial DNA is regularly used to estimate evolutionary history, it has some well-known drawbacks, including sex-biased dispersal and hybridization. Thus, **Hailer *et al.*** (p. 344) looked at neutral genetic data that are distributed more widely across the genome of a relatively large sample of polar, brown, and black bears. Consistent with fossil-based studies, the analysis reveals polar bears as a sister lineage to all brown bears, with an estimated divergence time of 300,000 to 900,000 years ago. Thus, polar bears are indeed of a more ancient lineage, and more recent estimates based on mitochondrial DNA are likely to have been affected by past hybridization with brown bear.

## Protein Tipping Point

Amyloid fibrils are insoluble protein aggregates that play a role in various degenerative diseases. Recent experiments have provided insight into fibrillar structures; however, the mechanisms of aggregation remain unclear. **Neudecker *et al.*** (p. 362; see the Perspective by **Eliezer**) report the structure of a transient folding intermediate in a protein SH3 domain known to undergo aggregation. The intermediate is stabilized by non-native interactions and exposes an aggregation-prone β strand. Thus, for this protein, folding from the intermediate state will compete with aggregation.

## Bad News for Bees

Neonicotinoid insecticides were introduced in the early 1990s and have become one of the most widely used crop pesticides in the world. These compounds act on the insect central nervous system, and they have been shown to be persistent in the environment and in plant tissues. Recently, there have been controversial connections made between neonicotinoids and pollinator deaths, but the mechanisms underlying these potential deaths have remained unknown. **Whitehorn *et al.*** (p. 351, published online 29 March) exposed developing colonies of bumble bees to low levels of the neonicotinoid imidacloprid and then released them to forage under natural conditions. Treated colonies displayed reduced colony growth and less reproductive success, and they produced significantly fewer queens to found subsequent generations. **Henry *et al.*** (p. 348, published online 29 March) documented the effects of low-dose, nonlethal intoxication of another widely used neonicotinoid, thiamethoxam, on wild foraging honey bees. Radio-frequency identification tags were used to determine navigation success of treated foragers, which suggested that their homing success was much reduced relative to untreated foragers.

## Thoroughly MODern Yeast

It is not clear if prion induction in yeast is truly linked to physiological roles. **Suzuki *et al.*** (p. 355) show that the yeast prion protein Mod5 (a transfer RNA isopentenyltransferase) responds to an environmental stressor by converting to an aggregated amyloid form, which leads to phenotypic changes in cell metabolism and drug resistance. Introduction of Mod5 amyloid into yeast resulted in the formation of a dominantly heritable prion state [*MOD*$^+$], in which Mod5 is aggregated. [*MOD*$^+$] yeast showed high ergosterol levels and acquired resistance to several antifungal agents. Selective pressure by antifungal drugs on nonprion [*mod*$^-$] yeast induced the [*MOD*$^+$] prion state, formation of amyloid, and increased cell survival.

## Joint Decisions

In many instances, decisions made by relatively homogeneous groups (two or more people) coalesce around the choice that people are most confident in, and this in turn stems from the sampling of representations that individuals perform when making their choices. **Koriat** (p. 360; see the Perspective by **Hertwig**) found that if most of the group members are able to form accurate judgments, then confidence and accuracy coincide and the consensus choice is the correct one. By contrast, if few people know the right answer, then heterogeneity in people's representations appeared to offer a surer path to accuracy.

CREDIT: NEUDECKER *ET AL.*

Alan I. Leshner is the chief executive officer of the American Association for the Advancement of Science and executive publisher of *Science*.

# Standards for Postdoc Training

POSTDOCTORAL (POSTDOC) TRAINING HAS BECOME VIRTUALLY INSTITUTIONALIZED IN MANY PARTS of the world as a discrete stage in the career progression in most science and engineering fields. However, there is far too much variability in what such training involves, across institutions and among the laboratories within them. Given its importance and pervasiveness—there are over 50,000 postdocs in the United States alone—we need to establish and enforce standards, norms, and expectations for mentors, mentees, and their institutions that are analogous to those for undergraduate and graduate education.

The original rationale for postdoc training was to acquire additional skills that were not included in one's graduate program. That motivation has persisted, but an extended postdoc period has also become a way to establish one's credentials, or a source of temporary employment when regular jobs are scarce. In many fields it is almost impossible to get a permanent job directly out of graduate school, and it is not unusual for researchers in some fields to have had two or more postdoc experiences. In addition, postdocs have become nearly indispensable members of many research groups, because they provide novel ideas and do much of the hands-on experimentation.

The U.S. National Academies' Committee on Science, Engineering, and Public Policy (COSEPUP) did an in-depth analysis of the postdoc experience in 2000* and is revisiting the issues with another study committee now. The 2000 report concluded that postdoc training is far too variable and recommended a set of remedial steps. Examples include the development of distinct goals, policies, and standards for postdoc experiences; institutional recognition, status, and compensation in keeping with the important roles postdocs play in the research enterprise; and career guidance to prepare postdocs for regular employment.

Unfortunately, none of these recommendations has been implemented on a broad scale. To convert them into reality requires oversight bodies both within and across research institutions that train postdocs. A critical COSEPUP recommendation was that every university should have a designated high-level office that oversees postdoc training across the entire institution. Although some institutions have established such offices, many lack the standing and influence needed to enforce adherence to standards and policies, and therefore the nature of postdoc training remains idiosyncratic from laboratory to laboratory.

Another barrier to implementing these recommendations is the absence of national bodies that support the institutional officials responsible for postdoc training, collecting data important for decision-making and articulating standards and best practices. In the United States, the Council of Graduate Schools (CGS) represents graduate school deans and serves these functions for graduation education. The National Postdoctoral Association (NPA) was founded by a small number of postdoc trainees in 2003 with the goal of improving the quality and consistency of U.S. postdoc experiences. The NPA now has about 171 institutional members, but, in contrast to the CGS, it lacks the full senior-level membership and official standing needed to foster consistency and standards across all institutions.

Every institution that trains postdocs should have a high-level office responsible for ensuring the quality and consistency of its training programs. And all such institutions should join together and either strengthen the NPA or form an alternative organization that will have the standing to recommend in detail best practices and standards and offer technical assistance to its institutional members. For any such efforts to succeed requires the full endorsement and participation of all elements of the scientific community—faculty, students, administrators, and funders. Today's postdocs are the future of the science and engineering enterprise. Let's commit to ensuring that all of them get the quality postdoc experiences they need and deserve.

**– Alan I. Leshner**

10.1126/science.1222476

*www.nap.edu/catalog.php?record_id=9831.







*Published by AAAS*

GENETICS

## Exons Encode Enhancers

Transcription factor binding to enhancer elements is critical for proper gene regulation. Enhancers are often found in noncoding sequences in close proximity to the gene that they regulate and sometimes even on another chromosome; however, whether they are also found in exons, the coding regions of DNA, is unclear. Birnbaum *et al.* analyzed 25 mouse and human enhancer-associated ChIP-seq data sets in order to identify enhancer peaks that overlap exons and found regulatory transcription factor binding to exonic regions. In fact, in mice, roughly 7% of enhancer peaks overlapped coding exons. Mutation of these elements in zebrafish and mouse enhancer assays showed that although exonic sequences are necessary, they are not sufficient for full enhancer function. Absence of an exon-encoded enhancer, however, did have functional consequences. Thus, exonic sequences may function in the regulation of nearby genes. Moreover, phenotypes seen in genetic knockout animals may be the result of not only the lack of expression of the deleted gene but also alterations in the expression of genes that are regulated by enhancers in the deleted exons. — BAP

*Genome Res.* **22**, 10.1101/gr.133546.111 (2012).

PLANT SCIENCES

## Toxic Lichens

Fungi and green algae can form symbioses called lichens—several involve cyanobacteria as the photosynthetic accessory. *Nostoc*, a filamentous cyanobacterium, is a common partner forming what are known as cyanolichens. Unfortunately, *Nostoc*, in common with freshwater bloom–forming cyanobacteria, can produce cyclic peptide toxins such as microcystins and nodularins, which target mammalian phosphatases and may be carcinogens. Kaasalainen *et al.* have discovered that many cyanolichens contain these toxins too, and have detected over 50 chemical variants of microcystins. The signature gene is *mcyE*, whose product is required for the synthesis of a variant amino acid; the bond between this amino acid and D-glutamate is essential for microcystin toxicity. But *mcyE* does not seem to be affected by the horizontal gene transfer that is rife among the cyanobacteria, and this amino acid is a constant in the otherwise variable peptide sequence of the toxin. So lichens with identical *mcyE* can have very different microcystin compositions. Being trapped in a relationship with a fungus tends to lead to local population bottlenecks, which may have been instrumental in the evolution of this surprising diversity of toxins. — CA

*Proc. Natl. Acad. Sci. U.S.A.* **109**, 10.1073/pnas.1200279109 (2012).

CLIMATE SCIENCE

## The Sun's Push

Unraveling the influence of the Sun on Earth's climate depends on having accurate chronologies of the variability of both climate and solar activity. Cosmic rays produced by stellar explosions interact with elements in the atmosphere and on the land to make the radionuclides $^{14}C$ and $^{10}Be$, both of which can be measured in order to construct a record of their fluxes at Earth's surface. That record, in turn, can be reinterpreted as a chronicle of solar activity, because the magnetic field of the Sun helps to control the intensity of cosmic rays that penetrate to Earth's surface. Steinhilber *et al.* present a high-resolution $^{10}Be$ data set derived from an Antarctic ice core and combine it with existing $^{10}Be$ and $^{14}C$ records, as well as data from a Chinese stalagmite, to provide a 9400-year-long history of solar activity, in order to determine the solar imprint on the Asian monsoon during that interval. Whereas solar forcing generally drives the monsoon, periods during which the two show little coherence indicate that other factors, such as volcanoes and greenhouse gases, also are important. — HJS

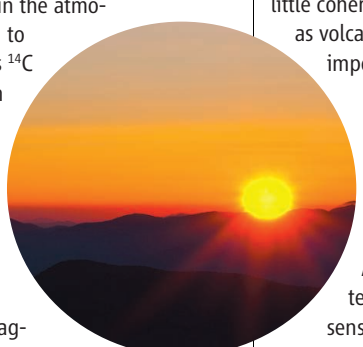

CREDITS (TOP TO BOTTOM): JOUKO RIKKINEN; ISTOCKPHOTO.COM

*Proc. Natl. Acad. Sci. U.S.A.* **109**, 10.1073/pnas.1118965109 (2012).

CHEMISTRY

## A Clean Sense

A primary goal in designing better sensors is to find ways to enhance sensitivity without sacrificing selectivity. Nanoscale materials such as carbon nanotubes should offer an easy route to better sensitivity because of their exceptionally high surface area–to–volume ratio and because their electronic properties are strongly affected by changes in their local environment. Thus, it should be possible to measure exposure to gases that bind to the nanotube surface through changes in electrical conductivity. However, the nanotube surface can easily be altered by low levels of contaminants or by incomplete recovery after an initial sensing cycle, thus changing the electronic properties in an undesired way. Chen *et al.* show that continuous illumination of single-walled carbon nanotubes by ultraviolet (UV) light leads to a cleaning of the nanotube surface. Detection of dry gases such as NO in an air stream was enhanced, but active sensor material degraded because of the formation of ozone. Detection of $NO_2$ and $NH_3$ in a nitrogen stream reached limits of a few parts per trillion (ppt), and for NO a sub-ppt amount was observed—an improvement of two to three orders of magnitude over other nanoscale devices. The UV light is also responsible for removing the detected gases from the nanotube surface, which enhances the rate at which the sensors can be cycled, but at the risk of increasing the detection limits. — MSL

*Sci. Rep.* **2**, 10.1038/srep00343 (2012).

## AROUND THE WORLD

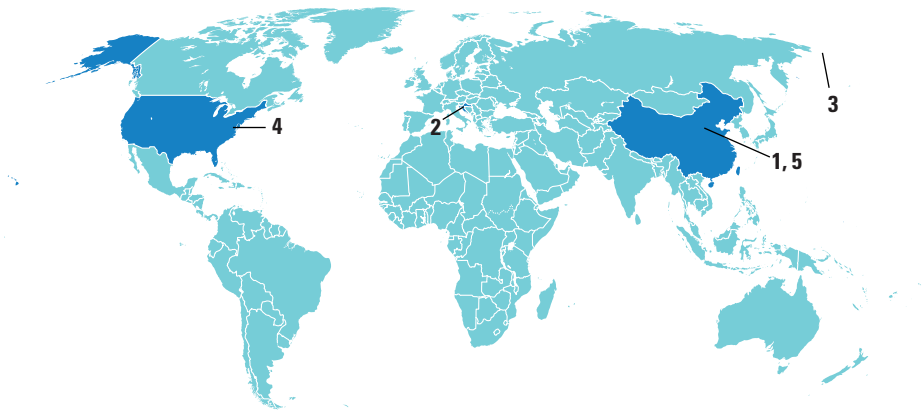


Beijing **1**

### A New Uproar Over Chinese Tobacco Research

A tobacco research project nominated for China's 2012 National Science and Technology Progress Award has produced an uproar among China's scientific community.

The project, titled "Formulation and Application of a Theoretical System for Chinese Cigarettes," was nominated by the State Tobacco Monopoly Administration. The cited achievements include improving quality and marketability of Chinese cigarettes and new sales revenue of about $27.5 billion over the last 3 years.

Yang Gonghuan, a professor at Peking Union Medical College's School of Basic Medicine, published an open letter to science minister Wan Gang on 3 April calling on the Ministry of Science and Technology (MOST) to ban tobacco research from being considered for national science awards. Editors at China's foremost science Web site and blog, ScienceNet.cn, began collecting signatures on 8 April from readers opposed to cigarette research's consideration for a science award.

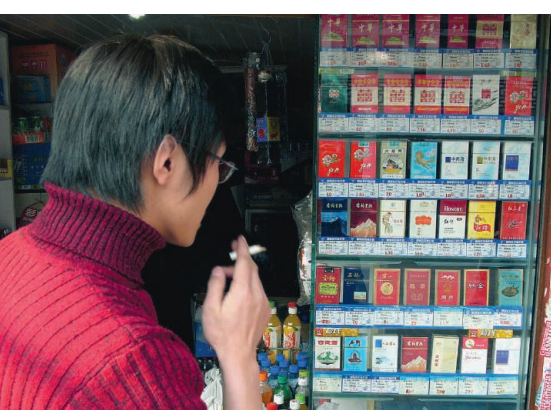

Tobacco research has garnered increased criticism in China: Last year, researchers protested the election of tobacco scientist Xie Jianping to the prestigious Chinese Academy of Engineering. Xie's low-tar research had received the National Science and Technology Progress Second Prize three times: in 2003, 2004, and 2010.
**http://scim.ag/Chinatobacco**

Zagreb **2**

### Director of Key Croatian Research Center Ousted

The head of one of Croatia's most important natural sciences institutes has lost her job. The official reason for the dismissal of Danica Ramljak, a medical researcher who took the helm of the Ruđer Bošković Institute (IRB) in Zagreb in 2009, is that she does not qualify as a "research associate/fellow" under Croatian law.

Ramljak, however, claims she's being punished for revealing corruption at the institute. She says that after she took over, she discovered several "large financial embezzlements" in past projects. At her invitation, police and Croatia's state attorney started an investigation at the institute in 2010, which was already under investigation by the Ministry of Finance's tax administration. In December 2011, a report by the tax administration concluded that IRB had failed to pay around $1.3 million in taxes as a result of various illegal activities by its scientists in 2008.

Croatia's science minister, Željko Jovanović, says he appointed a new management council in February to bring "stabilization" to the institute, and supported the conclusion that Ramljak did not meet formal requirements to head the institute in an 8 March letter to the council.
**http://scim.ag/Ramljak**


Ribbon seal

Bering and Okhotsk Seas **3**

### Monitoring Seals From On High

Last week, a group of scientists boarded equipment-laden airplanes, braved freezing temperatures, and began a massive accounting of seals in the Arctic. The project, which includes American and Russian scientists, is a 2-year effort aimed at understanding ice-associated seal populations in the Bering and Okhotsk seas.

Bearded (*Erignathus barbatus*), ringed (*Phoca hispida*), spotted (*P. largha*), and ribbon seals (*Histriophoca fasciata*) use springtime on the ice to give birth, mate, or molt—which makes it an ideal time to count them. The team plans to use a combination of thermal imaging and digital photographs to conduct their census.

"It's pretty widely anticipated that [the seals'] habitat will change over the next decade to centuries," says project leader and marine mammalogist Peter Boveng of the National Oceanic and Atmospheric Administration in Seattle, Washington. And getting a good handle on their population sizes is essential to any potential conservation efforts, he adds.

### NOTED

>For the second year in a row, Thomson Reuters named Eric Lander of the Broad Institute in Cambridge, Massachusetts, **the year's most influential researcher**. With 14 often-cited "hot papers," Lander topped the list of 15 Hottest Researchers of 2011. Genetics is also on fire, according to the report: It was the primary field of study for seven of the 15 researchers.

CREDITS (TOP TO BOTTOM): © JTB PHOTO COMMUNICATIONS INC./ALAMY; EUGENE HOSHIKO/AP PHOTO





Published by AAAS

Washington, D.C. **4**

## New Biodefense Lab in Limbo

The United States faces a stark choice between funding a new state-of-the-art laboratory for agricultural biodefense and paying for ongoing research on the topic, according to the government's top biosecurity research official.

"We are hard up against it now; you can't do research without modern facilities, but the money for modern facilities comes out of the same piggy bank that pays for research," Tara O'Toole, head of the Department of Homeland Security's (DHS's) Science and Technology Directorate, told a new study panel of the U.S. National Academies' National Research Council (NRC) on 13 April. DHS has asked the panel to examine plans for the proposed National Bio and Agro-Defense Facility (NBAF) in Manhattan, Kansas, which could cost $1 billion and is supposed to replace the aging Plum Island Animal Disease Center in New York. But funding issues and opposition to NBAF (*Science*, 24 February, p. 903) have prompted the Obama Administration to consider canceling or scaling back the laboratory. The NRC panel expects to release its recommendations by the end of June.
**http://scim.ag/biodef**

Beijing **5**

## Cleaning Up China's Journals

In what the Chinese press dubs a "war to protect academic honesty," publishers of more than 1000 journals have pledged to root out plagiarism and falsified research. The publishers, heads of journals under the China Association for Science and Technology, signed a pledge 10 April vowing to punish editors who misuse their positions or knowingly publish plagiarized papers.

China's General Administration of Press and Publication is intent on tidying up the bloated academic publishing industry (*Science*, 21 October 2011, p. 301), and journal publishers may be feeling the heat. Problems reach beyond faked research to fake journals that turn out citations to pad scientists' resumes. At some publications, the review process is just a matter of "going through the motions," the newspaper *China Science Daily* quoted former *Mechanics in Engineering* editor Li Jiachun as saying.

Others contend that punishing editors won't solve a problem rooted in the severe publish-or-perish mentality in China. Some Chinese institutions even pay scientists top dollar for publishing in journals with high impact factors. Says Meng Zhao, development editor at *Neural Regeneration Research*: "This is an ethical issue not just for the researchers, but for the whole academic society."

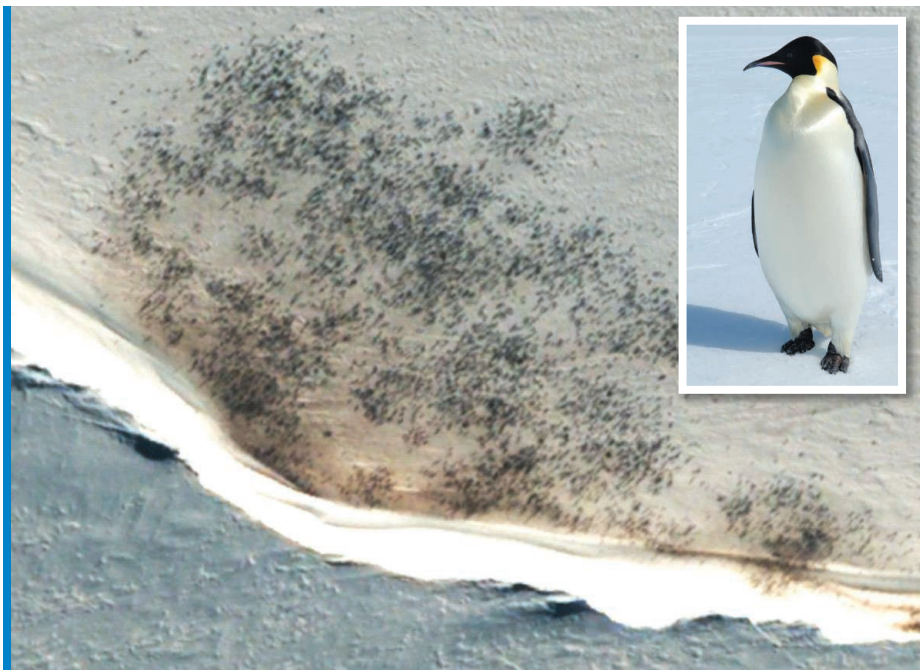

CREDITS (TOP TO BOTTOM): DIGITALGLOBE; (INSET) BRITISH ANTARCTIC SURVEY; COURTESY OF MOHAMED ISMAIL KHALED

## Counting Penguins From Space

**The hardest part of counting penguins isn't getting them to hold still; it's getting to the remote places where they live, especially Antarctica. Satellite images to the rescue: On 13 April, researchers reported the results of the first satellite image–based comprehensive study of penguins in *PLoS ONE*.**

**To count the birds, the team enhanced the images with pansharpening, making it possible to distinguish between shadows, guano, and actual penguins. The team found twice as many emperor penguins (*Aptenodytes forsteri*) as were thought to exist—roughly 595,000. They also counted seven new colonies, bringing the total to 44.**

**"This is a leap forward, but it doesn't change the conservation concern [about] emperor penguins and many other species," says penguin expert P. Dee Boersma of the University of Washington, Seattle. "Unfortunately, with climate warming and variation, we are likely to be studying the decline of emperor penguins. Satellite mapping will allow scientists to determine where the declines are occurring and by how much."**

NEWSMAKERS

## Three Q's

Khaled

During the 2011 Egyptian revolution, looters broke into the Museum of Egyptian Antiquities in Cairo and plundered storehouses at archaeological sites such as Saqqara. Last week, **Mohamed Ismail Khaled**, the Egyptian official in charge of foreign archaeological missions, spoke to a Yale University audience about the effects of the revolution. *Science* caught up with him there.

**Q: What challenges did you face during the revolution?**

We had many difficult times, beginning with what happened at the [Museum of Egyptian Antiquities]. The same wrong information was just multiplied by the media. People didn't believe us when we said that only 54 pieces were stolen from the museum and that now only 29 are missing. All the masterpieces relating to King Tut, thank God, they are back. >>





Published by AAAS

## >>NEWSMAKERS

**Q: Are all foreign archaeological missions back in the field again?**

The only missions that left Egypt were from the Cairo area, and they left because it was not safe. But missions in the Eastern and Western Desert, in Aswan, and in other areas, they did not see the revolution. They never stopped working.

**Q: Egypt's former minister of state for antiquities affairs, Zahi Hawass, campaigned for the return of Egyptian artifacts, such as the Rosetta Stone, from foreign museums. Is this still a priority?**

It is our cultural heritage. We will not leave the repatriation issues unsettled. But the problem now is that the Ministry of State for Antiquities is suffering from internal protests: people want jobs, increases in salaries. You have to solve these problems first and then think about the fight outside the country.

**Science LIVE**

Join us Thursday, 26 April, at 3 p.m. EDT for a live chat on the continuing science versus security debate sparked by two **H5N1 avian influenza studies**. **http://scim.ag/science-live**

## Exiled Chinese Physicist Fang Lizhi Dies

Astrophysicist **Fang Lizhi**, who died at 76 on 6 April, was a champion of freedom, human rights, and democracy in China.


Fang

Fang began his academic career as a physics lecturer in 1958 at the University of Science and Technology of China (USTC) in Beijing, but his career was interrupted by compulsory labor on farms and in a coal mine during the Cultural Revolution. In 1976, Fang resumed publishing academic papers, and was elected at age 44 to the Chinese Academy of Sciences's Division of Mathematics and Physics in 1980. In 1984, he was appointed vice president of USTC.

Fang called for political reform during the 1980s. In 1987, Deng Xiaoping, China's paramount leader, ordered Fang's removal as USTC vice president. The government labeled Fang a "black hand" behind student demonstrations that ended in a bloody crackdown in June 1989. Fang and his wife were eventually allowed to leave China, and in 1992 Fang joined the faculty at the University of Arizona in Tucson. He was elected a fellow of the American Physical Society in 2010 for "his important work in cosmology and early-universe physics … and his tireless, selfless, courageous and continuing advocacy of human rights in China." **http://scim.ag/FangLizhi**

## BY THE NUMBERS

**193** Number of papers co-authored by disgraced anesthesiologist Yoshitaka Fujii that journals may retract by 30 June. Fujii would hold the record for most retractions by a single author.

**56** Number of coral species in U.S. waters that likely face extinction by 2100, according to a 16 April National Marine Fisheries Service review of 82 corals being considered for protection under the Endangered Species Act.

## Random Sample

### Not-So-Silly Putty for Potholes

Non-Newtonian fluids are the stars of high school science demonstrations: Poured or pulled slowly, a gooey batter of corn starch and water, for example, will flow like a liquid, but when subjected to high stress, such as being hit firmly or pulled sharply, it becomes stiff like a solid. Unlike Newtonian fluids, which maintain their fluid state regardless of disturbances, the viscosity, or resistance, of a non-Newtonian fluid changes in response to forces applied to it. Different non-Newtonian fluids—such as mayonnaise, ketchup, Silly Putty, and blood—all contain some sort of particle, and the interaction of those particles explains their behavior under stress.

Those unusual physical properties gave a group of undergraduates at Case Western Reserve University in Cleveland, Ohio, an idea: Design a non-Newtonian fluid to fill potholes. "When there's no force being applied to it, it flows like a liquid does and fills in the holes," says 21-year-old team member Curtis Obert, "but when it gets run over, it acts like a solid."

The team created a powdered mixture stored in waterproof bags designed to stand up to the salt and freezing conditions of a Midwest winter. City workers would add water and seal the bag. It's less messy than packing potholes with asphalt, Obert says, and dropping the fluid-filled bags into potholes requires little training or experience. When the roads are repaired, the bags can be removed and reused.

The students devised the idea as part of an engineering contest sponsored by French materials company Saint-Gobain—and took first prize this month. They plan to patent their invention, so they won't divulge their exact formulation, but they say it's biodegradable and poses no danger to people or the environment. **http://scim.ag/puttypotholes**

CREDITS: (TOP) JAMES S. WOOD/*THE ARIZONA DAILY STAR*/AP PHOTO; (BOTTOM LEFT TO RIGHT) GRETCHEN CUDA KROEN; ISTOCKPHOTO.COM





Published by AAAS

**Vigilant.** State inspectors in California collect psyllids (*inset*) from a kumquat tree near where they detected citrus greening disease.

AGRICULTURE

# Dread Citrus Disease Turns Up in California, Texas

When the worst disease of citrus plants was detected in Florida in 2005, growers and researchers elsewhere in the country watched with trepidation. Citrus greening, also known as huanglongbing, turns fruit sour and kills trees within a few years. There is no cure. Transmitted by a tiny insect, the bacterial disease rapidly conquered Florida, doubling the cost of citrus production and raising questions about the future of the industry. Fred Gmitter of the University of Florida says, "The dilemma for Florida is: Where do we go from here?"

Now citrus greening has turned up in California and Texas, the second- and third-largest citrus producers in the United States. "We've been waiting for this and searching for it," says Beth Grafton-Cardwell of the University of California, Riverside's Lindcove Research and Extension Center in Exeter. She and other researchers are hoping that rapid action—hunting for and destroying infected trees and battling the sap-sucking insect vector—can contain the disease, buying enough time to develop treatments or even resistant trees.

Citrus greening afflicts most countries that grow the fruits. First seen in China at the end of the 19th century, it has become endemic in many parts of Asia, Africa, and Latin America, disrupting citrus production. The 4-mm-long psyllids, which are related to aphids and whiteflies, transmit the bacterium *Candidatus Liberibacter* between trees when they feed on new leaves. Several months to 2 years later, as the bacterium damages the vascular system, leaves start to turn yellow (*Science*, 28 April 2006, p. 523). Trees are infectious even before they show symptoms, which makes it hard to halt the disease's spread. So far, only Brazil, the world's largest producer of citrus, has succeeded, thanks to intensive surveillance, relentless removal of sick trees, and aggressive insecticide spraying.

Online
**sciencemag.org**
Podcast interview with author Erik Stokstad.
http://scim.ag/pod_6079

The Asian citrus psyllid turned up in Florida in 1998. Even though it was known to be the vector for citrus greening, growers were not very concerned. "We got caught with our eyes closed," Gmitter says. The psyllid soon reached most of the citrus-growing counties in the state, hitchhiking on orange jasmine, an ornamental plant used in landscaping. By the time citrus greening was detected in Miami-Dade County in 2005, it was already too late to stop the disease. Plant pathologists in Texas and California immediately took action, educating the public about the dangers of moving fruit trees, for example.

With the help of the U.S. Department of Agriculture (USDA), state inspectors also began monitoring for the psyllids. Plant pathologists suspect that the bacterium first arrives when residents unwittingly bring back infected twigs from other states or countries to graft onto their own trees. The psyllids probably arrive separately, on small plants or fruit. And when they do, they spread the disease from tree to tree. It's easier to test for the bacterium in psyllids than in leaves, because trees often don't show symptoms at first.

When the insects turned up in San Diego and Imperial counties in 2008, the California Department of Food and Agriculture went yard by yard spraying insecticides, and also quarantined nurseries. Despite these efforts, Asian citrus psyllids have become established in Los Angeles County and in southern Texas. Since 2005, researchers in both California and Texas have tested tens of thousands of psyllids for the bacterium. They found a *C. Liberibacter*-positive psyllid in January in Texas, in a small orange grove near the border with Mexico, where the disease is rapidly spreading north. About 60 trees in that orchard and a nearby grapefruit grove have since been confirmed infected. Some 20 trees have already been destroyed, with more culling planned, says John da Graça, who directs the Texas A&M University Kingsville Citrus Center in Weslaco: "The disease is here and everyone is taking it very seriously." Late last month, California inspectors found an infected psyllid in Los Angeles County. They raced back to the neighborhood and found a diseased lemon-pomelo tree, which they have destroyed. "We fully expect to find more infected trees," says Ted Batkin of the California Citrus Research Board in Visalia. "I get little sleep these days."

After these detections, both states have ramped up their monitoring. Researchers in California are releasing parasitoid wasps imported from Pakistan to help control the psyllids in urban areas, where widespread spraying isn't feasible. "It's not a silver bullet," says Mark Hoddle of the University of California, Riverside, who is leading the effort. Other experts put more stock in quarantines

CREDITS: REED SAXON/AP (2)





Published by AAAS

and in monitoring and spraying commercial groves. "We've been successful in slowing down the whole process," says Grafton-Cardwell. "We know we're just buying time until a solution comes about."

Researchers are pursuing a variety of approaches to combat the disease. One is to treat infected trees with antibiotics. USDA's Yongping Duan and colleagues reported in September that the combination of streptomycin and penicillin will eliminate the bacterium, but the U.S. Food and Drug Administration is unlikely to allow the use of penicillin in plants. Last year, the Citrus Research and Development Foundation (CRDF) in Florida offered a cash prize for new antibiotics; now it is funding Duan and others to test more than 50 candidates. Other researchers are trying to develop "plantibodies" to fight the bacterium, to find RNAs that will prevent the psyllid from transmitting the bacterium, and to develop ways to repel psyllids from citrus trees.

The ultimate hope is to create resistant trees, which many groups are trying to do. Erik Mirkov of Texas A&M University's AgriLife Research unit in Weslaco is the furthest along. He has added two genes from spinach that code for antimicrobial proteins into several types of citrus. After growing the transgenic trees for more than a year in a greenhouse with infected psyllids, Mirkov says he can't detect the bacterium in the trees. Field testing in Florida should begin later this year, but regulatory approval for commercial release is years away.

In the meantime, Florida growers are trying to make the best of the miserable situation. Many have begun coordinating insecticide spraying to better control the psyllids. But most growers no longer remove infected trees for fear that they won't have enough left to stay in business. Instead, they are trying to keep the trees productive as long as possible by applying extra fertilizer. David Hall of USDA is now testing whether this approach really works. The fundamental problem, however, is that the sick trees will infect any new ones that are planted.

Florida growers may have to move to a new type of agriculture in which they plant dense orchards and optimize the growth of young trees before citrus greening starts to damage the fruit. That may just keep citrus growing in Florida economical, says CRDF's Harold Browning, who urges continued funding of research. "It's difficult for an industry facing disaster to be patient," he says. Growers in the West have their fingers crossed that their dollars—and heightened vigilance—will pay off in time. **–ERIK STOKSTAD**

STEM CELLS

# Texas Medical Board Approves Rules for Controversial Treatment

Last week, the Texas Medical Board signed off on what's said to be the first state-level policy imposing oversight on experimental treatments using adult stem cells. The scientific community has mixed views on whether this is a good way to raise standards.

Some experts say the rule will allow unscrupulous doctors to avoid U.S. Food and Drug Administration (FDA) reviews. "They're acting as though there's no federal policy around stem cells," says bioethicist Leigh Turner of the University of Minnesota, Twin Cities. But others say it's a good-faith effort to bring oversight to controversial treatments that clinics around the world offer for diseases including arthritis and multiple sclerosis.

**Case study.** Governor Rick Perry asked for new rules after receiving therapy for back pain.

CREDIT: RICKPERRY.ORG

Texas has become a flashpoint thanks in part to Governor Rick Perry, who last summer received treatment from a Houston physician for a back injury that consisted of an injection of his own fat stem cells. Meanwhile, the company that prepared Perry's cells, Celltex Therapeutics of Sugar Land, Texas, has come under fire for allegedly charging patients to bank their cells for experimental treatments.

Perry asked the Texas Medical Board for a review; last summer it began drafting a rule governing physicians' use of "investigational agents," including stem cells. The final rule would require patients' informed consent for stem cell treatments. The cells' proposed use would also have to be part of a National Institutes of Health or FDA-approved protocol or study, or be approved by an ethics panel known as an Institutional Review Board (IRB).

Critics say most stem cell treatments offered at clinics clearly fall under FDA's purview. They note that stem cells are considered a biologic drug if they are more than "minimally manipulated" (by expanding the cells in culture, for example) or are meant to perform a function different from their original one. The rule "opens up a lot of opportunities for abuse or fairly lax regulation," says science policy expert Douglas Sipp of the RIKEN Center for Developmental Biology in Kobe, Japan.

Turner, who testified before the Texas board last week, also warns that the proposed rule would permit review by private, for-profit IRBs, which he argues can be under financial pressure to approve protocols. And stem cell researcher Irving Weissman of Stanford University in Palo Alto, California, told the *Houston Chronicle* that the draft rule is "a clever way around the FDA's appropriate role overseeing clinical trials" and violates guidelines from the International Society for Stem Cell Research (ISSCR). However, ISSCR hasn't taken a position. Its science director, Heather Rooke, says, "We've generally heard positive things about the intent" of the rule.

Sean Morrison, an ISSCR member at the University of Texas Southwestern Medical Center in Dallas, says the Texas board cannot require FDA oversight, noting that many legitimate U.S. clinical trials test treatments that don't meet FDA's definition of a regulated product. But the draft rule wouldn't stop FDA from stepping in, Morrison says, because "federal laws trump state laws."

Morrison does share concerns that the draft rule's requirements for IRB review are "weak." But he says the medical board "should be congratulated for trying to impede the proliferation of unproven stem cell therapies." Texas, he says, "has done more to address this problem than most other states."

The medical board's 10-to-4 vote, says Executive Director Mari Robinson, reflects a feeling that the FDA guidelines aren't clear and that, given that some doctors are already offering stem cell treatments, the board felt that it needed "to create a safety setup." She said the board expects to consider refinements to the rule at its June meeting. **–JOCELYN KAISER**





Published by AAAS



**In the limelight.** Virologist Ron Fouchier (*center*) discussed his paper on a popular Dutch talk show on 21 February.

CREDITS: DWDD/VARA (3)

BIOSECURITY

# Will Dutch Allow 'Export' of Controversial Flu Study?

**AMSTERDAM, THE NETHERLANDS**—He already defended the merits of his controversial H5N1 avian influenza study at meetings in Geneva, Washington, and London. Now, Dutch virologist Ron Fouchier will do the same at home. On 23 April, Fouchier will attend a meeting organized by the Ministry of Foreign Affairs in The Hague, a 25-minute drive from his lab at Erasmus MC in Rotterdam. That same evening, he's booked for a 2-hour public debate at the 17th century canal-side mansion of the Netherlands Royal Academy of Arts and Sciences, here in the capital.

The second meeting is expected to be well attended. But the first, held behind closed doors, will likely help decide the fate of Fouchier's paper on how he made the H5N1 virus transmissible in mammals. The Dutch government must decide if it will invoke export-control laws in a bid to prevent Fouchier from submitting a revised version of his paper to *Science*.

Last month, in a surprising shift, the U.S. National Science Advisory Board for Biosecurity (NSABB) recommended that Fouchier's study be published in full, along with a similar one by Yoshihiro Kawaoka of the University of Wisconsin, Madison, under review by *Nature* (*Science*, 6 April, p. 19). But the Dutch government still isn't sure. It says Fouchier needs an export license to publish the sensitive paper, because it involves "dual-use" research that could be used for good or evil. Whether it will grant one will depend in part on the meeting, says a spokesperson for the Ministry of Economic Affairs, Agriculture and Innovation. Among the 30-odd guests are Kawaoka and other scientists and officials from the United States, Japan, Indonesia, Vietnam, and the United Kingdom, as well as representatives from *Science*, *Nature*, and the World Health Organization (WHO).

Even if the government releases the paper, the debate is likely to have wider ramifications. Dutch parliamentarians have asked the government for stricter oversight of dual-use research, and health minister Edith Schippers has hinted she may support the creation of a European version of the NSABB.

Reactions to Fouchier's study in the Netherlands were relatively muted when news about it hit Dutch papers late last year. His lab's proactive, open media strategy and efforts to keep officials at the relevant ministries in the loop had "nipped the debate in the bud," Fouchier concluded. But the perception that Dutch officials hadn't properly considered the study's risks prompted criticism from members of the Dutch House of Representatives—especially after NSABB recommended last December that key details be redacted from Fouchier's paper. "We couldn't just ignore that opinion," says Henk Jan Ormel, a House member representing the Christian Democratic Appeal party.

But Ormel calls the government's response—requiring that Fouchier apply for an export permit—"a bit artificial." The demand is based on the government's interpretation of a 2009 European Union regulation governing the export of sensitive technologies and materials, including H5N1. Those rules exempt "basic scientific research," which lawyers for Erasmus MC say includes Fouchier's study. Fouchier didn't apply for a permit when he first submitted the paper to *Science*; the government says that omission may have broken the law.

Given NSABB's reversal—which followed a similar recommendation to publish in February from an expert group assembled by WHO—some believe the Dutch government is unlikely to resist publication. "Because they based the export-control decision on [NSABB's] recommendations, the expectation is they will lift it," says NSABB acting chair Paul Keim. That's not a foregone conclusion, the Dutch ministry spokesperson warns.

The fracas has led to a broader debate about dual-use research in the Netherlands. Fouchier "did everything he had to do" according to A Code of Conduct on Biosecurity, adopted by the Royal Academy in 2007, says Lous van Vloten-Doting, who chaired the panel that wrote the code. But the case has made it clear that an NSABB-like panel, preferably at the European level, is needed to weigh the risks and benefits of such studies, Van Vloten-Doting says. Ormel says he plans to introduce a motion in the House that asks the government to help establish such a panel.

Fouchier's H5N1 study proposal was green-lighted in 2007 by the Netherlands Commission on Genetic Modification (COGEM), a government advisory panel. The COGEM review focused on lab biosafety, but part of its remit is to inform the government about emerging ethical debates. "In retrospect, perhaps we should have looked at" the study's dual-use risks, says COGEM secretary Frank van der Wilk. "We missed it. … We didn't realize it would cause so much debate." Fouchier is COGEM's acting chair and chair of its Medical and Veterinary Aspects subcommittee, but he recused himself during the 2007 review and had "no influence whatsoever" on its outcome, Van der Wilk says.

Meanwhile, one of the six NSABB members who still opposes full publication of Fouchier's paper has strongly criticized the March meeting in which NSABB reached its new decision. The gathering was "designed to produce the outcome that occurred," and only "kicked the can down the road" in preventing future conflicts over potential dual-use studies, Michael Osterholm of the University of Minnesota, Twin Cities, wrote in a letter to Amy Patterson, the National Institutes of Health official who oversees NSABB. Fouchier—who describes the last 6 months of debate as "a big pain"—declined to respond to Osterholm's letter, which was obtained by *Science* (http://scim.ag/flaw-flv).

**–MARTIN ENSERINK**





Published by AAAS

BIOMEDICINE

# Nanoparticle Treatment Reverses Cerebral Palsy in Rabbits

By the time a child is diagnosed with cerebral palsy, typically around the age of 2, it's too late to figure out exactly what caused the neurological damage. Cerebral palsy affects roughly three in 1000 babies, and a far greater percentage of those born prematurely. It can result from genetic causes, infection and ensuing inflammation, a disruption in the brain's oxygen supply, or a combination of these. The injury to the brain happens before birth, but its impact persists for a lifetime, causing rigid muscles, a lack of coordination, and other permanent movement difficulties.

Or maybe not so permanent. This week in *Science Translational Medicine* (http://scim.ag/SKannan), researchers describe a treatment that restores nearly normal movement to rabbits with an induced form of cerebral palsy when given a few hours after birth. The therapy consists of an injection of an anti-inflammatory drug bound to nanoparticles that ferry the drug into the brain and deliver it to specific cells. The treatment's developers acknowledge it's not ready for clinical trials in humans, but they and others say the findings raise the possibility of a preventive treatment that could be given to high-risk infants soon after they're born.

"The big question is how late could you give that injection and still see an improvement in the outcome," says Janice Brunstrom-Hernandez, a pediatric neurologist specializing in cerebral palsy at Washington University in St. Louis in Missouri. In contrast to the current standard of care, which includes physical therapy and medications that improve mobility and reduce other symptoms, the new study suggests it may be possible to reduce the underlying brain damage, Brunstrom-Hernandez says: "We have to have more research like this."

While at Wayne State University in Detroit, Michigan, chemical engineer Rangaramanujam Kannan and his wife Sujatha Kannan, a pediatric critical care physician, developed the new therapy, whose key ingredient is an anti-inflammatory and antioxidant drug called *N*-acetyl-L-cysteine (NAC). The drug is already used to prevent liver damage in people who overdose on the painkiller acetaminophen, and its neuroprotective effects are being tested in clinical trials for conditions as diverse as autism and Alzheimer's disease. The Kannans reasoned that NAC might also have potential for treating cerebral palsy.

They and colleagues, including Roberto Romero of the Eunice Kennedy Shriver National Institute of Child Health and Human Development in Detroit, first tested this idea by injecting NAC alone into rabbits with cerebral palsy–like symptoms. These animals, whose mothers had been given a shot containing toxin from *Escherichia coli* bacteria 3 days before giving birth, exhibit abnormally rigid muscles and movement problems similar to those of children with cerebral palsy. Unlike healthy rabbit kits, they could barely walk and were unable to hop. NAC alone had only a barely discernible effect on these symptoms, however.

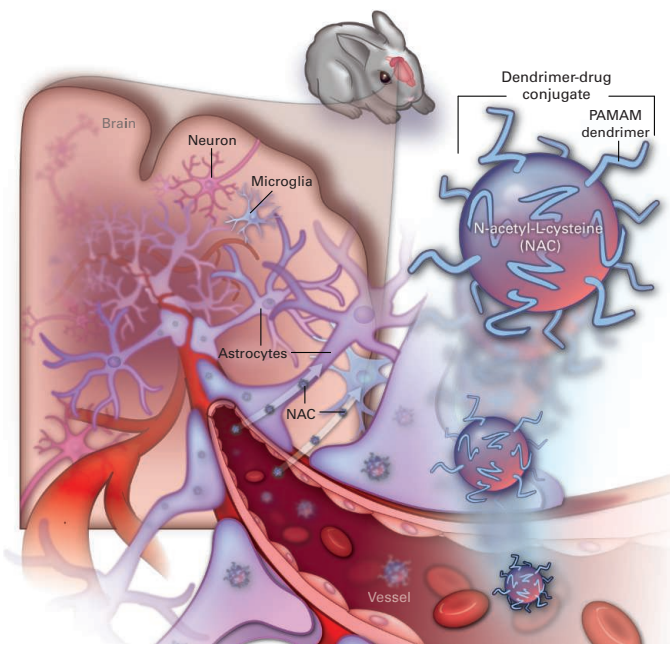


**Brain defense.** Drug-carrying nanoparticles (*top right*) injected into rabbits target microglia and astrocytes in the brain and reduce symptoms of cerebral palsy.

Rangaramanujam Kannan, who specializes in nanomedicine, knew that drugs coupled to nanoparticles have shown promise in treating cancer and other disorders, because they help target the drug where it's needed (see p. 292). So he chemically attached NAC to nanoparticles called dendrimers that branch out from the center to form tiny spheres. When given an injection of the dendrimer-coupled NAC a few hours after birth, kits with cerebral palsy showed improved muscle tone and were walking and hopping nearly as well as healthy animals within 5 days, which is as long as the researchers followed them in this study.

Exactly how the NAC-nanoparticle treatment works is not yet clear—the dendrimers alone don't have any effect—but follow-up experiments by the Kannans and their colleagues provide several clues. In rabbits with cerebral palsy, the nanoparticles seem to deliver their payload of NAC specifically to two types of cells in the brain: immune system cells called microglia, and multifunctional support cells called astrocytes. The treatment decreased several molecular markers of potentially harmful inflammation and oxidative stress, decreased the loss of neurons, and improved myelination, the fatty insulation on neurons that's essential for neural signaling.

"To my knowledge, this is the first demonstration that such a dendrimer-based approach is doable and efficient to protect the neonatal brain," says Pierre Gressens, a child neurologist at the French biomedical research agency INSERM in Paris. It's especially impressive, Gressens adds, that the nanoparticle treatment was effective at doses 100 times lower than those tried with NAC alone.

"This is on the threshold of something big," says Sidhartha Tan, a neonatologist at NorthShore University HealthSystem in Evanston, Illinois. Tan notes that although some clinical trials with nanoparticle therapies are already under way, the particular type of dendrimers used in the new study has not yet been approved for human use. More work will be needed to establish that they are safe, he says.

Other questions remain as well, says Zena Vexler, a neuroscientist who studies perinatal brain injury at the University of California, San Francisco. "The results are quite striking, but they need to follow up for much longer" to see if the benefits last longer than a few days and whether side effects develop, Vexler says. The Kannans, who have since moved to Johns Hopkins University in Baltimore, Maryland, say these experiments are already under way.

**–GREG MILLER**

CREDIT: BRICELYN STAUNCH/*SCIENCE*





Published by AAAS

NEWSMAKER INTERVIEW: ROBERT GROVES

# Saving Money Essential for Next Census, Says Departing Director

Sociologist Robert Groves interrupted his academic career 3 years ago to direct the Census Bureau on the eve of its massive decennial count. The largest peacetime mobilization in U.S. history—600,000 people knocking on 47 million doors from the Aleutians to Key West—was so successful that Democratic and Republican lawmakers alike expressed chagrin when Groves announced last week that he would be leaving the agency in August.

"His tenure is proof that appointing good people makes a big difference," said Representative Darrell Issa (R–CA), chair of the House of Representatives committee that oversees the bureau. "He was just what the doctor ordered," said Senator Tom Carper (D–DE), who leads the equivalent panel in the Senate.

The 2010 census cost $13.1 billion, and doing it the same way in 2020 could require more than twice that amount. Such a budget is just not in the cards, however, so the next director will need to figure out how to conduct an accurate and comprehensive tally for much less.

The Internet isn't the answer, Groves says—although next year it will be one option on the agency's ongoing American Community Survey (ACS) that has replaced the long-form census (*Science*, 9 April 2010, p. 158). A bigger step, he says, would be to mine existing government records, assuming the agency can clear technical, legal, and cultural hurdles.

Groves, 63, will remain in Washington, D.C., to become provost of Georgetown University. He says he's returning to academia in part to tackle "the gigantic mismatch" between the vast quantities of statistical data available to politicians and how little is actually used to shape policy.

Below are excerpts from a 13 April interview with *Science*.

–JEFFREY MERVIS

**Q: What can the Census Bureau do to reduce the cost of the next census?**
**R.G.:** We did a test using the [community survey], in which some people got the normal, paper request and others got a letter inviting them to go online to fill out the questionnaire. At the end of a month, the response rates of both groups were about the same. The Internet responses saved money, because you don't have to process the paper forms, but all of the scientific studies around the world say that won't solve the problem.

So many countries have asked the question: "For this address, are there other data that have been supplied to other government agencies that might allow us to estimate who's there?" In effect, it's a mode of data collection that doesn't require the active participation of the population.

The amount of money that one can save is vast. But there are three issues. Do the existing records cover the U.S. well? Is it legal to make use of these records? And third, what will people think about this? Will they say, "Thank God, you've finally gotten your act together"? Or will they say, "This is threatening to me"?


Robert Groves

CREDIT: ROSS D. FRANKLIN/AP

**Q: Do you need congressional approval?**
**R.G.:** Article 1, Section 2, of the Constitution says that the census will be taken "in such manner as they [Congress] shall by law direct." And we feel that an expression of congressional intent is important, because it would be a shift.

**Q: Last month, you testified at a House hearing on a bill to make ACS voluntary and said that such a change would raise the cost and lower response rates. What's the next step?**
**R.G.:** My intent was to say that we needed to do some research to address questions that weren't answered in a 2003 study before we could assure Congress on the impact, in terms of cost and quality, of making it voluntary. And I think what I promised is, if they wanted to pursue that research, I would be happy to lay out the projected cost and the nature of that research.

**Q: You've had very good relations with both sides of the aisle in Congress. What's your secret?**
**R.G.:** I must say, it's one of the more surprising developments following my announcement. I believe Congress does have the right to direct us in important ways. But I also felt the need to speak frankly when we had scientific results that were pertinent to something they wanted to do. I view my job as a scientific position, not a political position.

**Q: Would a fixed term, like the 6-year term given the National Science Foundation director, be a good idea?**
**R.G.:** I'm on record as saying that it would be useful. But rather than a fixed length, I favor a fixed term in time, beginning in year 2 and ending in year 7. That fits well with the periodicity of the census.

**Q: Why do you want to be a provost?**
**R.G.:** One thing I didn't fully understand before I took this job is the gigantic mismatch between the production of really good statistical information about what is going on and how decisions are made. For example, I'm much more aware of that mismatch with regard to decisions that are made affecting the U.S. economy and society.

**Q: Was that a disappointment to you?**
**R.G.:** Absolutely. I've devoted my life to trying to improve the quality of statistical information, and it is disappointing to see how little of that is used to make decisions. The second observation is how fundamentally data have changed. The Internet has reshuffled the deck of knowledge [to the point where] with a couple of keystrokes, we can become privy to what all disciplines know about any problem.

So I concluded that the most important thing we have to do is to prepare universities for that new world. That means restructuring curricula and research activities to take advantage of both opportunities, using knowledge for action and utilizing interdisciplinary perspectives. That's the kind of challenge that motivated me.





Published by AAAS

# Trouble on The Yangtze

**Upriver habitats—including a critical refuge created when construction began on the Three Gorges Dam—are now at risk from a series of new projects**

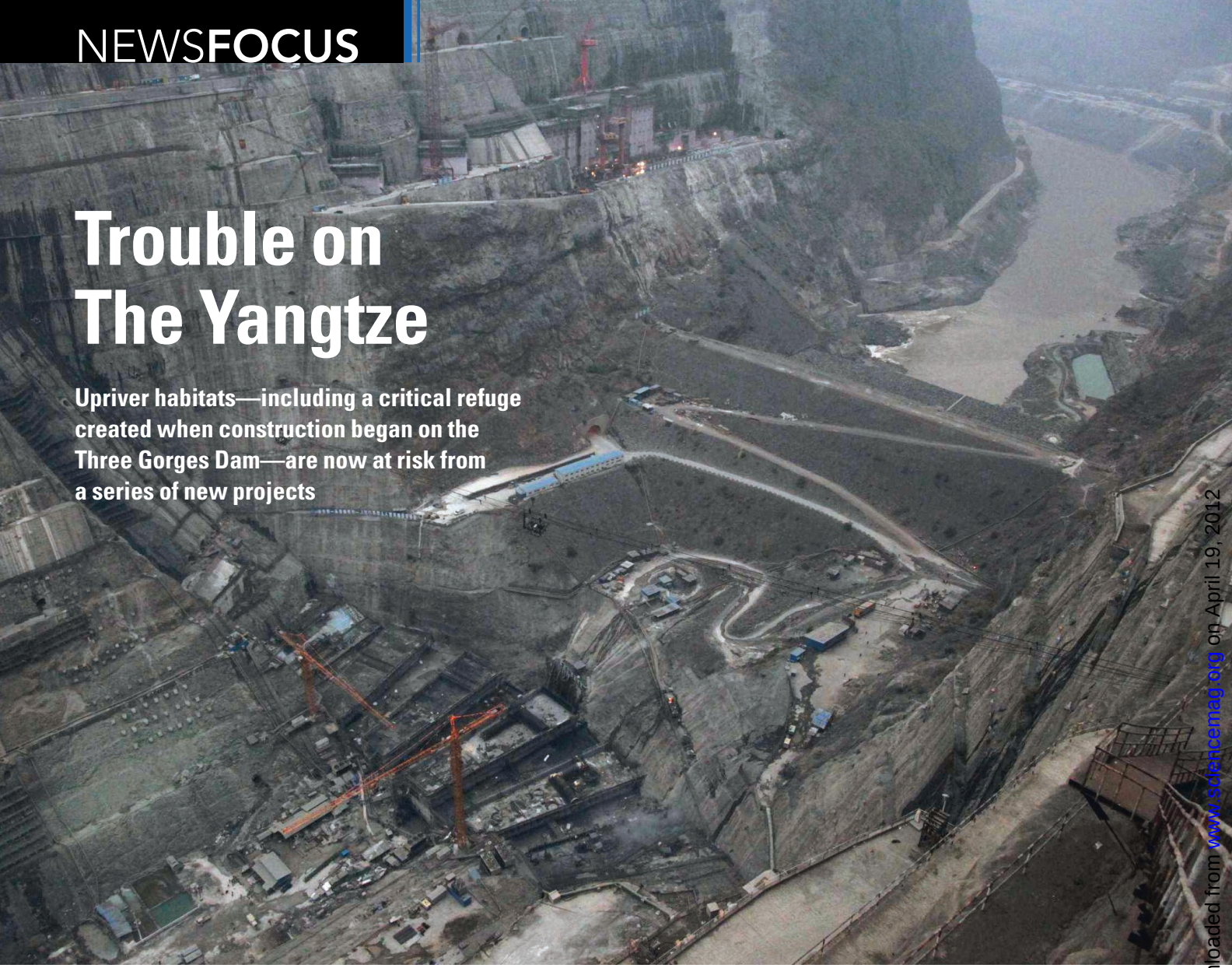

CREDIT: YANG YONG



**YONGSHAN, CHINA—**Among the hundreds of fish species that call the upper Yangtze River home is the largemouth bronze gudgeon. The species spawns in the rapids of this rocky waterway—also known as the Jinsha River—which descends from the Tibetan Plateau through the mountains of western China. Its eggs and larvae are kept afloat by the swift current until they hatch and mature hundreds of kilometers downstream. "They have evolved to live in fast-flowing rivers," says Cao Wenxuan, an ecologist at the Institute of Hydrobiology at the Chinese Academy of Sciences (CAS) in Wuhan.

But with dozens of new dams planned for the Yangtze system, that habitat will soon change. Last month, preparatory work began on the controversial Xiaonanhai Dam, with more projects to follow. Within a few years, the Jinsha will slow to a sluggish pace and its temperature will drop as a series of large dams release cold bottom water from their reservoirs into the river. Along with other endemic fish species, the largemouth bronze gudgeon may spawn up to 3 months later, and soon after, its eggs and larvae may sink to the bottom and die from lack of oxygen. For species already threatened by the Three Gorges Dam downriver, Cao says, the new series of hydropower dams will "take away their last refuge."

Last year, the central government solidified plans to increase China's reliance on non–fossil fuel energy from the 2010 level of 8% to 15% of the energy mix by 2020. Nearly two-thirds of that target will come from hydropower—an increase on par with adding nearly one Three Gorges Dam a year. "The scale of hydropower development in China is simply off the charts," says Edward Grumbine, an environmental policy researcher at CAS's Kunming Institute of Botany in Yunnan Province. Ecologists say China's hydropower push will threaten already-taxed ecosystems in the upper Yangtze.

Central to the spurt of construction is a 770-kilometer-long stretch of the lower Jinsha River flowing through Sichuan and Yunnan provinces. Last June, China announced an injection of $63.4 billion for hydropower in the region to cover four massive dams with a total capacity of 43,000 MW. "It's worrying to see so many proposed large dams, one immediately after another," says Zhang Xiaodong, deputy director of the China Earthquake Networks Center in Beijing.

In addition, three large dams are under construction and five are planned on the 560-kilometer-long middle Jinsha, with more planned for the 960-kilometer-long upper reach. At a combined height of 2 kilometers, the dams will convert "the rapidly flowing Jinsha River into a series of stepped lakes with few free-flowing sections," says Liao Wengeng, deputy director



Published by AAAS

**Building spree.** The Longkaikou (*top*), Xiangjiaba (*bottom*), and Xiluodu (*facing*) dams are among a series of new dams threatening the upper Yangtze River ecosystem.

CREDIT (TOP TO BOTTOM): YANG YONG

of the National Research Center for Sustainable Hydropower Development (NRCSHD) in Beijing. Also tagged for development are Yangtze tributaries such as the Yalong, Min, and Dahu rivers.

As construction of the Three Gorges Dam got under way in the 1990s, ecologists submitted petitions to the central government calling for an upstream reserve to protect fish populations. The result was the Upper Yangtze River Rare and Endemic Fish Reserve, a 500-kilometer-long protected stretch of river that includes 350 kilometers of the Yangtze mainstream. The reserve became a critical habitat for some 190 fish species—including the critically endangered paddlefish and the Yangtze sturgeon (*Science*, 1 August 2008, p. 628).

In 2005, officials sliced off 150 kilometers of the upriver portion to make way for the Xiangjiaba and Xiluodu dams. Now the Xiaonanhai Dam will chip away at the reserve even further. At a cost of $3.8 billion, the dam is expected to generate 1750 MW of electricity at its completion. Officials in Chongqing, the municipality overseeing the project, say that it will alleviate power shortages and boost the local economy. But it will also create a nearly 100-kilometer-long reservoir in the heart of the upstream protected area.

For years, ecologists have voiced fierce opposition against the Xiaonanhai Dam. But the battle was lost last December, when China's State Council green-lighted Chongqing's request to shrink the reserve. Road building and other preparation began 29 March. Critics like Fan Xiao, chief engineer at the Sichuan Bureau of Geology and Mineral Resources in Chengdu, fear that Xiaonanhai will pave the way for two additional upstream dams proposed by Sichuan authorities in the reserve area. And that could mean the end for the paddlefish, the Yangtze sturgeon, and other endemic fish: "The reserve would exist only in name," he says.

### Geological minefield

Driving on the narrow road clinging to a cliff above the Jinsha River is not for the faint-hearted. It circles mountains that have risen out of tens of millions of years of thrusting and folding of Earth's crust, overlooking a steep valley carved by the roaring river. Scars left by recent landslides cut across facing slopes.

Critics fear that China's hydropower expansion will collide with this stark topography. Crisscrossed with active faults hundreds of kilometers long, the region is "much more geologically complex than the Three Gorges," says geologist Guo Shunmin of the China Earthquake Administration's Institute of Geology in Beijing. Earthquakes of magnitude 7 or 8 are not uncommon. "A lot of the reservoirs will have active faults beneath them," he adds.

Given that some evidence links construction of the Zipingpu Dam to the 2008 Wenchuan earthquake (see sidebar, p. 291), "there should be studies on the effect of water impoundment on active faults beneath the [Jinsha area] reservoirs," says Hu Xianming, a geophysicist at the Sichuan Seismological Bureau's Institute of Reservoir-Induced Seismicity Research in Chengdu. The current safety evaluation, however, involves only surveys to avoid building dams on active faults.

Compounding the problem is the up to 2 meters in precipitation the Jinsha region gets every year. In monsoon season, torrential rains can tear apart steep slopes. Massive landslides have blocked the Jinsha for days at a time in the past, says Yang Yong, director of the environmental group the Hengduanshan Society in Chengdu.

Changes in water temperature will be stark as well. The 278-meter-high Xiluodu Dam will cool water temperature by an average of 1.5°C for the months of March through September, according to the project's environmental impact assessment (EIA). Deep reservoirs stratify water into layers of different temperature, with the coldest near the bottom. Water from the cold bottom layer will be released downstream, Liao says. Most fish species spawn in April or May, when the water warms to 16°C to 18°C. After the four dams on the lower Jinsha are built, the EIA says, downstream portions of the river won't reach such temperatures until 2 to





Published by AAAS

## Evidence Mounts for Dam-Quake Link

**CHENGDU**—Ever since the devastating magnitude-7.9 Wenchuan earthquake killed 80,000 people in 2008, Chinese hydrologists and geologists have wrangled over whether the reservoir behind the 156-meter-high Zipingpu Dam may be to blame (*Science*, 5 March 2010, p. 1184). Today, as China embarks on a spurt of new hydropower development (see main text, p. 288), the debate is getting increasingly heated. Newly published studies present the strongest evidence yet for the link.

Most scientists agree that the Wenchuan hypocenter, or depth of the initial rupture, is directly beneath the reservoir. But just how deep it lies is in dispute. The China Earthquake Networks Center (CENC) and geophysicist Liu Qiyuan of the China Earthquake Administration's (CEA's) Institute of Geology in Beijing calculate the hypocenter at 14 and 19 kilometers beneath the surface, respectively. At such depths, some scientists contend, water from the reservoir could not have reached the fault.

Others point out that Liu and CENC based their calculations on seismic data from stations tens of kilometers from the epicenter. Using data from the Zipingpu seismic network, including one station almost directly above the hypocenter, Xu Xiwei, deputy director of CEA's Institute of Geology, and colleagues reported last year in *Seismology and Geology* that the hypocenter is as shallow as 6 to 9 kilometers—within easy reach of water from the reservoir.

Some scientists also point to numerical modeling studies looking at stress changes caused by the weight of the reservoir and water infiltration. Xinglin Lei, a geophysicist at the Geological Survey of Japan in Tsukuba, concluded in a study published in the *Journal of Asian Earth Sciences* last year that the reservoir significantly impacted the Beichuan-Yinxiu fault, which runs along the reservoir, and increased the stress on the hypocenter of the Wenchuan Earthquake. That could hasten the occurrence of the earthquake by tens to hundreds of years, he argues. Shemin Ge, a hydrogeologist at the University of Colorado, Boulder, and colleagues came to a similar conclusion using a different model in an earlier study.

That finding was contradicted in 2010 studies by geophysicists Zhou Shiyong of Peking University in Beijing and Kalpana Gahalaut of the National Geophysical Research Institute in Hyderabad, India. But their results could be explained by the use of different numerical models and geometrical parameters for the faults, among other factors, says Jian Lin, a geophysicist at Woods Hole Oceanographic Institution in Massachusetts, who is not involved with any of the studies.

The strongest evidence for a Zipingpu-Wenchuan link may come from analyses by Xu's team of nearly 1000 seismic events recorded by the Zipingpu seismic network between August 2004 and May 2008, before the Wenchuan quake. The researchers found three clusters of seismicity—all under magnitude 3.5—after the reservoir was filled with water in September 2005. One, the Shuimo swarm, occurred along the Beichuan-Yinxiu fault, where the researchers concluded it was induced by the reservoir.

Despite the controversies, many Chinese geophysicists now agree that the reservoir may be connected to the Wenchuan earthquake. Even if the hypocenter lies 19 kilometers below the surface, Liu says, as his calculation shows, this doesn't exclude the possibility that Zipingpu hastened the quake because "small incremental stress changes due to the reservoir could rupture critically stressed faults—even without water reaching them."

The new studies highlight the need to consider reservoir-induced seismicity when building large dams in quake-prone regions, scientists say. With dozens of dams planned for the upper Yangtze, Ge says, "We need to assess whether the proposed reservoirs could significantly speed up the accumulation of stress and cause rock failures."

**–J.Q.**

3 months later. That will "hamper fish reproduction," Liao says. He points to the Three Gorges Dam: With spawning delayed by over a month, downstream carp populations have been decimated.

The problems brought on by that earlier dam are well documented. The river dolphin, or *baiji*, has been functionally extinct since 2007, and ecologists fear that the finless porpoise, or *jiangzhu*, may soon follow it.

Also of concern is silt accumulation: Sediment retention in the reservoir means the clearer downstream water can cut the riverbed deeper and lower water levels in lakes fed by the Yangtze. In January, Poyang Lake, China's largest freshwater lake, was hit by the worst drought in 6 decades: the water level dropped to a mere 8 meters, and much of the lake has become a plain of cracked mud. Such problems will snowball with "a cascade of upstream dams," Liao says.

### A stacked deck

Some hydrologists say that optimizing dam operation could alleviate problems with downstream water supply. But many are unconvinced. With so many new dams, says Guo Qiaoyu, director of The Nature Conservancy's Yangtze River project, "it will be extremely difficult to ensure proper coordination between provinces and companies that operate the dams."

With the new hydropower boom, criticism of China's EIA process is mounting. By law, dams cannot be constructed in nature reserves or their buffer zones. But the government is all too willing to redraw the boundaries to accommodate hydropower projects, some say. The Xiaonanhai Dam in particular, Guo says, is "yet another example of the country's disregard for the environment."

Critics say EIA committee members are often paid for their services by dam projects and deliver favorable assessments in order to be invited back. "The EIA is just about friends evaluating each other's projects," says Wang Mingna, a hydrologist at the Chinese Institute of Water Resources and Hydropower Research in Beijing. Scientists' warnings "often fall on deaf ears," adds ecologist Yang Junxing of CAS's Kunming Institute of Zoology.

Adding bias to the schedule, ecologists say, are rules that allow developers to start preparing for a proposed dam while project assessment is still under way. And EIAs are too narrow, examining projects in isolation, points out He Daming, an ecologist at Yunnan University, Kunming. "Even if the impact of individual dams is acceptable," he says, "the cumulative effects of stacking dams on top of one another could still be catastrophic."

The science ministry is funding research that takes additive impacts into account. The Ministry of Water Resources, meanwhile, may soon improve the EIA process, says Yu Xuezhong, chief engineer at the NRCSHD.

But such measures may come too late for the upper Yangtze's beleaguered fish species. Ecologists are scrambling to set aside small sanctuaries—in small tributaries near their current habitats, for example. The goal, Cao says, is to "save as many fish species as we can. All we can hope for is to slow down the extinction rate."

**–JANE QIU**

Jane Qiu is a writer in Beijing and London.





Published by AAAS

# Nanoparticles Offer 'Open Sesame' Keys to New Drugs and Vaccines

Drugs that rely on tiny strands of RNA to shut down the production of problem proteins have generated intense research interest in recent years. But they have to overcome a common difficulty: It's hard to get the RNA into target cells. Research presented at the meeting suggests there may be a straightforward solution: Pack the strands together to form nano-sized particles. And a second study indicated that a different kind of nanoparticle may lead to novel kinds of vaccines. Nanomedicine may be about to get a big boost.

A little over a decade ago, researchers demonstrated that it's possible to use short strands of RNA to knock down the expression of particular genes and prevent construction of key disease proteins. The RNA strands, called short interfering RNAs (siRNAs), are tailored to bind to target strands of messenger RNA (mRNA) that carry genetic instructions from the cell nucleus to the ribosomes, where proteins are built. The mRNAs then can't be translated into proteins by the ribosomal machinery. To do their work, however, siRNAs have to enter cells. The trouble is, says Chad Mirkin, a chemist at Northwestern University in Evanston, Illinois, because RNA is negatively charged, it is repelled by cell surfaces, which are also primarily negatively charged.

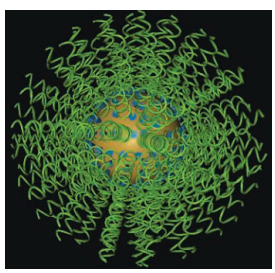

**Fuzzball.** Gene-silencing nanoparticles deftly slip inside cells.

Mirkin reported that he and his colleagues have overcome this problem by packing hundreds of copies of siRNA strands into a tight ball. The RNA ball attracts the attention of numerous positively charged cell surface proteins called scavenger proteins, which bind to it. The complex is then engulfed into the cell, and the spherical siRNA particles are later released to sop up their mRNA targets. Mirkin reported that in cell culture studies, the particles readily entered 49 of 50 different cell types (with red blood cells being the only exception) and knocked down the expression of target mRNAs.

Working with Alexander Stegh, a brain cancer expert at Northwestern University's Feinberg School of Medicine in Chicago, Illinois, Mirkin's team then designed siRNA particles targeted to prevent the expression of key proteins involved in brain cancer. When they injected the particles into mice with brain cancer, 1% of the particles crossed the blood-brain barrier, which stops most drugs from getting into the brain, and increased the average life expectancy of the animals by 20%. The hope, Mirkin says, is that the technique will enable a new generation of oncology drugs to work against brain cancer, currently one of the most difficult families of cancers to treat.

It was "just luck" that the particles managed to cross the blood-brain barrier, Mirkin says. But Joseph DeSimone, a chemist at the University of North Carolina, Chapel Hill, says Mirkin's team has been far more than lucky. "This has the potential to pull the siRNA field out of the toilet," DeSimone says.

At the meeting, DeSimone reported some heavy lifting of his own: using nanoparticles to make novel vaccines. DeSimone's group has pioneered a technique for making organic nanoparticles of almost any size, shape, and composition. Now the group has incorporated, in some cases, dozens of immunogenic fragments from pathogens such as influenza into nanoparticles. When the researchers injected mice with the particles, 30% to 40% of the particles were taken up by immune cells, compared with roughly 1% of normal vaccine compounds, and antibody titers against influenza and other diseases increased as much as 12-fold. Not only might the work lead to vaccines that are more effective and require fewer booster shots, DeSimone says, but it could also require far less of a given formulation, thus dropping their cost and making them more readily available.

Mirkin returns the favor, calling DeSimone's latest work "fantastic."

# Biofuels and City Air: A Marginal Effect

If drivers switch from gasoline to biofuels, will it lessen the air pollution that shrouds cities around the world? Studies of auto emissions have indicated it might. But the first citywide air quality study of its kind suggests that unless more than 26% of cars make the switch, it will have negligible effect.

CREDIT: JOSHUA I. CUTLER/NORTHWESTERN UNIVERSITY



# New Genetic Letters Augment DNA, and Soon Perhaps Life

AGCT. The letters of DNA, along with their RNA cousins, write the code for all life as we know it. But perhaps not for long.

At the ACS meeting, a pair of research groups reported that they now have alternative letters—synthetic nucleotides—that can be incorporated into DNA and can be copied with near perfection by enzymes that copy natural DNA. These additions to the genetic alphabet are already enabling researchers to write new chemical functions into DNA, which could help usher in a wide array of biotechnology advances. And they are a critical step along the way to making semisynthetic life forms, written in the first new type of genetic code that life has ever known.

The effort to rewrite life's genetic code has a long history. Researchers have already created dozens of novel nucleotides, designated by initials such as P and Z, and they have even managed to incorporate many of them into natural DNA. But getting them to work in living, reproducing organisms is a tough challenge. One major problem is that when enzymes called DNA polymerases try to copy unnatural nucleotides, either they grind to a halt like a printer with a paper jam or they make mistakes.

Last year, Steven Benner, a chemist and founder of the Westheimer Institute for Science and Technology, a private research institute in Gainesville, Florida, and colleagues came close to solving that


**Natural experiment.** An annual change in the price of gasoline relative to ethanol makes it possible to test how biofuels affect air pollution.

The new work, reported by Franz Geiger, a chemist at Northwestern University in Evanston, Illinois, grows out of a natural experiment that takes place every year in São Paulo, Brazil's largest city. São Paulo is home to 1.5 million flex-fuel cars capable of switching between using gasoline and 100% ethanol, made from fermenting sugar cane. Because virtually all gas stations in São Paulo offer both fuels, drivers of flex-fuel cars choose by calculating which will let them drive more cheaply, Geiger says. (Gasoline tends to be more expensive but also supplies about 30% more energy per liter.)

Unlike gas prices in the United States and Europe, which fluctuate with world oil prices, gas prices in Brazil are tightly regulated. The cost of ethanol, however, varies wildly with the cost of sugar cane. For most of the year, it's cheaper for drivers to fill up with ethanol. But for two of the past three winters, world hikes in the price of sugar have made gasoline a better value, prompting 1.5 million drivers—about 26% of the total of 5.8 million cars and light trucks—to switch for a couple of months.

Geiger and his colleagues, including Northwestern University economist Alberto Salvo, decided to see whether this change affected air quality. To their surprise, it didn't. Geiger reported at the meeting that they analyzed air sampling data taken at regular intervals every day from 22 stations throughout the city. The sampling tracked carbon monoxide, nitrous oxides, sulfur dioxide, ozone, and other compounds in both the high- and the low-ethanol seasons. But the researchers found no change in air quality. When they crunched the numbers further, performing numerous statistical regression analyses that attempted to isolate specific correlations with weather, traffic patterns, air-circulation patterns, and other possible links, they still saw no effect. "Any discernible change may require an even larger share of vehicles to switch fuels, or change to a new fuel altogether," Geiger says.

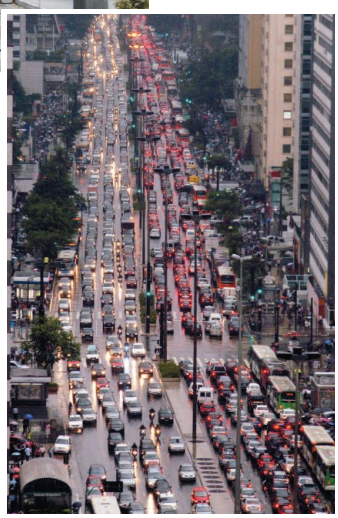

Geiger stresses that a larger scale switch to biofuels might affect air quality. And air quality may still improve over time, as older, higher-polluting cars and trucks are replaced by newer, more-efficient models. That has yet to be seen. But the Northwestern team's new study will provide valuable baseline data to spot such a future trend, Geiger says.

Paul Alivisatos, director of Lawrence Berkeley National Laboratory in California, says the new results should be seen as "good news for biofuels." The growth of sugar cane and other feedstocks removes carbon dioxide—the most abundant greenhouse gas—from the air, which is then returned to the atmosphere when the fuels are burned. Burning fossil fuels, by contrast, adds new $CO_2$. And the new study, Alivisatos says, suggests that switching to biofuels doesn't carry a penalty in air quality, which on balance makes them a winner.

**–ROBERT F. SERVICE**

CREDITS (TOP TO BOTTOM): BRUNO DOMINGOS/REUTERS; ANDERSON BARBOSA/AP

problem. He reported incorporating novel nucleotides into DNA and showed they could be copied with 99.8% fidelity. Still, 99.9% fidelity will be required to avoid mistakes building up in the new genetic code, or the replacement of novel bases by natural ones.

At the meeting, groups led by Ichiro Hirao of the RIKEN Yokohama Institute in Japan and Floyd Romesberg of the Scripps Research Institute in San Diego, California, reported the synthesis of new nucleotides that can be incorporated into DNA and copied with sufficient fidelity to work well in living organisms. Hirao and colleagues reported that their novel DNA was copied with as high as 99.97% fidelity. One limitation was that their new letters always had to be flanked by particular sequences of natural DNA to ensure high copying quality. Romesberg's team, meanwhile, got 99.9% fidelity with its system and showed that its novel letters could be incorporated anywhere in natural DNA strands without affecting the copying fidelity. Another group reports similar success with a different set of letters on page 341.

Now, the race will be on to get the new letters incorporated in living microbes. That won't be easy, Romesberg says.

Researchers still need to find ways to coax cells to import the new nucleotides or bring in the building blocks and assemble them once inside. They also need to show that the altered DNA is transcribed into RNA with corresponding novel letters and then translated into new amino acids that make up proteins. Researchers have previously coaxed cells to incorporate unnatural amino acids into proteins, but no one has yet started with novel genetic letters and gone the distance.

With several groups now zeroing in on that goal, life's genetic alphabet may soon be expanded for the first time. **–R.F.S.**




Published by AAAS

Complexities of genetic testing 297

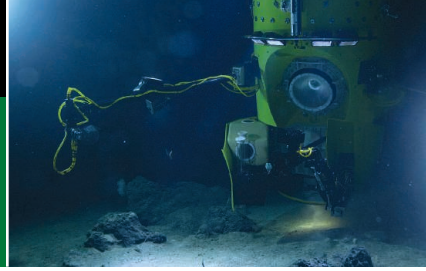

Exploring the Mariana trench 301



# LETTERS

*edited by Jennifer Sills*

## Environment-Friendly Reform in Myanmar

DECADES OF ECONOMIC AND POLITICAL ISOLATION HAVE TRANSFORMED MYANMAR. ONCE A regional leader [and the world's largest exporter of rice through the 1950s (*1*)], Myanmar now has some of the lowest human development and governance indicators in the world (*2*, *3*). Environmental governance has also suffered: Mineral and timber resources have been unsustainably exploited (*4*), wildlife populations have declined (*5*), environmental safeguards are negligible (*6*), and the protected-areas network is under-resourced and poorly enforced (*7*). Yet, Myanmar remains a global biodiversity hotspot and conservation priority. It hosts one of the largest contiguous forest blocks in Southeast Asia and sustains many endangered and endemic species, including the newly described Burmese snub-nosed monkey (*8*). New, rapid economic transformation has the potential to compound the challenges of safeguarding sensitive ecosystems.

**Democracy advocate Aung San Suu Kyi.** Recent elections bring Myanmar one step closer to reform.

The 2011 establishment of a quasi-democratic government and the subsequent release of hundreds of political prisoners prompted high-profile visits by representatives from numerous donor countries (*9*). With openly contested by-elections on 1 April, Myanmar has taken another step toward increased development assistance, reduced sanctions, and improved trade, in hopes of renewed economic opportunity. Myanmar's business environment is already changing, spurred by regional investment, the China-ASEAN Free Trade Agreement, and plans for large-scale industrial and agricultural development and currency stabilization.

Although potentially transformative, massive and rapid investment into Myanmar should prompt some concern. Myanmar's neighbors may view liberalization as an opportunity to export polluting industries, extract raw materials, and supply agricultural exports; domestic environmental groups are already sounding the alarm (*6*, *10*). Encouragingly, the new government has recently made several bold, high-profile steps toward environmental protection, including the suspension of the Chinese-supported Myitsone Dam and Thai-financed Dawei coal-fired power plant (*11*, *12*).

Much depends on the reform of Myanmar's environmental regulatory framework. Although Myanmar is already a signatory to international environmental agreements such as the Convention on Biological Diversity (in 1994) and the Ramsar Convention (in 2005), there is clear need for internal review, as well as capacity-building and financial support to promote best practices. During this period of re-engagement among government, donors (including nontraditional donors), and foreign investors, there is also a need for renewed dialogue about how to establish sustainable development and environmental agendas for Myanmar. In the face of rapid economic liberalization, it will be a major challenge to ensure sustainability and to conserve Myanmar's imperiled biodiversity.

**EDWARD L. WEBB,[1]* JACOB PHELPS,[1] DANIEL A. FRIESS,[2] MADHU RAO,[1,3] ALAN D. ZIEGLER[2]**

[1]Department of Biological Sciences, National University of Singapore, 117543, Singapore. [2]Department of Geography, National University of Singapore, 117570, Singapore. [3]Wildlife Conservation Society Singapore, 247671 Singapore.

*To whom correspondence should be addressed. E-mail: ted.webb@nus.edu.sg

**References and Notes**

1. D. Dawe, *Food Pol.* **27**, 355 (2002).
2. United Nations Development Program, "Human development report 2011" (http://hdr.undp.org/en/).
3. The World Bank's Worldwide Governance Indicators (http://info.worldbank.org/governance/wgi/index.asp).
4. Global Witness, "A conflict of interests" (2003); www.globalwitness.org/library/conflict-interest-english.
5. M. Rao, S. Htun, T. Zaw, T. Myint, *Environ. Manage.* **46**, 143 (2010).
6. Burma Environmental Working Group, *Burma's Environment: People, Problems, Policies* (Wanida Press, Chiang Mai, Thailand, 2011); www.bewg.org/en/pubs/finish/4/34.
7. M. Rao, A. Rabinowitz, A. T. Khaing, *Conserv. Biol.* **16**, 360 (2002).
8. T. Geissmann *et al.*, *Am. J. Primatol.* **72**, 1 (2010).
9. Ministry of Foreign Affairs, Government of the Republic of the Union of Myanmar (www.mofa.gov.mm).
10. A. Guilloux, *Contemp. Pol.* **16**, 383 (2010).
11. T. Fuller, "Myanmar backs down, suspending dam project," *The New York Times*, 1 October 2011, p. A4 (www.nytimes.com/2011/10/01/world/asia/myanmar-suspends-construction-of-controversial-dam.html).
12. J. S. Gaung, "Govt cuts coal plant from Dawei project," *Myanmar Times*, 16 January 2012 (www.mmtimes.com/2012/news/610/news61006.html).

13. E.L.W., D.A.F., and A.D.Z. are supported by the Singapore-Delft Water Alliance, National University of Singapore.

## India's Science: Elitism Prevails

AFTER READING THE NEWS FOCUS STORY "INDIA rising" (R. Stone, 24 February, p. 904) and the related Editorial, "India's 'science for all' academy" (R. Mashelkar, 24 February, p. 891), I can't escape asking: Why doesn't such a competent and highly educated scientific workforce produce? It seems that in







Published by AAAS

India, scientists who become successful or achieve some modicum of notoriety eventually become science administrators and preside over decades of myopic science policies and self-preservation, including handpicking those who are "respectful and compliant," ensuring vertical transmission of mediocrity and incompetence. This continuum of elitism, contaminated with favoritism, leaves Indian science bereft of new ideas and energies. The only time that this practice was defied was when Nehru (India's first prime minister) appointed a young, energetic visionary physicist named Homi Bhabha, much to the chagrin of the late Sir C.V. Raman (the Nobel laureate). It was Bhabha who ushered the Indian Atomic Energy program to its current stature and competence. In a nation of more than a billion people, there shouldn't be a dearth of energy or ideas. It is sad that Stone did not find any young Indian scientists to write about.

**SURAJ P. BHAT**

Department of Ophthalmology, Geffen School of Medicine, University of California, Los Angeles, Los Angeles, CA 90095, USA. E-mail: bhat@jsei.ucla.edu

## India's Science: Excellence Unrecognized

NEITHER R. MASHELKAR'S EDITORIAL ("INDIA'S 'science for all' academy," 24 February, p. 891) nor the News Focus story by R. Stone ("India rising," 24 February, p. 904) touched upon the biggest shortcoming of Indian science: its inability to reward, and hence inspire, excellence.

Among the multitudes who brave the largely patronizing and unimaginative education system in India, many researchers do emerge who are capable of emulating the best in the world. However, no mechanism exists to encourage demonstrated potential or to reward those who achieve better-than-average output. A university faculty member receives the same annual salary raise whether she or he has published 10 papers, one paper, or no papers in high–impact-factor journals in the preceding year. Not only is the system unable to provide personal benefits to achievers of excellence, it does not even facilitate their work with better research grants. An assistant professor must spend at least 11 years and must achieve a certain minimum research output in that time to be given associate professorship. But if someone achieves double, triple, or quadruple the stipulated minimum in less than 11 years, there is no provision for that person to move up faster than the lesser achievers. Apart from enduring the disinterest of the establishment, these scientists also have to contend with the hurdles placed in their path by envious colleagues.

Once in a while, policy-makers make noises about providing a faster track to those who put in exceptional effort, but the idea is quickly abandoned out of fear of displeasing the fence-sitting majority. Given this backdrop, those who pursue excellence in Indian universities and research institutions invoke a mixture of hostility and embarrassment. The treatment they receive becomes a demotivating example for others. The Indian scientific establishment keeps expressing the desire to promote excellence, but on the ground, it does everything to discourage it.

**TASNEEM ABBASI AND SHAHID ABBAS ABBASI***

Center for Pollution Control and Environmental Engineering, Pondicherry University, Pondicherry, 605014, India.

*To whom correspondence should be addressed. E-mail: prof.s.a.abbasi.@gmail.com

### Letters to the Editor

Letters (~300 words) discuss material published in *Science* in the past 3 months or matters of general interest. Letters are not acknowledged upon receipt. Whether published in full or in part, Letters are subject to editing for clarity and space. Letters submitted, published, or posted elsewhere, in print or online, will be disqualified. To submit a Letter, go to www.submit2science.org.

## CORRECTIONS AND CLARIFICATIONS

**Perspectives:** "Rapamycin paradox resolved" by K. J. Hughes and B. K. Kennedy (30 March, p. 1578). In the print and online HTML version of the figure, some of the chemical structures of rapamycin were mistakenly omitted. The correct figure is shown here (right). The online HTML version has now been corrected. The online PDF was corrected shortly after publication.

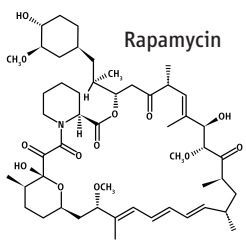


**Research Articles:** "A systematic survey of loss-of-function variants in human protein-coding genes" by D. G. MacArthur *et al*. (17 February, p. 823). In Fig. 3C, the axis labels "False Positive Rate" and "True Positive Rate" should have been swapped. The corrected figure is shown here (below). The figure has been corrected in the HTML version online.

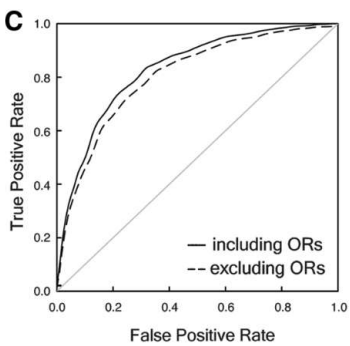


**Research Articles:** "The technology path to deep greenhouse gas emissions cuts by 2050: The pivotal role of electricity" by J. H. Williams *et al*. (6 January, p. 53). One of the affiliations of the corresponding author, Margaret S. Torn, was inadvertently omitted: Earth Sciences Division, 90R111, Lawrence Berkeley National Laboratory, Berkeley, CA 94720, USA.

**Reports:** "Effects of genetic perturbation on seasonal life history plasticity " by A. M. Wilczek *et al*. (13 February 2009, p. 930). A minor coding error was detected that affects the sunrise and sunset times used in the authors' photothermal model of *Arabidopsis* development. The computed photoperiods are correct, but the error had small effects on daytime degree-hour accumulations because temperatures are cooler near dawn than dusk. Correcting this error resulted in minor changes to estimated model parameters and modified photothermal unit values (tables S2 and S3) and insignificant changes in Figs. 2 to 4. There were no $R^2$ changes (Figs. 3 and 4B), and the conclusions of the paper are completely unaffected. The online supplement has been corrected. The authors thank Alex Cobb for detecting the error.

## TECHNICAL COMMENT ABSTRACTS

### Comment on "Detection of Emerging Sunspot Regions in the Solar Interior"

**Douglas C. Braun**

Ilonidis *et al*. (Reports, 19 August 2011, p. 993) report acoustic travel-time decreases associated with emerging sunspot regions before their appearance on the solar surface. An independent analysis using helioseismic holography does not confirm these travel-time anomalies for the four regions illustrated by Ilonidis *et al*. This negative finding is consistent with expectations based on current emerging flux models.

Full text at www.sciencemag.org/cgi/content/full/336/6079/296-c

### Response to Comment on "Detection of Emerging Sunspot Regions in the Solar Interior"

**Stathis Ilonidis, Junwei Zhao, Alexander Kosovichev**

Braun claims that his analysis using helioseismic holography does not confirm the detection of emerging sunspot regions. We examine his measurement procedure and explain why his method has different sensitivity than our method. We also discuss possible physical processes that may cause the detected phase travel-time shifts.

Full text at www.sciencemag.org/cgi/content/full/336/6079/296-d





Published by AAAS

# Comment on "Detection of Emerging Sunspot Regions in the Solar Interior"

Douglas C. Braun

Ilonidis *et al*. (Reports, 19 August 2011, p. 993) report acoustic travel-time decreases associated with emerging sunspot regions before their appearance on the solar surface. An independent analysis using helioseismic holography does not confirm these travel-time anomalies for the four regions illustrated by Ilonidis *et al*. This negative finding is consistent with expectations based on current emerging flux models.

Ilonidis *et al*. (*1*) claim the detection of acoustic travel-time decreases of 12 to 16 s, between 1 and 2 days before the maximum surface flux emergence rate, using a time-distance analysis of acoustic waves penetrating between 42 and 75 Mm below the solar surface. This result is contrary to recent numerical simulations of emerging magnetic flux tubes (*2*) that predict travel-time shifts due to flows of about 1 s and shifts on the order of $10^{-1}$ to $10^{-2}$ s due to magnetic field or temperature fluctuations. Ilonidis *et al*. (*1*) note this discrepancy and acknowledge that the physical origin of the observed travel-time shifts is unknown. The results, if confirmed, may offer hope for enabling the prediction of emerging magnetic flux 1 to 2 days in advance of its appearance at the surface, but would also challenge current understanding.

The goal of the present work is to ascertain whether the claimed travel-time anomalies are detectable with an independent analysis. This goal is distinct from an independent replication of the exact time-distance methodology of Ilonidis *et al*. (*1*). A variety of methods in local helioseismology (*3*) exist that are capable of detecting travel-time (or phase) shifts due to perturbations in subsurface conditions affecting wave propagation. Among these is helioseismic holography applied in the "lateral-vantage" or "deep-focus" scheme (*4*–*6*). To test for the presence of the signatures reported, I applied helioseismic holography (*7*) to 6-hour time segments of full-disk Doppler observations from the Michelson Doppler Imager (MDI) (*8*) on board the Solar and Heliospheric Observatory (SOHO) to compute travel-time maps of the four emerging flux regions presented by Ilonidis *et al*. (*1*).

The resulting maps (Fig. 1 and fig. S2) and statistics (fig. S3) of the travel-time shifts near the target regions do not support the existence of decreases in acoustic travel times on the order of 12 to 16 s at any of the expected depths and positions, although such signatures would be at least 5 times the background noise. Instead, the observed fluctuations in the depth-averaged travel-time maps appear to be consistent with realization noise (*9*), which for these measurements is ~2 s. The use of multiple arc configurations by Ilonidis *et al*. (*1*) implies that the signal-to-noise ratio of their maps may vary with the number of arc configurations employed. Figures S3 and S4 demonstrate that the signal in this holography analysis is not enhanced, nor is the noise reduced, by the cumulative addition of egression-ingression correlations using multiple arc configurations, particularly with the smaller arc configurations advocated by Ilonidis *et al*. (*1*).

The findings here are consistent with the expectations (*2*) that acoustic travel-time signatures of magnetic flux, at depths of ~50 Mm, are less than a second, and thus below the typical helioseismic noise for observations spanning less than a day (*6*). It is worth noting that both time-distance and holography methods are demonstrably capable

NorthWest Research Associates, 3380 Mitchell Lane, Boulder, CO 80301, USA. E-mail: dbraun@cora.nwra.com

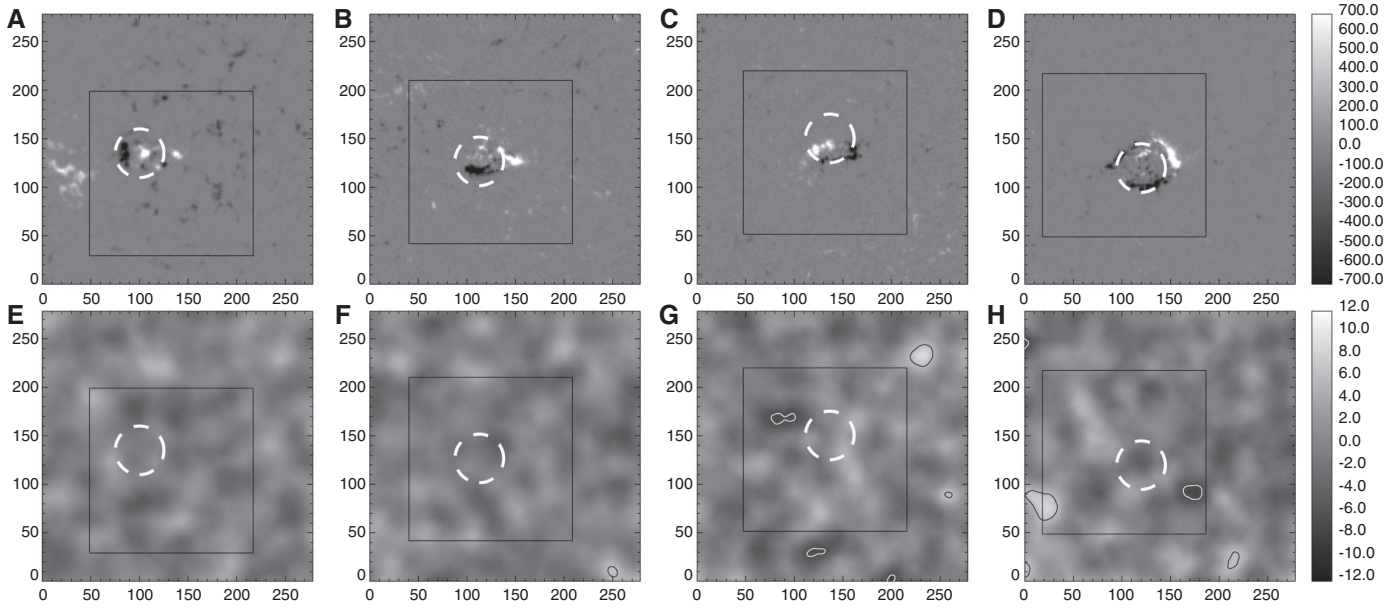


**Fig. 1.** (**A** to **D**) Line-of-sight MDI magnetograms (in units of Mx/cm$^2$) and (**E** to **H**) travel-time shift maps (in units of seconds) for the four active regions studied. From left to right, the active regions shown are AR 07978, AR 08164, AR 08171, and AR 10488, respectively. (A) to (D) show the photospheric magnetic field at post-emergence (at identical times as those shown by Ilonidis *et al*. in figures 4C, 3C, S2C, and 2C, respectively), and the boxes show the field of view as employed by them (with dimensions in Mm). The dashed white circles (50 Mm in diameter) approximately mark the size and location of the reported signatures. The black (white) contours in (E) to (H) indicate travel-time shifts of +6 (–6) s. The travel-time shift maps were made from 6-hour time series centered on the following times (from left to right): 6 July 1996 12:00 UT, 23 February 1998 00:00 UT, 27 February 1998 03:00 UT, and 26 October 2003 03:00 UT, all of which are near the times of the maximum travel-time shifts reported by Ilonidis *et al*. The computed maps extend beyond the region shown and represent averages over the four target depths (maps for the individual depths are shown in fig. S2).

(as a prominent example) of detecting ~10-s travel-time shifts caused by strong magnetic flux concentrations on the far surface of the Sun (*10*–*12*). The discrepancy between the results presented here and those of Ilonidis *et* al. (*1*) is difficult to reconcile in terms of the properties of known acoustic travel-time anomalies such as compact perturbations of sound speed. Ascertaining the potential consequences for the results of (perhaps subtle) changes in methodology may be important. For example, the holography analysis includes acoustic waves propagating through the target depths at impact angles up to ±45 degrees from the horizontal, as opposed to the selection of predominantly horizontally impacting waves by Ilonidis *et al*. (*1*). Quantitative measurements of variations of travel-time shifts with impact angle and other parameters may be critical in understanding the physical nature of the anomalies. The holography method used here is applied to fairly large regions of the Sun surrounding the targets, which allows the assessment of realization noise for each separate target region. Applying the time-distance procedure of Ilonidis *et al*. (*1*) over comparably large areas would be useful for future comparisons. Due to differences in methodology, I draw no conclusions regarding the replicability of the reported anomalies using the time-distance methods described by Ilonidis *et al*. (*1*). However, given the disparity of results and the lack of physical basis for such signatures, I consider the 12- to 16-s travel-time decreases reported by Ilonidis *et al*. to be controversial and suggest that a resolution of the issue might be achieved using blind tests with simulated and real data.

### References and Notes


1. S. Ilonidis, J. Zhao, A. Kosovichev, *Science* **333**, 993 (2011).
2. A. C. Birch, D. C. Braun, Y. Fan, *Astrophys. J.* **723**, L190 (2010).
3. L. Gizon, A. C. Birch, H. C. Spruit, *Annu. Rev. Astron. Astrophys.* **48**, 289 (2010).
4. C. Lindsey, D. C. Braun, *Astrophys. J.* **155** (suppl.), 209 (2004).
5. D. C. Braun, A. C. Birch, D. Benson, R. F. Stein, A. Nordlund, *Astrophys. J.* **669**, 1395 (2007).
6. D. C. Braun, A. C. Birch, *Astrophys. J.* **689**, L161 (2008).
7. Materials and methods are available as supplementary materials on *Science* Online.
8. P. H. Scherrer *et al*., *Sol. Phys.* **162**, 129 (1995).
9. L. Gizon, A. C. Birch, *Astrophys. J.* **614**, 472 (2004).
10. C. Lindsey, D. C. Braun, *Science* **287**, 1799 (2000).
11. D. C. Braun, C. Lindsey, *Astrophys. J.* **560**, L189 (2001).
12. J. Zhao, *Astrophys. J.* **664**, L139 (2007).



**Acknowledgments:** The author thanks A. Birch, A. Crouch, T. Duvall Jr., L. Gizon, K. D. Leka, C. Lindsey, P. Scherrer, and M. Woodard for useful comments on the manuscript. SOHO is a project of international cooperation between the European Space Agency and NASA. This work is supported by NASA Living With a Star Targeted Research and Technology contract NNH07CD25C, NASA Solar Dynamics Observatory Science Center contract NNH09CE41C, and a subcontract from the NASA-supported Helioseismic and Magnetic Imager project at Stanford University.


### Supplementary Materials

www.sciencemag.org/cgi/content/full/336/6079/296-c/DC1
Materials and Methods
Figs. S1 to S4
References (*13*, *14*)


18 October 2011; accepted 23 March 2012
10.1126/science.1215425

# Response to Comment on "Detection of Emerging Sunspot Regions in the Solar Interior"

Stathis Ilonidis,* Junwei Zhao, Alexander Kosovichev

Braun claims that his analysis using helioseismic holography does not confirm the detection of emerging sunspot regions. We examine his measurement procedure and explain why his method has different sensitivity than our method. We also discuss possible physical processes that may cause the detected phase travel-time shifts.

Ilonidis *et al.* (*1*) report that large sunspot regions can be detected before their appearance on the solar disc and as deep as 65,000 km below the solar surface. The detection method, based on time-distance helioseismology technique (*2*), employs a newly designed phase-speed filter and a measurement scheme with a high signal-to-noise (S/N) ratio. Braun claims that an independent analysis (*3*) with the helioseismic holography technique (*4*) is not able to detect the phase shifts associated with the emerging sunspot regions and considers our results controversial. In fact, Braun follows a completely different procedure that only shows that this particular method is not able to detect emerging sunspot regions. We mention below several important differences between our method and his and demonstrate with measurements that his method is not expected to provide a sufficiently high S/N ratio needed for a positive detection.

In our study, we used a specially designed non-Gaussian phase-speed filter [details of the filter can be found in (*5*)] because our tests with emerging-flux and quiet-Sun regions showed that it provides a higher S/N ratio than other Gaussian phase-speed filters at the same depth range (*5*). We also computed the exact pixel-to-pixel distances in spherical coordinates to avoid errors on the selection of annuli caused by the Cartesian approximation. Braun instead employed Cartesian coordinates in his analysis, although the radius of the largest pupil annulus is about 24.1° and the travel-time maps cover a region of about 22° by 22°. He also used four Gaussian phase-speed filters to compute travel-time maps at four target depths and then added these travel-time maps together.

Below, we followed our measurement method (*1*) but used the Cartesian approximation and four Gaussian phase-speed filters to construct travel-time maps at about the same target depths with (*3*) and then adding these travel-time maps together as in (*3*). The parameters of the phase-speed filtering are given in table S1. The final map (Fig. 1D) does not show, at the location of the emergence, signatures that can be determined as a positive detection. The reasons are (i) the Cartesian approximation mixes up the phases of the waves and smears out real signals (Fig. 1B), (ii) the Gaussian phase-speed filters do not provide as high a S/N ratio as the filter that we used (Fig. 1C), and (iii) focusing at four separate target depths, instead of combining the measurements from different depths as we did, further reduces the signal relative to the noise (Fig. 1D). This analysis confirms our initial finding that a successful detection is possible only if a procedure with a sufficiently high S/N ratio is used. Following the procedure that was used in (*3*), we also fail to detect significant signals.

Figure 2 shows that the measurement scheme used in (*3*) is significantly different from ours. We used acoustic waves with 1-skip horizontal distance of 111 to 198 Mm, whereas the corresponding range in (*3*) is 119 to 334 Mm.

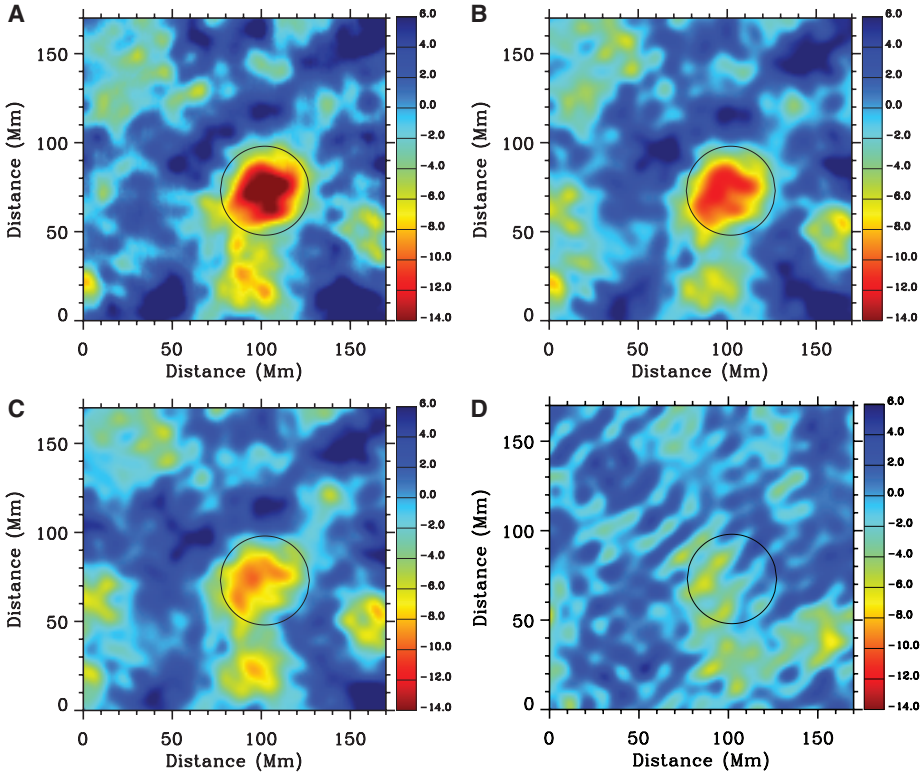


**Fig. 1.** (**A**) Mean phase travel-time perturbation map of AR 10488 obtained from an 8-hour data set centered at 03:30 UT, 26 October 2003. The cross-covariances were computed using our method (*1*), with arcs with a size of 45° and four different orientations. The phase shifts inside the circle, which are caused by the emerging sunspot region, have the maximum amplitude of 16.2 s. (**B**) Same as (A) except that the cross-covariances, following Braun's approach, were computed assuming Cartesian geometry (instead of the correct spherical geometry). The maximum amplitude of the phase shifts inside the circle is reduced to 12 s. (**C**) Same as (B) except that the cross-covariances were computed using a Gaussian phase-speed filter (instead of our specially designed filter). The signal inside the circle was further reduced to 9.7 s. (**D**) Mean phase travel-time perturbation map made with Braun's methodology: same as (C) except that the cross-covariances were computed using four Gaussian phase-speed filters at four target depths. The final phase travel-time map shown here is the average of the four individual maps. The strongest signal inside the circle is only 5.9 s, which is not sufficiently high to allow the detection of an emerging sunspot region. The strongest signal in this map, with amplitude of about 7.0 s as in Braun's comment, is more than 60 Mm away from the location of the emergence. These panels illustrate that only these three differences in Braun's analysis method can fully explain his negative result. Other factors, discussed in the text, may also be important.

W. W. Hansen Experimental Physics Laboratory, Stanford University, Stanford, CA 94305–4085, USA.

*To whom correspondence should be addressed. E-mail: ilonidis@sun.stanford.edu

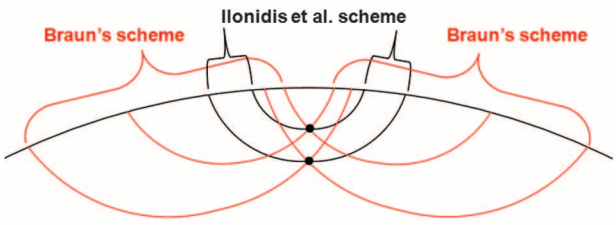


**Fig. 2.** Schematic representation of the largest ray paths for the smallest and largest focus depths used in our and Braun's measurement schemes. The largest 1-skip distance in our analysis is about 198 Mm, whereas in Braun's analysis it is about 334 Mm. The oscillation signals in Braun's scheme are selected from a much larger region of the solar disc, have much larger horizontal wavelengths and different wave vector orientations at the lower turning point, and they travel much deeper in the solar interior. These waves have also different acoustic power distribution over the frequency. All these factors can significantly affect the phase travel-time shifts.

These waves have very different physical properties. The horizontal wavelength at 3.5 mHz, for example, is 24 to 38 Mm in our case and 28 to 56 Mm in (*3*). It has been shown (*6*) that phase travel-time shifts can be caused by absorption of acoustic waves, and it is well known (*7*, *8*) that the absorption coefficient monotonically decreases with the horizontal wavelength. The use of much larger wavelengths (56 Mm instead of 38 Mm) may lead to a reduction of the measured phase shifts. The orientation of the wave vector at the focus point (which determines the angle with the magnetic field) is also different: It is horizontal in our case, and varies between 0° and 45° in (*3*) (Fig. 2). Further studies are required to determine how the measured phase shifts vary with this orientation angle. Last, acoustic waves suffer a 90° phase jump at the lower turning point (*9*), which, in our case, coincides with the focus point and is always located inside the magnetic region. Therefore, our method may be more sensitive to perturbations that cause phase shifts at this point.

The definition of the phase travel time in (*3*) is also different from ours. The phase shifts in our study are obtained by fitting the computed cross-covariances with a Gabor wavelet (*10*), and the phase travel time corresponds to the location of just one of the highest peaks of the cross-covariance function. The phase travel time in (*3*) represents the argument angle of the cross-covariance function (for a selected window) in the Fourier domain and most likely represents averaged phase shifts of all peaks in the selected window. These two definitions are not equivalent and may produce different values.

Regarding the physical origin of the perturbation, the observed phase shifts can be caused not only by sound-speed and magnetic-field perturbations or plasma flows but also by more complex effects such as absorption and scattering. There has been also evidence, both from observations and numerical simulations (*11*), that submerged magnetic regions can modify the acoustic power above them. This effect may also cause phase travel-time shifts in measurements. The estimates of acoustic travel times from a numerical model of emerging flux (*12*) mentioned in (*3*) are based on a simple assumption that the travel-time shifts are caused by sound-speed perturbations or flows. These theoretical estimates do not include other effects of acoustic waves and thus cannot justify Braun's claim that our results lack physical basis.

Overall, Braun (*3*) employs an analysis procedure that is different in many aspects from our analysis and does not provide a sufficiently high S/N ratio for the detection of emerging sunspot regions. We have demonstrated with measurements that the selection of filters, geometry, and measurement scheme can fully explain this negative result.

## References and Notes

1. S. Ilonidis, J. Zhao, A. Kosovichev, *Science* **333**, 993 (2011).
2. T. L. Duvall Jr., S. M. Jefferies, J. W. Harvey, M. A. Pomerantz, *Nature* **362**, 430 (1993).
3. D. C. Braun, *Science* **336**, 296 (2012); www.sciencemag.org/cgi/content/full/336/6079/296-c.
4. C. Lindsey, D. C. Braun, *Sol. Phys.* **192**, 261 (2000).
5. S. Ilonidis, J. Zhao, A. Kosovichev, http://arxiv.org/abs/1203.2546 (2012).
6. M. F. Woodard, *Astrophys. J.* **485**, 890 (1997).
7. D. C. Braun, T. L. Duvall Jr., B. J. LaBonte, *Astrophys. J.* **319**, L27 (1987).
8. S. Ilonidis, J. Zhao, *Sol. Phys.* **268**, 377 (2011).
9. D. O. Gough, in *Astrophysical Fluid Dynamics, Linear Adiabatic Stellar Pulsation (Les Houches 1987)*, J.-P. Zahn, J. Zinn-Justin, Eds. (Elsevier, Amsterdam, 1993), chap. 8.
10. A. G. Kosovichev, T. L. Duvall Jr., in *Proc. SCORe96 Workshop: Solar Convection and Oscillations and Their Relationship*, F. P. Pijpers, J. Christensen-Dalsgaard, C. S. Rosenthal, Eds. (Kluwer, Dordrecht, Netherlands, 1996), pp. 241–260.
11. T. Hartlep, A. G. Kosovichev, J. Zhao, N. N. Mansour, *Sol. Phys.* **268**, 321 (2011).
12. A. C. Birch, D. C. Braun, Y. Fan, *Astrophys. J.* **723**, L190 (2010).

**Acknowledgments:** This work was partly supported by NASA contracts NNX09AI90G and NAS5-02139 to Stanford University and by Living With a Star Targeted Research and Technology grant NNX07AP61.

## Supplementary Materials

www.sciencemag.org/cgi/content/full/336/6079/296-d/DC1
Table S1

21 November 2011; accepted 23 March 2012
10.1126/science.1215539

MEDICINE

# Perceived Inheritance

**Michael A. Goldman**

CREDIT: ©IKON IMAGES/CORBIS

Even within the lifetime of most Baby Boomers, it will become possible for any middle-class American to obtain a substantially complete sequence of his or her own genome. The interesting question is not when that will happen but what we will do with the data when we have them—how we will turn the personal sequences into actionable knowledge. These are the issues that Robert Klitzman grapples with in *Am I My Genes*?

Klitzman, a psychiatrist and bioethicist at Columbia University, conducted two-hour interviews of 64 individuals affected by or deemed to be at risk for one of three genetic conditions—Huntington's disease, breast cancer, or alpha-1-antitrypsin deficiency. He published a somewhat more technical account of his findings in a ten-page paper (*1*). The expanded space provided by the book allows him to present more direct quotes, to discuss matters at greater length, and to correct a few numerical errors. Nonetheless, the earlier journal article may strike health care professionals as more concise and to the point.

Many of the questions Klitzman asks were as relevant ten years ago as they are today. Even before the breast cancer–associated tumor suppressor genes (*BRCA1* and *BRCA2*) were mapped in the mid-1990s, the strong tendency of breast cancer to run in some families already presented individuals with important information about relative risk. Genetic counselors dealt with Huntington's disease, whereas most health professionals didn't understand it. And the basic ethical, legal, and social questions that Klitzman considers date back at least to the dawn of the Human Genome Project. The interviews he relates took place before the passage in 2008 of key U.S. legislation—the Genetic Information Nondiscrimination Act. Although the law is probably too narrow in scope to render the wealth of information in this book substantially out of date, genomic medicine has since outstripped education, understanding, law, and ethics in many ways.

Given that the study encompassed three different genetic conditions and 64 interviewees from an admirable array of socioeconomic and ethnic backgrounds, it's not surprising that it is hard to tease out a few salient take-home points. Klitzman makes a valiant effort to not only distill specific points but also rationalize them. For example, in discussing the decision about whether or not to share one's genetic "status" with those who hold a stake in it because they are relatives:

> The greater the genetic connection, the greater the social and moral bonds, since, as the biologist Richard Dawkins avers, genes seek to replicate themselves.
>
> Yet here the presence or absence of one specific mutation, not the overall percentage of one's genes, is important. I may share only 1/16th of my genes with my first cousin once removed (my cousin's child), but that small fraction is critical if it contains a lethal or treatable mutation. Whereas I might otherwise communicate little if at all with these extended relatives, genetics heightens the reasons to do so.… Such communication can be vital, if not morally obligatory.

Whereas patients may wrestle with issues of whom to tell about their genetic test results, physicians might have an obligation. This juxtaposes "patients' rights to confidentiality against physicians' broader social obligations." Klitzman notes that U.S. courts have held "that physicians at times have a duty to warn third parties about genetic risks" (*2*). It is sobering to imagine that position scaled up to deal with whole-genome sequencing data.

Klitzman strikes at the heart of the issue when he observes that "[o]verall, patients, physicians, and the public have relatively little knowledge about many aspects of genetics." He cites misconceptions: some individuals "believe that fathers contribute more genetic material than do mothers, and that a child is more likely to inherit a disease mutation if he or she more physically resembles the parent with the mutation." But the book doesn't do much to solve the problem of a lack of education in genetics. It provides only a short, selective introduction in an appendix that most readers will miss. Nor does Klitzman take advantage of the opportunity to clarify some of the simple mathematics of risk, which he recognizes as widely misunderstood. A good cost-benefit analysis might have been instructive.

The author comments that "genetic test results appear to function as a kind of Rorschach test that individuals interpret in a wide variety of ways based on broader psychological, cultural, and personal issues, needs, and beliefs." Patients weigh genetics and environment, and their own influence on the future, differently depending on their disposition and experience. These individuals face unusual challenges and unique perspectives on life: "A mutation can thus suggest not only the etiology, or cause of disease, but the *timing* of one's demise"—the expiration date envisioned in the film *Gattaca*. "Though intellectually humans are all aware that they will eventually die, few confront this inevitability with the certainty of those who know they have or may have a potentially lethal mutation."

In concentrating on single-gene disorders, Klitzman misses the real potential and complexity of genome-level analysis. The near future will bring tremendous challenges in understanding common, complex conditions that affect huge numbers of individuals and have a tremendous economic and social impact. The book offers neither novel ideas

**Am I My Genes?**
Confronting Fate and Family Secrets in the Age of Genetic Testing
***by Robert L. Klitzman***
Oxford University Press, New York, 2012. 375 pp. $29.95, £19.99.
ISBN 9780199837168.

The reviewer is at the Department of Biology, San Francisco State University, San Francisco, CA 94132–1722, USA. E-mail: goldman@sfsu.edu





Published by AAAS

nor a broad, didactic treatment of its sweeping subject. Nonetheless, engaged readers will find an opportunity for total immersion in some exciting questions and touching human experiences. *Am I My Genes?* should be required reading for students of genetic counseling—and for people facing the challenges of genomic health in their own lives.

**References**

1. R. L. Klitzman, *Genet. Med.* **11**, 880 (2009).
2. K. Offit, E. Groeger, S. Turner, E. A. Wadsworth, M. A. Weiser, *JAMA* **292**, 1469 (2004).

10.1126/science.1221226

ENVIRONMENT

# Inextricably Coupled

**Harald A. Mieg**

Sometimes it pays to start reading a book near the end, as that clarifies how the story's many lines fit in a cohesive plan. Such is the case with Roland Scholz's *Environmental Literacy in Science and Society*. Scholz (a sustainability scientist at the Swiss Federal Institute of Technology) aims to promote the "efficient use of scientific knowledge" that we require to cope with 21st-century environmental problems. The book's first several sections systematically explore an abundance of concepts (drawn from biology, psychology, sociology, economics, and industrial ecology) and transdisciplinary approaches and offer a comprehensive introduction to sustainability science. However, the full picture only emerges in the penultimate section, "A framework for investigating human–environment systems (HES)."

Scholz (joined by several coauthors) presents this framework as a "heuristic tool" for shaping studies of human-environment interactions and for dealing with the complexity of those interactions. The framework rests on seven postulates, assumptions that function as the basis for the authors' arguments.

The first four postulates (complementarity, hierarchy, interference, and feedback) are epistemological assumptions drawn from systems theory. With them, Scholz emphasizes a fundamental constraint of human life: that people and environments are coupled at every hierarchical level, from cellular processes to institution-building by societies. Neither the idea of coupled human-environmental systems nor that of hierarchies is new. However, in Scholz's HES model, human and environmental systems are rigorously, "inextricably" coupled. Among the book's highlights are the case studies on phosphorus cycles within coupled human-environment systems. These link material fluxes and related biogeochemical processes to decision-making at different levels, e.g., via consumer behavior (individual), farming and meat processing (organizational), media and public administration (institutional), and national and transnational policies (societal, supranational).

**Environmental Literacy in Science and Society**
From Knowledge to Decisions
***by Roland W. Scholz* et al.**
Cambridge University Press, Cambridge, 2011. 655 pp. $130, £80. ISBN 9780521192712. Paper, $75, £45. ISBN 9780521183338.

In the context of these examples, what does coupledness mean, as a fundamental constraint? When reconsidering the fundaments of ecology, Sven Jørgensen *et al.* (*1*) designated one principle—the openness of systems—as ontic, a matter of being. Ecology, a biological endeavor, attempts to define basic structures of complex life. In a slight contrast, Scholz sees the fundamental coupledness of human-environment systems as an epistemological matter (a matter of awareness and cognition), related to how we, as decision-making agents, should study human and environmental systems. Hence, Scholz speaks of postulates rather than principles or laws. His starting point is not biology but industrial ecology. Postulates five (decision) and six (awareness) introduce "agency": environments are perceived and are subject to decisions and subsequent actions. Therefore, postulate seven (environment-first) should be read not as "value the environment" (an ontological stance) but as an injunction to start our analysis by understanding environments.

The potential Achilles' heel of the HES model is its conceptualization of environment. From a systems perspective, environment comprises (roughly speaking) anything external to a system's borders. It is therefore a relative concept. For living systems, it is also underdetermined, as they perceive only parts of their environments. Scholz shows that conception of environment as "surrounding" dates from the Middle Ages. He supports the thesis that Herbert Spencer [in (*2*)] "invented" the modern idea of environment by extrapolating from individuals to life as a whole. The HES model is based on a refinement of this concept of a total environment, encompassing the "universe" minus a particular system. Its application to real problems presupposes that we know the structures of the environment as a whole. Yet, it is clear that we have only begun to understand the coupling of functional levels—for instance, in the example of the financial system, between stock markets and derivative markets and their consequences for phosphorus prices. From the perspective of being aware of what we can or cannot know, Scholz's concept of environment is somewhat overburdened and overdetermined. It has to incorporate not only conditions of varying proximity but also the mind-body complementarity and the emergence of human life and living cells "from the zygote and their (inter-)actions." In diagramming the HES model, the authors even represent environment as if it were a closed system, with its own boundaries (to where?). But if we want to provoke discussion and advance science, we have sometimes to make clear and strong assumptions—as Scholz does.

The book presents a highly structured account of the approach Scholz and his colleagues have developed since the late 1980s. Notwithstanding changes in terminology (from "systems thinking" to "transdisciplinarity"), they have consistently championed environmental literacy as a foundation of integrated and publicly focused sciences. The call for environmental literacy is also backed by ecology; Stephen Schneider formulated such literacy as a matter of "good citizenship" (*3*). Scholz goes one step further: the inextricable coupling of human and environmental systems requires that society become more scientific and science more practical. His hierarchical HES model also goes far beyond the sustainability-science approach of integrating economic, societal, and environmental concerns toward systematically linking all human decision-making to biogeochemical cycles. Thus, *Environmental Literacy in Science and Society* provides a potential basis for research and conceptual revisions in coming decades.

**References**

1. S. E. Jørgensen *et al.*, *A New Ecology: Systems Perspective* (Elsevier, Amsterdam, 2007).
2. H. Spencer, *The Principles of Psychology* (Longman, Brown, Green, and Longmans, London, 1855).
3. S. H. Schneider, *Trends Ecol. Evol.* **12**, 457 (1997).

10.1126/science.1221798

The reviewer is at the Institute for Advanced Sustainability Studies e.V., Berliner Strasse 130, D-14467 Potsdam, Germany. E-mail: harald.mieg@iass-potsdam.de

SCIENCE AND REGULATION

# FDA's Approach to Regulation of Products of Nanotechnology

A broadly inclusive initial approach may become more nuanced in light of experience, scientific information, and public input.

**Margaret A. Hamburg**

The U.S. Food and Drug Administration (FDA) has long encountered the combination of promise, risk, and uncertainty that accompanies new technologies. This is equally true for nanotechnology, which engenders both excitement and concern owing to the rapidly evolving science and range of applications. The very changes in biological, chemical, and other properties that make some applications so exciting may also present new questions about how to predict, identify, measure, and monitor possibly harmful effects.

FDA is generally responsible for overseeing the safety and effectiveness of drugs and devices for humans and animals and of biological products for humans, and the safety of foods (including food additives and dietary supplements), color additives, and cosmetics. The agency conducts these oversight functions under a variety of laws and regulations, which establish the specific premarket and/or postmarket oversight mechanisms applicable to a particular class of products (*1*). We focus below on identifying FDA products that involve nanotechnology, evaluating products that contain nanomaterials, and ensuring a responsive regulatory framework, which may be tailored to specific product areas over time.

### Identifying Nanomaterials for Regulation

FDA's regulatory science priorities are focused on issues relevant to oversight of products subject to its regulations. Identifying nanomaterials is an important first step. Materials can exhibit new physicochemical properties at nanoscale dimensions (*2*), and properties that are attributable to size can be seen or retained even when the material or end-product may not necessarily exist entirely within the nanoscale (*3*–*7*). Although one definition for "nanomaterial" may offer meaningful guidance in one context, that definition may be too narrow or broad in another. For this reason, FDA is not at this time adopting a regulatory definition of nanotechnology. Instead, it is initially taking a broadly inclusive approach to considering whether FDA-regulated products contain nanomaterials or involve nanotechnology.

FDA recently issued a draft guidance for industry on this topic (*8*) proposing that when evaluating whether an FDA-regulated product contains nanomaterials or involves nanotechnology, FDA and its stakeholders should consider the following: Does an engineered material or end-product have at least one dimension in the nanoscale range (~1 to 100 nm)?; or does it exhibit properties or phenomena, including physical or chemical properties or biological effects, that are attributable to its dimensions, even if these dimensions fall outside the nanoscale range, up to 1 μm? Structures such as agglomerates and aggregates are of interest in this context (*3*), as are coated, functionalized, or hierarchically assembled structures (*4*). This initial broadly inclusive approach may become more nuanced in light of experience, available scientific information (including the agency's own regulatory science research), and public input, which will inform any future agency issuance of regulatory documents or public communication efforts. There may also be an opportunity to pursue approaches specifically tailored to FDA's various product areas.

Until then, industry and developers should keep both of these broad size- and property-related factors in mind when considering whether their products might fall within FDA's attention for nanomaterials and are encouraged to consult with the agency early in their development process to resolve any uncertainties.

### Evaluating Products Containing Nanomaterials

Whether a product is subject to premarket review (e.g., new drugs, biological products, certain devices, and food and color additives) or not (e.g., cosmetics), industry is required to ensure that the product satisfies applicable safety standards and complies with other applicable requirements. Substantiation of safety requires scientific evidence. The FDA Nanotechnology Task Force made recommendations for a staged approach to determining whether current tests are adequate to support risk management decisions and where they are not, to collect data and update procedures (*9*). Of particular importance are the following:

- routes of exposure, including inhalation, dermal absorption, and ingestion (e.g., as related to cosmetics and foods), as well as exposure media (e.g., air, water, and food).
- properties related to absorption, distribution, metabolism, and excretion (ADME) (e.g., as related to drugs). Because biological interactions may be influenced by size changes, this may require additional analytical techniques capable of determining physical characteristics (e.g., size or aggregation) not previously assessed for tissue samples collected in ADME studies.
- size, size distribution, surface charge, surface properties, particle interactions, particle behavior, purity, stability, and general batch-to-batch variability. The new properties of materials and products that involve nanomaterials or applications of nanotechnology may require additional product-specific testing and manufacturing controls.

For FDA, regulatory science addresses these questions and involves developing new tools, standards, and approaches to assess the safety, efficacy, quality, and performance of FDA-regulated products, to help evaluate whether products are appropriate for marketing (*10*). FDA plans to continue to invest in a regulatory science program that includes such areas as nanomaterial characterization, in vitro and in vivo modeling, and product-focused research. There may be areas of application that deserve special attention, such as cosmetics, for which there is no premarket review that requires industry to provide the agency with product-specific data. For these products, better characterization of nanotechnology-based products—as well as the development and evaluation of models for predicting safety, effectiveness, and quality—will help industry fulfill their responsibility to ensure product safety before marketing and will help FDA in its postmarket surveillance. There may also be product-specific research needs in areas such as novel medical products for serious diseases. FDA is sharing information, coordinating its activities, and combining resources through interactions with other U.S. agencies, such as through the interagency National Nanotechnology Initiative (*11*). FDA is also participating in pub-

Commissioner, U.S. Food and Drug Administration, Silver Spring, MD 20993, USA. E-mail: margaret.hamburg@fda.hhs.gov







Published by AAAS

lic workshops on such topics as risk assessment and management methods (*12*), and has formed joint partnerships, including one with the National Institutes of Health and the National Institute of Standards and Technology, on establishing a transitional pathway from nanotechnology discovery research to clinical application (*13*).

### Ensuring a Responsive Regulatory Framework

Regulatory agencies around the world are considering how best to provide oversight, including the development of regulatory definitions and applicability of existing frameworks (*14*–*18*). FDA does not categorically judge all products containing nanomaterials or otherwise involving the application of nanotechnology as intrinsically benign or harmful. As with other emerging technologies, advances in both basic and applied nanotechnology science may be unpredictable, rapid, and unevenly distributed across product applications and risk management tools. Therefore, the optimal regulatory approach is iterative, adaptive, and flexible (*19*, *20*). It is iterative by developing and delivering incremental components of a regulatory system, such as guidances specific to product areas, each as warranted and when ready. It is adaptive by providing a mechanism, within statutory constraints, to change the rules, presumptions, or pathways for these regulatory components, in light of new information gained from research or from experience in regulating earlier products. And it is flexible by using all available means, ranging from workshops to consultations to guidances to rules, in order to match the burden of regulation to its need. To that end, FDA's regulatory approach will feature the following attributes:

*Maintain a product-focused, science-based regulatory policy*. Technical assessments will be product-specific, taking into account the effects of nanomaterials in the particular biological and mechanical context of each product and its intended use. Particular policies for each product area will vary according to the statutory authorities.

*Legal standards for risk vary among product classes*. Food additives are considered safe when there is a reasonable certainty of no harm from their intended use (*21*). New drugs, on the other hand, are approved on the basis not only of their risk profile but also their predicted benefit (*22*). Different legal standards can lead to different regulatory outcomes, even if products present similar levels of risk, on the basis of applicable standards for safety, efficacy, or public health impact.

*Where premarket review authority exists, attention to nanomaterials is being incorporated into standing procedures.* Premarket review requires applicants to submit data related (where applicable) to product safety, regulatory status, effectiveness, or other attributes. Individual premarket product review procedures include attention to whether the use of nanomaterials suggests the need for additional data on safety, efficacy, or other attributes, as applicable.

*Where statutory authority does not provide for premarket review, voluntary measures are encouraged*. Here, FDA has a more limited ability to evaluate product safety before its entry into commerce. Instead, FDA must rely on publicly available or voluntarily submitted information and on postmarket enforcement activities. In some of these cases, the law requires that information relied on in establishing safety be publicly available. In all cases, FDA encourages industry to provide safety information to FDA before taking their products to market. Such information can help FDA to advise companies and to carry out any necessary postmarketing safety oversight.

*Technical advice and guidance to industry.* FDA's recent draft guidance (*8*) on considerations for identifying products containing nanomaterials is intended to provide greater regulatory clarity to industry. As needed, FDA will develop additional product-specific guidance documents related to the use of nanomaterials in FDA-regulated products to assist industry to meet their regulatory and statutory obligations. These guidances may address interpretation of relevant statutory and regulatory standards and can provide guidance on the technical data needed to meet those standards.

*Continued postmarket monitoring*. FDA will continue to monitor the marketplace for products that contain nanomaterials and take actions, as needed, to protect consumers.

*Industry obligations.* Industry must work with current information in product development, and monitor products once marketed. Industry is encouraged to consult early with the agency, which may afford an opportunity to clarify the methodologies and data that will be needed to meet their obligations. Public meetings may be held to advance regulatory science, to identify product-specific data needs, and to seek input on specific issues.

Regulating an emerging technology is not a unique problem but rather a regularly encountered challenge. Flexible, iterative, product-focused, science-based approaches will be used in a spirit of collaboration to facilitate innovation and to fulfill FDA's mission to safeguard the public's health.

### References and Notes


1. For more information about FDA regulations, including between pre- and postmarket approval, review, and notification, see www.fda.gov/AboutFDA/Transparency/Basics/default.htm.
2. What's so special about the nanoscale? National Nanotechnology Initiative (NNI); www.nano.gov/nanotech-101/special.
3. G. Lövestam *et al*., *Considerations on a* Definition *of Nanomaterial for Regulatory Purposes* []oint Resource Centre, European Commission (EC), Luxembourg, 2010]; http://ec.europa.eu/dgs/jrc/downloads/jrc_reference_report_201007_nanomaterials.pdf.
4. Scientific Committee on Emerging and Newly Identified Health Risks, *Scientific Basis for the Definition of the Term "Nanomaterial"* (EC, Brussels, 2010); http://ec.europa.eu/health/scientific_committees/emerging/docs/scenihr_o_030.pdf.
5. F. Kesisoglou, S. Panmai, Y. Wu, *Adv. Drug Deliv. Rev.* **59**, 631 (2007).
6. S. M. Moghimi, A. C. Hunter, J. C. Murray, *FASEB J.* **19**, 311 (2005).
7. B. S. Zolnik, N. Sadrieh, *Adv. Drug Deliv. Rev.* **61**, 422 (2009).
8. FDA, Considering whether an FDA-regulated product involves the application of nanotechnology: Guidance for industry; www.fda.gov/RegulatoryInformation/Guidances/ucm257698.htm.
9. Nanotechnology Task Force Report 2007; www.fda.gov/ScienceResearch/SpecialTopics/Nanotechnology/NanotechnologyTaskForceReport2007/default.htm.
10. FDA, Nanotechnology Regulatory Science Research Categories, www.fda.gov/ScienceResearch/SpecialTopics/Nanotechnology/ucm196697.htm.
11. NNI, www.nano.gov/about-nni.
12. NNI, Capstone meeting: Risk management methods and ethical, legal, and societal implications of nanotechnology, Arlington, VA, 30 to 31 March 2010; www.nano.gov/events/meetings-workshops/capstone.
13. FDA Collaborations with National Cancer Institute, (NCI, NIH) and National Institute for Standards and Technology (NIST) on Nanotechnology; www.fda.gov/AboutFDA/PartnershipsCollaborations/PublicPrivatePartnershipProgram/ucm231125.htm.
14. EC, Directive on cosmetics; http://eur-lex.europa.eu/LexUriServ/LexUriServ.do?uri=OJ:L:2009:342:0059:0209:en:PDF.
15. EC, Recommendation on the definition of nanomaterial; http://ec.europa.eu/environment/chemicals/nanotech/pdf/commission_recommendation.pdf.
16. EPA's new proposed policy for nanotechnology in pesticides; www.epa.gov/pesticides/regulating/nanotechnology.html.
17. Health Canada, Policy statement on Health Canada's working definition for nanomaterial, 2011; www.hc-sc.gc.ca/sr-sr/pubs/nano/pol-eng.php.
18. National Industrial Chemicals Notification and Assessment Scheme, Australia's new chemical requirements for notification; www.nicnas.gov.au/Current_Issues/Nanotechnology.asp.
19. T. Earles, Office of Science and Technology, Emerging technologies committee lays out principles for guidance; www.whitehouse.gov/blog/2011/03/16/emerging-technologies-committee-lays-out-principles-guidance.
20. J. P. Holdren, C. R. Sustein, I. A. Siddiqui, Policy Principles for the U.S. decision-making concerning regulation and oversight of applications of nanotechnology and nanomaterials [memorandum] (Executive Offices, Washington, DC, 2011); www.whitehouse.gov/sites/default/files/omb/inforeg/for-agencies/nanotechnology-regulation-and-oversight-principles.pdf.
21. FFDCA § 409 (21 U.S.C. 348) and 21 CFR 170.3(i).
22. FFDCA § 505 (21 U.S.C. 355) and § 512 (21 U.S.C. 360b).


10.1126/science.1205441

OCEAN SCIENCE

# A Dive to Challenger Deep

A recent manned dive to the bottom of the Mariana Trench heralds new scientific discoveries.

**Richard A. Lutz and Paul G. Falkowski**

Humans have always been fascinated by the deep sea. Early sketches of submarines in the 16th century led to the construction of the first underwater vehicle in 1623. By the 18th century, submarines were used for warfare. In 1870, Jules Verne created a fictional world of sea monsters and life aboard the mystical submarine *Nautilus* that could descend 20 km into the sea. The novel captured the imagination of millions of people.

Reality caught up with fiction on 23 January 1960, when U.S. Navy Lieutenant Don Walsh and Swiss engineer and oceanographer Jacques Piccard descended in the bathyscaphe *Trieste* more than 10,800 m to the bottom of the deepest area of the world's ocean, the Challenger Deep in the Mariana Trench—and returned home safely. However, *Trieste* was extremely bulky and not designed for exploration. On 26 March 2012, a technologically advanced research submersible was finally ready to brave a return to the site, and another human made that same round trip, reigniting the excitement of exploring the deep ocean. But what James Cameron accomplished during his 7 hours in the *Deepsea Challenger* submersible (see the first figure) was far more than just one more journey to "the abyss." *Deepsea Challenger* is equipped with a hydraulic arm for taking samples and has elaborate lighting and photographic capabilities, enabling state-of-the-art research in the deepest parts of the ocean.

The imagination of the scientific community was sparked in 1977, when three occupants of the submersible deep submergence vehicle (DSV) *Alvin* discovered a chemosynthesis-based ecosystem teeming with life at deep-sea hydrothermal vents at a depth of 2500 m along the Galapagos Rift (*1*). That voyage to the deep was the first in a series of ongoing discoveries about the potential of animals to sustain life based on symbiotic associations with chemoautotrophic microbes in areas of seafloor spreading. It set the stage for decades of biological and geological research with human-occupied vehicles in arguably the most extreme environments on Earth.

Institute of Marine and Coastal Sciences, Rutgers University, New Brunswick, NJ 08901, USA. E-mail: rlutz@marine.rutgers.edu; falko@marine.rutgers.edu

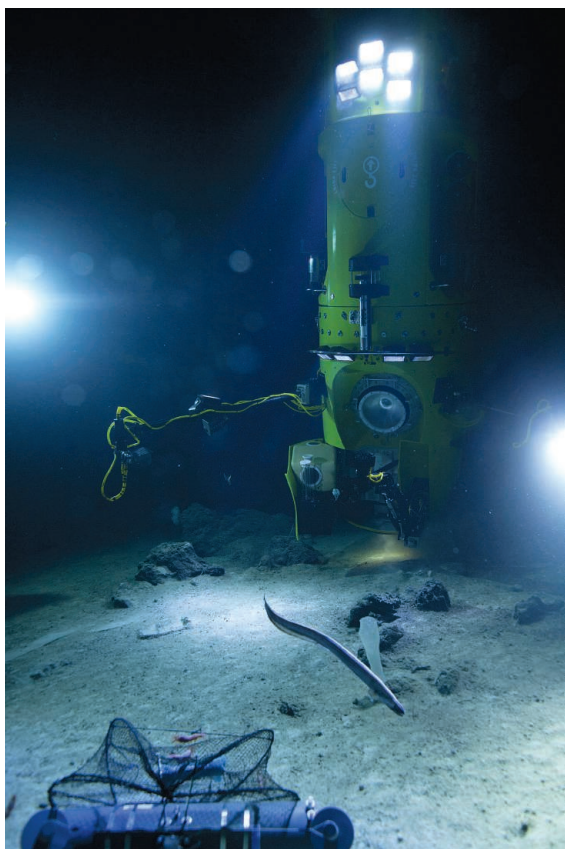

**Into the deep.** The DSV *Deepsea Challenger*, the one-man deep-diving submarine built by James Cameron, photographed on 1 April 2012 by the unmanned lander, deep ocean vehicle (DOV) *Mike*, built by Scripps Institution of Oceanography/University of California, San Diego. The pair met up at a depth of 1500 m on a checkout dive off Ulithi Atoll after Cameron's dive to the bottom of the Challenger Deep, East Pond, Mariana Trench, on 26 March 2012.

Since the discovery of these deep-sea ecosystems, researchers have spent countless hours in research submarines to experience firsthand these esoteric organisms in their remote environments. The physical reality of seeing the deep sea firsthand is totally different from viewing it on a television screen on the deck of a ship. Scientific exploration of these communities has stimulated interactions among scientists across many disciplines. Their collective and interactive research has provided clues to the origin of life, the reasons behind the phenomenal rates of mineral deposition and organism growth in vent environments (*2*, *3*) and the possibility of life on extraterrestrial bodies (*4*).

**Life under pressure.** This specimen of *Hirondellea gigas* was collected by ROV *Kaiko* at a depth of 10,920 m in the Challenger Deep.

The deepest-diving human-occupied research submersibles in today's scientific fleets can descend to depths of ~7000 m, thus covering more than 99% of the world's seafloor environments. However, 16 trenches throughout the world's oceans are deeper than 7000 m (*5*). Cameron's extraordinary feat shows that technology has advanced to the point where a vehicle can safely transport its occupant or occupants to the deepest depths of the ocean, providing access to areas that remain essentially unexplored.

In one of the few reported studies of seafloor ecosystems below 7000 m, Fujikura *et al*. used the Japanese unmanned remotely operated vehicle (ROV) *Kaiko* to explore and sample a dense, chemosynthetic-based community dominated by a previously undescribed species of a thyasirid bivalve, *Maorithyas hadalis*, at a depth of 7326 m in the Japan Trench (*6*). Yayanos *et al*. (*7*) isolated an obligate barophilic ("pressure-loving") microorganism from an amphipod collected in the Mariana Trench at a depth of 10,500 m with an insulated trap. The strain grew relatively well at 1000 atm and 2°C (the conditions at the bottom of the Mariana Trench), compared with its optimal growth at 690 atm. It failed to grow below 350 atm.

In 1996, ROV *Kaiko* performed its first sampling dive in the Mariana Trench (see the

CREDITS: (TOP) DEEPSEA CHALLENGE PROJECT; (BOTTOM) JAMSTEC





Published by AAAS

second figure). From sediments collected at a depth of 10,898 m during this dive, Kato *et al*. (*8*) isolated two strains of obligately barophilic bacteria. Growth of these isolates was optimal between 700 and 800 atm, with no growth detected below 500 atm. From sediment samples collected at the same depth in the Mariana Trench, Pathom-aree *et al*. isolated 38 strains of actinomycetes (a group of Gram-positive bacteria) (*9*).

The few bioactive compound screening studies reported to date on deep-sea actinomycetes have yielded extraordinary results. Unique compounds isolated from an actinomycete inhabiting deep-sea sediments in the South China Sea have shown potent activities against three tumor cell lines and also showed antibacterial activities (*10*). Compounds isolated from another deep-sea actinomycete exhibited cytotoxicities against five different human cancer cell lines (*11*).

Given the ongoing scientific interest in chemosynthetic communities, questions concerning the adaptations and tolerance of barophilic organisms to extreme pressures, and the potential medical and economic interest in deep-sea microbes and other organisms (*12*), the largely unexplored ocean environments at depths greater than 7000 m are fertile grounds for scientific exploration. With Cameron's recent journey to the Challenger Deep, the world now has a new technology (see the first figure) capable of transporting humans to these extreme high-pressure environments.


**References**

1. M. L. Jones, *Biol. Soc. Wash. Bull.* **6**, 1 (1985).
2. R. Lutz *et al*., *Nature* **371**, 663 (1994).
3. R. A. Lutz, R. M. Haymon, *Natl. Geogr. Mag.* **186**, 114 (1994).
4. R. A. Lutz, in *Life at Extremes: Environments, Organisms and Strategies for Survival*, E. M. Bell, Ed. (CAB International, Wallingford, UK, 2012), pp. 242–270.
5. http://en.wikipedia.org/wiki/List_of_submarine_topographical_features#List_of_oceanic_trenches
6. K. Fujikura *et al*., *Mar. Ecol. Prog. Ser.* **190**, 17 (1999).
7. A. A. Yayanos, A. S. Dietz, R. Van Boxtel, *Appl. Environ. Microbiol.* **44**, 1356 (1982).
8. C. Kato *et al*., *Appl. Environ. Microbiol.* **64**, 1510 (1998).
9. W. Pathom-aree *et al*., *Extremophiles* **10**, 181 (2006).
10. S. Li *et al*., *Mar. Drugs* **9**, 1428 (2011).
11. H. Huang *et al*., *J. Nat. Prod.* **75**, 202 (2012).
12. M. M. McNeil, J. M. Brown, *Clin. Microbiol. Rev.* **7**, 357 (1994).


Published online 12 April 2012
10.1126/science.1222641

APPLIED PHYSICS

# Solution-Processible Electrodes

Polymer-coated surfaces may provide a low-cost route for processing and fabricating organic-based electronic devices.

**Michael G. Helander**

Electronics based on thin-film organic materials offer the promise of low-cost flexible solar cells, displays, and light sources that have the potential to be manufactured on large-area plastic substrates via roll-to-roll printing techniques (*1*). These exciting applications are made possible by the relative ease of processing of organic compounds relative to traditional inorganic semiconductors such as silicon. Unfortunately, fabricating these organic-based devices is still prohibitively expensive because they require several costly vacuum-processing steps to manufacture. One of the key barriers to eliminating these steps, in order to realize a low-cost, all solution-processed device, is finding a suitable low–work function electrode material to replace the reactive metals that are typically used, such as calcium, magnesium, or aluminum. On page 327 of this issue, Zhou *et al*. (*2*) report on a general method of engineering low–work function electrode surfaces by means of polymeric surface modifiers containing simple aliphatic amine functional groups. Their method is applicable to a wide range of different electrode materials and can also be used in most state-of-the-art high-efficiency organic electronic devices, including organic solar cells, organic thin-film transistors, and organic light-emitting diodes.

Although the measurement of the work function of a material was first reported more than a century ago (*3*, *4*) as part of an observation of the photoelectric effect, new methods of engineering stable low–work function surfaces are still at the forefront of scientific discovery. The difficulty in realizing a suitably stable material is that the work function—the minimum energy required to remove an electron from the surface of a solid—scales with the electronegativity of the atoms in the bulk (*5*). As a result, low–work function materials are inherently more reactive and therefore typically require vacuum processing to prevent oxidation of the electrode contacts.

**The right solution.** The method of polymer-modified surfaces reported by Zhou *et al*. provides the potential to manufacture low-cost solution-processed organic electronics such as an all-polymer solar cell.

Zhou *et al*. circumvented this problem of surface oxidation by starting with more stable high–work function materials, such as gold, and then reducing the electrostatic potential at the surface [work function scales with electrostatic potential (*6*)] by adding a thin coating of polymer surface modifier. Although this approach has been used before, previous surface modifiers have relied on specific chemical interactions between the modification layer and the electrode surface, which only works for particular material combinations. In contrast, Zhou *et al*. used air-stable polyethylenimine (PEI) polymers, traditionally used for enzyme immobilization and carbon sequestration, that strongly physisorb to a wide range of different materials, including metals, oxides, polymers, and graphene. Because PEI is a cationic polymer, it strongly reduces the surface electrostatic potential when applied as a thin surface modification layer, thus lowering the work function.

Zhou *et al*. demonstrated the utility of their method by incorporating low–work function PEI-modified electrodes into various electronic devices, including simple organic diodes, organic solar cells, organic thin-film transistors, oxide thin-film transistors, and organic light-emitting diodes. Remarkably, the performance of the PEI-modified electrodes was comparable to that of standard low–work function metal contacts in most of these devices. Even more impressive, using PEI to lower the work function of the conductive polymer PEDOT:PSS [poly(3,4-ethylenedioxythiophene):poly(styrenesulfonate)], they fabricated an all-polymer solution-processed organic solar cell in which the substrate, anode, active layer, and cathode are

Department of Materials Science and Engineering, University of Toronto, Toronto, Ontario M5S 3E4, Canada. E-mail: michael.helander@utoronto.ca

all polymers (see the figure). Although Zhou *et al*. have made an appreciable step toward eliminating the costly vacuum deposition of low–work function metal electrodes, there is still much work to be done before low-cost roll-to-roll printing of organic electronics is fully realized.

The long-term stability and device lifetime of low–work function PEI-modified electrodes needs to be examined in various organic electronic devices. The preliminary lifetime testing data reported by Zhou *et al*. for an organic solar cell are promising, but longer-term testing on packaged devices operating under real conditions needs to be performed to ensure that the electrodes are stable for the lifetime of any commercial product in which they may be used. From a practical point of view, it is still not clear whether scale-up of solution-processing techniques for organic electronics to mass production is truly viable. For example, state-of-the-art flat-panel displays are manufactured on large-area substrates (2.2 m × 2.5 m); to date, only vacuum-processing techniques can handle such substrates with adequate uniformity, yield, and throughput time. Nonetheless, with the strong and growing momentum behind organic electronics, the present barriers to low-cost flexible devices are poised to be overcome in the near future.


**References**

1. S. R. Forrest, *Nature* **428**, 911 (2004).
2. Y. Zhou *et al*., *Science* **336**, 327 (2012).
3. H. Hertz, *Ann. Phys.* **267**, 983 (1887).
4. W. Hallwachs, *Ann. Phys.* **269**, 301 (1888).
5. W. Gordy, W. J. O. Thomas, *J. Chem. Phys.* **24**, 439 (1956).
6. C. Herring, M. H. Nichols, *Rev. Mod. Phys.* **21**, 185 (1949).


10.1126/science.1220829

PSYCHOLOGY

# Tapping into the Wisdom of the Crowd—with Confidence

The subjective confidence of individuals in groups can be a valid predictor of accuracy in decision-making tasks.

**Ralph Hertwig**

If research in psychology had a Dr. Jekyll and Mr. Hyde Award, it would go to—drum roll, please—the group as a decision-making instrument. Since the late 19th century, the group (also known as jury, team, crowd, and swarm) has been deplored as a source of intellectual inferiority (*1*) and disastrous policy decisions (*2*) and hailed as a source of near-magical creativity (*3*) and unparalleled wisdom and forecast accuracy (*4*, *5*). Some of these attributions have proved to be unfounded. For instance, with respect to creative potential, groups that engage in brainstorming lag hopelessly behind the same number of individuals working alone (*6*). The key to benefiting from other minds is to know when to rely on the group and when to walk alone. On page 360 of this issue, Koriat (*7*) explores the value of individual confidence in group decision-making.

After a medical test, the physician tells you that the results suggest a worrying abnormality. Despite the doctor's high confidence in her conclusion, you seek a second opinion. The second physician believes that the cause is probably benign. But his level of confidence is lower than the first physician's. Whose opinion should you believe?

Koriat's analysis speaks to such dilemmas. Presenting his participants with inference tasks involving two alternatives (such as which of two countries has a larger area), he shows that members of dyads—and, by extension, larger groups—can tap into the wisdom of two heads even in the absence of social interaction by using a simple heuristic: Select the response expressed with the higher—or in the case of more than two heads, highest—degree of confidence.

This maximum-confidence slating (MCS) heuristic enables humans to benefit from the presence of two or more opinions in choice tasks. Another simple and highly adaptive combination tool in choice tasks is the majority rule, but it requires at least three opinions (*8*). In estimation tasks, no combination strategy rivals the intelligent simplicity of averaging, which exploits the benefit of error cancellation (*9*).

Why and when does the MCS heuristic work? By using the subjective confidence of each judge in the accuracy of their response, the heuristic flexibly adopts the opinion of one or the other judge. It does not bet that the same person will always be the best judge (while not precluding this possibility), but rather adaptively aligns itself with the judge who produces the most confident response in a given trial. In his first two experiments, Koriat shows that using this heuristic enables a level of inferential accuracy that is substantially higher than that achieved by the dyad's higher-performing member. Furthermore, a person who responds to the same task twice, separated by an interval and thus enabling variability (for example by forgetting), can boost accuracy by select-

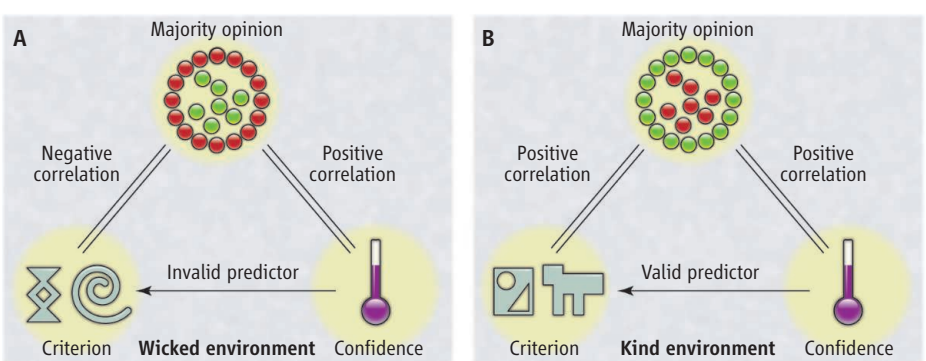


**The role of confidence.** In "wicked" environments (**A**), in which confidence correlates positively with the majority opinion (red dots) and the majority opinion correlates negatively with the criterion (correct response), confidence is an invalid predictor of the criterion. In contrast, Koriat shows that relying on the more confident response of a virtual dyad fosters accuracy in "kind" environments (**B**), in which confidence correlates positively with the majority opinion (green dots), and the latter correlates positively with the criterion.

CREDIT: P. HUEY/*SCIENCE*

Department of Psychology, University of Basel, Missionsstrasse 60-64, CH-4055 Basel, Switzerland, and Max Planck Institute for Human Development, Lentzealle 94, 14195 Berlin, Germany. E-mail: ralph.hertwig@unibas.ch

ing the response in which he has higher confidence, thus exploiting the wisdom of the crowd in a single mind (*10*).

The fact that a judge's confidence can be a valid predictor of accuracy is remarkable in light of the bad reputation that subjective confidence has acquired in many areas of psychology and behavioral economics. Numerous studies (*11*) have found that people's confidence in the accuracy of their judgments or predictions is systematically greater than the judgments' actual accuracy.

However, according to proponents of an ecological approach to understanding the human mind (*12*), overconfidence does not reflect faulty cognitive software. Rather, it results from experimenters' frequent practice of sampling questions in such a way that otherwise sound knowledge results in wrong inferences. For instance, one does not need to know much about the populations of French cities to infer correctly that Paris has more residents than Toulouse: Paris is the capital of France, and in many countries the capital is the largest metropolis. Yet the "capital" cue can suggest a wrong inference. For instance, residents of Zurich outnumber those of Bern, but the latter is the Swiss capital. Many disagreements in psychology about the reality and significance of overconfidence can be traced to how experimenters select their stimuli (such as knowledge questions) (*13*).

Koriat elegantly integrates this ecological approach to confidence with research on the wisdom of the crowd. His third and fourth experiments show that when tasks are sampled such that misleading ones are overrepresented, the accuracy of the MCS heuristic falls below that of each individual. In such "wicked" environments (see the figure, panel A), betting on the more confident response ceases to be adaptive. In contrast, in "kind" environments (*14*) (panel B), the MCS heuristic tops the better individual.

So what should one make of conflicting medical opinions? That depends on whether the medical world represents a predominantly wicked or kind environment and whether you can tell one from the other, which raises two questions for future research. First, is it possible to sort environments according to whether or not shared knowledge and majority opinions are more often right than wrong? One variable that may enable such classification is the degree to which an environment involves competitive or cooperative interactions (*15*). Second, are there probabilistic cues that can help to distinguish between kind and wicked environments (or help to infer whether the experimenter selected questions to trick us)? If so, an adaptive decision-maker can strategically choose between Koriat's MCS heuristic and its opposite: Select the response expressed with the lower degree of confidence.

In the absence of such cues, and given that human communication norms (*16*) presumably give rise to common knowledge that is more likely true than not, Koriat has sound advice: Take the more confident response.

**References**


1. G. LeBon, *The Crowd* (Transaction Publishers, New Brunswick, NJ, 1895/1995).
2. I. L. Janis, *Groupthink: Psychological Studies of Policy Decisions and Fiascoes* (Houghton Mifflin, Boston, MA, ed. 2, 1972).
3. A. F. Osborn, *Applied Imagination* (Scribner, New York, 1957).
4. F. Galton, *Nature* **75**, 450 (1907).
5. J. Surowiecki, *The Wisdom of Crowds* (Doubleday, New York, 2004).
6. N. L. Kerr, R. S. Tindale, *Annu. Rev. Psychol.* **55**, 623 (2004).
7. A. Koriat, *Science* **336**, 360 (2012).
8. R. Hastie, T. Kameda, *Psychol. Rev.* **112**, 494 (2005).
9. J. B. Soll, R. P. Larrick, *J. Exp. Psychol. Learn. Mem. Cogn.* **35**, 780 (2009).
10. S. M. Herzog, R. Hertwig, *Psychol. Sci.* **20**, 231 (2009).
11. D. Griffin, L. Brenner, in *Blackwell Handbook of Judgment and Decision Making*, D. J. Koehler, N. Harvey, Eds. (Blackwell, Oxford, 2004), pp. 177–199.
12. P. M. Todd, G. Gigerenzer, the ABC Research Group, *Ecological Rationality: Intelligence in the World* (Oxford Univ. Press, New York, 2012).
13. M. K. Dhami *et al*., *Psychol. Bull.* **130**, 959 (2004).
14. R. M. Hogarth, *Educating Intuition* (Univ. Chicago Press, Chicago, 2001).
15. R. Hertwig, U. Hoffrage, the ABC Research Group, *Simple Heuristics in a Social World* (Oxford Univ. Press, New York, 2012).
16. P. Grice, *Studies in the Way of Words* (Harvard Univ. Press, Cambridge, MA, 1989).


10.1126/science.1221403

CANCER

# Heterogeneity and Tumor History

What can genomic heterogeneity within a single tumor reveal about the tumor's evolution and its diagnosis?

**Darryl Shibata**

All cells are almost perfect copies of prior cells. Imperfect DNA replication creates random variation, which is the substrate for evolution. Such differences may be small [normally about one new mutation per human cell division (*1*)], but the accumulation of mutations over time can eventually transform a single cell. Progeny of this first transformed cell expand by bifurcating branching cell division (see the figure) to form visible billion-cell clonal tumor populations. Each one of these cancer cells is an almost perfect copy of the first transformed cell. Given this scenario, different genetic alterations in different parts of the same cancer should be found in most tumors. Such intratumor heterogeneity has been found in many cancers, but its true extent is becoming much more evident with the unprecedented ability to sequence genome-wide many times (deep sequencing).

Intratumor heterogeneity has been found whenever deep sequencing has been appropriately applied to different parts of the same cancer for the colon, pancreas, breast, and blood (*2*–*5*). The recent study by Gerlinger *et al*. (*6*) highlights this phenomenon, as over half the mutations in multiple different parts of the same advanced renal cell carcinoma (primary tumor and its metastases) were different. Topographical differences in chromosome copy-number variations and gene expression signatures were also readily found, indicating that with high-resolution methods, intratumor heterogeneity is present wherever one looks.

One conclusion drawn from this baffling intratumor heterogeneity is that applying molecular signatures of prognosis or therapy to individual patients will be extremely difficult because the "answer" will vary depending on what part of the tumor is sampled (*7*). Analyzing more biopsies and sequencing even deeper are likely to reveal even more abnormalities and heterogeneity. Because all genomes are almost perfect copies of prior genomes, potentially the history of a tumor is encoded by its heterogeneity. With a simple molecular clock hypothesis (the number of differences between two genomes increases with the number of divisions since a common ancestor), the heterogeneity within and between different parts of the same tumor can indicate how long ago transformation occurred and how cancer cells spread and migrate during progression. Heterogeneity

University of Southern California Keck School of Medicine, 1441 Eastlake Avenue, NOR2424, Los Angeles, CA 90033, USA. E-mail: dshibata@usc.edu

can be a list of mutations and a language of change.

One way to illustrate tumorigenesis is with ancestral trees, whose shapes can be inferred by comparing mutations in different parts of the same cancer (see the figure). Driver mutations (those that are causally implicated in oncogenesis) are therapeutic targets, but most of the historical information is encoded by the much more numerous passenger mutations (those that do not alter the fitness of a cell). Mutations can also be classified as founders or "public" (present in all cancer cells), "semiprivate" (present in a detectable fraction of cancer cells), or "private" (present in a single or few cancer cells). Public mutations accumulate between the zygote and the first transformed cell, whereas private mutations arise after transformation. The spread of a private mutation depends both on its selective value and when it was acquired after transformation. Current tumor sampling cannot easily determine whether private mutations are present in every cell (a single subclone) or in different cells (multiple subclones) within a small biopsy. Interestingly, at even finer physical resolution, genomic heterogeneity is still present within single cancer glands or between adjacent cancer cells (*8*, *9*), suggesting that many private mutations lack sufficient driver value to confer much local dominance. In the absence of selection, heterogeneity becomes a function of time, error rates, and random drift.

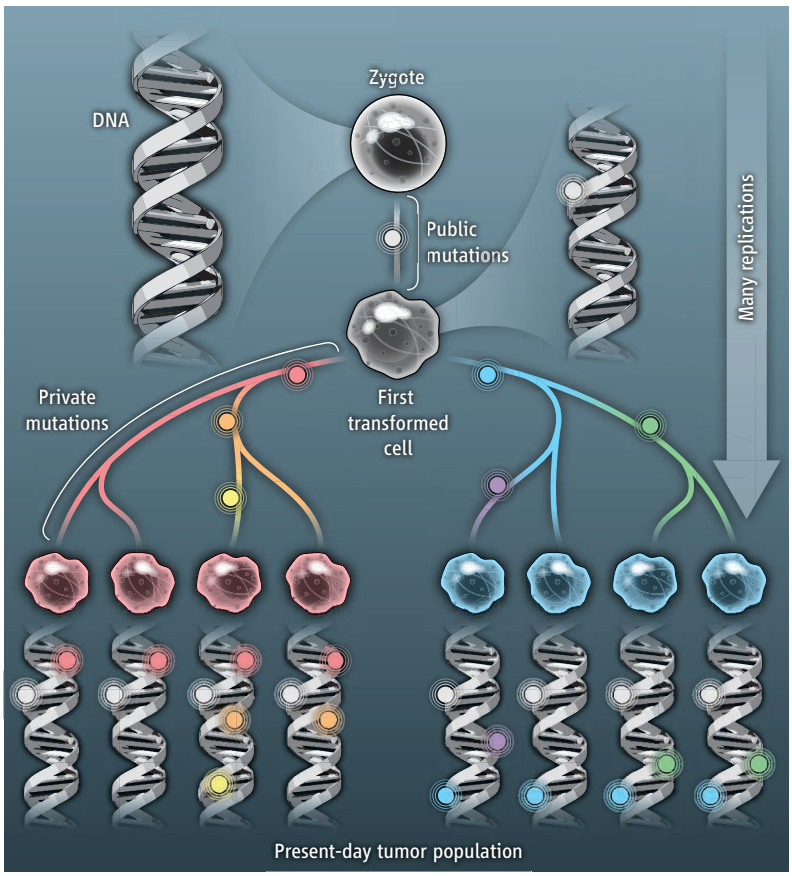


**Mutation history.** Tumorigenesis can be represented by an ancestral tree that starts from the zygote and ends with present-day cancer cells. Mutations (circles) accumulate with cell division and can be classified as public or private. Tumor heterogeneity is an inherent outcome of branching cell division, with the amount of genomic heterogeneity dependent on the time after transformation and how cancer cells divide and migrate. It should be possible to infer the past by characterizing mutations in different parts of the same tumor. The past, as recorded in the multiple heterogeneous genomes within a tumor, may help predict its future.

Driver mutations that confer selective advantages reduce heterogeneity through clonal evolution. A newly emerged tumor cell population has relatively few private mutations, but more will accumulate. Therefore, private mutation frequencies can encode the relative age of a human tumor—the greater the heterogeneity, the greater the time since transformation. The amount of tumor heterogeneity has clinical implications for chemotherapy. Targeted therapies should be directed at public driver mutations present in all cancer cells, but the probability of drug-resistant variants increases with cell division (*10*). Therefore, a more heterogeneous tumor with many private mutations is more likely to fail chemotherapy. The renal carcinoma data (*6*) illustrate this point. Tumor size and tumor heterogeneity were maintained despite therapy with everolimus, an mTOR inhibitor. More effective chemotherapy would be expected to cause more severe genetic bottlenecks by killing the majority of cells and their private mutations, thereby reducing the genetic diversity of the surviving cancer cells. By contrast, less initial heterogeneity and a greater bottleneck effect were apparent after leukemia chemotherapy (*5*), a treatment that often results in cures.

Heterogeneity cannot be fully sampled because of the logistical difficulties of obtaining a complete tumor "physical," but translating heterogeneity into inferred tumor "histories" provides an alternative roadmap for personalized cancer diagnosis and treatment. Initial studies of tumor heterogeneity have begun to reconstruct exactly how individual human cancers evolve, branch, and spread (*2*–*6*). For example, the topographical heterogeneity in present-day pancreatic cancer cells is consistent with initiation on average about 20 years ago and metastasis about 3 years ago (*3*). Instead of generating increasingly long lists of mutations, genomic alterations could be distilled into better patient-specific tumor histories with relatively simple outputs—how long ago transformation occurred, and how and when their tumors spread. Reading this fundamental information may provide actionable clues for treatment and prevention because like many human diseases, tumors with the same histories may have relatively predictable futures. Moreover, serial biopsies can help monitor treatment by measuring reductions in heterogeneity expected with more effective therapies. How to best reconstruct the histories written in tumor genomes is uncertain, with many challenges in developing optimal sampling schemes and algorithms. However, taking the additional time and effort to obtain a good tumor history may help make more sense of the multiple physical alterations in a cancer, and bring more effective personalized medicine to its unfortunate host.

**References**

1. T. L. Wang *et al.*, *Proc. Natl. Acad. Sci. U.S.A.* **99**, 3076 (2002).
2. S. Jones *et al.*, *Proc. Natl. Acad. Sci. U.S.A.* **105**, 4283 (2008).
3. S. Yachida *et al.*, *Nature* **467**, 1114 (2010).
4. L. Ding *et al.*, *Nature* **464**, 999 (2010).
5. L. Ding *et al.*, *Nature* **481**, 506 (2012).
6. M. Gerlinger *et al.*, *N. Engl. J. Med.* **366**, 883 (2012).
7. D. L. Longo, *N. Engl. J. Med.* **366**, 956 (2012).
8. K. D. Siegmund, P. Marjoram, S. Tavaré, D. Shibata, *PLoS ONE* **6**, e21657 (2011).
9. N. Navin *et al.*, *Genome Res.* **20**, 68 (2010).
10. J. H. Goldie, A. J. Coldman, *Cancer Treat. Rep.* **63**, 1727 (1979).

10.1126/science.1222361

DEVELOPMENT

# Making Waves for Segments

Vertebrates and arthropods share a common molecular mechanism for controlling body segmentation during development.

**Siegfried Roth and Kristen A. Panfilio**

Without a frame of reference, it is difficult to know what is moving. The first step is to make the moving object visible. On page 338 of this issue, Sarrazin *et al*. (*1*) have done just that to address a long-standing question about the evolution of segmentation in bilaterian animals.

Three prominent branches of the tree of life have a segmented body plan along the head-to-tail axis (*2*). Whether it is the repeated muscle blocks in vertebrate abdomens, the visible "rings" for which annelid worms are named, or the many leg-bearing segments of centipedes (arthropods), animals in these groups share a modular body structure. However, each group has closely related unsegmented relatives. What the common ancestor of all bilaterally symmetric animals (Urbilateria) looked like—and whether segmentation emerged independently in each lineage—has been an ongoing debate. One way to address this question is through a molecular understanding of how the body segments are formed during embryonic development. The extent to which they use the same developmental program informs the likelihood that this represents a shared ancestral feature.

The most complete causal analysis of segmentation has been achieved for the fruit fly *Drosophila melanogaster*, where all segments are formed simultaneously during early embryogenesis (*3*). This occurs through a hierarchical network of genes that specify progressively more refined domains. Surprisingly, this process does not use oscillatory mechanisms. At the level of the first periodically expressed genes (the pair-rule genes, with double segmental periodicity), each "stripe" of expression is specified independently by direct input from nonperiodically expressed regulators. Thus, periodicity in the expression of a gene across the embryo is the secondary result of a nonperiodic process.

By contrast, segmentation in vertebrates occurs sequentially within a posterior growth zone. Molecular oscillators generate waves of gene expression that determine segmental periodicity. Despite unresolved questions, a three-tier model has emerged of the vertebrate segmentation clock (*4*): growth zone cells harbor cell-autonomous oscillators based on negative transcriptional feedback circuits; these oscillators are synchronized by short-range cell-to-cell communication; and the synchronized oscillations are globally controlled by long-range signaling gradients emerging from boundaries of the growth zone. The interplay of these processes generates kinematic waves of gene expression that sweep through the growth zone, with a defined speed and time of termination that specify the size and number of single segmental units.

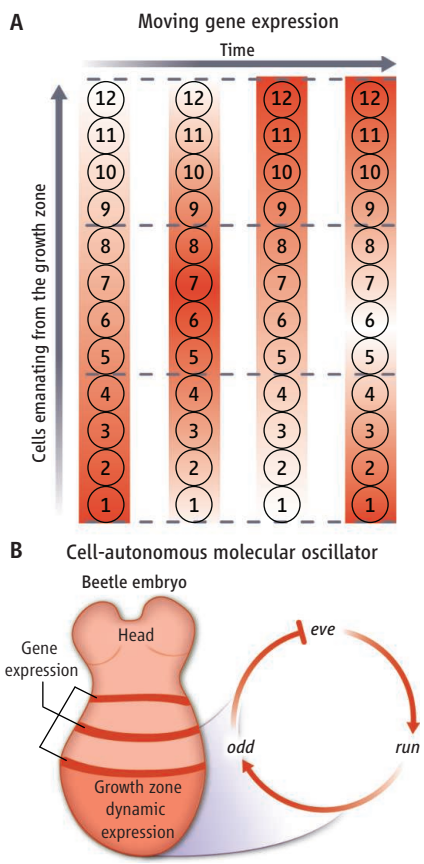


**Gene expression on the move.** (**A**) In vertebrates and some arthropods, high levels of gene expression (dark orange) pass through embryonic tissue in sequential waves, such that expression fluctuates in a given cell (numbered circles; the color gradient indicates high to low expression). (**B**) A *Tribolium* beetle embryo is illustrated showing three primary stripes of expression of the transcription factor *odd-skipped* (*odd*). The posterior growth zone might harbor a cell-autonomous oscillator, comprising three transcription factors: *even-skipped* (*eve*), *runt* (*run*), and *odd*.

Because the *Drosophila* and vertebrate modes of segmentation are radically different, it is impossible to make inferences about common ancestry. However, unlike *Drosophila*, most arthropods do not form their segments simultaneously (*3*). Rather, like vertebrates, posterior segments are added sequentially from a growth zone. This so-called short-germ mode of segmentation in insects differs from the long-germ mode seen in *Drosophila*. Indeed, there is molecular and functional evidence for a segmentation clock in spiders, centipedes, and some short-germ insects (*3*, *5*). What has been missing is the direct demonstration of waves of gene expression passing through the growth zone, which would indicate kinematic waves produced by cellular oscillators. This has now been achieved in a nonvertebrate, the red flour beetle, *Tribolium castaneum*.

Sarrazin *et al*. produced transgenic *Tribolium* beetles in which all cells of the developing embryo are labeled fluorescently; they also developed methods for culturing the embryo outside of the egg. This allowed the authors to generate time-lapse video data to determine patterns of cell movement. At the same time, careful culturing of bisected embryos allowed comparison of gene expression at different time points in a single embryo, eliminating inter-embryo variability. Thus, Sarrazin *et al*. determined the periodicity of waves of gene expression (95 min) and demonstrated that on this time scale, cell movements cannot account for the changing gene expression patterns. Rather, it is gene expression that moves relative to the cells (see the figure). As expected for a kinematic wave, the authors observed that a given cell will undergo cycles of high and low gene expression over time in what constitutes genuine molecular oscillations, which generate a double segmental pattern. Thus, as in *Drosophila*, initial periodicity comprises a two-segmental unit, but as in vertebrates, this is achieved through an oscillatory mchanism. The feedback loop among three transcription factors (encoded by pair-rule gene orthologs) provides a candidate for the cell-autonomous oscillator (*6*).

*Tribolium* has become the best system after *Drosophila* for functional studies in insects. Its genome is sequenced, and classical and transposon-mediated mutagenesis, transgenesis, and RNA interference are

Institute for Devlopmental Biology, University of Cologne, Biocenter, Zülpicher Str. 47b, 50674 Cologne, Germany. E-mail: siegfried.roth@uni-koeln.de; kristen.panfilio@alum.swarthmore.edu







Published by AAAS

established techniques for functional investigation (*7*). Moreover, Sarrazin *et al*. demonstrate that *Tribolium* is amenable to embryo culture and live imaging. Beetles belong to the large group of holometabolous insects (those undergoing metamorphosis) that also includes *Drosophila*. The majority of insect orders within this group, even some families of beetles, are long-germ insects (*8*). A deeper understanding of the *Tribolium* mode of segmentation will provide the basis for understanding the transition between short-germ and long-germ modes of segmentation—a fascinating problem for the evolution of complex regulatory gene networks. Morphologically, the growth zone of *Tribolium* is similar to that of representatives from more basally branching insect lineages and noninsect arthropods. Work on *Tribolium* should help to answer the question of whether there is a common clock mechanism within arthropods, providing the basis for broader comparisons with other phyla. The brief live imaging analysis of Sarrazin *et al*. suggests that the next step—exit from the oscillating growth zone region as newly formed segments mature—is another key aspect for which the integration of cell tracking and gene expression analyses will pay dividends in *Tribolium*.


**References**

1. A. F. Sarrazin *et al*., *Science* **336**, 338 (2012); 10.1126/science.1218256.
2. D. Tautz, *Dev. Cell* **7**, 301 (2004).
3. A. D. Peel *et al*., *Nat. Rev. Genet.* **6**, 905 (2005).
4. A. C. Oates *et al*., *Development* **139**, 625 (2012).
5. J. I. Pueyo, R. Lanfear, J. P. Couso, *Proc. Natl. Acad. Sci. U.S.A.* **105**, 16614 (2008).
6. C. P. Choe, S. C. Miller, S. J. Brown, *Proc. Natl. Acad. Sci. U.S.A.* **103**, 6560 (2006).
7. S. J. Brown *et al*., *Cold Spring Harb. Protoc.* **2009**, pdb.mo126 (2009).
8. S. Roth, in *Gastrulation*, C. D. Stern, Ed. (Cold Spring Harbor Laboratory Press, New York, 2004), pp. 105–122.


10.1126/science.1222242

EVOLUTION

# Toward an Alternative Biology

The fundamental processes of genetics have been captured with synthetic molecules.

**Gerald F. Joyce**

Genetics provides a mechanism for molecular memory and thus the basis for Darwinian evolution. It involves the storage and propagation of molecular information and the refinement of that information through experience and differential survival. Heretofore, the only molecules known to be capable of undergoing Darwinian evolution were RNA and DNA, the genetic molecules of biology. But on page 341 of this issue, Pinheiro *et al*. (*1*) expand the palette considerably. They report six alternative genetic polymers that can be used to store and propagate information; one of these was made to undergo Darwinian evolution in response to imposed selection constraints. The work heralds the era of synthetic genetics, with implications for exobiology, biotechnology, and understanding of life itself.

Departments of Chemistry and Molecular Biology, The Scripps Research Institute, 10550 North Torrey Pines Road, La Jolla, CA 92037, USA. E-mail: gjoyce@scripps.edu

These first steps outside of biological genetics are modest ones, involving XNA molecules, where NA stands for nucleic acid and X refers to the sugar moiety or its substitute. The compounds are analogs of biological nucleic acids (see the figure, panel A). However, the sugar or sugar-like component is not the ribose found in RNA or the deoxyribose found in DNA. It has been replaced by a different five-carbon sugar (arabinose in ANA, 2′-fluoroarabinose in FANA), a four-carbon sugar (threose in TNA), a "locked" ribose analog in LNA, or a six-member ring structure (cyclohexene in CeNA, anhydrohexitol in HNA) (see the figure, panel B).

The study of XNAs has been inspired by the question of what was the first genetic polymer of life on Earth. Perhaps this was RNA, but it may have been a simpler structure that was more readily accessible through prebiotic synthesis (*2*). TNA and glycol nucleic acid (GNA) are prime candidates (*3*, *4*). Another inspiration for the study of XNAs is their application as antisense agents that bind to and thereby inhibit the function of biological RNAs. All six XNAs studied by Pinheiro *et al*. bind to complementary RNA and DNA and are resistant to degradation by biological nucleases. Finally, construction of genetic systems based on alternative chemical platforms may ultimately lead to the synthesis of novel forms of life. For that goal to be realized, the XNA must be able to catalyze its own replication, without the aid of any

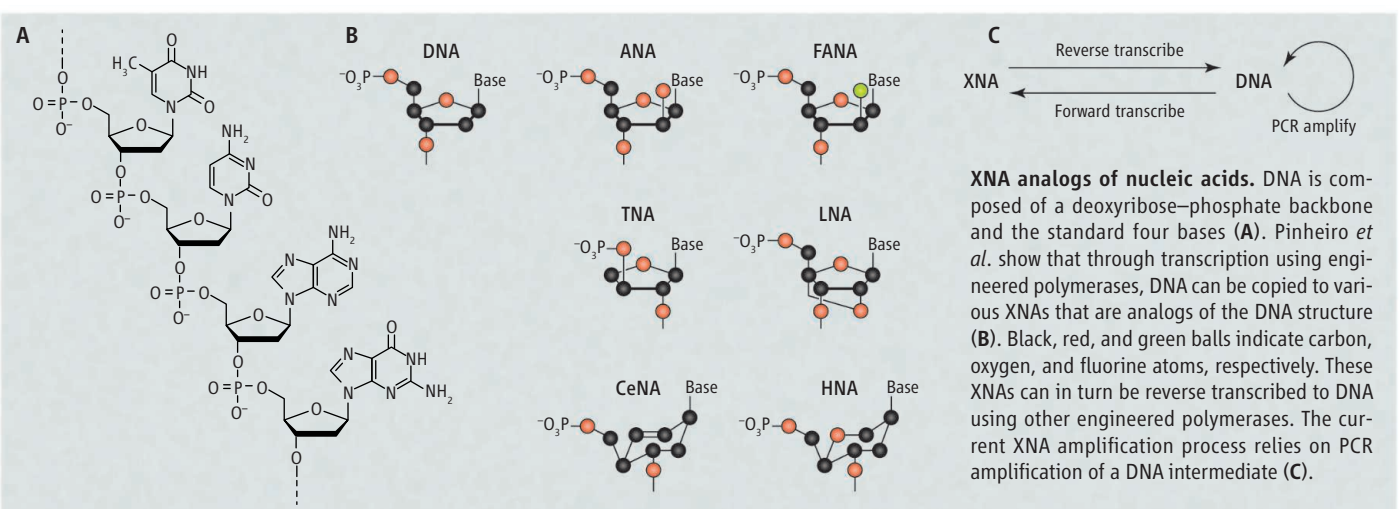


**XNA analogs of nucleic acids.** DNA is composed of a deoxyribose–phosphate backbone and the standard four bases (**A**). Pinheiro *et al*. show that through transcription using engineered polymerases, DNA can be copied to various XNAs that are analogs of the DNA structure (**B**). Black, red, and green balls indicate carbon, oxygen, and fluorine atoms, respectively. These XNAs can in turn be reverse transcribed to DNA using other engineered polymerases. The current XNA amplification process relies on PCR amplification of a DNA intermediate (**C**).





Published by AAAS

biological molecules, and thus be capable of undergoing Darwinian evolution in a self-sustained manner.

Pinheiro *et al*. have made great progress in showing that various XNAs can function as synthetic genetic polymers, but they have not yet realized a synthetic genetic system. In their system, the XNAs are replicated by reverse-transcribing them to DNA, amplifying the DNA using PCR, and then forward-transcribing the DNA back to XNA (see the figure, panel C). Each step uses a polymerase; amplification takes place with DNA. Another recent paper showed the storage and propagation of genetic information in TNA, but there, too, amplification occurred with DNA (*5*).

The key innovation of Pinheiro *et al*. is their use of sophisticated protein engineering techniques to develop variant polymerases that are adept at copying information between XNAs and DNA. They show that XNA polymers containing more than 70 subunits and having almost any sequence can be copied to and from DNA, with an average fidelity per subunit ranging from 95% (for LNA) to 99.6% (for CeNA). These attributes are sufficient to carry out the directed evolution of functional XNA molecules. The authors demonstrate this process for HNA polymers, which they evolved in the laboratory to obtain functional molecules (aptamers) that bind tightly and specifically to a particular RNA or protein target.

Pinheiro *et al*. give some hint of what will come next. They have begun to apply the same protein engineering techniques to develop polymerases that can copy an XNA to its own complement or copy information between two different XNAs. So far, both FANA and CeNA have been copied to their own complement and CeNA has been copied to HNA, but these processes are much less efficient than copying information between XNA and DNA.

Future studies are likely to yield improvements of the various XNA-to-XNA copying reactions. It also seems only a matter of time before there will be the first reported "XNAzyme"—a catalyst composed of XNA rather than protein or standard nucleic acid. A key aim will be the development of XNAzymes that catalyze the templated joining of XNA oligomers and ultimately the polymerization of XNA monomers. Synthetic biology studies of XNA may never catch up to those involving RNA because the former require more challenging preparative and analytical procedures and do not benefit from the technical infrastructure that supports RNA research. However, the comparative biochemistry of various XNA systems is itself a worthy pursuit, enabling one to investigate principles of macromolecular structure, molecular recognition, and catalysis across a series of related chemical polymers.

Another important reason to pursue the development of functional XNAs is to obtain compounds with potential applications in materials science, molecular diagnostics, and therapeutics. Nucleic acid aptamers have been widely adapted for these purposes, but because RNA and DNA are susceptible to biological nucleases, they must be modified to withstand exposure to the natural world. XNAs are unnatural and would pass through the biosphere unscathed. The benefits of their unusual chemical properties must be weighed against their greater cost, both literally and with regard to operating in the uncharted waters of XNA biochemistry.

As one contemplates all the alternative life forms that might be possible with XNAs and other more exotic genetic molecules, the words of Arthur C. Clarke come to mind. In *2010: Odyssey Two*, HAL the computer tells humanity: "All these worlds are yours" but cautions: "Except Europa. Attempt no landings there" (*6*). Synthetic biologists are beginning to frolic on the worlds of alternative genetics but must not tread into areas that have the potential to harm our biology.

**References**

1. V. B. Pinheiro *et al*., *Science* **336**, 341 (2012).
2. G. F. Joyce, A. W. Schwartz, S. L. Miller, L. E. Orgel, *Proc. Natl. Acad. Sci. U.S.A.* **84**, 4398 (1987).
3. K. Schöning *et al*., *Science* **290**, 1347 (2000).
4. L. Zhang *et al*., *J. Am. Chem. Soc.* **127**, 4174 (2005).
5. H. Yu, S. Zhang, J. C. Chaput, *Nat. Chem.* **4**, 183 (2012).
6. A. C. Clarke, *2010: Odyssey Two* (Ballantine Books, New York, 1983).

10.1126/science.1221724

BIOCHEMISTRY

# Visualizing Amyloid Assembly

Specific precursor states formed from soluble native proteins have been identified as leading to oligomerization and amyloid formation.

**David Eliezer**

Ordered amyloid fibril protein aggregates are a hallmark of a class of human diseases that includes Parkinson's and Alzheimer's. How proteins assemble into these structures is poorly understood (*1*) but is thought to play a direct role in disease. Two recent studies provide key insights into this problem. On page 362 of this issue, Neudecker *et al*. (*2*) have visualized the changes that convert a normally soluble protein into an aggregation-prone amyloid precursor. Laganowski *et al*. (*3*) have described the structure of a subsequent oligomeric amyloid intermediate of the kind currently believed to be responsible for amyloid-associated toxicity (*4*).

Neudecker *et al*. report a detailed characterization of an amyloid precursor, revealing structural changes that precede aggregation. The results were obtained through a combination of nuclear magnetic resonance (NMR) spectroscopy and computational algorithms that enabled visualization of this precursor, even though it appears so rarely that its characteristics cannot be measured directly by NMR. To better understand their approach, a loose analogy can be made between NMR spectroscopy and music. Each nucleus in the molecule can be considered to represent an instrument, and the spectrum of the protein is a snapshot of the melody played by the orchestra. Each instrument contributes a single note or resonance frequency—the latter reflecting the location of the associated nucleus in the protein relative to nearby nuclei.

However, some instruments spend a small fraction of the time playing a different tune, a harmony of sorts, that corresponds to a rare excited state, or alternative conformation adopted by the protein, which alters the positions of the nuclei and hence their frequencies. Each alternate note is too faint to be heard directly but has a detectable influence on the timbre, or spectral envelope, of the corresponding melodic part. By measuring this effect, Neudecker *et al*. recreated the notes of the faint harmony (*5*) and then used a computer algorithm (*6*) to allow them to determine what arrangement of the instruments, or nuclei, would most optimally reproduce each note. The result is a detailed description of the position of each nucleus in the excited state

Department of Biochemistry and Program in Structural Biology, Weill Cornell Medical College, New York, NY 10065, USA. E-mail: dae2005@med.cornell.edu

of the protein, that is to say, a structure of the amyloid precursor state.

The key feature revealed is the rearrangement of the final four amino acids of the 60–amino acid protein chain. Normally, this region forms a strandlike conformation, strand 5, that is hydrogen bonded, or woven, to another strand formed by the first few amino acids of the protein (strand 1) as part of a β sheet. Strand 5 caps the edge of this sheet of strands and contains the amino acid proline, which causes a kink that prevents the addition of any further strands. This mechanism is one that nature uses to prevent the addition of strands from different protein chains (*7*). In the amyloid precursor structure, strand 5 is unraveled and no longer able to prevent further strand addition. Indeed, when Neudecker *et al*. designed a version of their protein missing the last four amino acids, this form spontaneously assembled into amyloid fibrils, confirming the protective role of strand 5. A computational analysis highlighting protein regions with a propensity for aggregation (*8*) confirmed that strand 5 is a poor mediator of aggregation, whereas strand 1, uncovered in the amyloidogenic precursor, is a highly effective aggregation locus.

Neudecker *et al*. provide a view, at an unprecedented level of detail, into the structural changes that convert a normally soluble protein into an aggregation-prone precursor. Many questions remain open, and of particular interest are the intermediates that follow precursor formation but precede the appearance of mature fibrils.

The report by Laganowski *et al*. provides precisely this information. The authors used a different computational method (*9*) to identify amyloid-forming fragments in a protein found in the lens of the eye. One fragment produced stable toxic amyloid oligomers, which they crystallized to produce the first ever crystal structure of an oligomeric intermediate. This structure, termed a cylindrin by the authors, consists of six strands woven into a single sheet that is rolled into a tight nonporous barrel. Interestingly, the authors note that a similar structure is seen in part of a bacterial protein, PduU, comprising the shell of an organelle-like microcompartment (*10*). Seven residues near the start of that protein chain form a strand that is entirely separated in space from the remainder of the protein. Six such strands assemble into a hexameric sheet rolled into a tight barrel. This observation is particularly suggestive, given the finding by Neudecker *et al*. that strand 1, found at the beginning of their protein, is the likely driver of its aggregation. If, in the course of intermolecular interactions caused by the loss of strand 5, strand 1 detached from the sheet to which it normally belongs, it might be able, like in PduU, to participate in the formation of a cylindrin oligomer, as characterized by Laganowski *et al*. (see the figure).

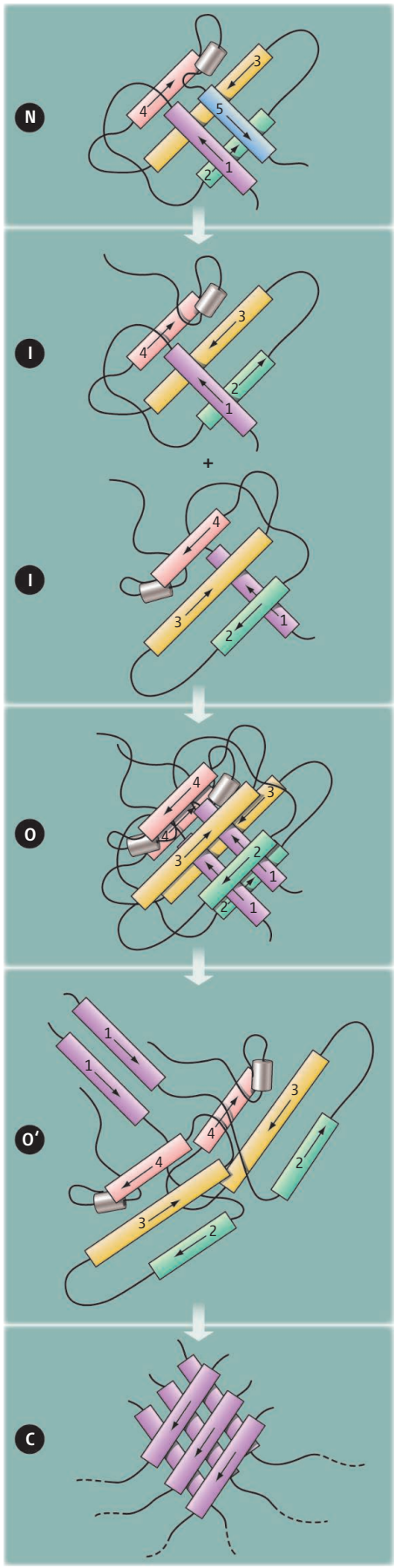


**Steps on the road to misassembly.** A potential pathway for amyloid formation is illustrated. The native state, N, converts to the amyloid precursor, I, by the unraveling of strand 5, as shown by Neudecker *et al*. Strand 1, which is highly aggregation prone, is thus exposed, and can mediate strand-strand interactions between different, largely native, monomers, leading to an as-of-yet uncharacterized oligomeric species, O, depicted here hypothetically as a dimer. The stably associated strand 1 sheets need to escape from the context of the native structure, rearranging O into O′ (via an unspecified mechanism) and allowing them to assemble, in a manner similar to that seen in the bacterial PduU protein, into the hexameric cylindrin structure, C, revealed by Laganowski *et al*. Formation of a parallel cylindrin is shown arbitrarily.

CREDIT: P. HUEY/ *CIENCE*

Together, the studies by Neudecker *et al*. and Laganowski *et al*. suggest a potentially general pathway for amyloid formation, in which protective native interactions are removed, facilitating intermolecular strand-strand interactions, accompanied by the escape of associated strands or hairpins from the native structure and their assembly into cylindrin barrel structures. These studies also sow a rich field for further inquiry. A mechanism by which intermolecular interactions facilitate eventual strand extraction is missing. Steps in the transition from cylindrins to higher-order aggregates and fibrils remain to be delineated. Importantly, many proteins that form disease-linked amyloid appear to be highly disordered and do not possess a native structure. Such proteins lack the protective interactions and preorganized strand structure that feature in the precursor characterized by Neudecker *et al*., so the interaction modes that drive the assembly of such proteins into cylindrin-like oligomers remain to be discovered.

**References**

1. T. Eichner, S. E. Radford, *Mol. Cell* **43**, 8 (2011).
2. P. Neudecker *et al*., *Science* **336**, 362 (2012).
3. A. Laganowsky *et al*., *Science* **335**, 1228 (2012).
4. C. Haass, D. J. Selkoe, *Nat. Rev. Mol. Cell Biol.* **8**, 101 (2007).
5. A. G. Palmer 3rd, *Chem. Rev.* **104**, 3623 (2004).
6. K. J. Kohlhoff *et al*., *J. Am. Chem. Soc.* **131**, 13894 (2009).
7. J. S. Richardson, D. C. Richardson, *Proc. Natl. Acad. Sci. U.S.A.* **99**, 2754 (2002).
8. S. Pechmann, E. D. Levy, G. G. Tartaglia, M. Vendruscolo, *Proc. Natl. Acad. Sci. U.S.A.* **106**, 10159 (2009).
9. M. J. Thompson *et al*., *Proc. Natl. Acad. Sci. U.S.A.* **103**, 4074 (2006).
10. C. S. Crowley *et al*., *Structure* **16**, 1324 (2008).

10.1126/science.1220356





Published by AAAS

# The State and Fate of Himalayan Glaciers

T. Bolch,[1,2]* A. Kulkarni,[3] A. Kääb,[4] C. Huggel,[1,5] F. Paul,[1] J. G. Cogley,[6] H. Frey,[1,5] J. S. Kargel,[7] K. Fujita,[8] M. Scheel,[1,5] S. Bajracharya,[9] M. Stoffel[5,10]

Himalayan glaciers are a focus of public and scientific debate. Prevailing uncertainties are of major concern because some projections of their future have serious implications for water resources. Most Himalayan glaciers are losing mass at rates similar to glaciers elsewhere, except for emerging indications of stability or mass gain in the Karakoram. A poor understanding of the processes affecting them, combined with the diversity of climatic conditions and the extremes of topographical relief within the region, makes projections speculative. Nevertheless, it is unlikely that dramatic changes in total runoff will occur soon, although continuing shrinkage outside the Karakoram will increase the seasonality of runoff, affect irrigation and hydropower, and alter hazards.

Almost 800 million people live in the catchments of the Indus, Ganges, and Brahmaputra rivers and rely to varying extents (in particular during dry seasons and in mountain valleys) on the water released from glaciers (*1*, *2*) that constitute the most extensive glacier cover outside Alaska and the Arctic (*3*). Published estimates of glacier coverage for the Himalaya and Karakoram (H-K), mostly based on historic data, vary between 43,178 km$^2$ and 49,650 km$^2$ (table S1). Our best estimate for H-K, as defined in fig. S1 (*4*), mainly based on mapping using recent satellite images (*4*) is ~40,800 km$^2$ (Himalaya, ~22,800 km$^2$; Karakoram, ~18,000 km$^2$) (table S2). Glacier volume cannot be measured directly over regional scales but must be modeled. Empirical estimates are highly uncertain and range from about 2300 km$^3$, taking the slope-dependent ice thickness into account, to ~3600 to ~6500 km$^3$ based on volume-area scaling (*4*) (table S2).

Glaciers are natural buffers of hydrological seasonality, releasing meltwater during summer and early autumn in particular. They represent a local water resource in the mountains but also influence runoff into lowland rivers, recharge river-fed aquifers, and contribute to global sea-level change (*1*, *5*). Regional climates are heterogeneous, and the socioeconomic importance of glacier meltwater varies over the H-K. It is a major source of stream flow in parts of the H-K having little summer precipitation, especially the Karakoram and northwestern Himalaya, but is less important in monsoon-dominated regions with abundant summer precipitation (*3*, *5*). This spatial variability influences meltwater regimes, in turn affecting the availability of water for hydropower generation, agriculture, and ecosystems (*6*). Glacier change also alters risks due to glacial hazards, not least from glacial lake outburst floods (GLOFs) (*7*).

Recent controversy about future Himalayan glacier change, largely fueled by an erroneous statement in the Intergovernmental Panel on Climate Change (IPCC) Fourth Assessment Report (*8*), has exposed major gaps in our knowledge of the behavior of the region's glaciers: Annual amounts of ice and snow melt along with its seasonal and spatial variability, as well as the contributions of precipitation to discharge, are all uncertain (*1*, *6*). These gaps are due to insufficient numbers of in situ measurements, for which remote sensing only partially substitutes. There are few high-elevation weather stations and no long-term field measurement programs on glaciers, and information about current ice extent is nonuniform and unsatisfactory in places (*4*). This can be attributed to the remote location of glaciers, the rugged terrain, and a complex political situation, all of which make physical access difficult. Here, we review the state of knowledge about key characteristics, current extent, and changes of H-K glaciers since the mid-19th century. We also discuss projections of possible future changes, summarize important implications for water resources and natural hazards, and close by

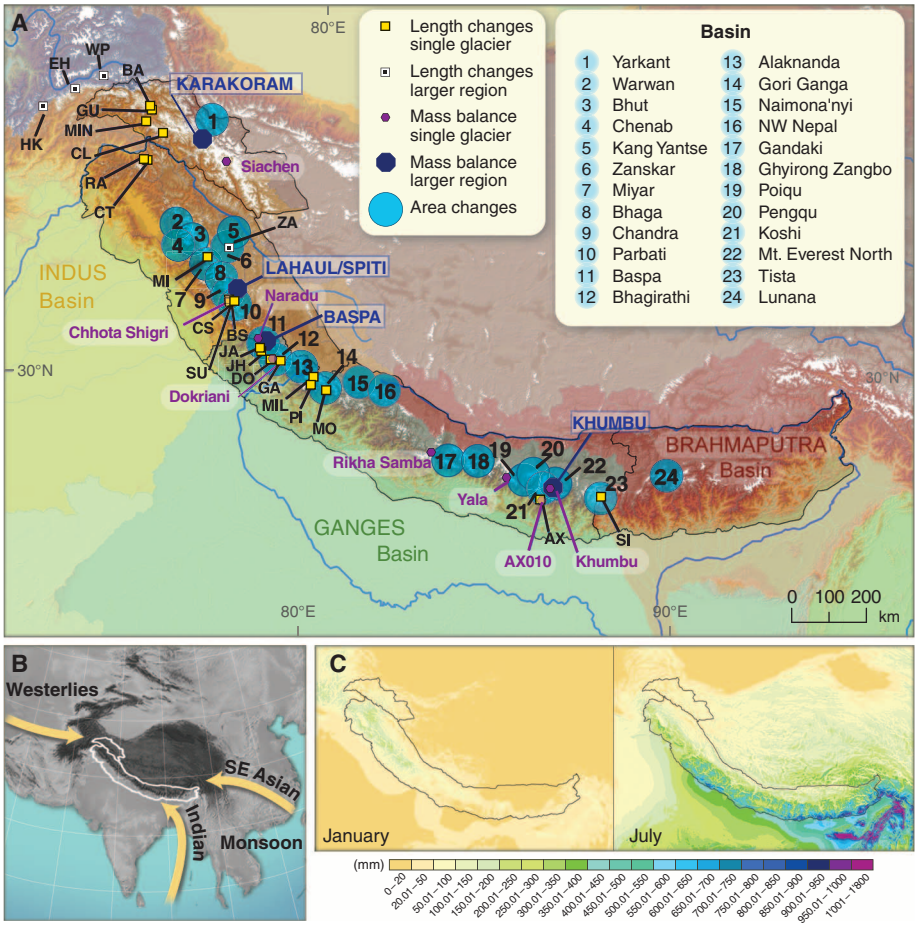


**Fig. 1.** (**A**) Map of the Karakoram and Himalaya showing the major river basins and the locations of measured rates of change in area and of a sample of glacier length change and mass budget measurements (*4*) (tables S3, S5, and S6). (**B**) Main wind systems. (**C**) Mean precipitation in January and July. [Source: (*9*)]

[1]Department of Geography, University of Zurich, 8057 Zürich Switzerland. [2]Institute for Cartography, Technische Universität Dresden, 01069 Dresden, Germany. [3]Divecha Center for Climate Change, Indian Institute of Science, Bangalore 560 012, India. [4]Department of Geosciences, University of Oslo, 0316 Oslo, Norway. [5]Institute for Environmental Sciences, University of Geneva, 1227 Geneva, Switzerland. [6]Department of Geography, Trent University, Peterborough, Ontario, Canada K9J 7B8. [7]Department of Hydrology and Water Resources, University of Arizona, Tucson, AZ 85721, USA. [8]Graduate School of Environmental Studies, Nagoya University, Nagoya 464-8601, Japan. [9]International Centre for Integrated Mountain Development (ICIMOD), Kathmandu, Nepal. [10]Institute of Geological Sciences, University of Bern, 3012 Bern, Switzerland.

*To whom correspondence should be addressed. E-mail: tobias.bolch@geo.uzh.ch

sketching a framework for integrated cryosphere research needed to fill the most critical gaps.

### Regional Variations of Himalayan Climate

The climate in H-K is strongly influenced by the varying dominance of the Asian monsoon and winds from the west (*9*, *10*). The westerlies are a more important moisture source in the northwest: about two-thirds of the high-altitude snowfall in the Karakoram is due to westerly cyclones, mainly in winter, whereas in the southeast more than 80% is provided by the summer monsoon (*10*). The mountains block transfer of most moisture to the Tibetan plateau; hence, precipitation decreases sharply northward in both the monsoonal and the westerly regimes (Fig. 1). The mean elevation of H-K glaciers, a rough proxy for the equilibrium line altitude (ELA), is ~5360 m above sea level (asl), with the highest values in the central (~5600 m) and the lowest in the western Himalaya (~5150 m) (table S2). The ELA is lower where accumulation is greater, requiring more ablation and higher temperatures to yield an annual mass budget of zero.

Little is known about the regional horizontal and vertical distribution of precipitation, especially at high elevations. Short records suggest precipitation of 1600 to 1800 mm year$^{-1}$ in the southwestern Karakoram near 5000 m asl (*11*). Himalayan precipitation records show little or no trend with time (*12*), whereas winter precipitation has increased in the Karakoram (*13*, *14*). Weather-station data indicate recent warming in the Himalaya but not in the Karakoram (*13*, *15*). Nearly all stations are far below the lower limit of glaciers, and some are affected by progressive urbanization, so that it is uncertain whether these trends are also valid for the glaciers. At the highest long-term weather station in the Himalaya, Tingri (4300 m asl), north of Mount Everest, mean annual air temperature (MAAT) increased by ~0.03 K year$^{-1}$ during 1959 to 2007, with greater warming in winter than in summer (*16*). This warming rate may be greater than the global average. In contrast, the MAAT in the Karakoram decreased—a global anomaly—mainly due to the decrease of summer temperatures (*13*, *14*).

### Characteristics of Himalayan Glaciers

Most glaciers in the eastern and central Himalaya belong to the "summer-accumulation type," gaining mass mainly from summer-monsoon snowfall (*17*), whereas winter accumulation is more important in the northwest (*18*) (Fig. 1). The very steep and rugged terrain above the glaciers leads to considerable accumulation by snow avalanching in H-K, especially for Karakoram glaciers, complicating the definition of accumulation areas and the calculation of responses to climatic changes (*19*–*21*). Many glaciers in H-K have heavily debris-covered tongues, a further consequence of the steep rocky terrain and avalanche activity. Debris cover, along with seasonal snow (*22*), complicates delineation of the glaciers, and different measures and definitions of the numerous tributaries of the larger glaciers make length and area determination difficult. The large proportion of low-elevation glacier area (fig. S2) in the western Himalaya may in part be a result of extensive debris cover. Our best estimate of total debris cover in H-K is ~10% (*4*). This percentage is important, because thick debris, which retards surface melting, is concentrated on the low-lying tongues where most melting is expected (*23*). However, many completely debris-covered glacier tongues have very low flow velocities or are stagnant (*23*, *24*) and are thus subject to additional melt processes, such as the development of thermokarst lakes from melt ponds (*25*). The flow speed of such glacier tongues is also controlled by the extent of the accumulation area and thus by the ice flux to the tongue.

In Bhutan, glaciers with large accumulation areas reach velocities of 100 to 200 m year$^{-1}$, decreasing gradually toward their termini, whereas those with small and steep accumulation areas have speeds >50 m year$^{-1}$ only in the zones beneath their rock-ice headwalls (*26*) (Fig. 2B). In contrast to this rather homogeneous regional pattern, which is typical for the central and eastern Himalaya (*23*) (fig. S5), glacier speeds in the Karakoram vary greatly in time and space (Fig. 2A). Glaciers in close proximity, in similar topographic settings, and with similar sizes and shapes have very different speeds at a given time, which points to a range of dynamical sensitivities and instabilities (*27*). Particularly in the Karakoram, many glaciers surge for reasons that are not directly related to climate (*27*, *28*). However, there is evidence that recent surges are favored by high-altitude warming (*18*). The number of glacier surges has almost doubled since 1990, which might be linked to positive mass budgets in this region in the recent period (*29*).

### General Changes in Himalayan Glaciers

Length changes (*22*, *30*) (tables S3 and S4) measured for more than 100 glaciers in H-K suggest that most Himalayan glaciers have been retreating since the mid-19th century (Fig. 3C), except for 1920 to 1940, when about half the records show stationary or advancing tongues (*30*). Some large glaciers have advanced or been stable recently in the northwestern Himalaya and in the Karakoram (*19*, *21*) (Fig. 3C and table S4). In the eastern Hindu Kush, west of the Karakoram, 25% of the glaciers were stable or advancing during 1976 to 2007 (*31*). North of the Karakoram, in the Wakhan Pamir, however, glaciers were retreating during a similar period (*32*).

Area changes (table S5) have been measured for several thousand glaciers in H-K. Area change data from the Karakoram exist only for the Yarkant basin north of the main ridge, where the loss rate was ~0.1% year$^{-1}$ between 1962 and 1999 (*33*). Small high-altitude glaciers in the Transhimalaya of Ladakh had a shrinkage rate of ~0.4% year$^{-1}$ from 1969 to 2010 (*34*). In the Indian Himalaya, shrinkage rates are regionally variable: ~0.2 to ~0.7% year$^{-1}$, 1960s to 2001–2004 [11 Indian catchments, (*35*)]; 0.12 ± 0.07% year$^{-1}$, 1968 to 2007 [Garhwal Himalaya, (*36*)]; ~0.3% year$^{-1}$, 1963 to 1993 [Bhutan, (*37*)]; and ~0.3 to 0.6% year$^{-1}$, ~1970 to ~2005 [Tibet, (*38*)]. There is also a clear tendency for area loss in Nepal (*39*) (table S5). Where measured, the debris-covered area has increased [e.g., (*36*)], indicating increasing debris production, reduced glacial transport capacity, or negative mass balances. Most studies investigating more than one time period show faster shrinkage rates in later periods. Notwithstanding the variability and the uncertainties, a consistent picture emerges of net area loss in recent decades in most parts of the Himalaya (Fig. 3B and fig. S4). Indications of positive mass budget suggest that net area gain is likely at least in the more humid parts of the Karakoram (*19*, *29*).

Measurements of the annual mass budget are relatively few and short-term. The longest series spans only 10 years (Fig. 3A and table S6). One geodetic (multiannual) measurement covers 1962 to 2007 (*20*). All budgets are negative on average with only a few positive years. Typical values vary from –0.32 m year$^{-1}$ water equivalent (w.e.) (Dokriani Glacier, 1992 to 2000) to –0.67 ± 0.40 m year$^{-1}$ w.e. (Chhota Shigri Glacier, 2002 to 2010) (*40*) to –1.60 m year$^{-1}$ w.e. (Hamtah Glacier, 2001 to 2006) (table S6). A space-borne geodetic assessment for 1999 to 2004 in Lahaul/Spiti (Western Himalaya) revealed substantial mass loss on several heavily debris-covered tongues (*41*). In the Mount Everest region, such glaciers had an average budget of –0.32 ± 0.08 m year$^{-1}$ w.e.

#### Glacial Response to Climate Change

Glaciers develop where mass gain (e.g., by snowfall and avalanches) exceeds mass loss (e.g., by melting and calving). Lower temperatures and greater snowfall favor mass gain (accumulation); conversely, higher temperatures favor mass loss (ablation). The sum of accumulation and ablation over any period is the mass budget. Mass is transferred by glacier flow from the accumulation area, at high elevation, to the ablation area at low elevation. The steeper the glacier, the faster the flow. If ablation dominates over several years, the mass flux is reduced and the glacier starts to retreat. Conversely, if net annual accumulation (positive balance) dominates for a long time, the glacier increases flow speed and eventually advances. Because the response of the terminus to a change in climate is delayed by flow dynamics, current changes in terminus position are integrated reactions to past climate changes. Glacier response times vary; the larger and slower (flatter) the glacier, the longer the delay under equal climatic conditions. Length and area changes are thus harder to interpret in climatic terms than are mass changes, but the latter are harder to measure.

(1970 to 2007) (*20*) (fig. S5). The only source of information for the Karakoram based on in situ data indicates an average budget of –0.51 m year$^{-1}$ w.e. for Siachen Glacier (1986 to 1991) (*42*), whereas a slight mass gain was observed for the Karakoram for the early 21st century based on a geodetic estimate (*43*). These measurements suggest that the mass budget over large parts of the Himalaya has been negative over the past five decades, that the rate of loss increased after roughly 1995 (Fig. 3), but also that the spatiotemporal variability is high (*44*). The region-wide loss rate is close to the global mean (*45*). Gravimetric measurements (*46*) indicate mass loss in the Himalaya and also possible mass gain in the Karakoram from 2002 to 2006, with a decrease thereafter. A more recent gravimetric study (*47*) is basically in line with this finding but shows considerably lower mass loss for the whole of High Mountain Asia (–4 ± 20 versus –47 ± 12 Gt year$^{-1}$) and only –5 ± 6 Gt year$^{-1}$ for the H-K from 2003 to 2010. The difference has been attributed mainly to different estimates of the groundwater depletion (*47*). The lower estimate could also be a sign of slight mass gain in the central Karakoram and moderate loss in the Himalaya during this period. It is beyond the scope of this contribution to discuss satellite gravimetry methods. However, it has to be noted that interpretation of Gravity Recovery and Climate Experiment (GRACE) satellite measurements in terms of glacier mass changes for a complex, large, and tectonically very active mountain range such as H-K, in close vicinity to a zone of substantial groundwater depletion in northern India, implies substantial uncertainties. These gravimetrically derived results need to be contrasted with existing mass budget data that show all negative values in the Himalaya outside the Karakoram (Fig. 3A)

Monsoon-affected glaciers are more sensitive to temperature change than winter-accumulation–type glaciers (*48*) because the temperature increase directly reduces solid precipitation (i.e., snow accumulation) and extends the melting period. Without a snow cover in summer, surface albedo is much lower and melt is further increased. In the Karakoram and northwestern Himalaya, glaciers that extend to higher elevations show irregular behavior and have retreated less rapidly or even advanced in recent years (the so-called Karakoram anomaly) (*19*, *29*) (tables S3 and S4). This is readily understandable for avalanche-fed glaciers where the extent of the accumulation area changes only slightly when the ELA is rising (*21*). Observed strong surface lowering of heavily debris-covered glaciers can be explained by their low elevations, by enhanced melting on exposed ice cliffs and beneath surface ponds (*25*), and maybe also by collapse of englacial conduits (for nearly stagnant ice). Dust and black soot, which increased melt on some Tibetan glaciers (*49*), are also likely to influence H-K glaciers, but this requires further investigation.

### Persistence of Himalayan glaciers

The statement that most H-K glaciers will likely disappear by 2035 is wrong (*8*), as shown by simple but physically robust modeling (*50*). More realistic projections (*5*), relying on degree-day modeling but reporting the H-K glaciers only as part of High Mountain Asia, are consistent with the simpler model in suggesting moderate mass loss over the 21st century. The only published study on catchment scale (Langtang Valley, Nepal) predicts somewhat higher mass loss (75% by 2088) (*51*), although melt processes beneath the extensive debris cover were only roughly addressed. Future changes of monsoon intensity will have an important effect on Himalayan glaciers, but current climate projections do not even agree on the sign of change, thus introducing further uncertainties (*6*). Nevertheless, all models project mass losses in coming decades that are substantial for most parts of the Himalaya, but consistently fall well short of complete region-wide glacier disappearance even by 2100. Information about total ice volume is essential

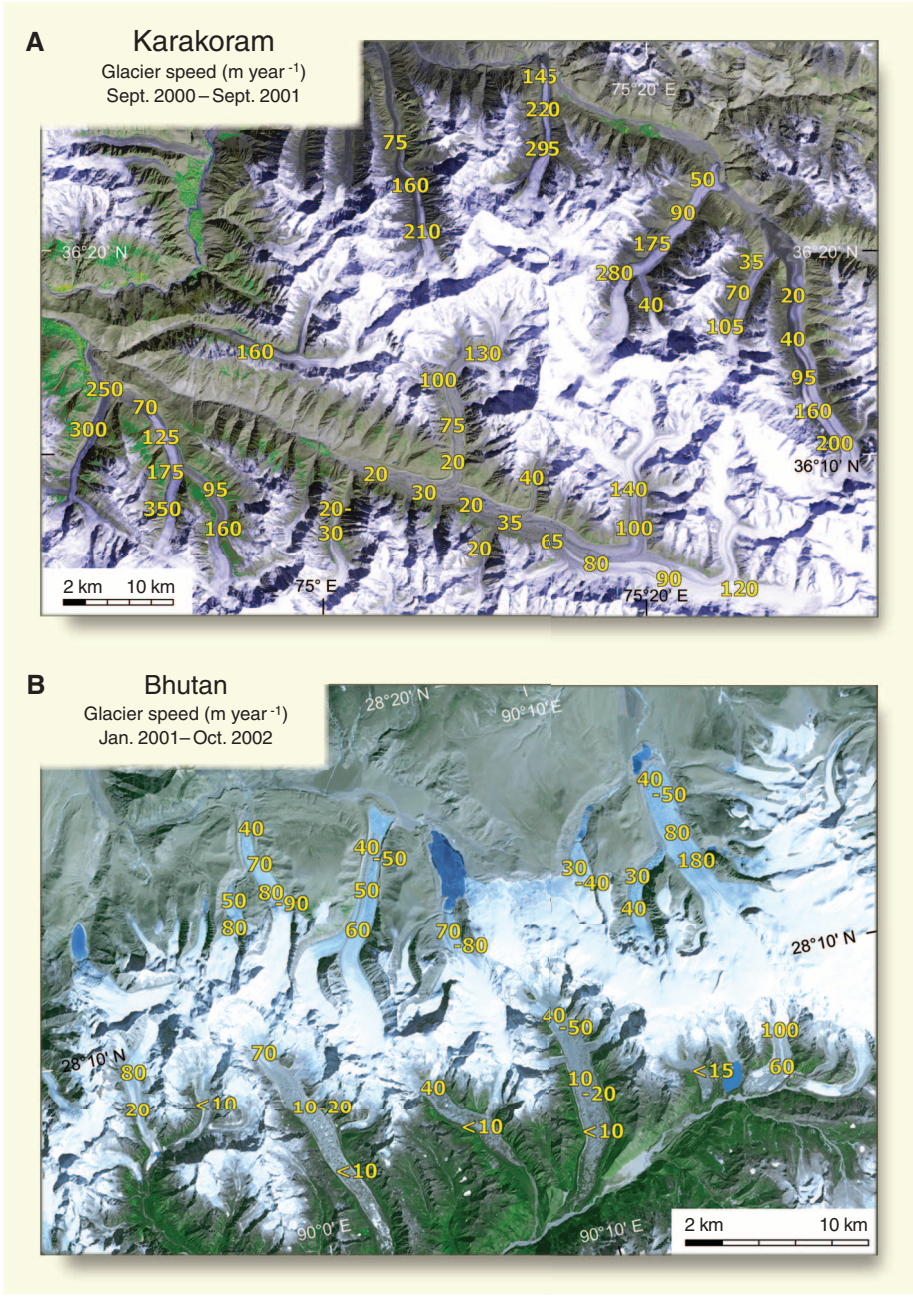


**Fig. 2.** (**A**) Representative horizontal speeds from Landsat data of October 2000 and October 2001 on glaciers in the Karakoram. Speeds vary greatly even for nearby and otherwise similar glaciers due to a large temporal variability in glacier dynamics, among other reasons because of glacier surges. (**B**) Representative horizontal surface displacements measured from repeat Advanced Spaceborne Thermal Emission and Reflection Radiometer satellite data of January 2001 and October 2002 on glaciers in Bhutan. The northern glaciers are debris-free, flow faster, and sustain their flow through their entire length, whereas the southbound glaciers have extensive debris cover on tongues that are nearly stagnant (for full measurements, see fig. S3).

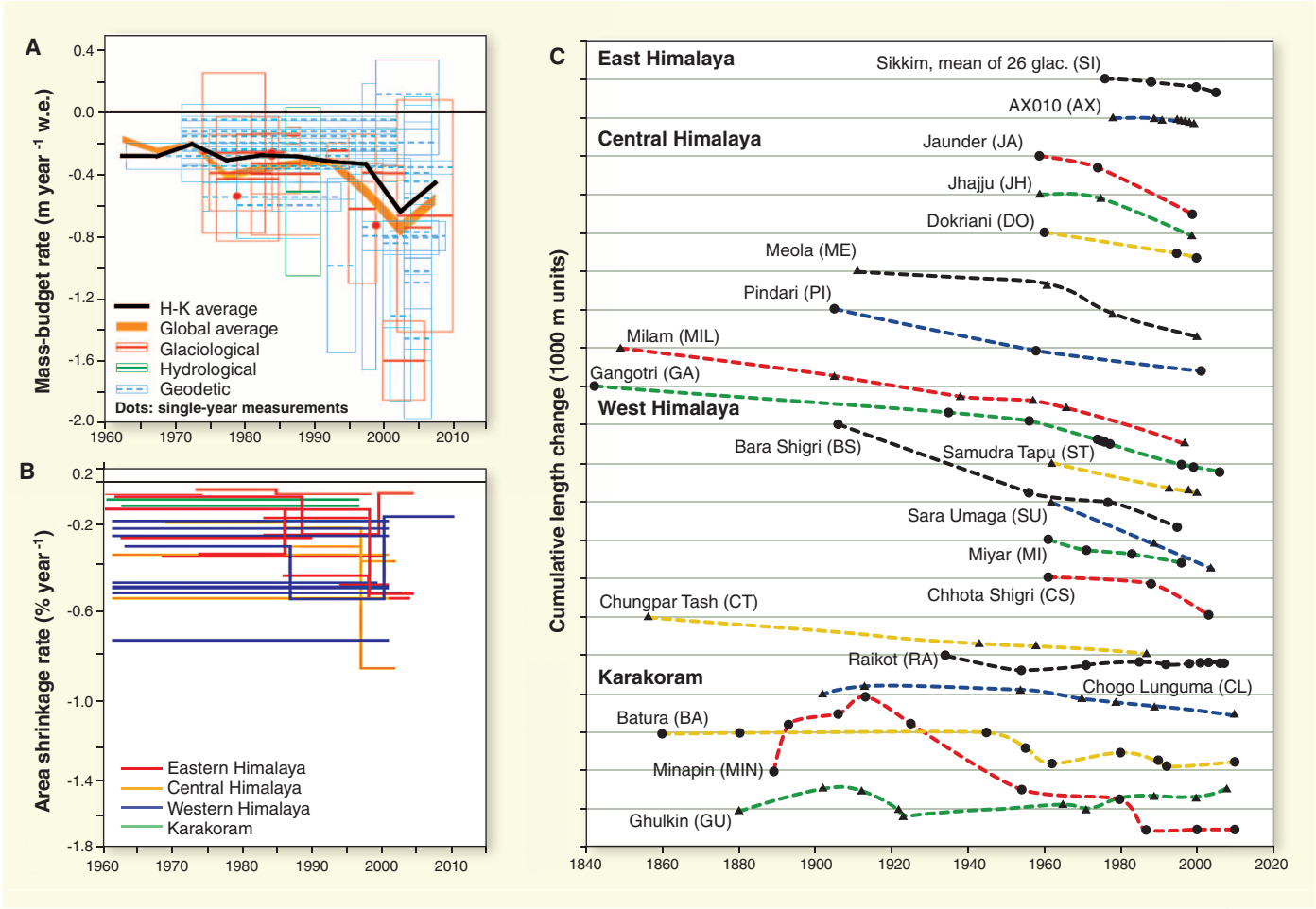


**Fig. 3.** Measured rates of change in mass budget (A) and area (B) and of a sample of cumulative length change measurements (C). For locations, see Fig. 1; for sources, see tables S3, S5, and S6. (**A**) Glaciological measurements are those made annually in situ; geodetic measurements, mostly multiannual, compare a later surface elevation (mostly derived from photogrammetric surveys) to an earlier one. Each budget is drawn as a thick horizontal line contained in a ±1 standard deviation box (±1 standard error for geodetic measurements). (**B**) Area shrinkage in recent decades. No statistically significant difference between the regions can be discerned. Uncertainties appear to be high but are as yet poorly assessed. (**C**) The glacier retreat since the mid-19th century is obvious in the Himalaya, with the exception of the glaciers at Nanga Parbat in the northwest (RA, CL). Glaciers in the Karakoram show complex behavior.

for predictions, but only very few measurements exist (*4*). Percentage changes in glacier volume are very likely to exceed percentage area changes, because a large part of the H-K ice is located in the low-lying and flat (and thus thick) tongues of the largest valley glaciers. Projections for the Karakoram glaciers will remain impractical until the reasons for their observed anomalous behavior, including their propensity to surge, are better understood (*27*, *29*). The evidence of stability or even mass gain in the Karakoram, which may be ascribable to increased winter precipitation and reduced summer temperature, was recently confirmed by direct measurement (*43*).

### Impacts of Glacier Changes in the Himalaya

Glacier change affects the hydrological cycle. A negative annual mass budget yields a surplus of runoff from glacier ice, whereas a positive budget yields a deficit of runoff because snow has gone into storage on the glacier. When glacier ice (as opposed to winter snow) is lost in the long term, the annual hydrograph evolves toward that of an equivalent glacier-free catchment. The relative importance of this loss of glacier ice necessarily decreases downstream, but it differs fundamentally under different precipitation regimes (*2*). The runoff contribution from glacier imbalance is relatively minor in the wetter monsoonal catchments of the Ganges and Brahmaputra but more substantial in the drier westerly dominated headwaters of the Indus (*1*, *2*) (table S7).

Projections of the diminishing contribution of seasonal snow to annual runoff indicate reduced maximum flows in spring and an increase by over 30% of the glacier contribution to total runoff (*52*). Runoff in strongly glaciated catchments, especially in the Karakoram, will likely not decrease due to deglaciation before the end of the 21st century (*53*). Currently, gauging stations in the extensively glaciated Hunza basin (Karakoram) show reduced runoff, consistent with climate records (*14*) and indications of a positive mass budget for glaciers in the Karakoram (*29*, *43*, *46*).

Rough predictions of runoff for the Langtang Valley (Nepal) suggest that total discharge might even increase during the next decades (*51*). However, this is mainly attributable to a projected increase in precipitation; the contribution of glaciers to discharge may decrease after ~2040. Unlike in regions with winter-accumulation–type glaciers, where an earlier peak of spring snowmelt is expected, the monsoon-influenced Himalaya will maintain peak discharge in summer even with strongly reduced glacier sizes (*1*, *2*). Runoff from less glaciated catchments will probably decrease, especially in the central and eastern Himalaya, as glaciers continue to shrink (*53*). In the absence of a clear trend in glacier shrinkage in the Karakoram and parts of the northwestern Himalaya, constituting important parts of the Indus catchment, we would not expect large changes in the discharge of the Indus River during the next decades. A corollary of the confirmation of the Karakoram anomaly is that the contribution of Karakoram glaciers to sea-level rise has been overestimated (*43*).

A further serious implication of glacier recession is the development of moraine-dammed glacial lakes (*54*) that, if their dams breach, can drain catastrophically (*7*). In the central and eastern Himalaya, both south and north of the main ridge, lake growth has been observed in recent decades, with much larger absolute growth rates in the east, while in the drier northwest, total lake area decreased (*54*, *55*). Lakes in contact with glacier ice efficiently transmit thermal energy to the ice front, accelerating melting, and also induce calving, accelerating retreat (*56*). In the H-K, growth of moraine-dammed lakes and disintegration of glacier tongues have been found to stem mostly from tongue stagnation and the rapid expansion of supraglacial lakes over a period of typically 50 years. The process may start when average surface slopes of glacier tongues become smaller than 2° (*57*). The associated thermokarst processes can be self-enhancing and irreversible, so that pond and lake development may lead to glacier shrinkage independently of climatic factors. Advancing glaciers may also cause threats if they dam tributary valleys, turning them into new lake basins (*58*). The risk related to glacial lakes in the H-K, in contrast to some other mountain regions such as the Alps or Andes, is characterized by the particularly large lake volumes and associated long outburst flood reaches rather than by a high population concentration close to the lakes (*7*).

## Perspectives

Most glaciers in H-K have retreated and lost mass since the mid-19th century. Loss rates have probably accelerated in recent decades, but the observed tendencies are not regionally uniform. In the Karakoram and parts of the northwestern Himalaya, many of the observed large glaciers have oscillated or surged since the beginning of the last century, with indications of positive mass balances for the 1990s and the beginning of the 21st century (*19*, *29*, *43*, *46*). This Karakoram anomaly stands out as a phenomenon that deserves further investigation to clarify the relation between climate forcing and glacier responses in the region, taking due account of the distinctive behavior of its many surge-type and dynamically variable glaciers.

The leading uncertainties about the state and fate of H-K glaciers relate to the contribution of glaciers to runoff (*51*), the projection of glacier changes (*50*), the variability of glacier changes within the region (*44*), the influence of debris cover on glacier melt (*20*, *23*), the role of ice and snow avalanches in the glacier mass budget (*21*), and the magnitude of past glacier changes as revealed from comparisons with maps (*22*). These uncertainties can be mainly attributed to deficient information (for example, about total glacier area and mass); lack of measurements, both of climatic forcing agents and of the glaciers themselves (mass budgets and length changes); and the use of unsuitable or uncertain data, such as imagery with extensive seasonal snow or maps drawn from such imagery. Nonpublication of existing data makes these problems worse.

To close the knowledge gaps, the most useful steps will be to release a regionally complete, up-to-date, and accurate glacier inventory conforming to international standards and including the most important topographic parameters; to continue to develop and refine remote-sensing methods for the estimation of glacier changes, including length, area, and volume changes, as well as gravimetric measurement of mass changes; to fill critical gaps in the climatic and hydrologic station network and establish transects from the lowlands in the south to the Tibetan Plateau, similar to that already established north and south of Mount Everest; to continue existing mass-budget measurements on reference glaciers and to establish new programs to cover more climate zones and glacier types in a more representative way, particularly in the Karakoram; to measure the thickness of selected glaciers as a basis for calibrating recently developed methods for modeling of subglacial topography [e.g., (*59*)] and hence glacier volume; and to strengthen modeling efforts, in particular for climate projections, future glacier evolution, GLOFs, and glacier runoff. Field and remote-sensing–based investigations should consider the needs of these models when designing and performing investigations. Finally, we recommend the continuation and extension of coordinated transboundary research on climate, cryosphere, and their impacts, including the exchange of all relevant data.

### References and Notes


1. W. W. Immerzeel, L. P. van Beek, M. F. Bierkens, *Science* **328**, 1382 (2010).
2. G. Kaser, M. Grosshauser, B. Marzeion, *Proc. Natl. Acad. Sci. U.S.A.* **107**, 20223 (2010).
3. M. B. Dyurgerov, M. F. Meier, "Glaciers and the Changing Earth System: A 2004 Snapshot" Occasional Paper **58**. (2005).
4. Methods and discussion are available as supplementary materials on *Science* Online.
5. V. Radić, R. Hock, *J. Geophys. Res.* **115**, (F1), F01010 (2010).
6. E. J. Moors *et al.*, *Environ. Sci. Policy* **14**, 758 (2011).
7. S. Richardson, J. Reynolds, *Quat. Int.* **65–66**, 31 (2000).
8. J. G. Cogley, J. S. Kargel, G. Kaser, C. J. van der Veen, *Science* **327**, 522 (2010).
9. J. Böhner, *Boreas* **35**, 279 (2006).
10. B. Bookhagen, D. Burbank, *J. Geophys. Res.* **115**, (F3), F03019 (2010).
11. M. Winiger, M. Gumpert, H. Yamout, *Hydrol. Processes* **19**, 2329 (2005).
12. A. Shrestha, C. Wake, J. Dibb, P. Mayewski, *Int. J. Climatol.* **20**, 317 (2000).
13. M. Shekhar, H. Chand, S. Kumar, K. Srinivasan, A. Ganju, *Ann. Glaciol.* **51**, 105 (2010).
14. H. Fowler, D. Archer, *J. Clim.* **19**, 4276 (2006).
15. A. Shrestha, C. Wake, P. Mayewski, J. Dibb, *J. Clim.* **12**, 2775 (1999).
16. X. Yang, T. Zhang, D. Qin, S. Kang, X. Qin, *Arct. Antarct. Alp. Res.* **43**, 147 (2011).
17. Y. Ageta, K. Higuchi, *Geogr. Ann. A* **66**, 249 (1984).
18. D. J. Quincey *et al.*, *Geophys. Res. Lett.* **38**, L18504 (2011).
19. K. Hewitt, *Mt. Res. Dev.* **31**, 188 (2011).
20. T. Bolch, T. Pieczonka, D. I. Benn, *The Cryosphere* **5**, 349 (2011).
21. L. Iturrizaga, *Zeit. für Geo.* **55**, (suppl.), 205 (2011).
22. R. Bhambri, T. Bolch, *Prog. Phys. Geogr.* **33**, 672 (2009).
23. D. Scherler, B. Bookhagen, M. R. Strecker, *Nat. Geosci.* **4**, 156 (2011).
24. D. Quincey, A. Luckman, D. I. Benn, *J. Glaciol.* **55**, 596 (2009).
25. A. Sakai, N. Takeuchi, K. Fujita, M. Nakawo, *IAHS Publication* **264**, 119 (2000).
26. A. Kääb, *Remote Sens. Environ.* **94**, 463 (2005).
27. T. Heid, A. Kääb, *The Cryosphere Discuss.* **5**, 3025 (2011).
28. L. Copland *et al.*, *Ann. Glaciol.* **50**, 41 (2009).
29. L. Copland *et al.*, *Arct. Antarct. Alp. Res.* **43**, 503 (2011).
30. P. A. Mayewski, P. A. Jeschke, *Arct. Alp. Res.* **11**, 267 (1979).
31. M. A. Sarikaya, M. P. Bishop, J. F. Shroder, J. A. Olsenholler, *Remote Sens. Lett.* **3**, 77 (2012).
32. U. K. Haritashya, M. P. Bishop, J. F. Shroder, A. B. G. Bush, H. N. N. Bulley, *Clim. Change* **94**, 5 (2009).
33. S. Liu *et al.*, *Ann. Glaciol.* **43**, 91 (2006).
34. S. Schmidt, M. Nüsser, *Arct. Antarct. Alp. Res.* **44**, 107 (2012).
35. A. V. Kulkarni, B. P. Rathore, S. K. Singh, I. M. Bahuguna, *Int. J. Remote Sens.* **32**, 601 (2011).
36. R. Bhambri, T. Bolch, R. K. Chaujar, S. C. Kulshreshtha, *J. Glaciol.* **57**, 543 (2011).
37. Karma, Y. Ageta, N. Naito, S. Iwata, H. Yabuki, *Bull. Glaciol. Res.* **20**, 29 (2003).
38. Y. Nie, Y. Zhang, L. Liu, J. Zhang, *J. Geogr. Sci.* **20**, 667 (2010).
39. S. R. Bajracharya, S. B. Maharjan, F. Shrestha, in *Climate Change, Geophysical Foundations and Ecological Effects*, J. Blanco, H. Kheradmand, Eds. (InTech, Rijeka, Croatia, 2011).
40. M. F. Azam *et al.*, *J. Glaciol.* **58**, 315 (2012).
41. E. Berthier *et al.*, *Remote Sens. Environ.* **108**, 327 (2007).
42. M. R. Bhutiyani, *J. Glaciol.* **45**, 112 (1999).
43. J. Gardelle, E. Berthier, Y. Arnaud, *Nat. Geosci.* (2012); 10.1038/ngeo1450.
44. K. Fujita, T. Nuimura, *Proc. Natl. Acad. Sci. U.S.A.* **108**, 14011 (2011).
45. M. Zemp, M. Hoelzle, W. Haeberli, *Ann. Glaciol.* **50**, 101 (2009).
46. K. Matsuo, K. Heki, *Earth Planet. Sci. Lett.* **290**, 30 (2010).
47. T. Jacob, J. Wahr, W. T. Pfeffer, S. Swenson, *Nature* **482**, 514 (2012).
48. K. Fujita, *Earth Planet. Sci. Lett.* **276**, 14 (2008).
49. B. Xu *et al.*, *Proc. Natl. Acad. Sci. U.S.A.* **106**, 22114 (2009).
50. J. G. Cogley, *Ann. Glaciol.* **52**, 69 (2011).
51. W. W. Immerzeel, L. P. H. Beek, M. Konz, A. B. Shrestha, M. F. P. Bierkens, *Clim. Change* **110**, 721 (2012).
52. T. P. Barnett, J. C. Adam, D. P. Lettenmaier, *Nature* **438**, 303 (2005).
53. H. G. Rees, D. N. Collins, *Hydrol. Processes* **20**, 2157 (2006).
54. J. Gardelle, Y. Arnaud, E. Berthier, *Global Planet. Change* **75**, 47 (2011).
55. W. Xin, S. Liu, W. Gou, J. Xu, *Mt. Res. Dev.* **28**, 310 (2008).
56. A. Sakai, K. Nishimura, T. Kadota, N. Takeuchi, *J. Glaciol.* **55**, 909 (2009).
57. A. Sakai, K. Fujita, *J. Glaciol.* **56**, 177 (2010).
58. K. Hewitt, J. Liu, *Physical Geography* **31**, 528 (2010).
59. D. Farinotti, M. Huss, A. Bauder, M. Funk, M. Truffer, *J. Glaciol.* **55**, 422 (2009).


**Acknowledgments:** This work has been supported by the European Union FP7 project HighNoon (grant 22708), the European Space Agency projects Glaciers_cci (4000101778/10/I-AM) and GlobGlacier (21088/07/I-EC), and the Global Land Ice Measurements from Space (GLIMS) initiative. J.S.K. acknowledges the support of NASA and T.B. the support of Deutsche Forschungsgemeinschaft (DFG). This review has benefited greatly from discussions with E. Berthier, M. Bishop, U. Haritashya, D. Quincey, A. Racoviteanu, J. Wahr, and M. Zemp. Glacier inventory data for Shyok Basin was provided by R. Bhambri.

### Supplementary Materials

www.sciencemag.org/cgi/content/full/336/6079/310/DC1
Materials and Methods
Supplementary Text
Figs. S1 to S5
Tables S1 to S7
References (*60*–*113*)

10.1126/science.1215828

# Oxidation of the Guanine Nucleotide Pool Underlies Cell Death by Bactericidal Antibiotics

James J. Foti,[1] Babho Devadoss,[1] Jonathan A. Winkler,[2] James J. Collins,[3,4] Graham C. Walker[1]*

A detailed understanding of the mechanisms that underlie antibiotic killing is important for the derivation of new classes of antibiotics and clinically useful adjuvants for current antimicrobial therapies. Our efforts to understand why DinB (DNA polymerase IV) overproduction is cytotoxic to *Escherichia coli* led to the unexpected insight that oxidation of guanine to 8-oxo-guanine in the nucleotide pool underlies much of the cell death caused by both DinB overproduction and bactericidal antibiotics. We propose a model in which the cytotoxicity of beta-lactams and quinolones predominantly results from lethal double-strand DNA breaks caused by incomplete repair of closely spaced 8-oxo-deoxyguanosine lesions, whereas the cytotoxicity of aminoglycosides might additionally result from mistranslation due to the incorporation of 8-oxo-guanine into newly synthesized RNAs.

Elevated levels of reactive oxygen species (ROS), such as superoxide, hydrogen peroxide, and hydroxyl radicals (OH$^{\bullet}$), within prokaryotic cells potentiate cell death. For example, three different classes of bactericidal antibiotics (β-lactams, quinolones, and aminoglycosides), regardless of macromolecular target, ultimately result in cell death in both Gram-negative and Gram-positive bacteria via a common mechanism that produces OH$^{\bullet}$ (*1*). Because elevated intracellular levels of OH$^{\bullet}$ can damage DNA, lipids, and proteins, generalized oxidation catastrophe could result in cell death; however, our current work suggests that cell death is predominantly elicited by specific oxidation of the guanine nucleotide pool and its subsequent use in nucleic acid transactions.

**DinB overproduction lethality due to 8-oxo-deoxyguanosine (8-oxo-dG) incorporation.** The ribonucleotide reductase inhibitor hydroxyurea, although best known for stalling DNA replication forks and eliciting double-strand DNA breaks (DSBs), also causes bacterial cell death through the production of OH$^{\bullet}$ (*2*). This stimulated us to test whether the cytotoxicity associated with overproduction of the *E. coli* translesion DNA polymerase DinB (DNA Pol IV) might result from an OH$^{\bullet}$-dependent process, because, like hydroxyurea, it slows the speed of replication forks and results in bacterial cell death presumably because of DSBs (*3*, *4*). To test whether OH$^{\bullet}$ radicals underlie cell death resulting from DinB overproduction, we measured cell survival in the presence of thiourea (OH$^{\bullet}$ scavenger) and 2,2′-dipyridyl (an iron chelator that prevents the Fenton reaction required for OH$^{\bullet}$ production) (*5*–*8*). Thiourea and 2,2′-dipyridyl, which do not strongly affect cell growth (*1*), completely prevent cell death caused by DinB overproduction (Fig. 1A). In addition, DinB overproduction is not toxic in an anaerobic environment (Fig. 1B), which is consistent with OH$^{\bullet}$'s mediating DinB-induced cell death. However, in contrast to hydroxyurea, which significantly increases intracellular OH$^{\bullet}$ levels (~10-fold) (*2*), DinB overproduction has a more modest effect (~1.6-fold) (Fig. 1D). Thus, it seemed most likely that the elevated levels of DinB were lethal because of the increased use of oxidized deoxynucleotides, rather than because of the induction of high levels of OH$^{\bullet}$.

The nucleotide pool is an important target of ROS, and guanine is particularly susceptible to oxidation because of its low redox potential (*9*, *10*). One of the most intensively studied major products of guanine oxidation is 7,8-dihydro-8-oxoguanine (8-oxo-guanine) (*10*). Its deoxyribonucleotide, 8-oxo-dG, is potentially mutagenic because of its ability to form base pairs with both cytosine and adenine (fig. S1). DinB, like its human ortholog DNA Pol κ (*11*), is a translesion DNA polymerase that can use 8-oxo-deoxyguanosine triphosphate (8-oxo-dGTP) as the incoming nucleotide, pairing it with either deoxycytidine or deoxyadenosine (dC or dA), with a preference for dA (Fig. 1C). Mutation of DinB's steric gate (F13V, in which Phe$^{13}$ is replaced by Val) severely reduces its ability to use 8-oxo-dGTP as an incoming nucleotide (Fig. 1C), as does mutation of the corresponding steric gate of Pol κ (Y112A, in which Tyr$^{112}$ is replaced by Ala) (*11*). Therefore, to test the hypothesis that DinB overproduction causes cell death by incorporating more 8-oxo-dG than the cell can tolerate, we overproduced DinB F13V and, as predicted, observed that this variant is not cytotoxic (Fig. 1A).

Although the observation that DinB F13V is not cytotoxic is consistent with our hypothesis that DinB overproduction is incorporating more 8-oxo-dG than the cell can handle, it does not exclude the possibility that the ability of DinB to copy over $N^2$-dG adducts (*12*) is contributing to cell death. Therefore, we cooverproduced MutT, a nucleotide sanitizer of the GO system that, together with MutM and MutY, minimizes the deleterious effects of oxidized guanine (*13*). MutT, which hydrolyzes 8-oxo-dGTP to 8-oxo-deoxyguanosine monophosphate (dGMP) (*13*), eliminates the cytotoxicity of DinB when cooverproduced (Fig. 1A). DinB overproduction in a Δ*mutT* strain is as cytotoxic as it is in wild-type (fig. S2), which suggests that DinB levels are rate-limiting for death, even though levels of 8-oxo-dGTP are extremely low in a Δ*mutT* mutant (*14*), a conclusion that is consistent with trace amounts of 8-oxo-dGTP usage during replication potentially having important biological consequences (*15*).

Our results are consistent with the hypothesis that DinB is incorporating more 8-oxo-dG than the cell can tolerate, but two potential mechanisms of intolerance are possible: the accumulation of lethal mutations or the formation of lethal DSBs. It is unlikely that ~50% of the cells have obtained a lethal mutation within 90 min (Fig. 1A), as DinB moves as slowly as 1 base pair (bp) per s and thus has only copied ~5400 bp per replication fork (*4*). Instead, it seems more likely that cells are dying from DSBs as previously suggested (*3*), a possibility consistent with our observation that DinB overproduction results in the up-regulation of the SOS response as measured by microarray analysis (tables S1 and S2) and cell filamentation as measured by flow cytometry (4.76-fold increase) (Fig. 1D).

Although the absolute levels of 8-oxo-dG present in DNA in an unstressed Δ*mutT* strain are too low to cause chromosomal fragmentation (*16*), a change in the levels of 8-oxo-dGTP and/or a change in the ratios of the particular DNA polymerases operating in a cell (i.e., DinB overproduction in this case) could result in closely spaced 8-oxo-dG nucleotides. Closely spaced DNA lesions are potentially problematic, because the proximity of individual DNA lesions can alter the cell's ability to repair damage (*17*) and subsequently result in DSBs (*18*). A single DSB in an *E. coli* cell has been known for decades to be potentially lethal (*19*). Thus, in principle, incomplete base excision repair by MutM and MutY glycosylases acting at closely spaced dC:8-oxo-dG and dA:8-oxo-dG pairs, respectively, could result in the generation of a lethal DSB (fig. S3). A DNA polymerase prone to using 8-oxo-dGTP as a substrate, such as DinB, would increase the likelihood of two 8-oxo-dG lesions being incorporated in close proximity and, thus, the potential for a DSB. Direct incorporation of an 8-oxo-dG by a DNA polymerase close to an existing 8-oxo-dG could also lead to a lethal DSB event via the action of GO system glycosylases (fig. S3). DSB formation by either of these mechanisms could be

[1]Department of Biology, Massachusetts Institute of Technology, Cambridge, MA 02139, USA. [2]Program in Molecular Biology, Cell Biology, and Biochemistry, Boston University, Boston, MA 02215, USA. [3]Howard Hughes Medical Institute, Department of Biomedical Engineering, and Center for BioDynamics, Boston University, Boston, MA 02215, USA. [4]Wyss Institute for Biologically Inspired Engineering, Harvard University, Boston, MA 02118, USA.

*To whom correspondence should be addressed. E-mail: gwalker@mit.edu

suppressed by MutT overproduction. In principle, the occurrence of a closely spaced dC:8-oxo-dG and 8-oxo-dG:C pair as a consequence of direct oxidation of DNA could also result in DSBs (fig. S3), but these would not be suppressible by overproduction of MutT.

The processivity of DinB interacting with the β clamp is 300 to 400 nucleotides (*20*), and thus, in principle, it could continue to replicate long enough to introduce multiple 8-oxo-dGs into DNA and so set up the potential for a MutM- and MutY-mediated DSB. Consistent with this model, a Δ*mutM* Δ*mutY* mutant is less sensitive to the cytotoxic effects of DinB overproduction (Fig. 1E). The protective effect of Δ*mutM* Δ*mutY* may be less than that of MutT overproduction, because other base excision repair enzymes that recognize 8-oxo-dG may additionally contribute to DSB formation (*13*). In addition, it is possible that MutT is also able to sanitize another oxidized deoxynucleotide triphosphate, as can the human MutT homolog (*21*), and that its incorporation into DNA contributes to DSB formation through a MutM- and MutY-independent process. Because cells repair DSBs by homologous recombination, the increased sensitivity of a Δ*recA* strain to DinB overproduction (Fig. 1E) is consistent with this model of 8-oxo-dG–mediated DSB formation. Collectively, the above data suggest that incorporation of 8-oxo-dG into DNA during replication is cytotoxic because of DSBs generated by the incomplete action of base-excision repair systems designed to protect cells from the mutagenic effects of oxidized nucleotides, i.e., the cellular protector has become the executioner.

**Bactericidal antibiotic lethality due, in part, to the oxidation of guanine nucleotides.** We then wondered whether the principle revealed by these experiments—an increase in closely spaced 8-oxo-dG lesions leading to DSBs—might also underlie cell death induced by bactericidal antibiotics. Antibiotics can generally be classified as being bacteriostatic (preventing cell growth) or bactericidal (killing cells) (*22*). Bactericidal antibiotics had long been thought to kill by means of class-specific drug interactions, which usually fall into three categories: inhibitors of cell wall biosynthesis, of DNA replication, and of protein synthesis (*23*). However, it was recently shown that a common pathway that produces $OH^{\bullet}$ substantially contributes to killing induced in Gram-negative and Gram-positive bacteria by major classes of bactericidal antibiotics (*1*). Despite having different macromolecular targets, β-lactams (cell wall synthesis inhibitors), quinolones (DNA gyrase inhibitors), and aminoglycosides (protein synthesis inhibitors) generate $OH^{\bullet}$ through the tricarboxylic acid cycle, a transient depletion of the reduced form of nicotinamide adenine dinucleotide, destabilization of iron sulfur clusters, and a stimulation of the Fenton reaction (*1*). Because $OH^{\bullet}$ are the most powerful oxidizing agent in living cells and have a half-life of nanoseconds (*24*), cell death could result from the cumulative effect of oxidizing various classes of cellular molecules and macromolecules. However, from the insights we gained into the mechanistic basis of DinB overproduction cytotoxicity, we hypothesized that, instead, the oxidation of the guanine nucleotide pool is specifically responsible for much of the death caused by bactericidal antibiotics.

To test this hypothesis, we overproduced MutT in *E. coli* and treated the resulting culture with representatives of the three different classes of antibiotics that increase $OH^{\bullet}$: ampicillin (β-lactam), norfloxacin (quinolone), and kanamycin (aminoglycoside). It was striking that simply overproducing MutT was sufficient to reduce the sensitivity of *E. coli* cells to killing by all three drugs, consistent with the hypothesis that oxidation of the guanine nucleotide pool underlies much of the cytotoxicity of bactericidal antibiotics (Fig. 2A and fig. S4A). Similarly, overproduction of RibA, an alternative 8-oxo-dGTP sanitizer (*25*), was also sufficient to reduce sensitivity to killing by ampicillin and norfloxacin (Fig. 2B). The inability of RibA to reduce the sensitivity of cells to kanamycin (Fig. 2B) is probably the consequence of kanamycin's blocking of protein synthesis coupled with the inherent instability of the RibA protein, which results in a substantial reduction of RibA protein levels after addition of the drug (fig. S5). In contrast, overproduction of NudB, a nucleotide sanitizer that preferentially hydrolyzes 8-OH-deoxyadenosine triphosphate (8-OH-dATP) in vitro and has only a twofold effect on mutation rate when overproduced in a Δ*mutT* mutant (*26*, *27*), did not affect antibiotic sensitivity (Fig. 2C).

The amount of 8-oxo-dG incorporated into DNA is influenced by a combination of the levels of 8-oxo-dGTP in the conditions being examined and the levels and characteristics of the individual polymerases that are present. To gain insights into which of the *E. coli* polymerases might be contributing to cell death

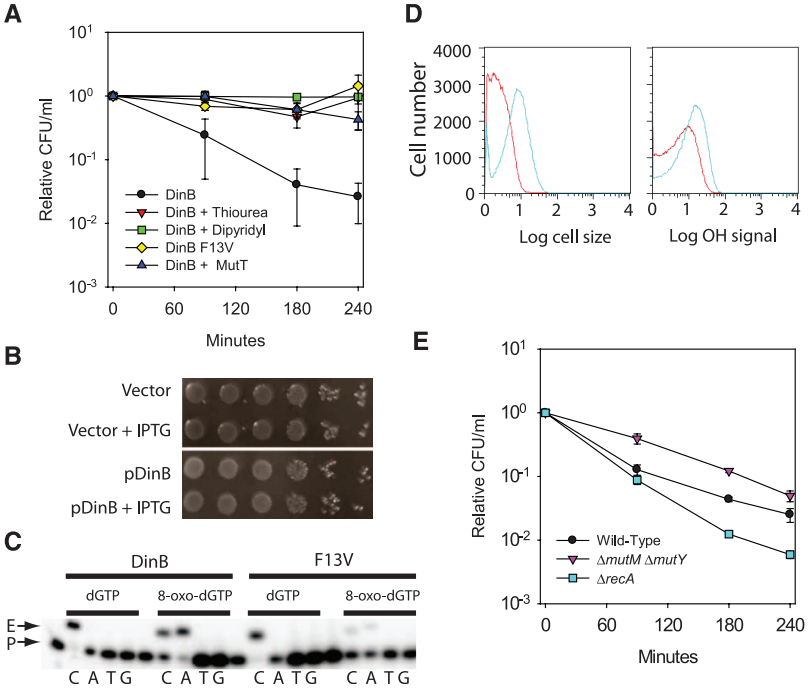


**Fig. 1.** DinB overproduction results in DSBs because of closely spaced 8-oxo-dG lesions. (**A**) Lethality of DinB overproduction (black), measured by colony-forming units (CFU) per ml relative to time zero, is reduced by thiourea (red), 2,2′-dipyridyl (green), and cooverproduction of MutT (blue). Overproduction of DinB F13V (yellow), which is incapable of incorporating 8-oxo-dG, is not lethal. (**B**) Under anaerobic conditions, DinB overproduction is not cytotoxic; cell viability was assayed by 10-fold serial dilutions of cells overproducing DinB with isopropyl-β-D-thiogalactopyranoside (pDinB + IPTG) and compared with noninduced (pDinB) and vector controls (vector and vector + IPTG). (**C**) DinB and DinB F13V (F13V) primer extension analysis using dGTP and 8-oxo-dGTP as the incoming nucleotide and the four different templating bases. The starting primer (P) and extended product (E) are indicated. Lanes 1, 6, 11, and 16 are unextended primer controls. (**D**) Overproduction of DinB for 3 hours (blue) results in cell filamentation but does not result in a substantial increase in intracellular $OH^{\bullet}$ levels when compared with an uninduced control (red). The forward-scatter histogram (left) of a DinB overproducing strain suggests cell elongatation (cell size, arbitrary units). (Right) Conversely, a modest increase in the 3′-(*p*-hydroxyphenyl) fluorescein fluorescence signal (1.6-fold) compared with the control is observed in a DinB-overproducing strain, which suggests that intracellular $OH^{\bullet}$ levels do not substantially increase ($OH^{\bullet}$ signal arbitrary units). (**E**) The lethality of DinB overproduction (black) is minimized in a Δ*mutM* Δ*mutY* background (purple) but enhanced in a Δ*recA* background (blue).

from bactericidal antibiotics by incorporating 8-oxo-dG into DNA, we tested the effect of mutating each polymerase on ampicillin cytotoxicity (fig. S6). Deletion of Δ*dinB* (DNA Pol IV) and Δ*umuDC* (DNA Pol V) reduced killing by ampicillin, which suggested that these two polymerases both contribute to ampicillin sensitivity, whereas mutations of *polA* (DNA Pol I) or *polB* (DNA Pol II) had no effect. The essential replication DNA polymerase Pol III is also involved in 8-oxo-dG incorporation because an antimutator allele of the catalytic subunit (*dnaE911*), which decreases the mutation frequency of a Δ*mutT* strain (*28*), also reduced ampicillin cytotoxicity (fig. S6). We then generated and tested a *dnaE911* Δ*dinB* Δ*umuDC* triple mutant and observed a striking reduction in sensitivity to all three classes of antibiotics (Fig. 2D and fig. S4B), consistent with Pol III, Pol IV, and Pol V's incorporation of more 8-oxo-dG than the cell can handle.

We hypothesized that the action of these polymerases under the conditions of elevated $OH^{\bullet}$ caused by the antibiotics could lead to increased 8-oxo-dG incorporation and, hence, a lethal MutM- and MutY-dependent DSB, as with DinB overproduction. We therefore treated a Δ*mutM* Δ*mutY* strain with the three different classes of antibiotics and, as anticipated, observed a significant decrease in killing, consistent with the action of these base excision repair enzymes resulting in DSBs (Fig. 3A and fig. S4C).

Deletion of Δ*recA*, which prevents DSB repair, has previously been shown to sensitize cells to antibiotics (*1*). To test whether the DSBs generated are repaired by the major RecA-dependent RecBCD pathway, we introduced a Δ*recB* mutant allele into cells and tested its effect on antibiotic cytotoxicity. The Δ*recB* mutant displayed approximately the same sensitivity as a Δ*recA* deletion, consistent with the hypothesis that the RecBCD pathway is used to repair the DSBs that are generated as a consequence of 8-oxo-dG incorporation (Fig. 3B).

To further support our hypothesis that DSBs, many of which are MutM and MutY dependent, are responsible for bactericidal cell death rather than being the result of DNA degradation in dead cells, we used the terminal deoxynucleotidyl transferase–mediated deoxyuridine triphosphate nick end labeling (TUNEL) assay. The TUNEL assay covalently attaches a fluorescent molecule to the 3′ terminus of a DNA molecule and, thus, can be used to directly measure DSBs. Thirty minutes after antibiotic treatment of wild-type cells, a time at which little cell death has occurred (Fig. 3C), we observed a qualitative increase in TUNEL-positive cells when analyzed by microscopy (Fig. 3D and fig. S7). We then quantified the number of TUNEL-positive cells in wild-type and Δ*mutM* Δ*mutY* populations after antibiotic treatment via flow cytometry (Fig. 3, E and G) and observed MutM- and MutY-dependent DSBs. Moreover, the median TUNEL signal for the Δ*mutM* Δ*mutY* strain is less than that of wild-type cells after treatment with antibiotics (Fig. 3, F and H). Collectively, these results are consistent with the hypothesis that bactericidal antibiotics lead to cell death largely by increasing the number of DSBs, a substantial fraction of which are MutM and MutY dependent.

**Extension of common mechanism model.** From the data described above, we are able to extend the model for a common mechanism of cell death induced by bactericidal antibiotics. Instead of generalized oxidative damage resulting in cell death, oxidation of the guanine nucleotide pool to 8-oxo-guanine results in several lethal outcomes. The approximately equal degree of protection from killing by β-lactams because of MutT overproduction, *dnaE911* Δ*dinB* Δ*umuDC*, and Δ*mutM* Δ*mutY* (Fig. 4) suggests that a substantial portion of the bactericidal effect of β-lactams is because of MutM- and MutY-mediated DSBs that are a consequence of Pol III, Pol IV, and Pol V's incorporation of 8-oxo-dG lesions into the daughter strand during replication (fig. S8). Penicillin, a β-lactam bactericidal antibiotic, was the first antibiotic described and was thought to kill cells primarily and specifically via inhibition of cell wall synthesis (*23*). It is noteworthy that our results suggest oxidation

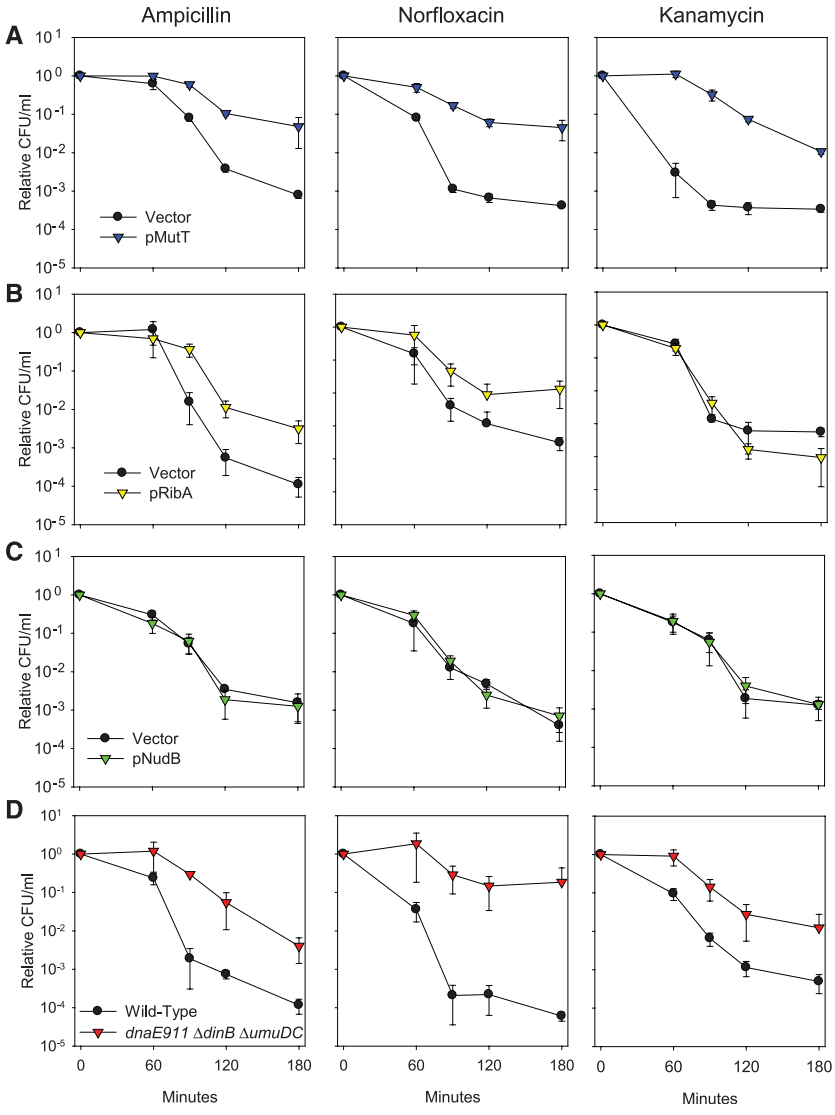


**Fig. 2.** The sensitivity of wild-type *E. coli* cells to killing by ampicillin, norfloxacin, and kanamycin is reduced when incorporation of 8-oxo-dG is minimized. (**A**) Overproduction of the 8-oxo-dGTP sanitizer MutT (blue) in wild-type MG1655 cells was sufficient to significantly reduce the sensitivity of cells to the bactericidal effects of all three classes of drugs compared with the vector control (black). (**B**) Overproduction of the alternative 8-oxo-dGTP sanitizer RibA (yellow) in MG1655 cells is also sufficient to reduce the sensitivity of cells to ampicillin and norfloxacin, but not kanamycin, probably because of its instability (fig. S5). (**C**) Overproduction of the 8-OH-dATP sanitizer NudB (green) does not reduce the antibiotic sensitivity. (**D**) A mutant strain that lacks the two Y-family DNA polymerases and expresses an antimutator replicative polymerase (*dnaE911* Δ*dinB* Δ*umuDC*) strain (red) is more resistant to killing by bactericidal antibiotics than wild-type cells (black).

of guanine nucleotides also contributes to cell death by penicillin (Fig. 4); this finding provides a new insight into the mechanism of action of the oldest known antibiotic. The approximately similar degrees of protection from killing by norfloxacin because of MutT overproduction and *dnaE911 ΔdinB ΔumuDC* indicate that an analogous mechanism is responsible for its bactericidal effects. However, the lesser degree of protection afforded by Δ*mutM* Δ*mutY* (Fig. 4) suggests that DNA gyrase inhibition additionally contributes to the DSBs caused by 8-oxo-dG incorporation (fig. S8).

This 8-oxo-dG–dependent DSB mechanism accounts for some of the bactericidal effects of kanamycin, as there is protection from killing by *dnaE911 ΔdinB ΔumuDC* and Δ*mutM* Δ*mutY*. However, our observation that the degree of protection caused by MutT overproduction is larger (Fig. 4) than that conferred by *dnaE911 ΔdinB ΔumuDC* or Δ*mutM* Δ*mutY*, together with the relatively modest increases in sensitivity conferred by the Δ*recA* and Δ*recB* mutants, suggests that an additional mechanism of cell killing is involved in the case of kanamycin. The reduced involvement of the 8-oxo-dG–dependent DSB mode of killing may, in part, be due to its translational inhibitory effects, which prevent the synthesis of SOS-regulated proteins (including the *dinB*- and *umuDC*-encoded DNA polymerases), other proteins required for stress responses, and antitoxins (leading to activation of their cognate toxins). Nevertheless, the strong suppression of kanamycin cytotoxicity by MutT overproduction suggests that, in addition to their known direct effect on the ribosome (*29*), a substantial amount of the cytotoxicity caused by aminoglycosides in vivo is due to oxidation of guanine nucleotides.

An intriguing hypothesis is that the protective effect of MutT overproduction is due to MutT's ability to sanitize the guanine ribonucleotide pool [8-oxo-guanosine triphosphate (8-oxo-rGTP) and 8-oxo-guanosine diphosphate (8-oxo-rGDP)] (*30*, *31*), as well as the guanine deoxynucleotide pool (fig. S8). RNA polymerase proficiently uses 8-oxo-rGTP as a substrate, incorporating 8-oxo-guanosine (8-oxo-rG) into transcripts at 1/10th the rate that it incorporates rG (*30*). These potentially altered transcripts could lead to mistranslated proteins, which is consistent with the previous observation that Δ*mutT* strains exhibit higher levels of protein carbonylation (*32*), a consequence of protein mistranslation. Moreover, the effect of 8-oxo-rGTP on protein mistranslation would be exacerbated by its misincorporation into ribosomal RNA and transfer RNA, which would be expected to further reduce the fidelity of protein synthesis. This potential for kanamycin-induced 8-oxo-rGTP–dependent mistranslation of cell envelope proteins could, in turn, cause more membrane alterations and could lead to increased drug uptake and further stimulation of the $OH^{\bullet}$ radical pathway through membrane stress two-component systems (Cpx) and

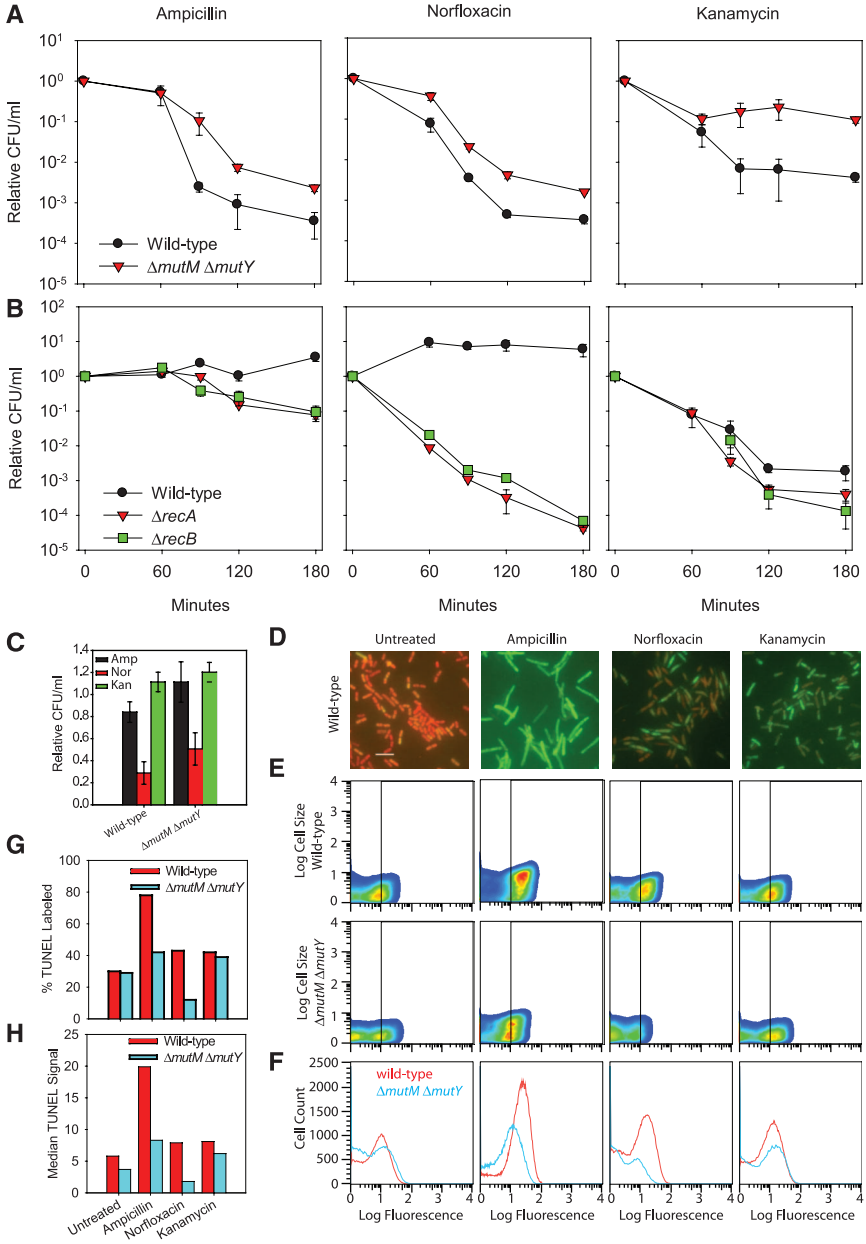


**Fig. 3.** Bactericidal antibiotics cause lethal DSBs. (**A**) A Δ*mutM* Δ*mutY* strain is less sensitive than wild-type cells to bactericidal antibiotic killing. (**B**) Deletion of Δ*recA* and Δ*recB* sensitizes cells to killing by bactericidal antibiotics. Relative CFU/ml of wild-type (black), Δ*recA* (red), and Δ*recB* (green) cells treated with 2 μg/ml ampicillin, 25 ng/ml norfloxacin, and 3 μg/ml kanamycin. (**C**) Neither ampicillin nor kanamycin treatments for 30 min significantly reduced the number of viable wild-type or Δ*mutM* Δ*mutY* cells. Norfloxacin treatment for 30 min results in a reduction in viable cell number for both wild-type (29% survival) and Δ*mutM* Δ*mutY* cells (51% survival). (**D**) Representative fields of wild-type cells after 30 min of treatment. Cells containing a DSB (TUNEL-positive, green) were overlaid on the propidium iodine staining of all cells (red). Scale bar, 5 μM. (**E**) Pseudocolor plot of cell size versus TUNEL fluorescence for untreated and treated wild-type and Δ*mutM* Δ*mutY* cells at 30 min. The vertical line at 10 fluorescence units is the cutoff of TUNEL-positive cells, which results in 30% of untreated wild-type cells being TUNEL-positive consistent with our microscopy results (~28% TUNEL-positive cells: 81 green out of 292 cells). The number of TUNEL-positive wild-type cells increases after antibiotic treatment (top), and Δ*mutM* Δ*mutY* cells (bottom) have fewer TUNEL-positive cells than wild-type. Both cell size (forward scatter) and fluorescence signal (TUNEL signal) are in arbitrary units (A.U.). (**F**) The distributions of the fluorescence intensity of wild-type (red) and Δ*mutM* Δ*mutY* (blue) TUNEL-stained cells suggest that Δ*mutM* Δ*mutY* cells have fewer dsDNA breaks. (**G**) The percentage of positive TUNEL-labeled cells (≥10 A.U.) determined in (E) is plotted for both wild-type (red) and Δ*mutM* Δ*mutY* (blue). (**H**) Histogram of the median TUNEL signal for the wild-type and Δ*mutM* Δ*mutY* populations shown in (F).

changes in metabolic function (Arc) (*29*). Thus, kanamycin treatment could potentially result in a catastrophic cycle of mistranslation driven by 8-oxo-rGTP.

It is also possible that 8-oxo-rGTP and 8-oxo-rGDP contribute to cell killing by interfering with the functioning of guanosine triphosphatases (GTPases), 13 of which are conserved in 75% of bacteria and most of which have critical functions in translation (*33*). For example, the reduced ability of the essential *E. coli* GTPase, Era, to hydrolyze 8-oxo-rGTP, compared with GTP (fig. S9), could alter the ratio between its GTP- and GDP-bound forms. In addition, oxidation of guanosine pentaphosphate or tetraphosphate [(p)ppGpp] could potentially interfere with the proper operation of the bacterial stringent response (*34*). Such bactericidal effects stemming from oxidation of the guanine ribonucleotide pool likely contribute to bactericidal effects of ampicillin and norfloxacin as well, but they appear to be less important than those mediated by the oxidation of the guanine deoxyribonucleotide pool.

**Broad implications.** Our model has two broad implications for the effectiveness of bactericidal antibiotics. First, in addition to a bacterial cell's intrinsic permeability to a drug and its ability to excrete it through drug pumps, our results suggest that its complement of DNA polymerases, DNA repair enzymes, and nucleotide sanitizers, such as MutT, could also play a role in a bacterium's intrinsic susceptibility to antibiotics. It is known that *E. coli* cells maintain a constant level of MutT after antibiotic stress (*1*), which suggests that a fitness cost may be associated with up-regulation of nucleotide sanitizers, perhaps decreasing mutagenesis that could lead to multidrug resistance (*35*). Second, the enhanced utilization of 8-oxo-guanine in nucleic acid transactions resulting in bacterial cell death could provide an avenue for identifying targets for the use of antimicrobial adjuvants. In the last few decades, only a handful of new classes of antibiotics have been introduced, which has led many to lament that the antibiotic pipeline is broken (*36*, *37*). Although new antimicrobial therapies are needed, adjuvants have the potential to extend the usefulness of current therapies. Our results suggest, for example, that bactericidal antibiotics could be potentiated by targeting proteins involved in repairing dsDNA breaks, e.g., inhibiting RecA or RecBCD, or by influencing the incorporation of 8-oxo-guanine into the DNA and RNA or the consequences of this incorporation.

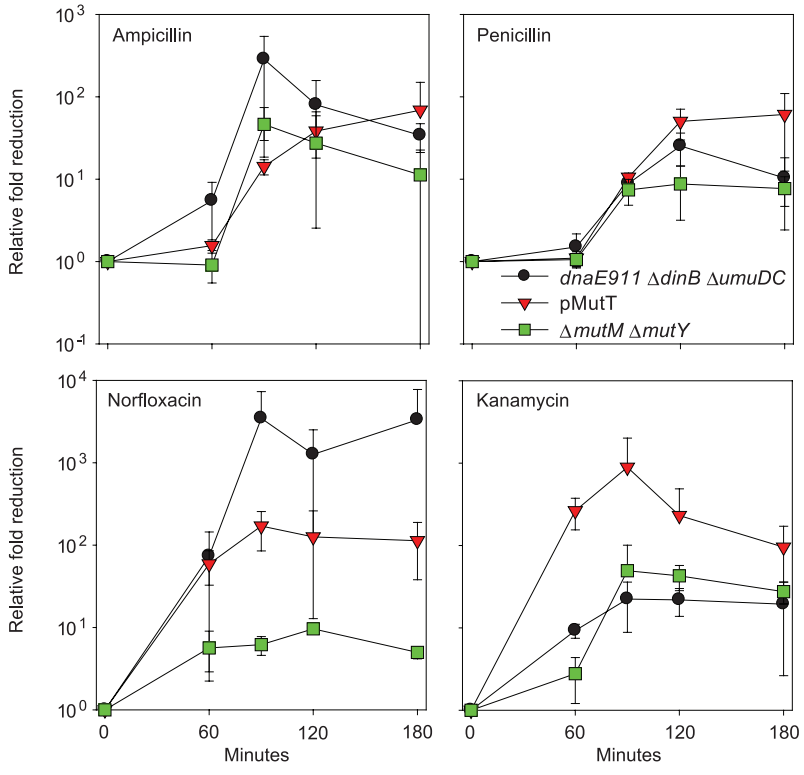


**Fig. 4.** Relative protective effect against killing because of MutT overproduction, mutation of three DNA polymerases (*dnaE911 ΔdinB ΔumuDC*), and *ΔmutM ΔmutY* for β-lactams, norfloxacin, and kanamycin suggests oxidation of guanine mediates bactericidal antibiotic–induced cell death. For β-lactams (ampicillin and penicillin), a similar fold rescue is observed for all three conditions. For norfloxacin, a similar degree of protection is afforded by MutT overproduction and mutation of the DNA polymerases, but a lesser degree of protection is observed for *ΔmutM ΔmutY*. For kanamycin, the greater fold rescue associated with MutT overproduction compared with *dnaE911 ΔdinB ΔumuDC* and *ΔmutM ΔmutY* suggests oxidation of the guanine to 8-oxo-rGTP is additionally contributing to cell death.


**References and Notes**

1. M. A. Kohanski, D. J. Dwyer, B. Hayete, C. A. Lawrence, J. J. Collins, *Cell* **130**, 797 (2007).
2. B. W. Davies *et al.*, *Mol. Cell* **36**, 845 (2009).
3. K. Uchida *et al.*, *Mol. Microbiol.* **70**, 608 (2008).
4. C. Indiani, L. D. Langston, O. Yurieva, M. F. Goodman, M. O'Donnell, *Proc. Natl. Acad. Sci. U.S.A.* **106**, 6031 (2009).
5. J. A. Imlay, S. M. Chin, S. Linn, *Science* **240**, 640 (1988).
6. A. Novogrodsky, A. Ravid, A. L. Rubin, K. H. Stenzel, *Proc. Natl. Acad. Sci. U.S.A.* **79**, 1171 (1982).
7. J. E. Repine, R. B. Fox, E. M. Berger, *J. Biol. Chem.* **256**, 7094 (1981).
8. D. Touati, M. Jacques, B. Tardat, L. Bouchard, S. Despied, *J. Bacteriol.* **177**, 2305 (1995).
9. S. Haghdoost, L. Sjölander, S. Czene, M. Harms-Ringdahl, *Free Radic. Biol. Med.* **41**, 620 (2006).
10. W. L. Neeley, J. M. Essigmann, *Chem. Res. Toxicol.* **19**, 491 (2006).
11. A. Katafuchi *et al.*, *Nucleic Acids Res.* **38**, 859 (2010).
12. D. F. Jarosz, V. G. Godoy, J. C. Delaney, J. M. Essigmann, G. C. Walker, *Nature* **439**, 225 (2006).
13. E. C. Friedberg *et al.*, *DNA Repair and Mutagenesis* (American Society for Microbiology, Washington, DC, ed. 2, 2005).
14. M. L. Tassotto, C. K. Mathews, *J. Biol. Chem.* **277**, 15807 (2002).
15. Z. F. Pursell, J. T. McDonald, C. K. Mathews, T. A. Kunkel, *Nucleic Acids Res.* **36**, 2174 (2008).
16. E. Rotman, A. Kuzminov, *J. Bacteriol.* **189**, 6976 (2007).
17. J. F. Ward, J. W. Evans, C. L. Limoli, P. M. Calabro-Jones, *Br. J. Cancer Suppl.* **8**, 105 (1987).
18. D. J. Brenner, J. F. Ward, *Int. J. Radiat. Biol.* **61**, 737 (1992).
19. T. Bonura, C. D. Town, K. C. Smith, H. S. Kaplan, *Radiat. Res.* **63**, 567 (1975).
20. J. Wagner, S. Fujii, P. Gruz, T. Nohmi, R. P. Fuchs, *EMBO Rep.* **1**, 484 (2000).
21. K. Fujikawa *et al.*, *J. Biol. Chem.* **274**, 18201 (1999).
22. G. A. Pankey, L. D. Sabath, *Clin. Infect. Dis.* **38**, 864 (2004).
23. C. Walsh, *Nature* **406**, 775 (2000).
24. B. Goodell *et al.*, *J. Biotechnol.* **53**, 133 (1997).
25. M. Kobayashi *et al.*, *J. Biol. Chem.* **273**, 26394 (1998).
26. M. Hori, K. Fujikawa, H. Kasai, H. Harashima, H. Kamiya, *DNA Repair (Amst.)* **4**, 33 (2005).
27. M. Hori *et al.*, *Biol. Pharm. Bull.* **29**, 1087 (2006).
28. I. J. Fijalkowska, R. L. Dunn, R. M. Schaaper, *Genetics* **134**, 1023 (1993).
29. M. A. Kohanski, D. J. Dwyer, J. Wierzbowski, G. Cottarel, J. J. Collins, *Cell* **135**, 679 (2008).
30. F. Taddei *et al.*, *Science* **278**, 128 (1997).
31. R. Ito, H. Hayakawa, M. Sekiguchi, T. Ishibashi, *Biochemistry* **44**, 6670 (2005).
32. S. Dukan *et al.*, *Proc. Natl. Acad. Sci. U.S.A.* **97**, 5746 (2000).
33. C. E. Caldon, P. Yoong, P. E. March, *Mol. Microbiol.* **41**, 289 (2001).
34. J. Wu, J. Xie, *J. Cell. Physiol.* **220**, 297 (2009).
35. M. A. Kohanski, M. A. DePristo, J. J. Collins, *Mol. Cell* **37**, 311 (2010).
36. M. A. Cooper, D. Shlaes, *Nature* **472**, 32 (2011).
37. C. M. Morel, E. Mossialos, *BMJ* **340**, c2115 (2010).



**Acknowledgments:** The authors thank S. Bell and D. Kim for use of equipment and S. Lovett for strains. This work was supported by NIH grants R01 CA021615 (to G.C.W.), F32 GM079885 (to J.J.F.), DP1 OD003644 (to J.C.C.), and P30 ES002019 (to the Massachusetts Institute of Technology Center for Environmental Sciences) as well as the Howard Hughes Medical Institute. G.C.W. is an American Cancer Society Professor.


**Supplementary Materials**

www.sciencemag.org/cgi/content/full/336/6079/315/DC1
Materials and Methods
Figs. S1 to S9
Tables S1 to S3
References (*38*–*48*)


16 January 2012; accepted 13 March 2012
10.1126/science.1219192

# Interplay of Intra- and Intermolecular H-Bonding in a Progressively Solvated Macrocyclic Peptide

Natalia S. Nagornova, Thomas R. Rizzo, Oleg V. Boyarkin*

Studying solvation of a large molecule on an atomic level is challenging because of the transient character and inhomogeneity of hydrogen bonding in liquid water. We studied water clusters of a protonated macrocyclic decapeptide, gramicidin S, which were prepared in the gas phase and then cooled to cryogenic temperatures. The experiment spectroscopically tracked fine structural changes of the clusters upon increasing the number of attached water molecules from 1 to 50 and distinguished vibrational fingerprints of different conformers. The data indicate that only the first two water molecules induce a substantial change of the gramicidin S structure by breaking two intramolecular noncovalent bonds. The peptide structure remains largely intact upon further solvation, reflecting the interplay between the strong intramolecular and weaker intermolecular hydrogen bonds.

A particularly important property of water molecules is their formation of hydrogen bonds with one another and with hydrophilic parts of solutes such as proteins. The subtle balance between these intermolecular interactions and the internal noncovalent bonds in a biomolecule largely determines its three-dimensional (3D) structure and biological functionality (*1*, *2*). The interactions of biomolecules with the surrounding water network are difficult to study in liquids because of inhomogeneity of these interactions, the dynamical nature of the hydrogen bonds, and the essentially infinite number of molecular degrees of freedom of the solvent (*3*). Isolation of biomolecules in the gas phase removes all interactions with the solvent but also enables stepwise control of these interactions by progressively increasing the number of the bound water molecules, ultimately bridging the gap between the gas phase and aqueous conditions. Here, we report a spectroscopic study that tracks changes in the structure of a decapeptide antibiotic, gramicidin S (GS), upon addition of 1 to 50 water molecules in a gas-phase cluster. Cryogenic cooling of the clusters initially formed at room temperature suppresses dynamical effects on the spectra, whereas the use of a conformer-selective spectroscopic scheme enables detection of vibrational transitions in single conformations. We learn about the most stable binding sites of water and the nature of the H-bonded network that grows as the number of incorporated water molecules increases.

Laboratoire de Chimie Physique Moléculaire, École Polytechnique Fédérale de Lausanne (EPFL), CH-1015 Lausanne, Switzerland.

*To whom correspondence should be addressed. E-mail: oleg.boiarkin@epfl.ch

Mass spectrometry, ion mobility, and laser spectroscopy, as well as combinations of these techniques, have demonstrated the ability to characterize pure water clusters and hydrated biomolecular complexes (*4*–*14*). To solve a 3D molecular structure, spectroscopy relies on measuring a "fingerprint" (a set of frequencies and intensities) of electronic or vibrational transitions, which must be reproduced by theory. To be uniquely characteristic, a spectroscopic fingerprint has to contain a sufficiently high number of vibrationally resolved transitions. This, however, becomes problematic for large clusters because of the thermal congestion in room temperature spectra, the presence of conformational heterogeneity, and the increasing number of vibrational modes of such species. Currently, structural identifications via vibrational spectroscopy are limited to amino acids and small peptides complexed with a few water molecules (*11*, *15*–*23*). Although such studies are valuable, there is a clear and pressing need for investigation of larger peptides with more direct biological relevance, solvated by a sufficiently large number of water molecules to approximate at least the first solvation shell. Here, we present well-resolved spectroscopic fingerprints for a protonated decapeptide solvated by up to a few tens of water molecules.

The 3D structure of the antibiotic gramicidin S (cyclo-VOLFPVOLFP, where O designates ornithine; F, the D rather than L enantiomer of phenylalanine; V, valine; L, leucine; and P, proline) was solved by nuclear magnetic resonance (NMR) spectroscopy (*24*) and x-ray diffraction (*25*) in the condensed phase and recently by the method of cold ion spectroscopy in the gas phase (fig. S1) (*26*, *27*). Doubly protonated gramicidin S, $[GS + 2H]^{2+}$, exhibits strong antibacterial activity in vivo by binding to phospholipids of bacteria cell membranes (*28*). The structure of the antibiotic under such conditions has yet to be determined in silico by using the intrinsic and native structures of $[GS + 2H]^{2+}$ as starting points together with an understanding of the interplay between the intra- and intermolecular hydrogen bonding. Our study of gradually solvated $[GS + 2H]^{2+}$ provides the opportunity for detailed modeling of this interplay in a large molecule.

Water clusters of $[GS + 2H]^{2+}$ were produced directly from an aqueous solution by using electrospray ionization (fig. S2). The clusters of a desired size were selected by a quadrupole mass filter, cooled to ~12 K in an ion trap (*29*), and then photofragmented by pulsed ultraviolet (UV) excitation of the phenylalanine chromophores.

Figure 1 shows UV photofragmentation spectra of cold $[GS + 2H]^{2+}(H_2O)_n$ clusters, where $n$ indicates the number of water molecules ($0 \leq n \leq 50$). Cooling allows vibrational resolution in the UV spectra of $[GS + 2H]^{2+}$ with up to 29 water molecules. The spectra shown in Fig. 1 provide some hints for structural changes of the clusters upon their gradual solvation. The 3D structure of bare $[GS + 2H]^{2+}$ exhibits four strong hydrogen bonds between Val and Leu residues, as well as binding of the protonated amino group of the ornithine to carbonyls on the Phe and Orn residues and to the Phe aromatic rings (fig. S1) (*27*). The latter $NH_3^+$-π electron interaction leads to a ~200 $cm^{-1}$ shift of the UV band origin to higher energy (blue shift) relative to that of several reference species where the charge is remote from the phenylalanine chromophore (*26*). Binding two water molecules to $[GS + 2H]^{2+}$ leads to a large shift halfway back (red shift) toward the band origin of these reference species, whereas further hydration exhibits little influence on the UV band origin of the clusters.

This observation suggests that the first two water molecules bind to protonated amino groups, weakening the $NH_3^+$-π interactions such that the two aromatic rings become almost decoupled from the $[GS + 2H]^{2+}$ backbone. Although the details of the peptide structure reflected in UV spectra (Fig. 1 and fig. S3) still change upon further solvation, this decoupling by only two water molecules leads to a substantial elongation of $[GS + 2H]^{2+}$, its structure thereby approaching that of the fully solvated species (*24*, *25*). The fact that red shifts of the UV band origins of all larger clusters are at least as large as for the $n = 2$ species implies that the hydration sites near the two charges remain occupied in all studied water complexes, although not necessarily in all their conformations.

In addition to the strongly red-shifted peaks, the UV spectrum of the $n = 2$ cluster in Fig. 1 exhibits another group of intense peaks that are close to the band origin of bare $[GS + 2H]^{2+}$. This observation suggests a certain conformational heterogeneity of the clusters, in which some may contain either one or two unsolvated ammonium groups. To verify this hypothesis, we

performed infrared (IR)–UV double resonance studies, wherein vibrational preexcitation of peptides by an IR pulse alters their subsequent UV fragmentation yield (*30*–*32*). Figure 2 shows selected conformer-specific IR spectra for clusters with $n \leq 15$. Beyond the typical well-resolved free OH stretches (~3700 $cm^{-1}$), all the spectra exhibit rich structure with many sharp peaks, making them highly specific fingerprints of the cluster structures. The characteristic CH stretch band around 2970 $cm^{-1}$ also exhibits sharp peaks that remain unshifted and almost identical, even for large clusters. This persistence reflects a high degree of hydrophobicity of GS and the low sensitivity of CH stretch frequencies to the binding of water molecules.

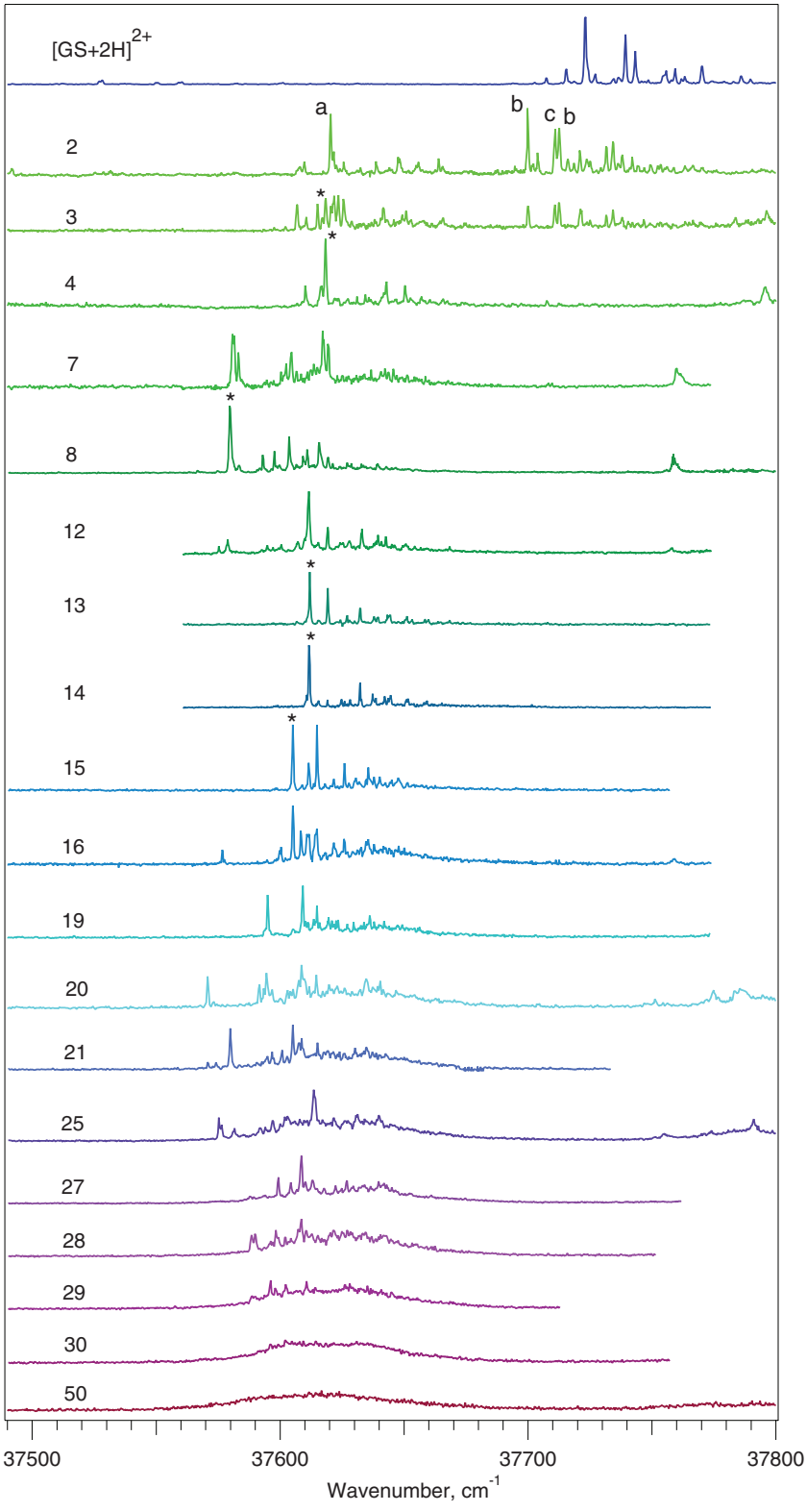


**Fig. 1.** Electronic spectra of cold, doubly protonated gramicidin S and its complexes with $n$ water molecules, $[GS + 2H]^{2+}(H_2O)_n$ ($2 \leq n \leq 50$), measured by detecting the fragment complexes $[GS + 2H]^{2+}(H_2O)_m$ with $m = n - 16 \pm 1$ for $n > 16$ but $[GS + 2H]^{2+}$ for $2 \leq n \leq 15$. Letters a, b, c and asterisks label the transitions used for conformer-selective IR spectroscopy (Fig. 2).

Figure 2, a to c, shows IR spectra of $[GS + 2H]^{2+}(H_2O)_2$ measured on the UV peaks, labeled as a, b, and c in Fig. 1. The specific fingerprint of the two water molecules comprises a sharp band near 3700 $cm^{-1}$ (free OH) and a broad band within 3350 to 3430 $cm^{-1}$ (H-bonded OH). The fact that these three spectra are different indicates that the species associated with the UV transitions a, b, and c in Fig. 1 have different structure and therefore must be assigned to three different conformers (labeled respectively a, b, and c) of the $n = 2$ clusters. Only one of them is associated with the red-shifted peak (a) in the UV spectrum and should have a structure in which both phenylalanine aromatic rings are free of strong cation-π bonding to the $NH_3^+$ of the ornithine side chains. Solvation of $[GS + 2H]^{2+}$ by two water molecules substantially shifts the $NH_3^+$ stretch bands near 3240 $cm^{-1}$ (assigned to the NH bonds that point to the aromatic rings) to lower energy and the NH stretch band of the Phe backbone to the high-energy side for this conformer only; this conformer also exhibits the lowest free water-OH stretch frequency among the three. These observations support our assessment that in conformer a the water molecules are strongly H bonded to the charged amine groups, decoupling the aromatic rings from the backbone of the peptide.

The higher frequencies of the free OH-stretch water band in the two other conformers imply weaker couplings between $[GS + 2H]^{2+}$ and $H_2O$ molecules. The NH stretch band of the Orn backbone is the only one that experiences a substantial wave number shift upon hydration, because the nearest peaks that can be assigned to this vibration appear 26 $cm^{-1}$ to the red (Fig. 2, b) and 70 $cm^{-1}$ to the blue (Fig. 2, c) from the position of this band in the bare molecule. On the basis of this observation and taking into account hydrogen bonding of the Orn amide NH to the Pro carbonyl group in isolated $[GS + 2H]^{2+}$ (*27*), we suggest an involvement of these residues as hydration sites in conformers b and c in the doubly solvated species. These conformer-selective IR spectra provide a challenge and a benchmark for theory, and only when agreement is reached in the positions and assignments of vibrational transitions can we have confidence in the exact binding sites and structures of these three conformers of $[GS + 2H]^{2+}(H_2O)_2$.

This computational challenge becomes more acute for GS hydrated with an increasing number of water molecules. To help in making spectral assignments for larger clusters, we used

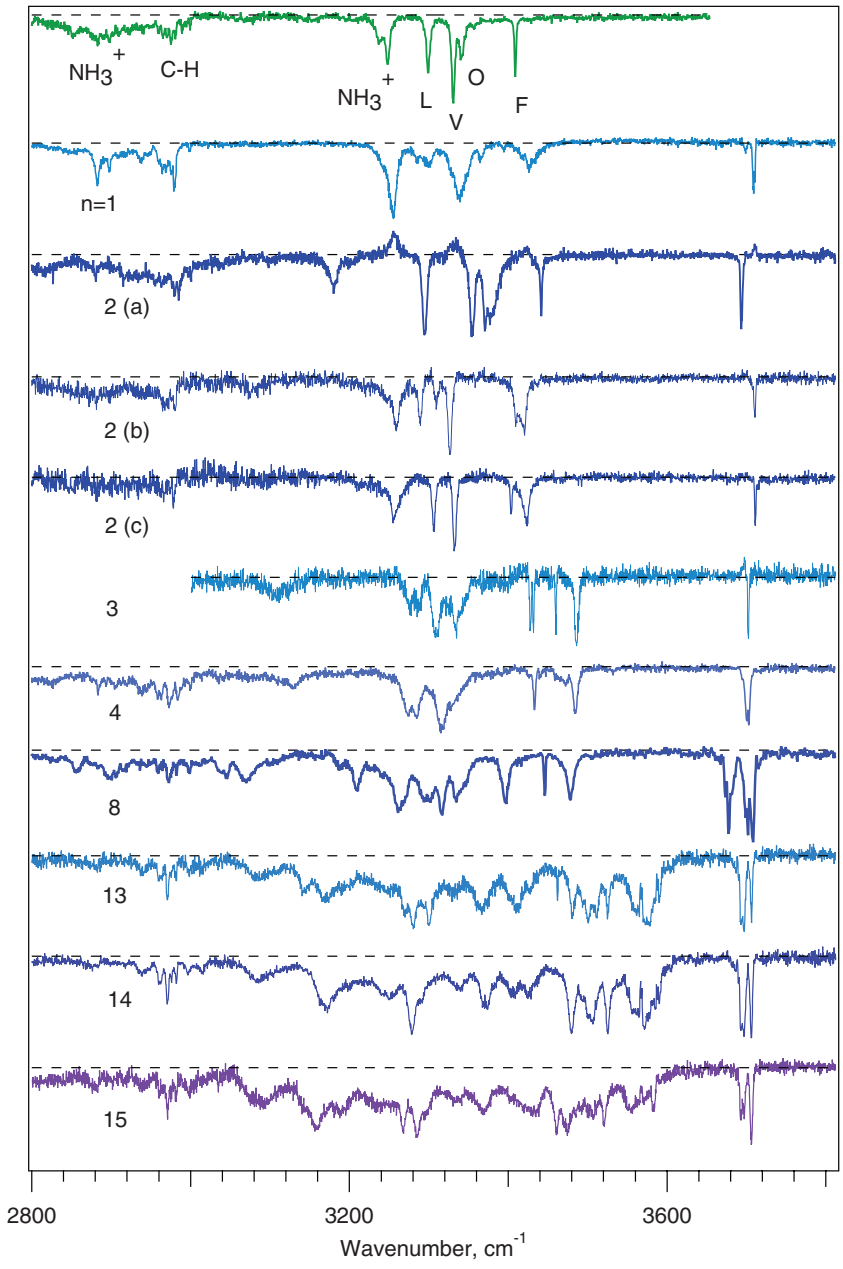


**Fig. 2.** Samples of conformation-selective, IR-UV depletion spectra of $[GS + 2H]^{2+}(H_2O)_n$ ($n$ = 2 to 15) complexes measured by fixing the UV wave number at the electronic transitions labeled in Fig. 1. The spectrum of singly hydrated gramicidin S ($n$ = 1) has been measured by IR photodissociation of the complex, detecting the bare $[GS + 2H]^{2+}$ fragment, and it is not conformer-selective. The spectra of conformers a, b, and c of the $n$ = 2 clusters are labeled respectively. For comparison, a spectrum of $[GS + 2H]^{2+}$ (*27*) with the assignments of the amide N-H stretches of the phenylalanine (F), ornithine (O), valine (V), and leucine (L) residues; the N-H stretches of the ornithine $NH_3^+$ groups; and the C-H stretches of the molecule are shown on the top of the figure.

isotopic substitution to distinguish vibrational bands of water from those of $[GS + 2H]^{2+}$. Figure 3 illustrates this approach by comparing conformation-selective IR spectra of $n$ = 8 clusters composed of $H_2{}^{16}O$ with those of its isotopologue, $H_2{}^{18}O$. Oxygen-18 isotopic substitution lowers the wave number of OH stretch vibrations by ~10 $cm^{-1}$ but doesn't influence noticeably the vibrational frequencies of $[GS + 2H]^{2+}$ itself. This allows a straightforward assignment of the remaining peaks in Fig. 3 to NH and CH stretch vibrations of solvated $[GS + 2H]^{2+}$, whereas the shifted peaks are assigned to water stretch vibrations.

The assignment of the $[GS + 2H]^{2+}$ bands to particular vibrations is more complicated because of the effect of bound water in broadening and shifting the bands or splitting the doubly degenerate amide NH bands of the Phe, Orn, Val, and Leu residues. The only band that we can confidently assign on the basis of its sharpness and a substantial blue shift (relative to that in $[GS + 2H]^{2+}$) is the isolated peak at 3445.7 $cm^{-1}$, which we attribute to the NH stretch of Phe. Similar to our consideration of doubly solvated $[GS + 2H]^{2+}$, such a shift indicates some remoteness of the phenylalanine ring from the peptide backbone and suggests solvation of the $NH_3^+$ charges by water molecules. This suggestion is fully consistent with our earlier conclusion that the large red shift of the UV transition that we used for measuring the IR spectra (Fig. 1) indicates hydration of the $NH_3^+$ groups in the $n$ = 8 species. Occupation of these binding sites would be consistent with an assignment of the split band at ~3050 $cm^{-1}$ to the two $NH_3^+$ stretches in which hydrogen atoms are involved in the coupling to the aromatic rings in $[GS + 2H]^{2+}$. We observed a very similar red shift and splitting of this band in IR spectra of $[GS + 2H]^{2+}$ complexed with two crown ether molecules (18-crown-6) (*27*), which form particularly strong hydrogen bonds with $NH_3^+$, although the use of crown ether molecules to model charge solvation by water is only a very rough approximation. For $n \leq 15$, the largest red shifts of both the UV band origin and the $NH_3^+$ stretch bands in the IR spectrum observed for $n$ = 8 clusters correlate with the elevated abundance of the species with this "magic" number in the cluster distribution measured earlier (*6*)

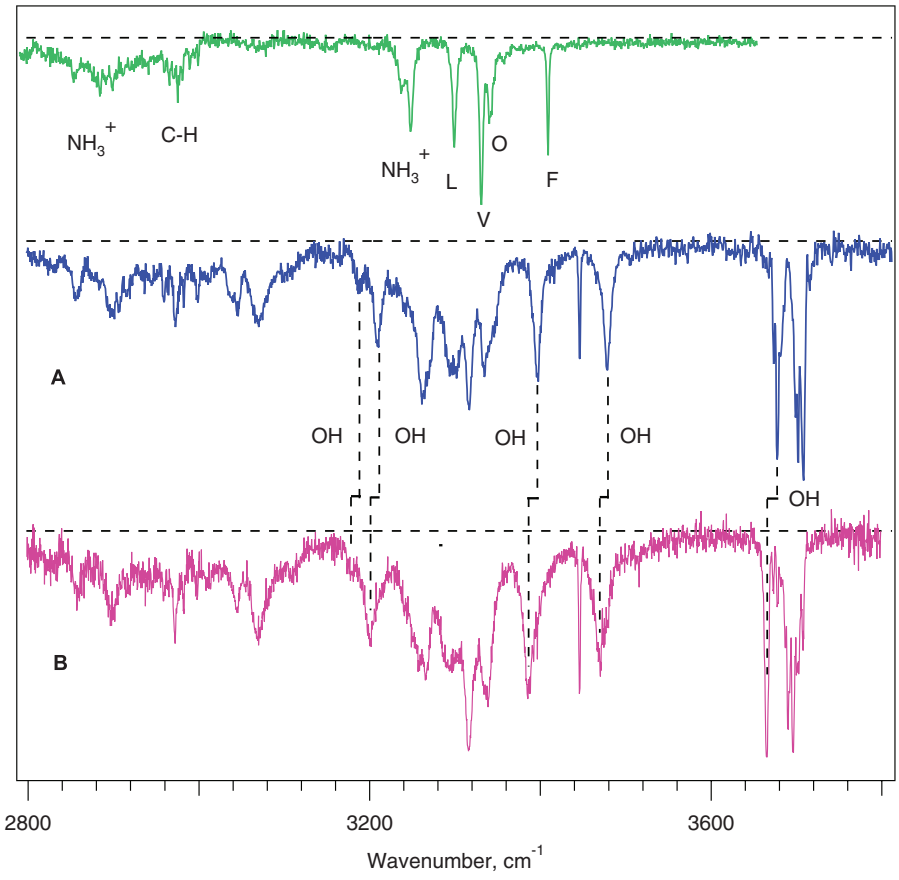


**Fig. 3.** Conformation-selective IR-UV depletion spectra of the (**A**) $[GS + 2H]^{2+}(H_2{}^{16}O)_8$ and (**B**) $[GS + 2H]^{2+}(H_2{}^{18}O)_8$ complexes, measured by fixing the UV wave number on the band origins of electronic transitions in the respective complexes. For comparison, an IR-UV depletion spectrum of fully dehydrated $[GS + 2H]^{2+}$ (*27*) with peak assignments is shown on the top of the figure.

and here (fig. S2). This prompts us to suggest that the elevated local stability of $n = 8$ clusters originates from the high degree of hydration of the $NH_3{}^+$ groups.

In addition to the commonly observed free OH stretch vibrations, the spectrum in Fig. 3A reveals four narrow ($\leq$10 $cm^{-1}$) bands associated with strongly hydrogen-bonded stretch vibrations of $H_2O$. The observation of only four such bands to describe binding of eight water molecules may indicate double degeneracy of these bands, implying certain symmetry for the water network structure of this cluster, although we cannot fully rule out the possibility that overlap with the bands of GS obscures some water OH bands. Another surprising observation is that the phenylalanine amide NH stretch band remains characteristically narrow in the IR spectrum of $n = 13$ clusters (Fig. 2), implying that it does not form a hydrogen bond even in the presence of 13 water molecules.

Ahead of yet-challenging calculations, our UV and IR spectra suggest a large structural change of the doubly protonated decapeptide, gramicidin S, induced by the first two bound water molecules, which solvate charges and break internal cation π bonds. Further solvation by water fails to interrupt the strong intramolecular hydrogen bonds of GS and causes little additional structural change. We demonstrate that a complex spectroscopic fingerprint of a cold cluster can be decomposed into the features that reflect structure of the peptide itself and to those that are ascribed to the bonded water network. These data provide two sets of accurate constraints for theory to model the structure of the solvated antibiotic GS itself and the pattern of the surrounding water network on an atomic level.

### References and Notes


1. W. Kauzmann, *Adv. Protein Chem.* **14**, 1 (1959).
2. A. R. Fersht *et al.*, *Nature* **314**, 235 (1985).
3. E. S. Manas, Z. Getahun, W. W. Wright, W. F. DeGrado, J. M. Vanderkooi, *J. Am. Chem. Soc.* **122**, 9883 (2000).
4. L. I. Yeh, M. Okumura, J. D. Myers, J. M. Price, Y. T. Lee, *J. Chem. Phys.* **91**, 7319 (1989).
5. C. J. Gruenloh *et al.*, *Science* **276**, 1678 (1997).
6. S. E. Rodriguez-Cruz, J. S. Klassen, E. R. Williams, *J. Am. Soc. Mass Spectrom.* **8**, 565 (1997).
7. M. Miyazaki, A. Fujii, T. Ebata, N. Mikami, *Science* **304**, 1134 (2004); 10.1126/science.1096037.
8. J.-W. Shin *et al.*, *Science* **304**, 1137 (2004); 10.1126/science.1096466.
9. D. Liu, T. Wyttenbach, P. E. Barran, M. T. Bowers, *J. Am. Chem. Soc.* **125**, 8458 (2003).
10. J. M. Headrick *et al.*, *Science* **308**, 1765 (2005).
11. A. Kamariotis *et al.*, *J. Am. Chem. Soc.* **128**, 905 (2006).
12. B. Gao, T. Wyttenbach, M. T. Bowers, *J. Am. Chem. Soc.* **131**, 4695 (2009).
13. T. Hamashima, K. Mizuse, A. Fujii, *J. Phys. Chem. A* **115**, 620 (2011).
14. J. S. Prell, T. M. Chang, J. T. O'Brien, E. R. Williams, *J. Am. Chem. Soc.* **132**, 7811 (2010).
15. T. S. Zwier, *J. Phys. Chem. A* **105**, 8827 (2001).
16. E. G. Robertson, J. P. Simons, *Phys. Chem. Chem. Phys.* **3**, 1 (2001).
17. L. C. Snoek, R. T. Kroemer, J. P. Simons, *Phys. Chem. Chem. Phys.* **4**, 2130 (2002).
18. P. Çarçabal *et al.*, *Phys. Chem. Chem. Phys.* **6**, 4546 (2004).
19. T. Ebata *et al.*, *Phys. Chem. Chem. Phys.* **8**, 4783 (2006).
20. S. R. Mercier *et al.*, *J. Am. Chem. Soc.* **128**, 16938 (2006).
21. N. C. Polfer, J. Oomens, *Mass Spectrom. Rev.* **28**, 468 (2009).
22. H. S. Biswal, Y. Loquais, B. Tardivel, E. Gloaguen, M. Mons, *J. Am. Chem. Soc.* **133**, 3931 (2011).
23. K. Schwing, C. Reyheller, A. Schaly, S. Kubik, M. Gerhards, *ChemPhysChem* **12**, 1981 (2011).
24. Y. Xu, I. P. Sugár, N. R. Krishna, *J. Biomol. NMR* **5**, 37 (1995).
25. A. L. Llamas-Saiz, G. M. Grotenbreg, M. Overhand, M. J. van Raaij, *Acta Crystallogr. D Biol. Crystallogr.* **63**, 401 (2007).
26. N. S. Nagornova, T. R. Rizzo, O. V. Boyarkin, *J. Am. Chem. Soc.* **132**, 4040 (2010).
27. N. S. Nagornova *et al.*, *Angew. Chem. Int. Ed.* **50**, 5383 (2011).
28. E. J. Prenner, R. N. A. H. Lewis, R. N. McElhaney, *Biochim. Biophys. Acta* **1462**, 201 (1999).
29. O. V. Boyarkin, S. R. Mercier, A. Kamariotis, T. R. Rizzo, *J. Am. Chem. Soc.* **128**, 2816 (2006).
30. R. H. Page, Y. R. Shen, Y. T. Lee, *J. Chem. Phys.* **88**, 5362 (1988).
31. C. J. Gruenloh *et al.*, *J. Chem. Phys.* **109**, 6601 (1998).
32. J. A. Stearns *et al.*, *J. Am. Chem. Soc.* **129**, 11814 (2007).


**Acknowledgments:** We thank EPFL, Swiss National Science Foundation (FNS) (grant no. 200020-130579), and Science and Technology Swiss-Russian cooperation program for their generous support of this work; O.V.B. thanks T. Zwier and A. Vilesov for useful discussions.

### Supplementary Materials

www.sciencemag.org/cgi/content/full/336/6079/320/DC1
Supplementary Text
Figs. S1 to S3
References (*33*–*35*)

4 January 2012; accepted 20 March 2012
10.1126/science.1218709

# Enantioselective C-H Crotylation of Primary Alcohols via Hydrohydroxyalkylation of Butadiene

Jason R. Zbieg, Eiji Yamaguchi, Emma L. McInturff, Michael J. Krische*

The direct, by-product–free conversion of basic feedstocks to products of medicinal and agricultural relevance is a broad goal of chemical research. Butadiene is a product of petroleum cracking and is produced on an enormous scale (about 12 × $10^6$ metric tons annually). Here, with the use of a ruthenium catalyst modified by a chiral phosphate counterion, we report the direct redox-triggered carbon-carbon coupling of alcohols and butadiene to form products of carbonyl crotylation with high levels of *anti*-diastereoselectivity and enantioselectivity in the absence of stoichiometric by-products.

Although many important methods for catalytic asymmetric carbon-carbon bond formation exist, much of this technology is not well suited for implementation on a large scale. Consequently, there is a need to discover and develop carbon-carbon–forming reactions that embody the principal characteristics of process relevance; in particular, the ability to transform abundant, ideally renewable, feedstocks to value-added products in the absence of stoichiometric by-products (*1*–*4*). This quality is embodied by alkene hydroformylation, the prototypical carbon-carbon bond–forming hydrogenation and largest-volume application of homogenous catalysis (*5*, *6*). Accordingly, systematic efforts toward the discovery and development of carbon-carbon bond–forming hydrogenations were initiated in our laboratory (*7*, *8*). We have found that diverse π-unsaturated reactants reductively couple to carbonyl compounds and imines under hydrogenation conditions or transfer hydrogenation conditions employing a sacrificial reductant (such as isopropanol), offering an alternative to the use of stoichiometric organometallic reagents. Most significantly, under transfer hydrogenation conditions, primary alcohols serve dually as hydrogen donors and aldehyde precursors, enabling carbonyl addition directly from the alcohol oxidation level in the absence of stoichiometric by-products.

In the course of advancing hydrogenative methods for polyketide construction, *anti*-diastereoselective and enantioselective carbonyl crotylations from the alcohol or aldehyde oxidation level were developed, using α-methyl allyl

Department of Chemistry and Biochemistry, University of Texas at Austin, Austin, TX 78712, USA.

*To whom correspondence should be addressed. E-mail: mkrische@mail.utexas.edu

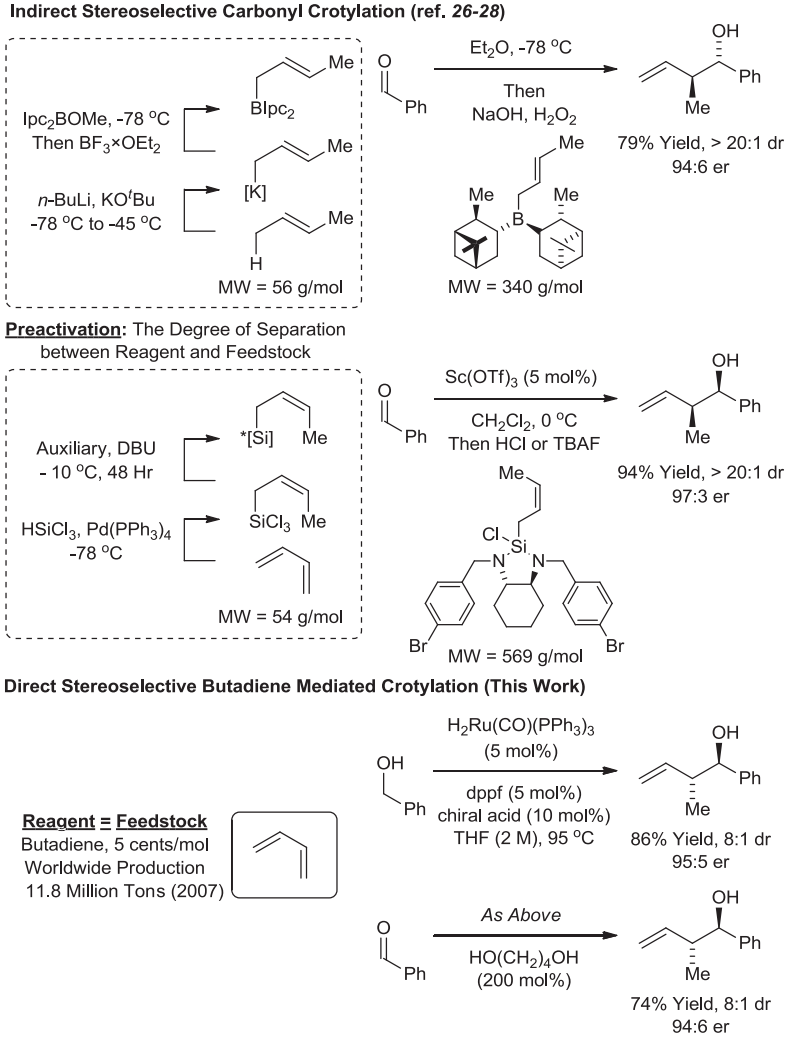


**Fig. 1.** Direct and indirect carbonyl crotylation. IPC, (-)-isopinocampheyl; DBU, 1,8 diazabicyclo[5.4.0]undec-7-ene; dppf, 1,1,-bis(diphenylphosphino)ferrocene, TBAF, tetrabutylammonium fluoride; MW, molecular weight; dr, diastereomeric ratio.

Eq. 1.

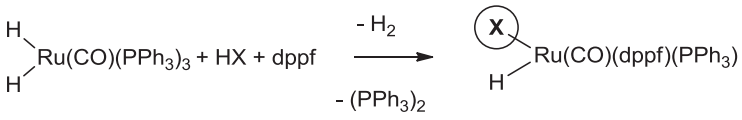


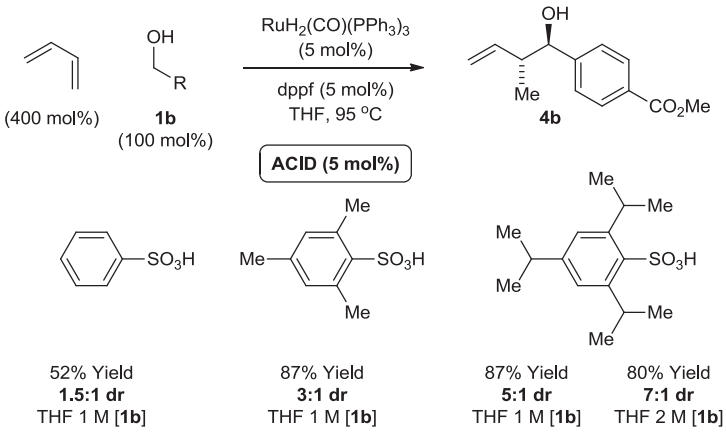


**Fig. 2.** Enhanced *anti*-diastereoselectivity in response to increasing steric demand of the ruthenium counterion in the hydrohydroxyalkylation of benzylic alcohol **1b**. Yields are of material isolated by silica gel chromatography. Diastereomeric ratios were determined by $^1$H NMR analysis of crude reaction mixtures. See the supplementary materials for further details.

**Table 1.** Optimization of *anti*-diastereoselectivity and enantioselectivity in the hydrohydroxyalkylation of benzylic alcohol **1b** using BINOL-derived phosphate counterions. Yields are of material isolated by silica gel chromatography. Diastereomeric ratios were determined by $^1$H NMR analysis of crude reaction mixtures. ERs (er) were determined by chiral stationary-phase high-performance liquid chromatography analysis. These data represent only a small sampling of conditions and phosphoric acids that were screened. For additional details, see supplementary materials text.

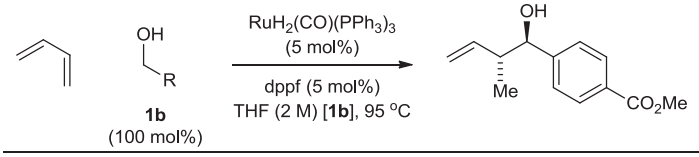


| Entry | Acid (mol%) | Butadiene | Time (hrs) | Yield% | er (dr) |
|---|---|---|---|---|---|
| 1 | $A_1$ (5) | 400 mol% | 19 | 45 | 52:48 (1:1) |
| 2 | $A_2$ (5) | 400 mol% | 19 | 91 | 57:43 (5:1) |
| 3 | $A_3$ (5) | 400 mol% | 19 | 83 | 69:31 (2:1) |
| 4 | $A_4$ (5) | 400 mol% | 19 | 84 | 87:13 (3:1) |
| 5 | $A_4$ (5) | 100 mol% | 19 | 72 | 87:13 (3:1) |
| 6 | $A_4$ (5) | 200 mol% | 19 | 80 | 87:13 (3:1) |
| 7 | $A_4$ (5) | 800 mol% | 19 | 50 | 87:13 (3:1) |
| 8 | $A_5$ (5) | 400 mol% | 19 | 15 | 85:15 (6:1) |
| 9 | $A_6$ (5) | 400 mol% | 19 | 21 | 85:15 (5:1) |
| 10 | $A_7$ (5) | 400 mol% | 19 | 45 | 89:11 (3:1) |
| 11 | $A_8$ (5) | 400 mol% | 19 | 15 | 86:14 (5:1) |
| 12 | $A_9$ (5) | 400 mol% | 19 | 29 | 86:14 (4:1) |
| 13 | $A_6$ (10) | 400 mol% | 19 | 33 | 92:8 (7:1) |
| 14 | $A_7$ (10) | 400 mol% | 19 | 48 | 90:10 (3:1) |
| 15 | $A_9$ (10) | 400 mol% | 19 | 50 | 94:6 (7:1) |
| ⇨ **16** | **$A_9$ (10)** | **400 mol%** | **48** | **80** | **94:6 (7:1)** |

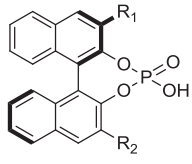


$A_1$: $R_1$=H $R_2$=H
$A_2$: $R_1$=Ph $R_2$=Ph
$A_3$: $R_1$=Ph $R_2$=H
$A_4$: $R_1$=Mes $R_2$=H
$A_5$: $R_1$=Mes $R_2$=Me
$A_6$: $R_1$=Mes $R_2$=Et

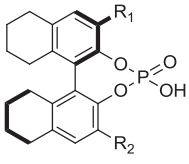


$A_7$: $R_1$=Mes $R_2$=H
$A_8$: $R_1$=Mes $R_2$=Me
$A_9$: $R_1$=Mes $R_2$=Et

acetate as the crotyl donor (*9*–*11*). Butadiene-alcohol carbon-carbon coupling potentially enables by-product–free access to identical crotylation products. However, although catalytic systems displaying the essential reactivity were defined (*12*–*14*), stereocontrolled hydrohydroxyalkylation of butadiene has proven elusive when both iridium (*12*) and ruthenium (*13*, *14*) catalysts were used. Here we report that ruthenium catalysts bearing $C_1$-symmetric 1,1'-bi-2-naphthol (BINOL)–derived phosphate counterions (*15*–*22*) promote *anti*-diastereoselective and enantioselective carbonyl crotylations from the alcohol or aldehyde oxidation level. This protocol bypasses the use of premetallated reagents for carbonyl crotylation, which are prepared from 2-butene or butadiene itself (*23*–*28*) (Fig. 1).

In ruthenium-catalyzed carbonyl *syn*-crotylation from the alcohol or aldehyde oxidation level (*14*), 2-silyl-butadienes were required to enforce the intervention of a single geometrical isomer at the stage of the transient σ-crotylruthenium species, which appears to engage in stereospecific carbonyl addition through a closed transition structure. Although the (*E*)- and (*Z*)-σ-crotylruthenium intermediates obtained upon butadiene hydrometallation are considerably closer in energy and thus harder to discriminate, increasing steric congestion at the ruthenium center should bias formation of the thermodynamically more stable (*E*)-isomer. Based on this reasoning, we further postulated that ruthenium complexes bearing counterions of variable size could be prepared in situ through the acid-base reaction of $H_2Ru(CO)(PPh_3)_3$ and HX (Eq. 1) (*29*, *30*), enabling a systematic evaluation of diastereoselectivity in response to the steric demand of the counterion. As revealed in the hydrohydroxyalkylation of butadiene employing ruthenium catalysts modified by benzenesulfonate, mesitylsulfonate (mesityl = 2,4,6-trimethylphenyl), and trisylsulfonate (trisyl = triisopropylphenyl) counterions, diastereoselectivity increases with the increasing size of the counterion. In the case of the trisylsulfonate, concentration-dependent diastereoselectivity is attributed to a steric inhibition of the acid-base reaction (Fig. 2).

These data suggested the feasibility of directing both relative and absolute stereochemistry, using BINOL-derived phosphate counterions. Whereas the parent (*R*)-BINOL phosphoric acid $\mathbf{A_1}$ conferred poor stereoselectivity, the corresponding 3,3′-diphenyl derivative $\mathbf{A_2}$ promoted promising levels of diastereoselectivity and a 57:43 enantiomeric ratio (ER) (Table 1, entries 1 and 2). The related $C_1$-symmetric phosphoric acid, which incorporates only a single phenyl moiety at the 3-position $\mathbf{A_3}$, displayed higher enantioselectivity than $\mathbf{A_1}$ or $\mathbf{A_2}$ (Table 1, entries 1 to 3). Based on this observation, the 3-mesityl phosphoric acid $\mathbf{A_4}$ was prepared and assayed, revealing an ER of 87:13 (Table 1, entry 4). The loading of butadiene can be decreased to 100 mol % with little impact on yield and stereoselectivity, although 400 mol % loadings provided optimal results and facilitated transfer of the volatile reagent on a small scale

(Table 1, entries 4 to 7). At higher loadings of butadiene (800 mol %), catalytic efficiency is decreased, presumably due to nonproductive coordination of butadiene to coordination sites on the catalyst required for binding of the transient aldehyde. Increasing the size of the 3-aryl substituent did not improve stereoselectivity (see the supplementary materials for additional experiments); however, enhanced diastereoselectivity was observed in connection with the 3-mesityl-3′-methyl phosphoric acid $\mathbf{A_5}$ and 3-mesityl-3′-ethyl phosphoric acid $\mathbf{A_6}$ (Table 1, entries 8 and 9). Further, we found that the 3-mesityl-$H_8$-BINOL $\mathbf{A_7}$ promoted higher enantioselectivity (89:11 ER) than the corresponding $H_4$-derivative $\mathbf{A_4}$ (87:13 ER) (Table 1, entry 10). An improvement in diastereoselectivity was observed in connection with the 3′-methyl and 3′-ethyl $H_8$-derivatives $\mathbf{A_8}$ and $\mathbf{A_9}$, yet a slight decrease in enantioselectivity was observed (Table 1, entries 11 and 12). Attributing decreased enantioselectivity to an incomplete acid-base reaction for such sterically demanding acids, we explored higher loadings of acid (10 mol %), using the $H_4$-derivative $\mathbf{A_6}$ and the $H_8$-derivatives $\mathbf{A_7}$ and $\mathbf{A_9}$ (Table 1, entries 13 to 15), which ultimately led to identification of $\mathbf{A_9}$ as the chiral acid of choice (Table 1, entry 16).

Using the chiral acid $\mathbf{A_9}$, benzylic alcohols **1a** to **1f** were assayed in the hydrohydroxyalkylation of butadiene to form the products of carbonyl crotylation **3a** to **3f**. The purity of alcohols **1a** to **1f** proved to be important, because trace quantities of carboxylic acid contribute to a racemic background reaction. Also, $^{31}P$ nuclear magnetic resonance (NMR) analysis was essential in terms of evaluating the purity of the chiral acid $\mathbf{A_9}$, because $^{1}H$ NMR was ineffective in this regard. With attention to these precautions, crotylation proceeds in good yield with *anti*-diastereoselectivities ranging from 5:1 to 9:1 and ERs ranging from 93:7 to 96:4 (Table 2). An identical set of adducts **3a** to **3f** are accessible from aromatic aldehydes **2a** to **2f** upon the use of 1,4-butanediol (*31*) (200 mol %) as the terminal reductant under otherwise identical conditions. Comparable *anti*-diastereoselectivities (4:1 to 8:1) and ERs (94:6 to 93:7) are observed (Table 2).

A plausible catalytic mechanism is depicted in Fig. 3. Hydrometallation of butadiene, as observed in stoichiometric reactions of $RuHCl(CO)(PPh_3)_3$ with 1,2- and 1,3-dienes (*32*, *33*), delivers the π-allylruthenium complex. Counterion-dependent partitioning of the (*E*)- and (*Z*)-σ-crotylruthenium isomers precedes stereospecific carbonyl addition by way of the σ-crotylruthenium haptomer through a closed transition structure. The resulting homoallylic ruthenium alkoxide, which resists dehydrogenation because all coordination sites at the metal center are occupied, participates in alkoxide exchange with a reactant alcohol to release the product of crotylation and provide a pentacoordinate ruthenium alkoxide. The vacant coordination site at this stage enables dehydrogenation to form an aldehyde and regenerate the ruthenium hydride to close the catalytic cycle (Fig. 3).

**Table 2.** Direct *anti*-diastereoselective and enantioselective carbonyl crotylation via hydrohydroxyalkylation of butadiene and related aldehyde-reductive couplings using the BINOL-derived phosphate counterion $\mathbf{A_9}$. Characterization methods were as described in Table 1.

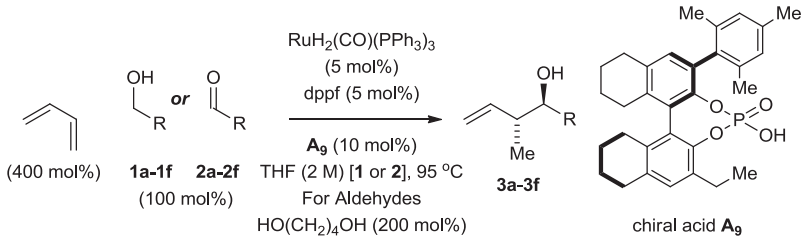


| Entry | Product | [o] Level | Y [%] **4a** (dr) | er |
|---|---|---|---|---|
| 1 | 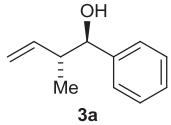 **3a** | Alcohol | 86 (8:1) | 95:5 |
| | | Aldehyde | 74 (8:1) | 94:6 |
| 2 | 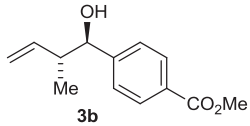 **3b** | Alcohol | 80 (7:1) | 94:6 |
| | | Aldehyde | 80 (6:1) | 93:7 |
| 3 | 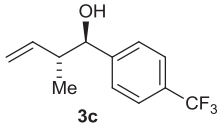 **3c** | Alcohol | 83 (7:1) | 96:4 |
| | | Aldehyde | 63 (6:1) | 94:6 |
| 4 | 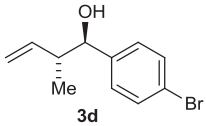 **3d** | Alcohol | 97 (5:1) | 93:7 |
| | | Aldehyde | 78 (5:1) | 93:7 |
| 5 | 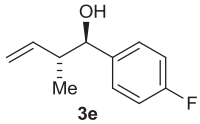 **3e** | Alcohol | 85 (6:1) | 93:7 |
| | | Aldehyde | 80 (5:1) | 94:6 |
| 6 | 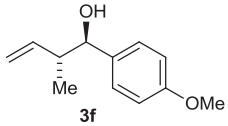 **3f** | Alcohol | 72 (6:1) | 93:7 |
| | | Aldehyde | 66 (6:1) | 94:6 |
| 7 | 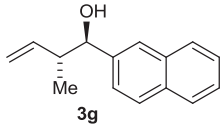 **3g** | Alcohol | 95 (9:1) | 94:6 |
| | | Aldehyde | 79 (4:1) | 93:7 |

Because organic molecules are compounds composed of carbon and hydrogen, the formation of carbon-carbon bonds under hydrogenation and transfer hydrogenation conditions is a natural end point in the evolution of strategies for organic synthesis. As illustrated here in the case of carbonyl crotylation, alcohol-butadiene hydrohydroxyalkylations enhance synthetic efficiency by removing the degrees of separation between reagent and feedstock, while bypassing discrete alcohol oxidation and the generation of stoichiometric byproducts. These initial findings set the stage for the development of catalysts that exhibit enhanced stereoselectivities and substrate scope.

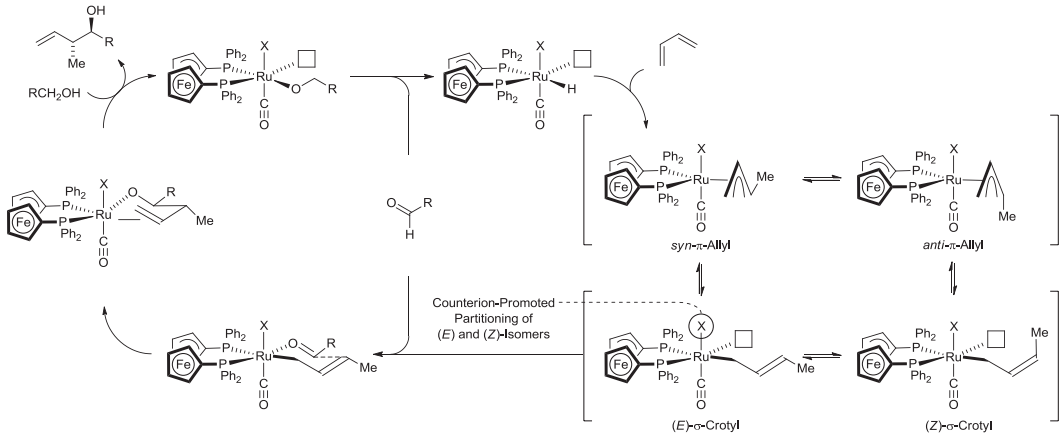


**Fig. 3.** Proposed mechanism for ruthenium-catalyzed hydrohydroxyalkylation of butadiene, illustrating the counterion-dependent partitioning of (*E*)- and (*Z*)-σ-crotylruthenium isomers.


**References and Notes**

1. M. Butters *et al*., *Chem. Rev.* **106**, 3002 (2006).
2. R. A. Sheldon, E. The, *Green Chem.* **9**, 1273 (2007).
3. C. A. Busacca, D. R. Fandrick, J. J. Song, C. H. Senanayake, *Adv. Synth. Catal.* **353**, 1825 (2011).
4. J. Magano, J. R. Dunetz, *Chem. Rev.* **111**, 2177 (2011).
5. C. D. Frohning, C. W. Kohlpaintner, in *Applied Homogeneous Catalysis with Organometallic Compounds*, B. Cornils, W. A. Herrmann, Eds. (Wiley-VCH, Weinheim, Germany 1996), pp. 29–104.
6. P. W. N. M. van Leeuwen, in *Homogeneous Catalysis: Understanding the Art* (Kluwer, Dordrecht, Netherlands, 2004), pp. 139–174.
7. J. F. Bower, M. J. Krische, *Top. Organomet. Chem.* **34**, 107 (2011).
8. A. Hassan, M. J. Krische, *Org. Process Res. Dev.* **15**, 1236 (2011).
9. I. S. Kim, S. B. Han, M. J. Krische, *J. Am. Chem. Soc.* **131**, 2514 (2009).
10. X. Gao, I. A. Townsend, M. J. Krische, *J. Org. Chem.* **76**, 2350 (2011).
11. X. Gao, H. Han, M. J. Krische, *J. Am. Chem. Soc.* **133**, 12795 (2011).
12. J. R. Zbieg, T. Fukuzumi, M. J. Krische, *Adv. Synth. Catal.* **352**, 2416 (2010).
13. F. Shibahara, J. F. Bower, M. J. Krische, *J. Am. Chem. Soc.* **130**, 6338 (2008).
14. J. R. Zbieg, J. Moran, M. J. Krische, *J. Am. Chem. Soc.* **133**, 10582 (2011).
15. H. Alper, N. Hamel, *J. Am. Chem. Soc.* **112**, 2803 (1990).
16. V. Komanduri, M. J. Krische, *J. Am. Chem. Soc.* **128**, 16448 (2006).
17. G. L. Hamilton, E. J. Kang, M. Mba, F. D. Toste, *Science* **317**, 496 (2007).
18. M. Rueping, A. P. Antonchick, C. Brinkmann, *Angew. Chem. Int. Ed.* **46**, 6903 (2007).
19. S. Mukherjee, B. List, *J. Am. Chem. Soc.* **129**, 11336 (2007).
20. S. Liao, B. List, *Angew. Chem. Int. Ed.* **49**, 628 (2010).
21. G. Jiang, B. List, *Chem. Commun. (Camb.)* **47**, 10022 (2011).
22. B. Xu, S.-F. Zhu, X.-L. Xie, J.-J. Shen, Q.-L. Zhou, *Angew. Chem. Int. Ed.* **50**, 11483 (2011).
23. S. E. Denmark, J. Fu, *Chem. Rev.* **103**, 2763 (2003).
24. M. Yus, J. C. González-Gómez, F. Foubelo, *Chem. Rev.* **111**, 7774 (2011).
25. R. W. Hoffmann, W. Ladner, *Tetrahedron Lett.* **20**, 4653 (1979).
26. H. C. Brown, K. S. Bhat, *J. Am. Chem. Soc.* **108**, 293 (1986).
27. H. C. Brown, K. S. Bhat, *J. Am. Chem. Soc.* **108**, 5919 (1986).
28. H. Kim, S. Ho, J. L. Leighton, *J. Am. Chem. Soc.* **133**, 6517 (2011).
29. A. Dobson, S. R. Robinson, M. F. Uttley, *J. Chem. Soc., Dalton Trans.* **1975**, 370 (1975).
30. J. R. Zbieg, E. L. McInturff, J. C. Leung, M. J. Krische, *J. Am. Chem. Soc.* **133**, 1141 (2011).
31. H. C. Maytum, B. Tavassoli, J. M. J. Williams, *Org. Lett.* **9**, 4387 (2007).
32. K. Hiraki, N. Ochi, Y. Sasada, H. Hayashida, Y. Fuchita, S. J. Yamanaka, *Chem. Soc. Dalton Trans.* **1985**, 873 (1985).
33. P. Xue *et al*., *Organometallics* **23**, 4735 (2004).



**Acknowledgments:** The Robert A. Welch Foundation (grant F-0038) and the NIH's National Institute of General Medical Sciences (grant RO1-GM069445) are acknowledged for financial support.


**Supplementary Materials**

www.sciencemag.org/cgi/content/full/336/6079/324/DC1
Materials and Methods
Tables S1 to S4
References (*34*–*42*)


17 January 2012; accepted 8 March 2012
10.1126/science.1219274


# A Universal Method to Produce Low–Work Function Electrodes for Organic Electronics


**Yinhua Zhou,[1] Canek Fuentes-Hernandez,[1] Jaewon Shim,[1] Jens Meyer,[2] Anthony J. Giordano,[3] Hong Li,[3] Paul Winget,[3] Theodoros Papadopoulos,[3] Hyeunseok Cheun,[1] Jungbae Kim,[1] Mathieu Fenoll,[1,4] Amir Dindar,[1] Wojciech Haske,[1] Ehsan Najafabadi,[1] Talha M. Khan,[1] Hossein Sojoudi,[5] Stephen Barlow,[3] Samuel Graham,[5] Jean-Luc Brédas,[3] Seth R. Marder,[3] Antoine Kahn,[2] Bernard Kippelen[1]***



Organic and printed electronics technologies require conductors with a work function that is sufficiently low to facilitate the transport of electrons in and out of various optoelectronic devices. We show that surface modifiers based on polymers containing simple aliphatic amine groups substantially reduce the work function of conductors including metals, transparent conductive metal oxides, conducting polymers, and graphene. The reduction arises from physisorption of the neutral polymer, which turns the modified conductors into efficient electron-selective electrodes in organic optoelectronic devices. These polymer surface modifiers are processed in air from solution, providing an appealing alternative to chemically reactive low–work function metals. Their use can pave the way to simplified manufacturing of low-cost and large-area organic electronic technologies.


Organic-based thin-film optoelectronic devices, such as organic solar cells (OSCs), organic light-emitting diodes (OLEDs), and organic thin-film transistors (TFTs), hold great economic potential; they may lead to a new generation of consumer electronic devices that could be printed or processed at low cost on large areas, have very low weight, and conform to free-form and flexible substrates (*1*–*4*). However, most printed optoelectronic devices require at least one electrode with a work function (WF) that is sufficiently low to either inject electrons into or collect electrons from the lowest unoccupied molecular orbital (LUMO) of a given organic semiconductor. Low-WF metals, such as alkaline-earth metals (Ca, Mg) or metals co-deposited or coated with alkali elements (Li, Cs), meet this requirement; however, they are chemically very reactive and easily oxidize in the presence of ambient oxygen and


[1]Center for Organic Photonics and Electronics (COPE), School of Electrical and Computer Engineering, Georgia Institute of Technology, Atlanta, GA 30332, USA. [2]Department of Electrical Engineering, Princeton University, Princeton, NJ 08544, USA. [3]Center for Organic Photonics and Electronics (COPE), School of Chemistry and Biochemistry, Georgia Institute of Technology, Atlanta, GA 30332, USA. [4]Solvay SA, rue de Ransbeek 310, 1120 Brussels, Belgium. [5]Center for Organic Photonics and Electronics (COPE), George W. Woodruff School of Mechanical Engineering, Georgia Institute of Technology, Atlanta, GA 30332, USA.

*To whom correspondence should be addressed. E-mail: kippelen@ece.gatech.edu

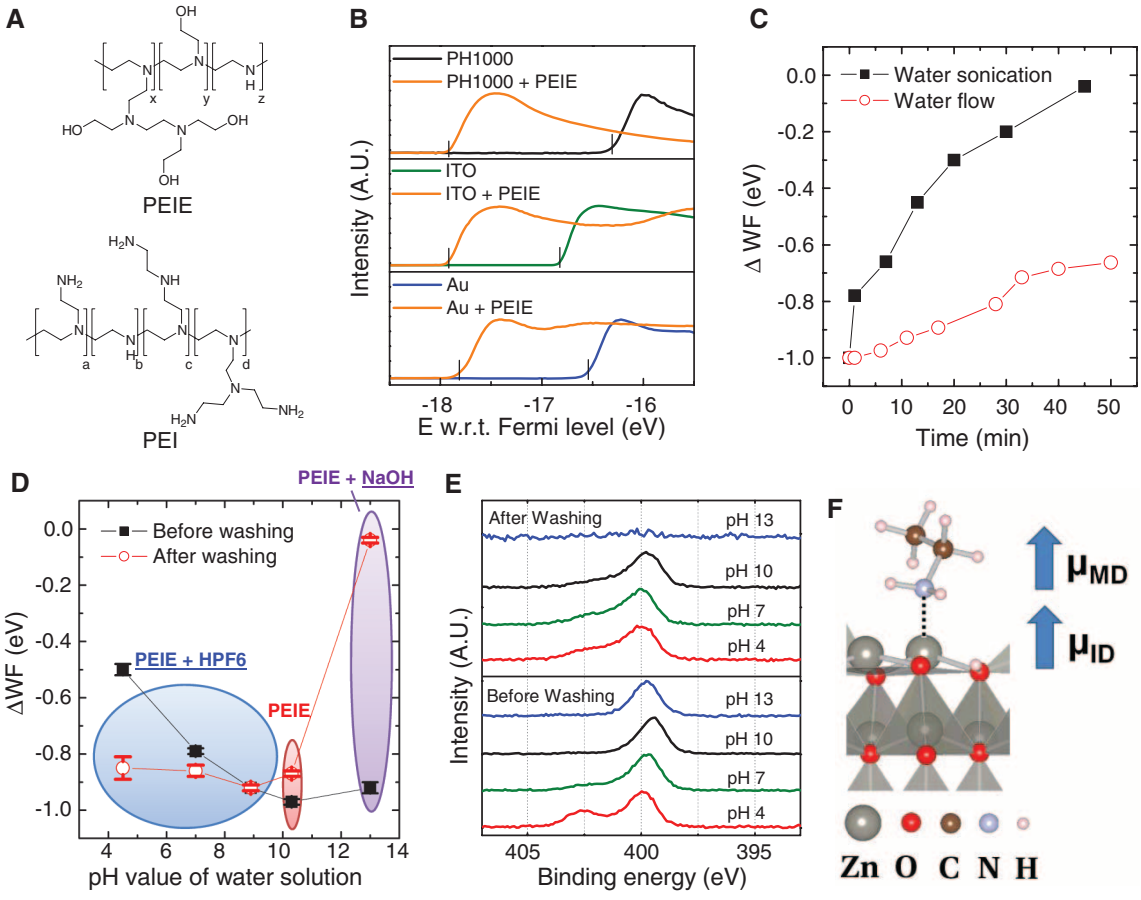


**Fig. 1.** (**A**) Chemical structure of PEIE and PEI. (**B**) Photoemission cutoff obtained via UPS for PEDOT:PSS PH1000, ITO, and Au samples, with and without PEIE. (**C**) WF change, relative to bare ITO, of ITO/PEIE after different washing conditions. (**D**) WF change, relative to bare ITO, upon modification from PEIE water solution, PEIE with $HPF_6$ water solution, and PEIE with NaOH water solution before (solid squares) and after (open circles) water washing. (**E**) N1s core level recorded via XPS on the samples in (D) before and after washing. (**F**) Proposed model of molecular dipole–induced and surface dipole–induced WF reduction on ZnO surface.

water. Thus, their use in printed electronics presents limitations that can only be overcome by the fabrication of devices in an inert atmosphere and their subsequent encapsulation with barrier-coating technologies, which increases both the cost and complexity of the device architectures.

Several strategies for replacing low-WF metals have been explored. In one approach, a film of a conducting or semiconducting material, typically thicker than 10 nm and displaying a low WF, is coated on a high-WF electrode. This film, an electron transport material, mediates charge injection and transport between the higher-WF conductive electrode onto which it is coated and a semiconducting layer in the device. Common examples of this approach have included coating indium tin oxide (ITO) with thin metal-oxide films—such as ZnO (*5*), $In_2O_3$ (*6*), Al-doped ZnO (*7*), or In-doped ZnO (*8*)—that present a lower WF (around 4.3 eV) than ITO. In another approach, the surface of the conductive electrode is coated with an ultrathin layer (≤10 nm) of a material that is chemically or physically adsorbed onto the conductor surface; the surface modifier is chosen in such a way as to create strong interface and/or molecular dipoles that induce a vacuum-level shift and modify the WF of the conductor. In this context, the chemisorption of small molecules onto the surface of conductors has been the most common route. For example, the WF of ITO could be decreased from 4.4 to 3.9 eV when treated with a basic solution of $N(C_4H_9)_4OH$ (*9*). The chemisorption of amine-containing conjugated small molecules such as tetrakis(dimethylamino)ethylene (TDAE) led to even greater reductions (up to 0.9 eV) of the WF of ITO (*10*), Au (*11*, *12*), and poly(3,4-ethylenedioxythiophene):poly(styrenesulfonate) (PEDOT:PSS) (*13*, *14*). However, molecules such as TDAE are highly unstable in air in their neutral state and undergo spontaneous oxidation, which limits their practical use. Chemisorbed self-assembled monolayers (SAMs) of dipolar molecules can also substantially modify the WF of metals and metal oxides (*15*–*17*), but specific surface chemistry is required to ensure chemisorption; a similar problem is faced by other inorganic-based modifiers such as $Cs_2CO_3$ when processed from solution (*18*). Polyethylene oxide and conjugated polymers have also been used but yield reductions in WF that are generally smaller (0.3 to 0.5 eV) (*19*–*21*).

**Table 1.** Work function of conducting materials with and without polymer modifiers, as independently measured by Kelvin probe in air and by UPS. Empty cells indicate no measurement for the corresponding sample.

| Electrodes | Work function (eV) | | | | | |
|---|---|---|---|---|---|---|
| | Kelvin probe in air | | | UPS | | |
| | Pristine | With PEIE | With PEI | Pristine | With PEIE | With PEI |
| Metal oxides | | | | | | |
| ITO | 4.62 ± 0.06 | 3.60 ± 0.06 | 3.50 ± 0.06 | 4.40 | 3.30 | 3.27 |
| | 5.16 ± 0.06* | 3.60 ± 0.06* | — | 5.00* | 3.30* | — |
| ZnO | 4.26 ± 0.06 | 3.28 ± 0.06 | 3.10 ± 0.06 | 3.96 | 3.55 | 3.17 |
| FTO | 4.68 ± 0.06 | 3.80 ± 0.06 | 3.60 ± 0.06 | — | — | — |
| Metals | | | | | | |
| Au | 5.10 ± 0.10 | 3.90 ± 0.06 | 3.94 ± 0.06 | 4.70 | 3.40 | — |
| Ag | 4.60 ± 0.06 | 3.70 ± 0.06 | 3.60 ± 0.06 | — | — | — |
| Al | 3.40 ± 0.06 | 2.75 ± 0.06 | — | — | — | — |
| PEDOT:PSS | 4.90 ± 0.06 | 3.58 ± 0.06 | 3.88 ± 0.06 | 4.95 | 3.32 | 3.16 |
| Graphene | 4.60 ± 0.06 | 3.80 ± 0.10 | — | — | — | — |

*Substrate was treated with an $O_2$ plasma for 2 min prior to measurements or polymer modifier deposition.

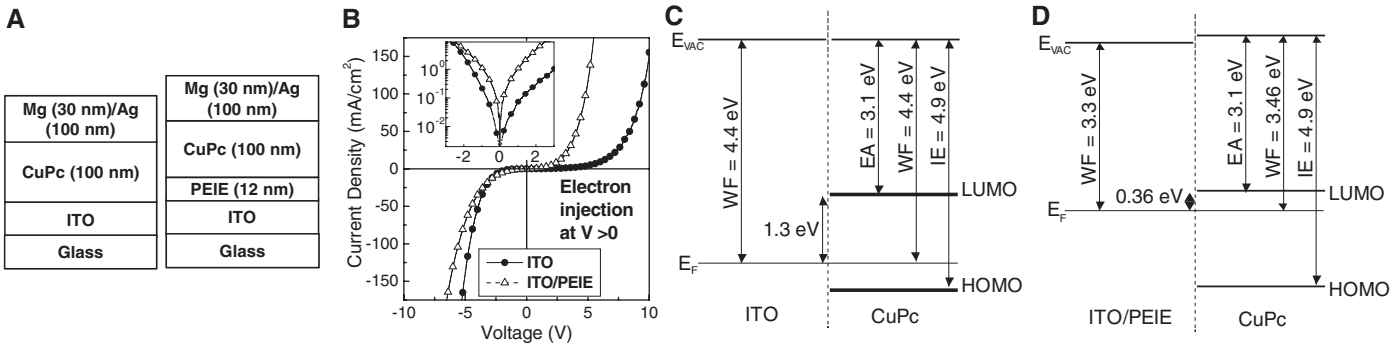


**Fig. 2.** (**A**) Structure of devices using ITO with and without PEIE as the bottom electrode. (**B**) *J-V* characteristics of these devices (without correction for built-in potential); inset shows the *J-V* characteristics on a semilogarithmic scale at low voltage. (**C** and **D**) Energy level alignment of CuPc (10 nm) on top of (C) ITO and (D) ITO/PEIE.

Here, we report on what appears to be a "universal" approach to reducing the WF of a conductor, in which an ultrathin layer (1 to 10 nm) of a polymer containing simple aliphatic amine groups is physisorbed onto the conductor surface. In contrast to the π-conjugated amine-containing small molecules and polymers considered earlier, the polymers exploited in this work are large band-gap insulators and should not be regarded as charge-injection layers but rather as surface modifiers. The intrinsic molecular dipole moments associated with the neutral amine groups contained in such an insulating polymer layer, and the charge-transfer character of their interaction with the conductor surface, together reduce the WF of a wide range of conductors. The commercially available polymer modifiers can be easily processed in air, from dilute solutions in environmentally friendly solvents such as water or methoxyethanol. Their low cost and ease of processing make them compatible with roll-to-roll large-area mass production techniques and suited for organic or printed electronic devices. To illustrate their potential, we evaluate their performance in various device platforms, such as OSCs (including the demonstration of all-polymeric OSCs), organic and metal-oxide TFTs, and OLEDs.

Figure 1A shows the chemical structure of polyethylenimine ethoxylated (PEIE) and branched polyethylenimine (PEI). The high content of amine groups (primary, secondary, and tertiary) in the polymer structures yields high pH values in water and methoxyethanol solutions; the pH values were measured to be 10.3 for PEIE and 10.5 for PEI in water, and 10.1 for PEIE and 10.3 for PEI in methoxyethanol solutions with a polymer concentration of 0.4 weight percent. Figure 1B displays the results of ultraviolet photoemission spectroscopy (UPS) measurements on a series of conductors before and after deposition of an ultrathin layer of PEIE; the spectra revealed WF reductions from 4.95 to 3.32 eV for PEDOT:PSS (high-conductivity grade PH1000), from 4.40 to 3.30 eV for ITO, and from 4.70 to 3.40 eV for Au. Separate Kelvin probe measurements in air further indicate that PEIE reduced the WF of metal oxides (ITO, FTO, ZnO), metals (Au, Ag, Al), and PEDOT:PSS PH1000 as well as graphene. Table 1 summarizes the values of the WF obtained by Kelvin probe and UPS experiments for several conductors modified with 10-nm-thick PEIE or PEI layers. Discrepancies between the two techniques are caused by the different atmospheres and the different experimental conditions under which the Kelvin probe and UPS experiments were conducted (*22*).

The thermal stability of the WF of PEIE- and PEI-coated ITO substrates was studied by Kelvin probe measurements in air. The WF of PEIE-coated ITO substrates did not suffer any change until a temperature of 190°C, making them compatible with the processing of printed electronic devices on plastic substrates (typically at temperatures below 200°C) (fig. S1). For PEI-coated ITO electrodes, the WF was unaffected until 150°C (fig. S1). PEIE-coated ITO electrodes also remained fairly stable under normal ambient conditions for more than 4 weeks; during that period, the WF varied by less than 0.2 eV (fig. S1). Furthermore, aqueous solutions of PEIE or PEI are stable in air (i.e., remain effective agents for reducing the WF) for more than 1 year.

Inverse photoemission spectroscopy (IPES) and UPS measurements on PEIE-coated Au indicate electron affinity and ionization potential energy values of 0.3 eV and 6.5 eV, respectively (fig. S2). These results imply that, in contrast to water/alcohol-soluble polymers based on a π-conjugated main chain that can display good electron-transporting properties (*23*–*26*), PEIE is likely to function as an insulator with a gap of 6.2 eV, and to exhibit large barriers for both hole and electron injection. We investigated the PEIE thickness dependence (from 2 to 22 nm) of the WF modification (ΔWF) of ITO and found a variation of <10% (fig. S3). However, even if the thickness of the PEIE layer did not influence ΔWF, its insulating nature would cause thicker polymer layers to adversely affect device performance.

Atomic force microscopy (AFM) measurements on PEIE-coated, non–plasma-treated ITO show that a 10-nm-thick PEIE layer did not uniformly cover the ITO surface, but formed islands separated by areas with a much thinner PEIE coating (fig. S4, C to F). These PEIE islands could be easily washed away by subjecting the PEIE-coated ITO substrate to a mild flow of running distilled water for 1 min (fig. S4, G and H). After washing, |ΔWF| decreased by less than 0.1 eV. This observation indicates that only an ultrathin layer of PEIE is needed to produce a large ΔWF and that the processes leading to such modifications are truly confined to the surface of the conductor.

To explore the strength of the binding between PEIE and substrate, we monitored the WF of a PEIE-coated ITO substrate over time as a function of controlled washing cycles with water. Figure 1C shows the evolution of ΔWF when the substrates were subjected to a total of 50 min of mild washing conditions (*22*). After such a period of time, |ΔWF| became less than 0.34 eV. The apparent resilience of the PEIE layer on the surface of ITO might at first glance point to a strong binding interaction between the polymer and the electrode; however, the WF reduction entirely disappeared after the PEIE-coated ITO substrate was subjected to a 50-min water wash in an ultrasonic bath (Fig. 1C). This result suggests that the PEIE layer is physisorbed on the conductor's surface, which would be consistent with the seemingly universal ability of PEIE to substantially reduce the WF of such a diverse group of conducting materials (Table 1).

To further explore the nature of the interaction between PEIE and the conductor surface, we modified the pH values of the original PEIE/water solution by adding either hexafluorophosphoric acid ($HPF_6$) or NaOH. PEIE was deposited on ITO from solutions with pH values of 4.5, 7.1, 9.2, 10.3, and 13. Figure 1D displays the ΔWF values induced before and after washing for 1 min with running water. Differences in the solution pH values were expected to primarily affect the degree of protonation of the amine groups in PEIE. The degree of PEIE protonation was followed with x-ray photoelectron spectroscopy (XPS) by tracking the position and shape of the N1s peak and the appearance of the F1s peak for PEIE solutions with pH values below

10.3 (fig. S5). When PEIE was processed from the most basic solution, ΔWF was −0.92 eV and the presence of neutral amine groups was indicated by the N1s peak at 399.8 eV (Fig. 1E). The same N1s peak appeared in the PEIE layers processed from a pH = 10.3 solution that yielded ΔWF = −0.97 eV. These results indicate that neutral amine groups are primarily involved in the interactions leading to the formation of the interface dipoles and the substantial changes in WF. In contrast, when the PEIE layers were processed from the more acidic solutions with a higher proportion of protonated amines, smaller WF reductions were observed. In films processed from solutions with pH values of 7.1 and 4.1, the appearance of a shoulder in the N1s peak at 402.5 eV (Fig. 1E) is indicative of protonated amines; at the same time, an F1s peak appeared, which is consistent with the inclusion of $PF_6^-$ counterions accompanying the protonated amines (fig. S5). After a 1-min water wash, with the exception of the PEIE layer coated from the most basic solution (which was completely removed from the ITO surface), all layers yielded similar ΔWF values around −0.86 eV (Fig. 1D). The XPS spectra of these layers show N1s peaks with a similar shape and a small shoulder at 402.5 eV, as well as the disappearance of the F1s peak (fig. S5). Similar trends were found when the polymer layers were deposited on FTO (fig. S6A) or Au (fig. S6B), or with the use of HCl instead of $HPF_6$ (fig. S6C). Interestingly, these results are different from those in previous reports where poly(amidoamine) dendrimers reduced the WF of ITO (*27*, *28*). In those reports, it was speculated that protonated amine groups were primarily responsible for ΔWF of ITO. Our results show that in the case of PEIE, neutral amine groups are primarily responsible for the largest ΔWF observed.

To understand the possible mechanism leading to the WF decrease, we carried out density functional theory (DFT) calculations for the Au (111) surface and the polar (0002) and nonpolar (10-10) ZnO surfaces (*22*). A SAM of ethylamine ($C_2H_5NH_2$) molecules was used to model the amine-containing thin molecular layer adsorbed on the electrode surface (fig. S7). The adsorption energy per amine group is on the order of −0.47 eV for Au (111), −0.88 eV for ZnO (0002), and −0.78 eV for ZnO (10-10). In all cases, physisorption of the ethylamine groups is calculated to be energetically favored over dissociative chemisorptions (for example, by 0.7 eV on the ZnO (0002) surface), which is consistent with the experimental observations. The ΔWF values of the three model surfaces induced by a SAM of ethylamine molecules are calculated to be −1.3 eV for Au (111), −1.7 eV for ZnO (0002), and −1.7 eV for ZnO (10-10); these results are fully in line with the UPS and Kelvin probe data.

The mechanism leading to ΔWF has been analyzed by decomposing it into contributions from (i) the ethylamine molecular dipole ($\mu_{MD}$) within the SAM along the direction perpendicular to the surface (leading to an electrostatic potential energy change denoted as $\Delta V_{MD}$), and (ii) the dipole ($\mu_{ID}$) formed at the interface between the molecular SAM and the electrode surface ($\Delta V_{ID}$) (*29*–*31*) (Fig. 1F and table S1). In all instances, the contributions to ΔWF from the molecular dipole and the interface dipole were of the same order of magnitude—for instance, −0.5 eV and −0.8 eV, respectively, on Au (111). The contribution to ΔWF from the interface dipole is attributed to a slight electron transfer [0.16 e for ethylamine on Au (111), 0.07 e on ZnO (0002), and 0.06 e on ZnO (10-10)] from the amine-containing molecules to the electrode surface.

We tested PEIE-coated conductors as electrodes in various device geometries. First, we investigated the ability of PEIE-coated ITO substrates to inject electrons into an organic semiconductor. The devices comprised a 100-nm-thick layer of copper(II) phthalocyanine (CuPc, with an electron affinity of 3.1 eV) deposited on top of a glass/ITO/PEIE substrate with a top Mg/Ag electrode (WF = 3.6 eV), as shown in Fig. 2A. A comparison of the current density–voltage (*J-V*) characteristics of such devices to identical devices without the PEIE layer is shown in Fig. 2B. The voltage was applied to the top Mg/Ag contact. Devices without the PEIE layer present *J-V* characteristics resembling those of a diode because of the large energy barrier for electron injection from ITO to CuPc. Figure 2C illustrates that the energy level alignment of a CuPc (10 nm) layer deposited on top of ITO, as determined by UPS and IPES measurements, yielded a value of

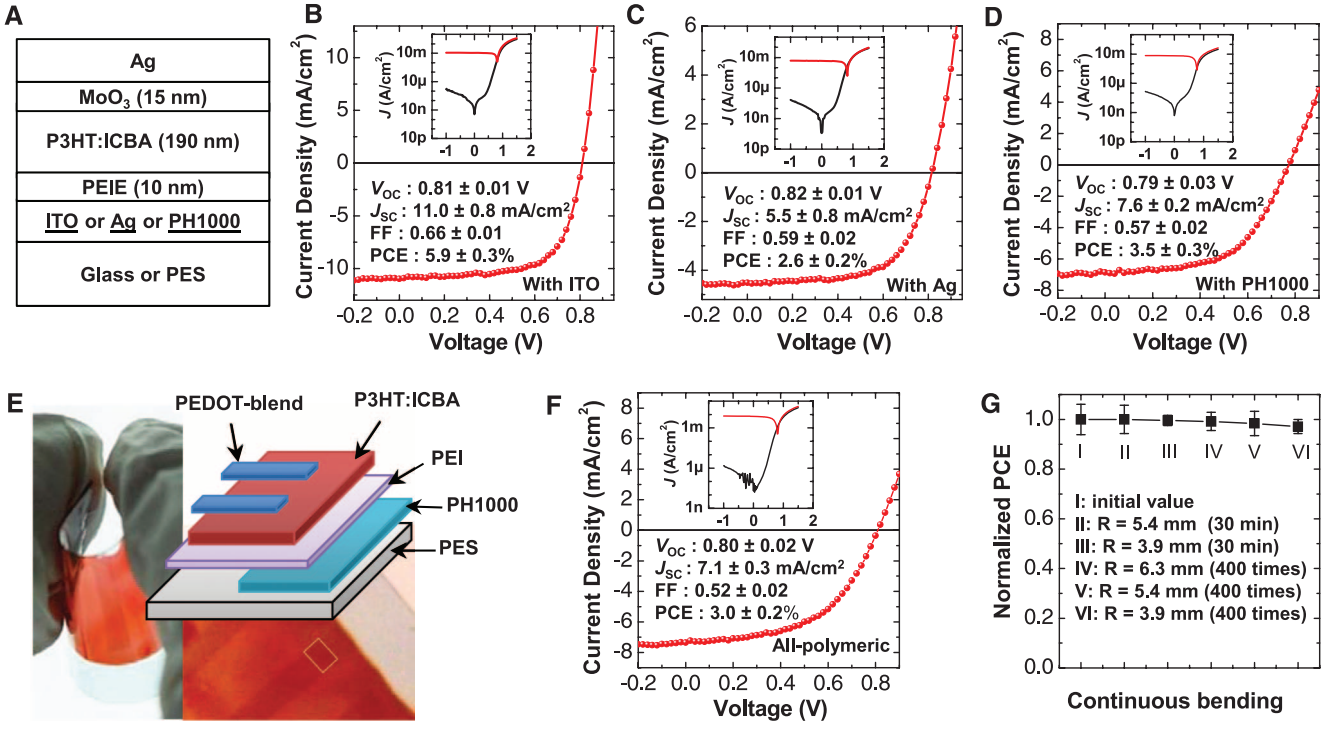


**Fig. 3.** (**A**) Device structure of inverted solar cells. (**B** to **D**) *J-V* characteristics of devices with PEIE-modified ITO (B), Ag (C), and PH1000 (D) electrodes under air mass (AM) 1.5 illumination (100 mW/cm$^2$). (**E**) Device structure and two photographs of all-polymeric solar cells. (**F**) *J-V* characteristics of all-polymeric solar cells under AM1.5 illumination (100 mW/cm$^2$). (**G**) Normalized PCE of all-polymeric solar cells after continuous bending tests with different bending radii (R). Insets in (B), (D), (E), and (F) are the *J-V* characteristics in the dark and under illumination on a semilogarithmic scale.

1.3 eV for the height of this barrier. In contrast, as shown in Fig. 2D, in a device with an ITO/PEIE electrode, this barrier was greatly reduced to a value of 0.36 eV. Thus, the *J-V* characteristics became nearly symmetric, with the current injected from the ITO/PEIE electrode slightly greater than that injected from Mg/Ag (Fig. 2B). This result confirms that, despite the insulating nature of PEIE, electrons can be injected efficiently into the semiconductor through the PEIE layer by processes such as tunneling or thermionic injection.

In a second step, the low-WF electrodes were tested in a variety of OSC geometries. OSCs were fabricated with PEIE-coated ITO, Ag, and PH1000 as the bottom electrode to demonstrate their electron selectivity (Fig. 3A). The top Ag layer was 150 nm for the devices with glass/ITO/PEIE and polyethersulfone (PES)/PH1000/PEIE, and it was 20 nm for the devices with glass/Ag/PEIE. A mixture of poly(3-hexylthiophene) (P3HT) and an indene-$C_{60}$ bis-adduct (ICBA) (weight ratio 1:1) was used as the photo-active layer (*32*). Figure 3, B to D, displays the *J-V* characteristics of these solar cells in the dark and under illumination. In all cases, the *J-V* characteristics in the dark show a large rectification and small reverse saturation currents; this result demonstrates the excellent electron selectivity of the PEIE-modified electrodes. Solar cells with PEIE-coated ITO electrode (Fig. 3B) yielded a power conversion efficiency (PCE) of 5.9% [open-circuit voltage ($V_{OC}$) = 0.81 V, short-circuit current density ($J_{SC}$) = 11.0 mA/cm$^2$, fill factor (FF) = 0.66], averaged over 10 devices. Such a large FF value also provides indirect evidence of the good electron selectivity of the PEIE-coated ITO electrode (*33*, *34*). Note that the PCE measured in these devices is comparable with that previously reported in other inverted solar cells that use the same active layer (*35*).

We studied the shelf air stability of cells with an ITO/PEIE electrode and found that the PCE remained nearly constant after 30 days in air and was still about 70% of its initial value after 102 days (fig. S8). PEIE-coated ITO electrodes were also tested in devices with an active layer comprising a blend of poly[(4,8-bis-(2-ethylhexyloxy)-benzo[1,2-*b*:4,5-*b*′]dithiophene)-2,6-diyl-*alt*-(4-(2-ethylhexanoyl)-thieno[3,4-*b*]thiophene)-2,6-diyl] (PBDTTT-C) and 3′-phenyl-3′*H*-cyclopropa-[1,9][$C_{60}$-$I_h$][5,6]fullerene-3′-butanoic acid methyl ester ($PC_{60}BM$). Devices with an inverted architecture consisting of glass/ITO/PEIE/PBDTTT-C:$PC_{60}BM$/$MoO_3$/Ag yielded an average PCE of 6.6% and excellent reproducibility (fig. S9). In comparison, devices consisting of glass/ITO/PEDOT:PSS(4083)/PBDTTT-C:$PC_{60}BM$/Ca/Al yielded a PCE of 6% (fig. S9 and table S2).

In the case of the solar cells with a PEIE-coated Ag bottom electrode (Fig. 3C), light enters the device through the $MoO_3$ (15 nm)/Ag (20 nm) top electrode. In these devices, a relatively high FF of 0.60 was also measured but $J_{SC}$ was lower (5.5 mA/cm$^2$) because of the low transmittance of the top electrode (fig. S10); as a result, the PCE was only 2.6%. Devices with a PEIE-coated PH1000 bottom electrode yielded a PCE of 3.5% (averaged over five devices), with $V_{OC}$ = 0.79 V, FF = 0.57, and $J_{SC}$ = 7.6 mA/cm$^2$. The slightly smaller FF value is attributed to the increased series resistance introduced by the relatively low conductivity of PH1000 (600 S/cm) relative to ITO or Ag, whereas the relatively small $J_{SC}$ is mainly caused by the lower transmittance of PH1000 (*36*–*38*) and differences in the thickness of the active layer (fig. S10).

Having transformed PEDOT:PSS into an efficient electron-collecting electrode upon modification, we fabricated all-polymeric OSCs on flexible substrates [Fig. 3E and fig. S11). As shown in Fig. 3F, OSCs with PEDOT:PSS/PEI electrodes show excellent rectification in the dark in contrast to samples without PEI (fig. S12). Under illumination, semitransparent all-polymeric OSCs showed a PCE of 3.0% averaged over seven devices, with $V_{OC}$ = 0.80 V, FF = 0.52, and $J_{SC}$ = 7.1 mA/cm$^2$. When a thick Ag layer was placed behind the semitransparent OSC to reflect some of the light back into the active layer, $J_{SC}$ increased to 8.2 mA/cm$^2$, yielding a PCE of 3.4% (table S3 and fig. S13), comparable to that of a device that uses a $MoO_3$/Ag hole-collecting electrode (Fig. 3D). Because the all-polymeric OSCs only present polymer-polymer interfaces, they demonstrate excellent mechanical properties under multiple bending conditions (Fig. 3G). They provide a proof of principle that OSCs can be fabricated using in-line, all-additive solution-based coating and/or printing of polymers. However, the design of large-area cells and modules could require the integration of some highly conductive electrodes to compensate for the lower sheet resistance of conducting polymers (*38*).

Air-stable, low-WF electrodes are also needed for organic semiconductor–based or metal oxide–based n-channel TFTs. In a TFT, the existence of large energetic barriers for electron injection at the source electrode and collection at the drain electrode can lead to a large threshold voltage ($V_{TH}$); it can also potentially result in low field-effect mobility (μ) when the contact resistance exceeds the channel resistance (*39*), a particularly critical issue for TFTs with short channel lengths. We fabricated examples of organic and metal-oxide n-channel TFTs that use air-stable PEIE-coated Au source and drain electrodes. In the first example, top-gate bottom-contact organic-based n-channel TFTs with a bilayer gate dielectric were fabricated (*40*) (Fig. 4A). For comparison purposes, two sets of TFTs were fabricated with Au source and drain electrodes, either coated with a PEIE layer or uncoated. In both instances, the organic semiconductor poly[*N*,*N*′-bis(2-octyldodecyl)-naphthalene-1,4:5,8-bis(dicarboximide)-2,6-diyl]-alt-5,5′-(2,2′-bithiophene) [P(NDI2OD-T2), also called N2200] (*4*) was inkjet-printed on top of the

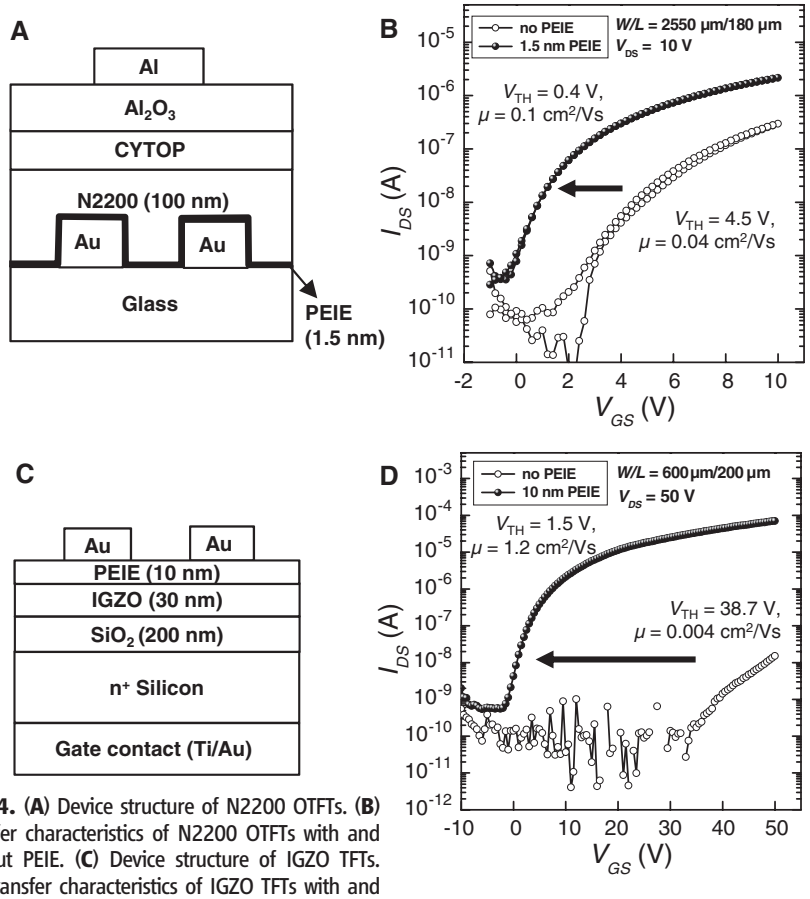


**Fig. 4.** (**A**) Device structure of N2200 OTFTs. (**B**) Transfer characteristics of N2200 OTFTs with and without PEIE. (**C**) Device structure of IGZO TFTs. (**D**) Transfer characteristics of IGZO TFTs with and without PEIE. CYTOP (CTL-809M) is a perfluorinated polymer purchased from Asahi Glass.

source and drain electrodes. Figure 4B displays a comparison of the transfer characteristics of both TFTs. In the TFTs with PEIE-coated source and drain electrodes, $V_{TH}$ dropped from 4.5 to 0.4 V, the average μ increased from 0.04 to 0.1 $cm^2 V^{-1} s^{-1}$ and the device yield improved from 60% to 95%. We note that whereas μ values obtained after the PEIE modification are comparable to those of similar TFTs previously reported, the $V_{TH}$ in our devices is lower (*4*). In this example, PEIE also coats the gate insulator inside the channel. PEIE layers thicker than 1.5 nm led to n-doping of the organic semiconductor channel. Similar doping was also observed on bottom-gate bottom-contact $PC_{60}BM$ TFTs that used PEIE-coated Au electrodes with PEIE thicknesses greater than 10 nm (fig. S14). This doping could assist the injection/collection of carriers by producing band-bending in the vicinity of the conductor surface; this effect is also likely present in OSCs containing fullerene-based acceptors (Fig. 3).

In a second example, bottom-gate top-contact amorphous InGaZnO (IGZO) TFTs were fabricated as shown in Fig. 4C. In contrast to the devices described above, PEIE was first deposited directly on top of the semiconductor (to prevent any damage from the radio frequency–sputtering deposition of IGZO) and the Au source and drain electrodes were evaporated on top of the PEIE layer. Figure 4D provides a comparison of the transfer characteristics of IGZO TFTs with and without PEIE. As in the n-channel organic-based TFTs, the $V_{TH}$ of the IGZO TFTs dropped from 38.7 to 1.5 V and μ increased from 0.004 to 1.2 $cm^2 V^{-1} s^{-1}$ in the devices with the PEIE-modified electrodes.

Finally, we tested the use of PEIE in OLEDs by replacing a LiF/Al cathode with PEIE/Al in benchmark devices based on 4,4′-bis(carbazol-9-yl)biphenyl (CBP) and an emitter of *fac*-tris(2-phenylpyridinato-$N,C^{2'}$) iridium [$Ir(ppy)_3$], and achieved an external quantum efficiency of 15% (fig. S15). Although the performance of these devices was not optimized, it illustrates the applicability of this method to OLED platforms.

Polymers containing simple aliphatic amine groups such as PEIE and PEI appear to be "universal" surface modifiers that allow the fabrication, at very low cost and from environmentally friendly solvents, of air-stable low-WF electrodes. This approach should enable the mass production of low-WF electrodes from processes that are compatible with the large-area roll-to-roll manufacturing techniques required for the commercialization of low-cost organic and printed electronic devices. The specific properties of the polymers can be further optimized for other applications, and conceptually the approach could be applied to the development of polymers for high-WF electrodes.

### References and Notes


1. H. Y. Chen *et al.*, *Nat. Photonics* **3**, 649 (2009).
2. R. H. Friend *et al.*, *Nature* **397**, 121 (1999).
3. G. Yu, J. Gao, J. C. Hummelen, F. Wudl, A. J. Heeger, *Science* **270**, 1789 (1995).
4. H. Yan *et al.*, *Nature* **457**, 679 (2009).
5. H. Cheun *et al.*, *J. Phys. Chem. C* **114**, 20713 (2010).
6. L. Wang *et al.*, *Nat. Mater.* **5**, 893 (2006).
7. J. Meyer *et al.*, *Appl. Phys. Lett.* **93**, 073308 (2008).
8. H. Cheun *et al.*, *Opt. Express* **18** (suppl. 4), A506 (2010).
9. F. Nüesch, L. J. Rothberg, E. W. Forsythe, Q. T. Le, Y. Gao, *Appl. Phys. Lett.* **74**, 880 (1999).
10. W. Osikowicz *et al.*, *Appl. Phys. Lett.* **85**, 1616 (2004).
11. L. Lindell *et al.*, *Appl. Phys. Lett.* **92**, 163302 (2008).
12. B. Bröker *et al.*, *Appl. Phys. Lett.* **93**, 243303 (2008).
13. L. Lindell *et al.*, *Chem. Mater.* **18**, 4246 (2006).
14. F. L. E. Jakobsson *et al.*, *Chem. Phys. Lett.* **433**, 110 (2006).
15. A. Sharma, P. J. Hotchkiss, S. R. Marder, B. Kippelen, *J. Appl. Phys.* **105**, 084507 (2009).
16. X. Bulliard *et al.*, *Adv. Funct. Mater.* **20**, 4381 (2010).
17. S.-N. Hsieh *et al.*, *Org. Electron.* **10**, 1626 (2009).
18. J. Huang, Z. Xu, Y. Yang, *Adv. Funct. Mater.* **17**, 1966 (2007).
19. Y. Zhou *et al.*, *Sol. Energy Mater. Sol. Cells* **93**, 497 (2009).
20. G. Jo *et al.*, *Appl. Phys. Lett.* **97**, 213301 (2010).
21. S. I. Na *et al.*, *Appl. Phys. Lett.* **97**, 223305 (2010).
22. See supplementary materials on *Science* Online.
23. F. Huang, H. B. Wu, Y. Cao, *Chem. Soc. Rev.* **39**, 2500 (2010).
24. F. Huang *et al.*, *Adv. Mater.* **19**, 2010 (2007).
25. S. H. Oh, D. Vak, S.-I. Na, T.-W. Lee, D.-Y. Kim, *Adv. Mater.* **20**, 1624 (2008).
26. W. Ma *et al.*, *Adv. Mater.* **17**, 274 (2005).
27. R. Schlapak *et al.*, *Langmuir* **23**, 8916 (2007).
28. G. Latini, M. Wykes, R. Schlapak, S. Howorka, F. Cacialli, *Appl. Phys. Lett.* **92**, 013511 (2008).
29. G. Heimel, L. Romaner, J.-L. Brédas, E. Zojer, *Phys. Rev. Lett.* **96**, 196806 (2006).
30. G. Heimel, L. Romaner, E. Zojer, J.-L. Brédas, *Acc. Chem. Res.* **41**, 721 (2008).
31. H. Li, P. Paramonov, J.-L. Brédas, *J. Mater. Chem.* **20**, 2630 (2010).
32. Y. He, H.-Y. Chen, J. Hou, Y. Li, *J. Am. Chem. Soc.* **132**, 1377 (2010).
33. H. Schmidt *et al.*, *Appl. Phys. Lett.* **96**, 243305 (2010).
34. A. Wagenpfahl, D. Rauh, M. Binder, C. Deibel, V. Dyakonov, *Phys. Rev. B* **82**, 115306 (2010).
35. Y. J. Cheng, C.-H. Hsieh, Y. He, C.-S. Hsu, Y. Li, *J. Am. Chem. Soc.* **132**, 17381 (2010).
36. Y. H. Zhou *et al.*, *Appl. Phys. Lett.* **97**, 153304 (2010).
37. O. Inganäs, *Nat. Photonics* **5**, 201 (2011).
38. S. Choi, W. J. Potscavage Jr., B. Kippelen, *Opt. Express* **18** (suppl. 3), A458 (2010).
39. A. Rolland, J. Richard, J. P. Kleider, D. Mencaraglia, *Jpn. J. Appl. Phys.* **35**, 4257 (1996).
40. D. K. Hwang *et al.*, *Adv. Mater.* **23**, 1293 (2011).



**Acknowledgments:** Supported by the Center for Interface Science: Solar Electric Materials, an Energy Frontier Research Center funded by the U.S. Department of Energy, Office of Science, Office of Basic Energy Sciences, under award DE-SC0001084 (Y.Z., J.S., J.M., H.C., H.L., P.W., S.B., J.-L.B., S.R.M., and S.G.), the NSF Science and Technology Centers program under agreement DMR-0120967 (C.F.-H., J.K., E.N., and A.D.), Office of Naval Research grant N00014-04-1-0120) (T.M.K. and B.K.), NSF grants DMR-1005892 (A.K.) and CMMI-0927736 (H.S.), the U.S. Department of Energy, Office of Science, Office of Basic Energy Sciences under award DE-FG02-05ER46165 (W.H. and T.P.), the Deutsche Forschungsgemeinschaft postdoctoral fellowship program (J.M.), and the National Defense Science and Engineering Graduate Fellowship program and NSF graduate research fellowship DGE-0644493 (A.J.G.).


**Supplementary Materials**

www.sciencemag.org/cgi/content/full/336/6079/327/DC1
Materials and Methods
Figs. S1 to S16
Tables S1 to S3
References (*41*–*52*)


6 January 2012; accepted 29 February 2012
10.1126/science.1218829


# Dislocation Damping and Anisotropic Seismic Wave Attenuation in Earth's Upper Mantle


**Robert J. M. Farla,[1]*† Ian Jackson,[1] John D. Fitz Gerald,[1] Ulrich H. Faul,[2] Mark E. Zimmerman[3]**



**Crystal defects form during tectonic deformation and are reactivated by the shear stress associated with passing seismic waves. Although these defects, known as dislocations, potentially contribute to the attenuation of seismic waves in Earth's upper mantle, evidence for dislocation damping from laboratory studies has been circumstantial. We experimentally determined the shear modulus and associated strain-energy dissipation in pre-deformed synthetic olivine aggregates under high pressures and temperatures. Enhanced high-temperature background dissipation occurred in specimens pre-deformed by dislocation creep in either compression or torsion, the enhancement being greater for prior deformation in torsion. These observations suggest the possibility of anisotropic attenuation in relatively coarse-grained rocks where olivine is or was deformed at relatively high stress by dislocation creep in Earth's upper mantle.**


A rheologically weak sublithospheric mantle (the asthenosphere) is widely invoked to explain the motion of the tectonic plates on Earth [e.g., (*1*)]. Laboratory experiments underpin an emerging understanding of the anomalous seismic properties of the asthenosphere (*2*, *3*). In particular, the seismic anisotropy of this part of the upper mantle is attributed to crystallographic preferred orientation in olivine-rich rocks—testimony to their deformation by dislocation creep (*4*–*11*). Several studies have demonstrated that anelastic relaxation attributed to grain-boundary sliding can affect the shear modulus and attenuation of upper mantle rocks (*12*–*16*), but evidence for strain-energy dissipation from mechanically forced vibrations of dislocations has been largely circumstantial until now.


[1]Research School of Earth Sciences, Australian National University, Canberra, Australian Capital Territory 0200, Australia. [2]Department of Earth Sciences, Boston University, Boston, MA 002215, USA. [3]Department of Geology and Geophysics, University of Minnesota, Minneapolis, MN 55455, USA.

*To whom correspondence should be addressed. E-mail: robert.farla@yale.edu

†Present address: Department of Geology and Geophysics, Yale University, New Haven, CT 06520, USA.

**Table 1.** Specimen characterization. Uncertainty is calculated as 1 SD. wt. ppm, concentration of species by weight in parts per million.

| Specimen | $d_i$* (μm) | $d_f$ (μm) | $\rho_i$† ($\mu m^{-2}$) | $\rho_f$ ($\mu m^{-2}$) (Fig. 3) | Water content‡ (wt. ppm $H_2O$) | Forced oscillation conditions: Maximum flow stress (MPa) | Forced oscillation conditions: Maximum strain ($\times 10^{-5}$) |
|---|---|---|---|---|---|---|---|
| H6585 | 3.1 (1.8) | 3.1 (1.4) | 1.0 (0.7) | 1.0 (0.9) | 3/2 | 0.53 | 1.00 |
| D6618 | 5.0 (2.6) | 4.9 (2.5) | 4.8 (1.6) | 1.9 (0.8) | 4/2 | 0.19 | 0.46 |
| D6646 | 4.8 (2.6) | 5.0 (3.2) | 7.1 (1.8) | 5.1 (2.0) | 2/2 | 0.35 | 0.95 |
| T0436 | 6.7 (4.7) | 5.7 (3.7) | 2.4 (1.0) | 1.3 (1.1) | 5/2 | 0.38 | 0.78 |

*Grain size $d$, where $i$ and $f$ indicate before and after forced-oscillation testing, respectively. †Dislocation density ρ, where $i$ and $f$ indicate before and after forced-oscillation testing, respectively. ‡Water content before/after forced-oscillation testing [calibration as in (*28*)].

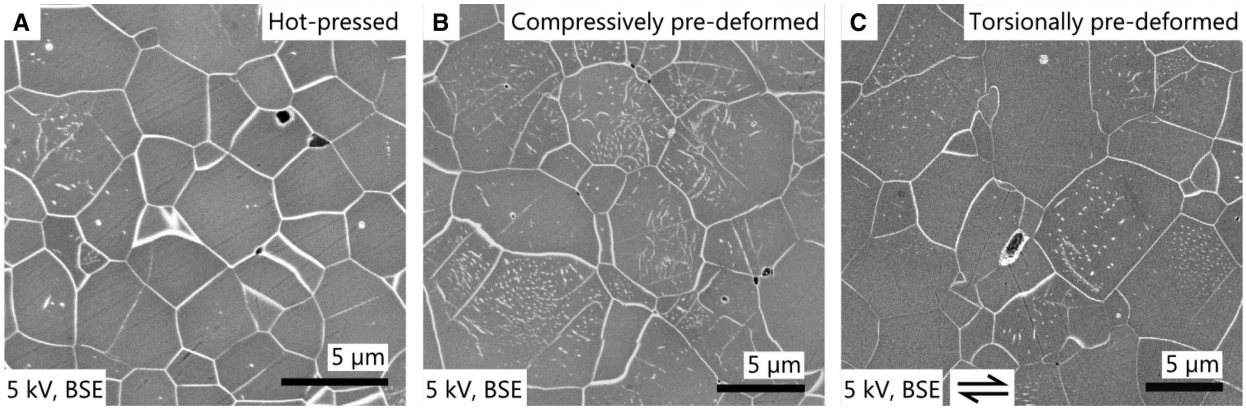


**Fig. 1.** Backscattered electron (BSE) micrographs of (**A**) a hot-pressed and un-deformed olivine specimen (H6585), (**B**) a compressively pre-deformed specimen (D6646), and (**C**) a torsionally pre-deformed specimen (T0436) after forced-oscillation testing. The dislocation density increased during deformation and remained higher than a that of a hot-pressed specimen after forced-oscillation testing. The average grain size is typically from 3 to 6 μm.

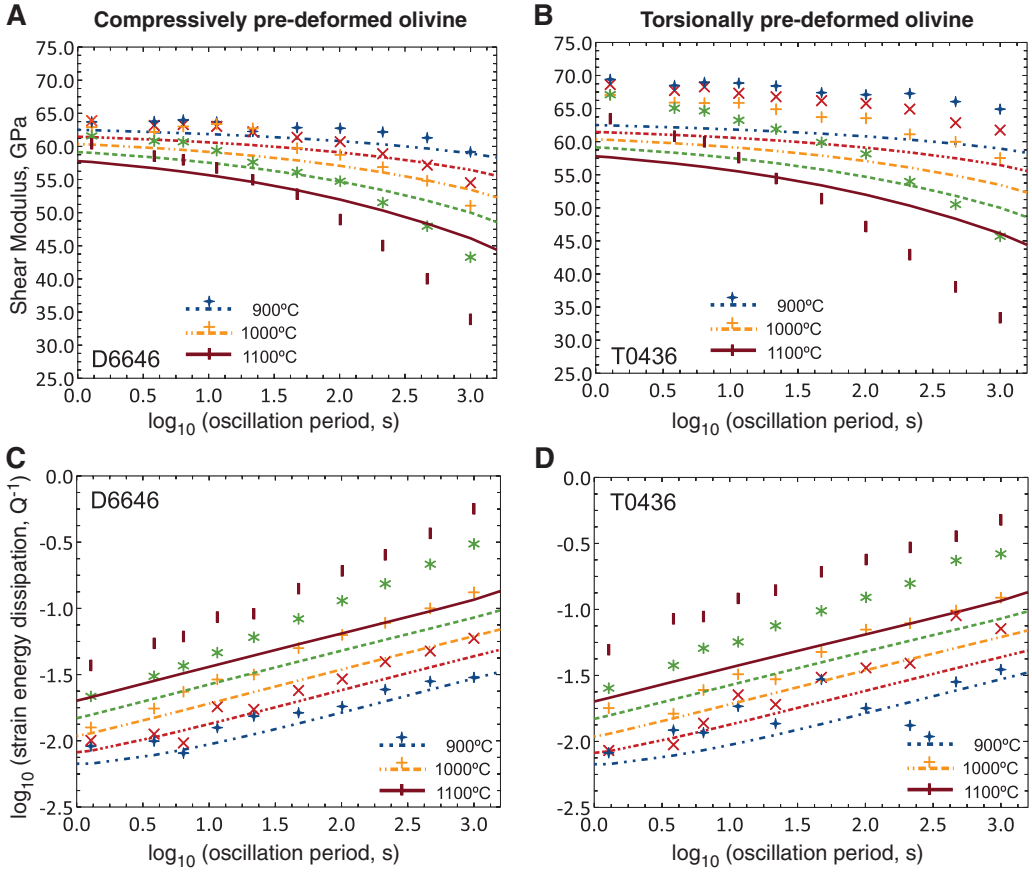


**Fig. 2.** Shear modulus (**A** and **B**) and dissipation (**C** and **D**) plotted against $\log_{10}$(oscillation period) for selected pre-deformed sol-gel olivine specimens, color-coded for representative temperatures as follows: 1100°C (maroon), 1050°C (green), 1000°C (orange), 950°C (red), and 900°C (blue). The dashed curves represent a model involving a Burgers-type creep function fitted to data for a suite of un-deformed hot-pressed olivine specimens (*16*). The model was evaluated at the grain size relevant for each specimen. Shear moduli for specimen T0436 higher than the (isotropic) anharmonic value (66.5 GPa at 900°C) are tentatively attributed to elastic anisotropy associated with crystallographic preferred orientation.

A single exploratory study of dislocation damping to date has demonstrated enhanced strain-energy dissipation in favorably oriented pre-deformed specimens of single-crystal forsterite (*17*).

Following this promising lead, we present a systematic study of pre-deformed polycrystalline olivine to determine the influence of dislocation density on shear wave speeds and attenuation within Earth's upper mantle. We deformed olivine specimens in either triaxial compression or torsion to introduce populations of differently oriented dislocations. A simple analysis of the resolved shear stress for dislocation glide in polycrystalline olivine samples containing randomly oriented crystallites, pre-deformed in either compression or torsion, suggests that prior deformation in torsion is likely to yield higher levels of strain-energy dissipation in subsequent torsional oscillation tests (supplementary materials). The shear modulus ($G$) and strain-energy dissipation ($Q^{-1}$) were derived from the measured complex torsional compliance of experimental assemblies, each containing a deformed specimen, and were compared to a model fitted to equivalent data for a suite of undeformed (hot-pressed) olivine specimens, tested under similar conditions of temperature, pressure, and forced-oscillation period.

We performed microstrain forced torsional oscillation tests under conditions of simultaneous high temperature and pressure (*16*, *18*). Based on dislocation recovery rates measured in olivine at a range of temperatures under similar oxygen fugacity conditions (*19*), the conditions for forced-oscillation testing of the pre-deformed specimens were limited to 1100°C, at which recovery is expected to decrease the free dislocation density by only 10% over a period of 50 hours. We initially monitored the forced-oscillation response for several tens of hours at 200 MPa, confining pressure and the maximum temperature in order to ensure broadly stable grain-scale microstructure without excessive dislocation recovery. Thereafter, forced-oscillation tests at 1- to 1000-s periods were performed at selected temperatures, spaced by 25° to 200°C, during staged cooling to room temperature. A final excursion back to high-temperature conditions verified the reproducibility of the forced-oscillation data. The maximum shear stress at 1100°C during a 1000-s period of oscillation was about 0.5 MPa (Table 1), associated with a maximum strain of $1 \times 10^{-5}$ (*20*), without any compelling evidence of nonlinear behavior associated, for example, with dislocation multiplication (*17*, *21*, *22*).

Microstructures of the hot-pressed and pre-deformed specimens, in particular the markedly different densities of dislocations, were imaged by backscattered electrons (Fig. 1). The reduction in dislocation density during high-temperature forced-oscillation testing was around 50% higher than predicted by a previous study of recovery kinetics (*19*). There was otherwise little microstructural evolution of the compressively pre-deformed specimens. A clean foam texture was preserved, with straight grain boundaries and only minor grain growth (Fig. 1 and Table 1). After the forced-oscillation testing, we found the torsionally pre-deformed specimen T0436 to have a somewhat smaller grain size and a more uniform fabric than before testing (fig. S4).

Forced-oscillation testing of both compressively and torsionally pre-deformed solution-gelation (sol-gel) olivine (supplementary materials) demonstrates a systematic reduction of shear modulus with increasing oscillation period and temperature (Fig. 2, A and B). We find a similar period dependence for $Q^{-1}$ of both specimens (Fig. 2, C and D), with systematically and monotonically higher dissipation toward longer oscillation periods and higher temperatures. The $G$ and $Q^{-1}$ data from the more highly pre-deformed specimens (D6646 and T0436) are similar in many respects, consistent with their similar grain sizes. However, the final dislocation density of T0436 was lower by a factor of 4 and close to that of the hot-pressed specimen H6585 (Table 1). If we compare our data for the two more-highly pre-deformed specimens with a Burgers-type creep function (JF) model describing the behavior of undeformed but otherwise equivalent specimens (*16*), it becomes clear that the shear modulus measured on each of the pre-deformed specimens (Fig. 2, A and B) is more strongly period-dependent above 1000°C than in the JF model (Fig. 2). Also, $G$ is higher at low temperature for the torsionally pre-deformed specimen, possibly reflecting elastic anisotropy associated with crystallographic preferred orientation (fig. S4). The dissipation measured for each pre-deformed specimen (Fig. 2, C and D) is substantially higher across the entire range of oscillation periods than in the JF model, especially at relatively high temperatures (Fig. 2). The increased dissipation and shear modulus dispersion of pre-deformed specimens as compared to the JF model for the behavior of undeformed specimens suggest that dislocations introduced during prior deformation are responsible for the substantial enhancement of a broad anelastic absorption band. We did not observe a dissipation peak that is diagnostic of a narrow distribution of relaxation times.

Overall, dissipation increased systematically with increasing strain or dislocation density in prior compressive deformation (D6618 and D6646) as compared to undeformed olivine (H6585) (Fig. 3). Furthermore, the torsionally pre-deformed specimen T0436 was 2.4 times as dissipative as a compressively pre-deformed specimen of the same final dislocation density (Fig. 3). The linear $Q^{-1}(\rho)$ trends

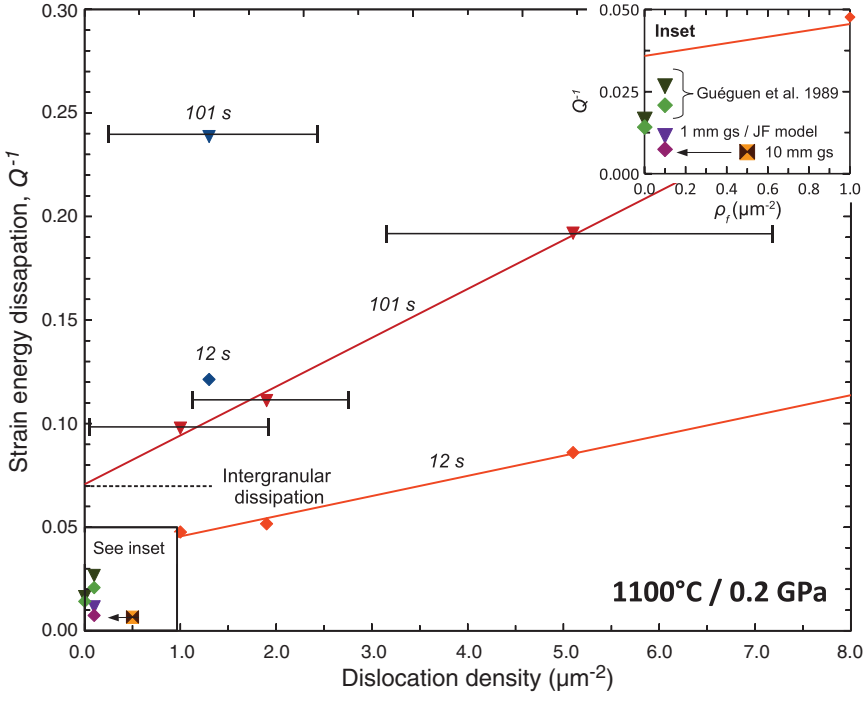


**Fig. 3.** Dissipation data (red/orange symbols) plotted against final dislocation density at 1100°C and 0.2 GPa confining pressure, for two representative oscillation periods: 12 s (inverted triangles) and 101 s (diamonds). Data for compressively pre-deformed olivine define the red linear trends, whose intercepts represent dissipation inferred for the intergranular relaxation processes acting alone. The data for torsionally pre-deformed olivine are shown by the blue symbols. The error bars attached to the 101-s data represent 1 SD for the population of estimates of dislocation density. Uncertainties in $G$ and $Q^{-1}$ are best estimated a posteriori from the scatter of the data around the generally systematic trends with varying oscillation period and temperature. Results from forced-oscillation testing on single-crystal forsterite (un-deformed and pre-deformed) are shown by the light- and dark-green symbols (*17*). The results of evaluating the JF model (*16*) for upper-mantle grain sizes (gs's) of 1 mm (purple inverted triangle for 101 s and magenta diamond for 12 s) and 10 mm (brown bowtie for 101 s and orange square for 12 s) are positioned at $\rho \sim 0.1\ \mu m^{-2}$ (see inset).

(where ρ is the dislocation density) for the hot-pressed and the compressively deformed specimens for the representative 12- and 101-s oscillation periods, which intercept the $Q^{-1}$ axis at ~0.035 and 0.07 respectively, reflect contributions from intergranular relaxation processes, such as grain-boundary sliding, in the fine-grained (3 to 6 μm) polycrystalline olivines of this study. The additional dissipation, attributable to dislocation damping, was approximately $Q^{-1} = 0.024 \times \rho\ (\mu m^{-2})$ at a 101-s period for the compressively pre-deformed materials. Thus, dislocation damping may account for about 25% of the dissipation measured in the fine-grained (3.1 μm) hot-pressed specimen 6585.

In order to assess the relative contributions of these two dissipation mechanisms for the larger grain sizes expected of Earth's mantle, we used the previously mentioned JF model (*16*), describing the behavior of undeformed, essentially dry and melt-free polycrystalline olivine (including H6585), of average dislocation density ~0.1 $\mu m^{-2}$. This model, evaluated under laboratory conditions of 0.2 GPa and 1100°C and at the experimental periods near 12 and 101 s for representative upper-mantle grain sizes of 1 and 10 mm, yields values of $Q^{-1}$ between 0.0065 and 0.0115 (Fig. 3, inset). Such dissipation is largely due to intergranular relaxation rather than dislocation damping. For compressively pre-deformed olivine tested at a 101-s period, comparable levels of dissipation would be expected from dislocation damping alone for upper-mantle dislocation densities of 0.3 to 0.5 $\mu m^{-2}$. The torsionally pre-deformed specimen (T0436) of the present study, with a population of dislocations similarly favorably oriented for glide, displayed much higher levels of dislocation damping than did compressively pre-deformed materials of comparable dislocation density. We conclude therefore that dislocation damping associated with typical upper-mantle dislocation densities (~0.01 to 0.1 $\mu m^{-2}$) (*10*, *23*) may contribute comparably with grain-boundary–related dissipation (with associated shear wave dispersion), especially in regions of Earth's upper mantle that are subject to relatively high prevailing (or fossil) deviatoric stress σ and consequently high dislocation density (*11*), and for shear waves with propagation/polarization directions that provide high resolved shear stress for dislocation glide.

Deformation in and beneath the oceanic lithosphere spreading away from a mid-ocean ridge involves simple shear in the vertical plane parallel to the spreading direction. This shear, if accomplished by glide on the dominant [100](010) slip system of olivine, will tend to result in rotation of the (010) planes of individual olivine crystals toward the horizontal so that [100] is preferentially aligned with the spreading direction. A crystallographic preferred orientation of this type, commonly measured in mantle xenoliths, provides the accepted explanation of the azimuthal anisotropy of compressional ($P_n$) wave speed (*6*, *24*, *25*). This fabric provides favorable average $V_{SH} > V_{SV}$ ($V_{SH}$, shear wave velocity with horizontal polarization; $V_{SV}$, shear wave velocity with vertical polarization) in transversely isotropic seismological wave speed models (*26*) that account for the discrepancy between Rayleigh and Love surface wave velocities (*27*). This fabric offers optimal average resolved shear stress for [100](010) dislocation glide for the geometry of the simple shear stress field controlling ongoing tectonic deformation beneath the oceanic plate. The same stress field applies to vertically travelling shear waves polarized parallel to the direction of plate motion direction. Accordingly, we predict that these seismic waves should be most strongly attenuated by dislocation glide in the suboceanic mantle.

Our data demonstrate that strain-energy dissipation (and shear modulus dispersion) associated with grain-boundary relaxation phenomena are augmented by the effects of dislocation relaxation. The relaxation strength is expected to vary linearly with the dislocation density, and in turn with the magnitude of the fossil/prevailing stress field as $\rho \propto \sigma^2$ (*11*). However, only in relatively cool parts of the lithosphere is a high dislocation density, reflecting a high fossil stress, likely to survive the process of static dislocation recovery. Under these circumstances, the relevant tectonic settings of high potential for dislocation damping will be regions in the lower lithosphere and asthenosphere, where olivine is or was deformed via (steady-state) dislocation creep. These regions include suboceanic mantle, deep-lithosphere shear zones, and the material immediately above and beneath an actively subducting slab.

### References and Notes


1. D. L. Kohlstedt, B. Evans, S. J. Mackwell, *J. Geophys. Res.* **100**, 17587 (1995).
2. F. Cammarano, B. Romanowicz, *Geophys. J. Int.* **175**, 116 (2008).
3. C. A. Dalton, G. Ekström, A. M. Dziewonski, *Earth Planet. Sci. Lett.* **284**, 65 (2009).
4. I. M. Artemieva, M. Billien, J. Lévêque, W. D. Mooney, *Geophys. J. Int.* **157**, 607 (2004).
5. H. W. Green II, S. V. Radcliffe, *Earth Planet. Sci. Lett.* **15**, 239 (1972).
6. H. H. Hess, *Nature* **203**, 629 (1964).
7. S. Zhang, S. Karato, *Nature* **375**, 774 (1995).
8. A. Tommasi, D. Mainprice, G. Canova, Y. Chastel, *J. Geophys. Res.* **105**, 7893 (2000).
9. T. Mizukami, S. R. Wallis, J. Yamamoto, *Nature* **427**, 432 (2004).
10. C. Goetze, D. L. Kohlstedt, *J. Geophys. Res.* **78**, 5961 (1973).
11. J. B. Minster, D. L. Anderson, *Philos. Trans. R. Soc. Lond.* **299**, 319 (1981).
12. T. T. Gribb, R. F. Cooper, *J. Geophys. Res.* **103**, 27267 (1998).
13. R. F. Cooper, *Rev. Mineral. Geochem.* **51**, 253 (2002).
14. B. H. Tan, I. Jackson, J. D. Fitz Gerald, *Phys. Chem. Miner.* **28**, 641 (2001).
15. I. Jackson, U. H. Faul, J. D. Fitz Gerald, S. J. S. Morris, *Mater. Sci. Eng. A* **442**, 170 (2006).
16. I. Jackson, U. H. Faul, *Phys. Earth Planet. Inter.* **183**, 151 (2010).
17. Y. Gueguen, M. Darot, P. Mazot, J. Woirgard, *Phys. Earth Planet. Inter.* **55**, 254 (1989).
18. I. Jackson, M. S. Paterson, *Pure Appl. Geophys.* **141**, 445 (1993).
19. R. J. M. Farla *et al.*, *Phys. Chem. Miner.* **38**, 363 (2011).
20. I. Jackson, *Geophys. Res. Lett.* **20**, 2115 (1993).
21. Y. Gueguen, J. M. Mercier, *Phys. Earth Planet. Inter.* **7**, 39 (1973).
22. I. Jackson, in *Treatise on Geophysics,* G. Schubert, Ed. (Elsevier, Amsterdam, Netherlands, 2007), pp. 493–525.
23. M. Toriumi, *Contrib. Mineral. Petrol.* **68**, 181 (1979).
24. R. W. Raitt, G. G. Shor Jr., T. J. G. Francis, G. B. Morris, *J. Geophys. Res.* **74**, 3095 (1969).
25. D. Barnford, S. Crampin, *Geophys. J. R. Astron. Soc.* **49**, 1 (1977).
26. D. Mainprice, in *Treatise on Geophysics,* G. Schubert, Ed. (Elsevier, Oxford, 2007), vol. 2, pp. 437–492.
27. D. W. Forsyth, *Geophys. J. R. Astron. Soc.* **43**, 103 (1975).
28. M. S. Paterson, *Bull. Mineralogie* **105**, 20 (1982).


**Acknowledgments:** We thank H. Kokkonen, C. Saint, H. Miller, and F. Brink for experimental help and D. Kohlstedt for allowing us to use his laboratory at the University of Minnesota. The Australian government (an Endeavor International Postgraduate Research Scholarship), a Mervyn and Katalin Paterson Fellowship (Research School of Earth Sciences–Australian National University), and NASA grant NNX11AF58G supported this work. We thank three anonymous reviewers for helping to improve the manuscript. The raw data are available in the supplementary materials.

### Supplementary Materials

www.sciencemag.org/cgi/content/full/336/6079/332/DC1
Materials and Methods
Figs. S1 to S4
Databases S1 to S5
References (*29*–*37*)

22 December 2011; accepted 20 March 2012
10.1126/science.1218318



# Dynamic Causes of the Relation Between Area and Age of the Ocean Floor

**N. Coltice,[1,2]* T. Rolf,[3] P. J. Tackley,[3] S. Labrosse[1,2]**

**The distribution of seafloor ages determines fundamental characteristics of Earth such as sea level, ocean chemistry, tectonic forces, and heat loss from the mantle. The present-day distribution suggests that subduction affects lithosphere of all ages, but this is at odds with the theory of thermal convection that predicts that subduction should happen once a critical age has been reached. We used spherical models of mantle convection to show that plate-like behavior and continents cause the seafloor area-age distribution to be representative of present-day Earth. The distribution varies in time with the creation and destruction of new plate boundaries. Our simulations suggest that the ocean floor production rate previously reached peaks that were twice the present-day value.**

The distribution of ages of the ocean floor is a first-order observation that determines the evolution of Earth's surface and interior (*1*). Because heat flow and bathymetry directly depend on the age of the ocean floor (*2*), a shift in the area-age distribution profoundly modifies Earth's cooling (*3*), sea level (*4*, *5*), and consequently global climate (*6*, *7*). The characterization

of the age of the ocean floor has shown that its present-day area per unit age decreases roughly linearly with increasing age (*8*, *9*), defining a function triangular in shape (Fig. 1A) for which a common expression is

$$\frac{dA(t)}{dt} = C_0\left(1 - \frac{t}{t_{max}}\right) \quad (1)$$

where $A(t)$ is the area of ocean floor that is younger than age $t$, $C_0$ is the rate of generation of new ocean floor, and $t_{max}$ is the age of the oldest seafloor [where present-day $C_0$ and $t_{max}$ are 3.01 km$^2$ year$^{-1}$ and 180 million years (My), respectively, and $C_0(t_{max}/2)$ is the total oceanic surface].

If such a distribution were to define a steady state, it would result from a constant production of ocean floor for the past 180 My combined with a consumption of seafloor, with a probability independent of its age (*1*, *10*). However, an evolving crustal production could explain the variance of the data equally well (*11*) and one-dimensional (1D) models provide a good fit to the present-day observations as long as spreading rates have varied (*12*). Indeed, seafloor spreading reconstructions have shown variations of ocean floor production, essentially through creation of mid-ocean ridges after the breakup of Pangea (*13*–*15*). As a consequence, the distribution has differed from the triangular shape we observe today (*12*, *15*).

The dynamic origin of the area-age distribution is a subject of debate, because subduction of young and buoyant seafloor seems at odds with the principles of convection that predict instabilities of the top boundary layer occurring for old and cooled material only. Continents may geometrically impose subduction of seafloor independently of the age (*3*), but other mechanisms could also reduce the dependence of subduction on seafloor age. Most of them involve rheological complexities of plates such as plate bending (*16*) and dehydration stiffening (*17*). However, simulations of mantle convection have never predicted any consistent triangular area-age distribution, thereby failing to satisfy an elementary geological constraint on mantle dynamics.

We performed 3D spherical mantle convection simulations introducing minimal complexity to study the causes of the triangular area-age distributions (*18*). In the following models, we varied the number of continents (for a constant surface fraction of 30%) and the rheology (isoviscous or inducing plate-like behavior). In these simulations, we calculated synthetic ages for the ocean floor from the computed local heat flow by means of the half-space cooling approximation (*18*), which is a very good approximation for a mantle convection model (*3*). However, the synthet-

[1]Laboratoire de Géologie de Lyon, Université Lyon 1; Ecole Normale Supérieure de Lyon; Université de Lyon; CNRS, 69100 Villeurbanne, France. [2]Institut Universitaire de France. [3]Institute of Geophysics, ETH Zürich, 8092 Zürich, Switzerland.

*To whom correspondence should be addressed. E-mail: nicolas.coltice@univ-lyon1.fr

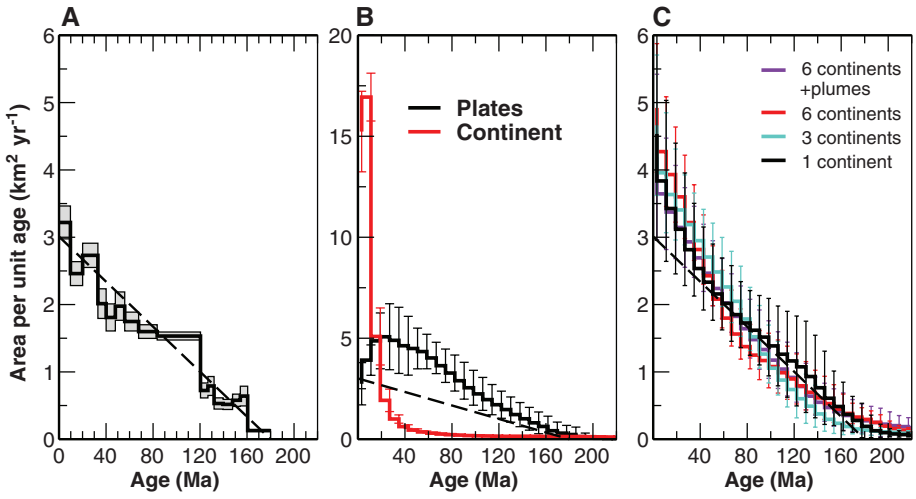


**Fig. 1.** (**A**) Distribution of area versus age (Ma, millions of years ago) of the ocean floor on the present-day Earth from (*9*). (**B**) Time-averaged distribution computed in 3D spherical simulations implementing continents (red) or plate-like behavior (black) over 5 billion years. (**C**) Time-averaged distribution computed in 3D spherical simulations implementing continents (their cumulative area is 30% of the total) and plate-like behavior. The model with plumes (purple) has 15% of core heating generating hot plumes. The straight dashed line in each panel represents the best triangular fit for the present-day distribution. The error bars show the standard deviation of the distribution.

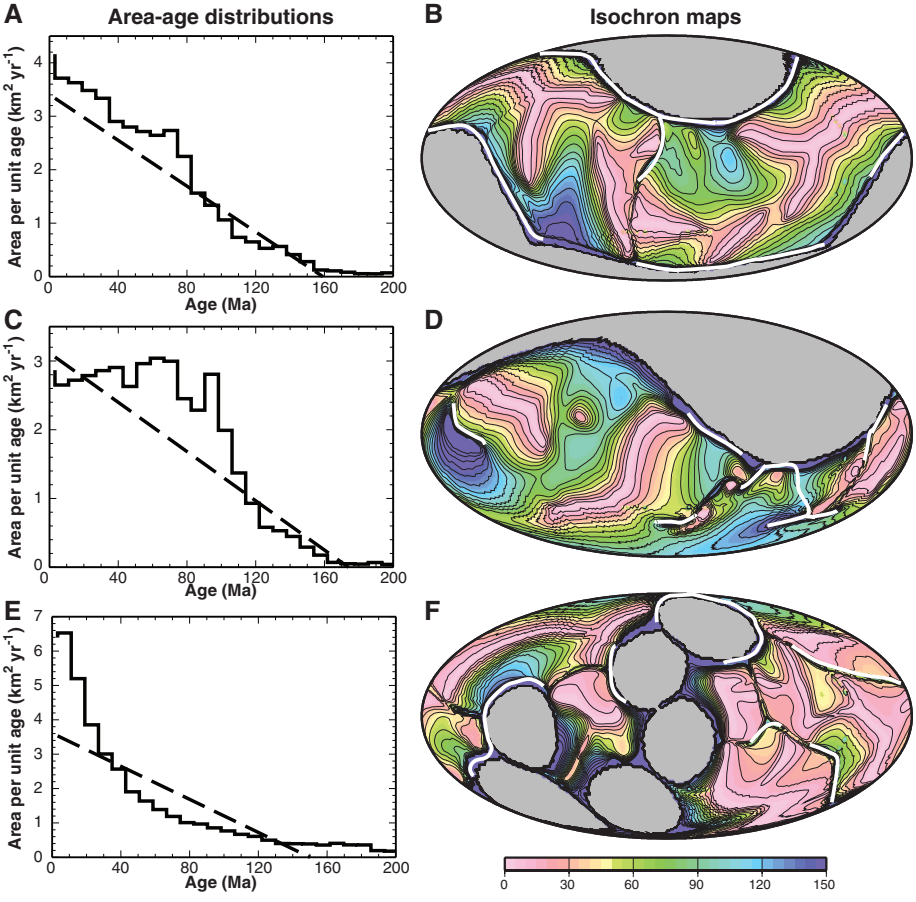


**Fig. 2.** Snapshots of the distribution of the area versus age of the ocean floor along with the corresponding best triangular fit in dashed lines (left) and maps of synthetic isochrons (right) computed in the 3D spherical convection models. The gray areas on the maps represent the continents, the white lines are the positions of the downwellings, and the age contours are plotted at 10-My intervals. (**A** and **B**) An example corresponding to a triangular distribution (with three continents covering respectively 15%, 10%, and 5% of the surface). (**C** and **D**) An example for a flat distribution (one supercontinent). (**E** and **F**) An example for a skewed distribution (six continents covering 5% of the surface each).

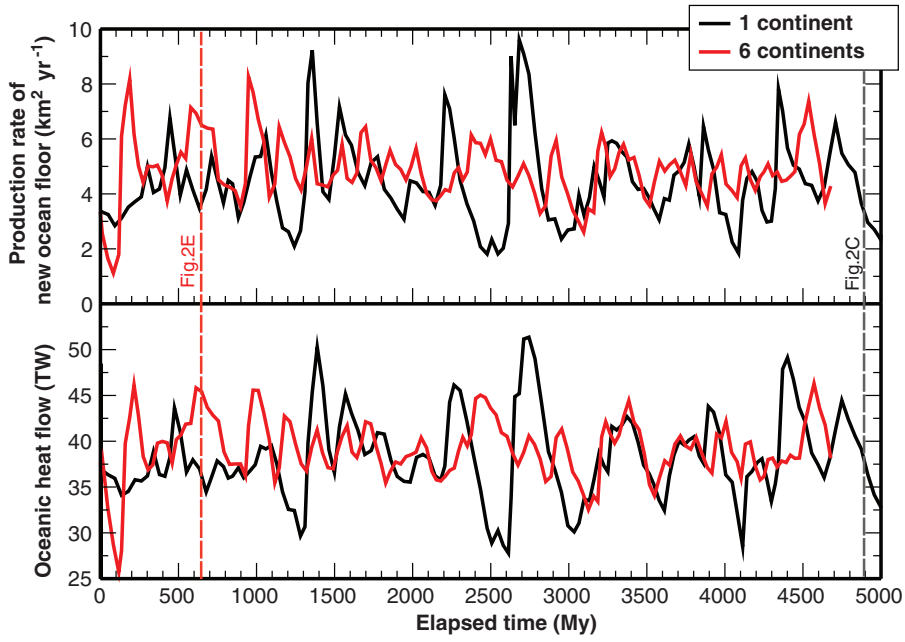


**Fig. 3.** Production rate of new ocean floor (top) and oceanic heat flow (bottom) as a function of elapsed time in models with the supercontinent covering 30% of the surface (black) and with six continents each covering 5% of the surface (red). The average productions are 4.91 km year$^{-1}$ with one continent and 4.55 km year$^{-1}$ with six continents, with standard deviations of 1.59 km year$^{-1}$ and 0.97 km year$^{-1}$, respectively. The transit time $\tau_s$ of 85 My is used for the scaling (*18*). The averages of the heat flow are 38.2 TW with one continent and 39.3 TW with six continents, with standard deviations of 4.8 TW (12%) and 2.8 TW (7%), respectively. The vertical dashed lines illustrate the points in time represented in Fig. 2C and Fig. 2E. The distributions computed over the time period give the average distributions in Fig. 1C.

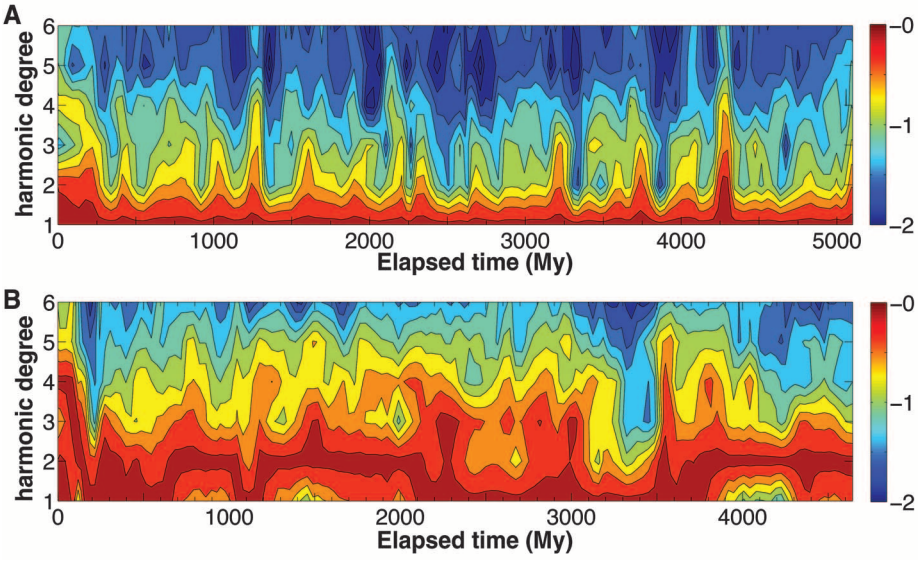


**Fig. 4.** (**A** and **B**) Evolution of the average spectral heterogeneity of the temperature field in (A) the supercontinent case and (B) the six-continent case, corresponding to the evolution depicted in Fig. 3. Shown are powers of the first six harmonic degrees in a logarithmic scale, depth-averaged over the upper mantle. For each point in time, the spectrum is normalized separately with the maximum spectral power occurring at this time. The color scale corresponds to the normalized power.

ic ages can be biased in regions of downwellings and in diffuse zones of extension or compression where heat transport is more complex.

Convection simulations integrated over 5 billion years generated time-averaged distributions of the area versus synthetic age of ocean floor. For the model with six continents (each covering 5% of the surface area) but without plate-like behavior (i.e., the viscosity is constant for each material), the synthetic area-age distribution is not triangular but the area decreases with age faster than exponentially (Fig. 1B). As previously observed, this is typical of internally heated convection (*3*, *19*). The area-age distribution for the model without continents but with plate-like behavior is also not triangular (Fig. 1B); it displays a skewed plateau. The plateau expresses the fact that young and hot material is not entrained in subduction and only the lithosphere that has reached a certain age (here, around 60 My) can be subducted. These distributions are consistent with those already computed in models without continents and in cartesian geometry (*3*).

When plate-like behavior and continents are combined, the average area-age distribution is close to a triangular shape with an approximately linear decrease of the area with increasing age and a present-day production of seafloor slightly larger than the observed present-day value (Fig. 1C). The averaged synthetic distributions given by the convection models with continents and plate-like behavior are in good agreement with the observed triangular distribution for the present-day Earth and with a 1D distribution corresponding to a model with a subduction probability depending on the square root of age (*12*). Simulations with different numbers and sizes of continental blocks, with and without a reasonable amount of core heating (15% of the total heat flow), yield results with very little differences.

Within the course of a simulation, the area-age distribution is mostly triangular but evolves with the birth of new plate boundaries and the vanishing of others. When the distribution is triangular (Fig. 2A), ridge-like structures with "young" ocean floor end at triple junctions and regions of transform motion (Fig. 2B). The downwellings here are mostly located on the edges of the continents. Several of the ridge-like structures are cut by downwellings, highlighting the sinking of "young" material in these models. Here, continents seem to act as a geometrical constraint that imposes the location of downwellings at the continent-ocean boundary.

A first type of nontriangular distribution (Fig. 2C) is relatively flat with a smaller value for the production of new ocean floor ($t_{max}$ is about the same as for the triangular shape), where downwellings are not all located on the edges of the continents (Fig. 2D). Such a distribution is more likely encountered in simulations with few continents (one or two), rather than with many. This distribution is close to that observed with plate-like behavior and without continents described above. Hence, a flat distribution could occur when the geometrical influence of the continents on the location of downwellings is minimal and when the flow is self-organized so that ocean floor is free to reach a critical buoyancy before starting to sink.

A second type of nontriangular distribution, observed in all the simulations at times where new plate boundaries are generated (Fig. 2E), has two characteristics: a large production of new ocean floor (here almost twice the time-averaged one) and a relative skewness. In this snapshot, ridge-like structures dominate and are very irregular.

They are formed in response to the onset of new cold instabilities. They develop and a reorganization of the flow takes place to progressively produce a more triangular distribution. Variations in the shape of the distribution with time are consistent with reconstructions for the past 150 My (*12*, *14*, *15*). The shape of the distribution may have evolved from flat-like, when Pangea was barely splitting, to a skewed distribution after the birth of new ridges (*15*), ultimately transforming to the present-day triangular shape with dispersed continents.

Like the shape of the area-age distribution, the rate of production of new ocean floor (younger than 10 My) in the mantle convection models varies with time (Fig. 3). Fluctuations are moderate—32% and 21% of the mean value for the supercontinent and six-continent cases, respectively—but they can reach 100% at times, doubling or halving the production of new ocean floor. The strongest variations occur on a time scale of 500 million years, which corresponds to the time scale of flow reorganization through the onset of new plate boundaries. The peaks of production are generally correlated with the generation of new plate boundaries and peaks in heat flow (like the configuration in Fig. 2F). The fluctuations are stronger with one continent than with six continents. Many small continents make the flow adopt a smaller wavelength, so that a change in plate organization has a smaller contribution to the total (Fig. 4). The smaller wavelength imposes a higher time-averaged heat flow than for the supercontinent case (*20*). The magnitudes and time scales of the computed variations of the production of new ocean floor are comparable to those extracted from seafloor spreading reconstructions (*12*, *13*).

Our models provide a fundamental basis for realistically simulating Earth's mantle convection. Although they have relatively low Rayleigh numbers and simplified parameters for the interior of the mantle, they show that plate-like behavior and the presence of continents are the two necessary ingredients to build a model in which young seafloor is subducted like on Earth. Continents constrain the location and geometry of the downwellings that cool Earth's mantle. When subduction is confined at an ocean-continent boundary, convection forces the subduction of very young seafloor. Such a situation is favored by continental growth and dispersal. The distribution of seafloor age is a primary observation that should be used as a diagnostic when simulating Earth's mantle, predicting the long-term cooling of Earth, the fluctuations of sea level caused by tectonics (*21*) that ultimately condition climate change on geological time scales.

### References and Notes


1. B. Parsons, *J. Geophys. Res.* **87**, (B1), 289 (1982).
2. C. Stein, S. Stein, *Nature* **359**, 123 (1992).
3. S. Labrosse, C. Jaupart, *Earth Planet. Sci. Lett.* **260**, 465 (2007).
4. S. Gaffin, *Am. J. Sci.* **287**, 596 (1987).
5. L. Husson, C. Conrad, *Geophys. Res. Lett.* **33**, L18303 (2006).
6. R. Berner, Z. Kothavala, *Am. J. Sci.* **301**, 182 (2001).
7. N. Flament, N. Coltice, P. Rey, *Earth Planet. Sci. Lett.* **275**, 326 (2008).
8. J. Sclater, C. Jaupart, D. Galson, *Rev. Geophys.* **18**, 269 (1980).
9. J.-P. Cogné, E. Humler, *Earth Planet. Sci. Lett.* **227**, 427 (2004).
10. D. Rowley, *Geol. Soc. Am. Bull.* **114**, 927 (2002).
11. R. Demicco, *Geology* **32**, 485 (2004).
12. T. Becker, C. Conrad, B. Buffett, R. Müller, *Earth Planet. Sci. Lett.* **278**, 233 (2009).
13. C. Conrad, C. Lithgow-Bertelloni, *Geology* **35**, 29 (2007).
14. R. Müller, M. Sdrolias, C. Gaina, W. Roest, *Geochem. Geophys. Geosyst.* **9**, Q04006 (2008).
15. M. Seton, C. Gaina, R. Müller, C. Heine, *Geology* **37**, 687 (2009).
16. C. Conrad, B. Hager, *J. Geophys. Res.* **104**, 17551 (1999).
17. C. Lee, A. Lenardic, C. Cooper, F. Niu, A. Levander, *Earth Planet. Sci. Lett.* **230**, 379 (2005).
18. See supplementary materials on *Science* Online.
19. T. Yanagisawa, Y. Hamano, *Geophys. Res. Lett.* **26**, 791 (1999).
20. C. Grigné, S. Labrosse, P. Tackley, *J. Geophys. Res.* **110**, B03409 (2005).
21. R. D. Müller, M. Sdrolias, C. Gaina, B. Steinberger, C. Heine, *Science* **319**, 1357 (2008).



**Acknowledgments:** We thank R. D. Müller and T. W. Becker for fruitful reviews. Supported by Institut Universitaire de France and ANR grant DynBMO (Dynamique de l'océan de magma basal) ANR-08-JCJC-0084-01 (N.C. and S.L.) and by Crystal2Plate, a FP-7 funded Marie Curie action under grant agreement PITN-GA-2008-215353 (T.R.). Supercomputing resources were provided by ETH and the Swiss Supercomputer Centre (CSCS).


### Supplementary Materials

www.sciencemag.org/cgi/content/full/336/6079/335/DC1
Materials and Methods
Data File and Codes
References (*22*–*27*)


13 January 2012; accepted 21 March 2012
10.1126/science.1219120


# A Segmentation Clock with Two-Segment Periodicity in Insects


**Andres F. Sarrazin,*† Andrew D. Peel,† Michalis Averof‡**



**Vertebrate segmentation relies on a mechanism characterized by oscillating gene expression. Whether this mechanism is used by other segmented animals has been controversial. Rigorous proof of cyclic expression during arthropod segmentation has been lacking. We find that the segmentation gene *odd-skipped (Tc-odd)* oscillates with a two-segment periodicity in the beetle *Tribolium castaneum*. By bisecting embryos and culturing the two halves over different time intervals, we demonstrate that *Tc-odd* cycles with a period of about 95 minutes at 30°C. Using live imaging and cell tracking in green fluorescent protein–expressing embryos, we can exclude that cell movements explain this dynamic expression. Our results show that molecular oscillators represent a common feature of segmentation in divergent animals and help reconcile the contrasting paradigms of insect and vertebrate segmentation.**


Many animals generate body segments sequentially from a posterior region known as the growth zone (*1*, *2*). Whether there are common mechanisms underlying this process of segmentation in disparate segmented animals, such as vertebrates, annelids, and arthropods, has been intensely debated (*3*–*8*). A role for molecular oscillators in segmentation was initially proposed on theoretical grounds by Cooke and Zeeman (*9*). Their "clock and wavefront" model explained how the temporal periodicity of a clock could be translated into a repetitive spatial pattern during sequential segmentation. Subsequent studies showed that oscillating patterns of gene expression sweeping through the growth zone play a key role in vertebrate segmentation (*10*–*13*).

A number of studies have indicated that an equivalent segmentation clock may operate in the presegmental zone of arthropods (*3*–*5*, *14*, *15*). These studies revealed changing patterns of gene expression in the presegmental zone of an insect, a centipede, and a spider. They also showed that disrupting *Notch* signaling, which is an important element of the vertebrate segmentation clock (*13*, *16*), leads to defects in segmentation in some of these species. These results have been interpreted by some researchers as evidence that a common mechanism for segmentation was inherited by vertebrates and arthropods from a segmented common ancestor.

However, several doubts remain regarding this interpretation. First, Notch signaling is known to be involved in many other developmental processes, such as specification of the presegmental zone. These diverse functions may provide alternative explanations for segmentation defects (*8*, *17*, *18*). Second, cycling expression patterns have been inferred from in situ hybridization stainings on fixed embryos and comparison of similarly staged embryos. However, embryo-to-embryo variation and difficulty in accurately staging embryos (relative to the speed of segment formation) limits the reliability of this approach. Moreover, it has not yet been proven that these dynamic expression patterns reflect intracellular changes in gene expression, rather than cell movements. Thus, there is no rigorous demonstration that cyclic waves of expression are sweeping through the growth zone of arthropods. We use embryo culture and live imaging in the insect *Tribolium castaneum* to address these issues.


Institute of Molecular Biology and Biotechnology (IMBB), Foundation for Research and Technology Hellas (FORTH), Nikolaou Plastira 100, GR-70013 Heraklio, Crete, Greece.

*Present address: Instituto de Química, Pontificia Universidad Católica de Valparaíso, Casilla 4059, Valparaiso, Chile.
†These authors contributed equally to this work.
‡To whom correspondence should be addressed. E-mail: averof@imbb.forth.gr

We focus on the expression of the pair-rule ortholog *odd-skipped (Tc-odd)* during early germband elongation. *Tc-odd* is expressed in primary "pair-rule" stripes, corresponding to alternate segments, emerging from the growth zone (*19*); secondary segmental stripes appear later. Knockdown of *Tc-odd* arrests segmentation (*19*). We noticed that *Tc-odd* expression in the growth zone and in the overlying amnion varies among similarly staged embryos (Fig. 1). In particular, embryos that have the same number of primary *Tc-odd* stripes in the segmented part of the embryo show differences in the extent and strength of *Tc-odd* expression within the posterior growth zone (e.g., compare panels A′ to F′ in Fig. 1). These differences are also evident when *Tc-odd* expression is compared to the expression of the *Tribolium* ortholog of *even-skipped (Tc-eve)* (fig. S3). *Tc-odd* expression appears dynamic both in the ectoderm, the mesoderm, and the amnion (fig. S4). Taking the extent of amnion closure, the emergence of the secondary (segmental) *Tc-odd* stripes, and the overall shape of the germband as reference points (Fig. 1, A to F), we placed embryos in a putative temporal sequence and subdivided the period that leads to the production of each new *Tc-odd* stripe into three phases, named I, II, and III (see supporting online material and Fig. 1). By comparing these stainings to time-lapse recordings of live embryos (movie S1), using amnion closure as a reference, we roughly estimate that a new primary *Tc-odd* stripe is generated within 40 to 110 min at 30°C.

To address the criticism that different expression patterns may reflect variation among embryos, rather than temporal changes, we need to observe gene expression in the same embryo during successive time points. We achieved this using the approach taken by Palmeirim *et al*. (*10*) to prove oscillations in the vertebrate presomitic zone. First, we developed a method for *Tribolium* embryo culture, which allows the developing germband (embryo proper) to be dissected away from the surrounding yolk and serosa and to be grown in cell culture medium (Fig. 2). Germbands taken during early segmental stages (phase 3.III) continue to form segments for up to 5 hours in culture, at normal speed, with no overt morphological defects (Fig. 2C). This enabled us to bisect embryos in culture and to sample the expression pattern of *Tc-odd* at different time points in each half-embryo: Immediately after dissection, we cut individual germbands along the midline into halves (Fig. 2B); one half was fixed immediately after bisection ($t$ = 0), whereas the other was cultured over different time intervals (15 to 105 min) before fixation. Both halves were then simultaneously subjected to in situ hybridization for *Tc-odd*. By comparing expression in these half-embryos, we demonstrate that *Tc-odd* expression in the growth zone changes from high to low levels, and back to high levels again, during production of the third and fourth primary stripes (Fig. 2, D and E). These experiments allow us to define more precisely the cycling period of *Tc-odd*, which we estimate to be ~95 min at 30°C (fig. S5).

Next, we asked whether the observed changes in *Tc-odd* expression might be explained by cell movements in the growth zone, rather than changes in expression levels within cells. To directly address this, we established live imaging in *Tribolium* embryos and dissected germbands. We generated a transgenic line expressing nuclear-localized green fluorescent protein (GFP) driven by a *Tribolium* ubiquitous promoter (see supporting online material) and developed methods for imaging live *Tribolium* embryos under a spinning-disc confocal microscope. Whole embryos could be kept alive for more than 5 hours, with no apparent defects in morphogenesis, allowing us to visualize morphogenetic processes such as embryo condensation, amnion formation, germband elongation, and segmentation (Fig. 3A and movies S1 and S2). Dissected germbands were viable under a coverslip and could be imaged for 2 to 3 hours, allowing us to track the movements of individual nuclei in the growth zone and elongating germband (movie S3). Although only a small number of nuclei can be tracked reliably over a period of 1 hour at 30°C, this is sufficient to provide a map of cell movements in the early *Tribolium* germband (Fig. 3B). Compared with *Tc-odd* expression in corresponding stages, this map shows that cell movements could not account for the changes in *Tc-odd* expression that we observe in the growth zone

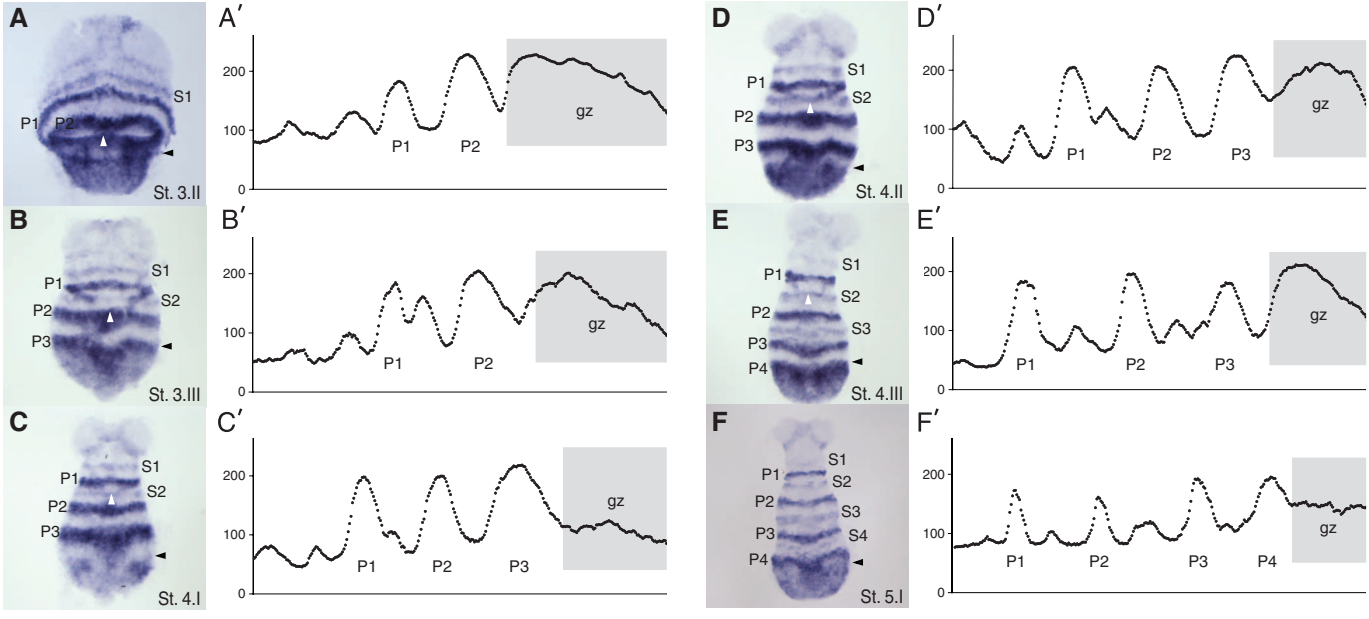


**Fig. 1.** Expression of *Tc-odd* during early germband elongation. (**A** to **F**) In situ hybridization for *Tc-odd* in elongating germbands at stages 3.II to 5.I, in ventral view (for staging, see supporting online material). The growth zone is located posterior to the black arrowheads. White arrowheads mark the posterior edge of the amniotic fold. (**A′** to **F′**) Intensity profiles of *Tc-odd* expression along the anterior-posterior axis of germbands. The intensity of staining was measured on the lateral part of the germbands shown in (A) to (F), encompassing the ectoderm and the amnion (for explanations, see fig. S1). Note the changing profile of *Tc-odd* expression within the posterior growth zone (gray area) during the emergence of new primary *Tc-odd* stripes from that zone. During phase I of stripe formation [(C) and (F)], the growth zone has low levels of *Tc-odd*, except for two lateral spots of expression that mark the initiation of a new cycle of *Tc-odd* expression. At phase II [(A) and (D)], *Tc-odd* expression extends through the growth zone, such that a posterior domain of high *Tc-odd* expression is established. At phase III [(B) and (E)], *Tc-odd* expression in the posterior-most part of the growth zone is reduced to low levels, whereas cells at the anterior of the growth zone still express high levels, establishing a broad primary stripe. In a typical collection of embryos, each phase is found in roughly equal numbers. P1 to P4, primary stripes; S1 to S4, intercalating secondary stripes; gz, growth zone.

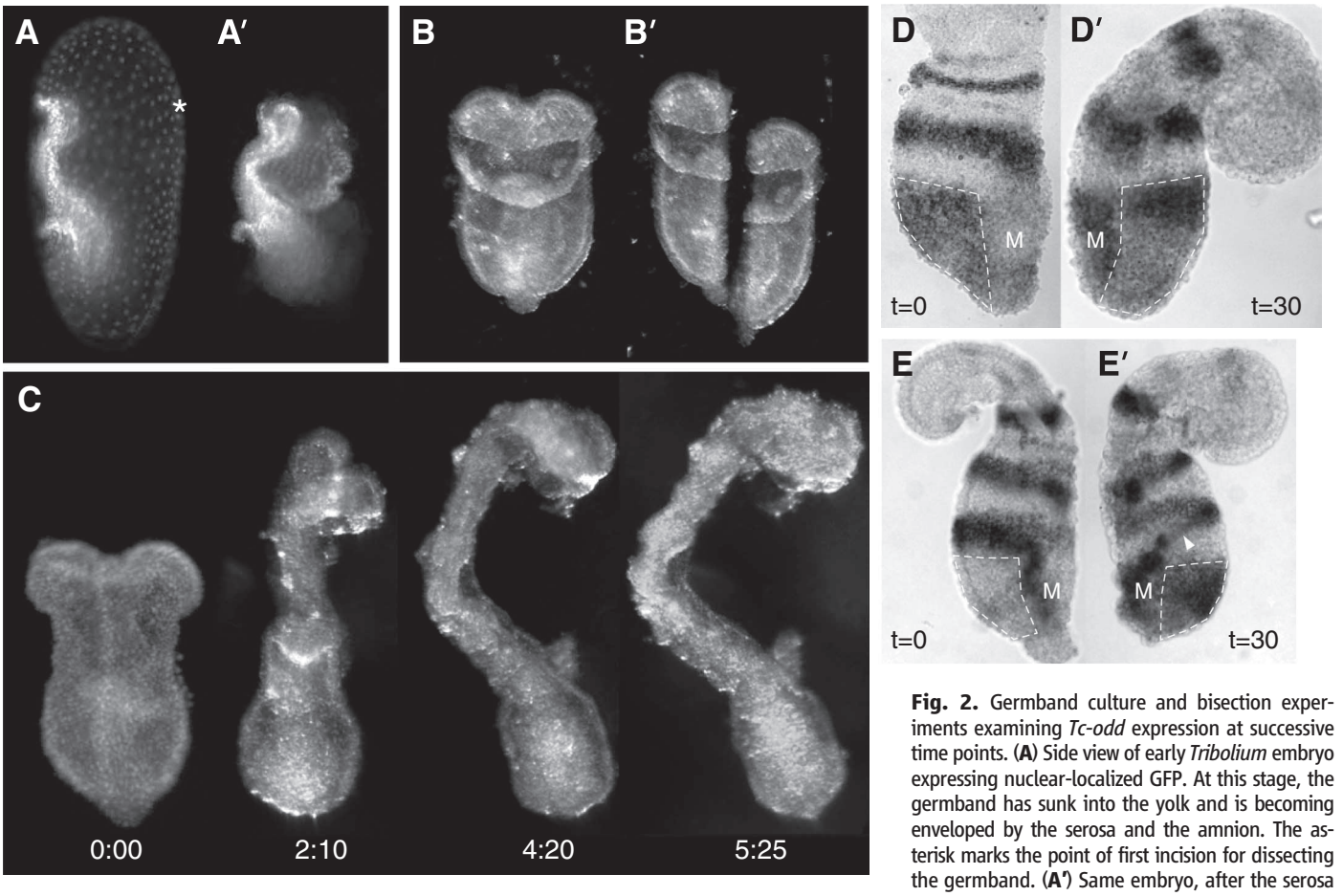


**Fig. 2.** Germband culture and bisection experiments examining *Tc-odd* expression at successive time points. (**A**) Side view of early *Tribolium* embryo expressing nuclear-localized GFP. At this stage, the germband has sunk into the yolk and is becoming enveloped by the serosa and the amnion. The asterisk marks the point of first incision for dissecting the germband. (**A′**) Same embryo, after the serosa and yolk have been partially removed. (**B**) Ventral view of fully dissected germband in culture. (**B′**) Same embryo shown after bisection along the midline. (**C**) Successive pictures of a germband in culture. The germband was mounted under a coverslip and cultured for more than 5 hours at 30°C. (**D** and **D′**) In situ hybridization for *Tc-odd* on two halves of the same embryo. One half was fixed immediately after dissection (D), whereas the other was cultured for 30 min at 30°C before fixation (D′). *Tc-odd* expression in each half-embryo is at phase 3.II and 3.III, respectively. (**E** and **E′**) Same experiment, with half-embryos at phases 4.I and 4.II. The lateral part of the growth zone, encompassing the ectoderm and amnion, is outlined with a dashed line; the medial part, which also includes mesoderm, is marked M (see fig. S1). In panel E′, the oblique stripe of *Tc-odd* expression (white arrowhead) is in the amnion. Anterior is toward the top in all panels.

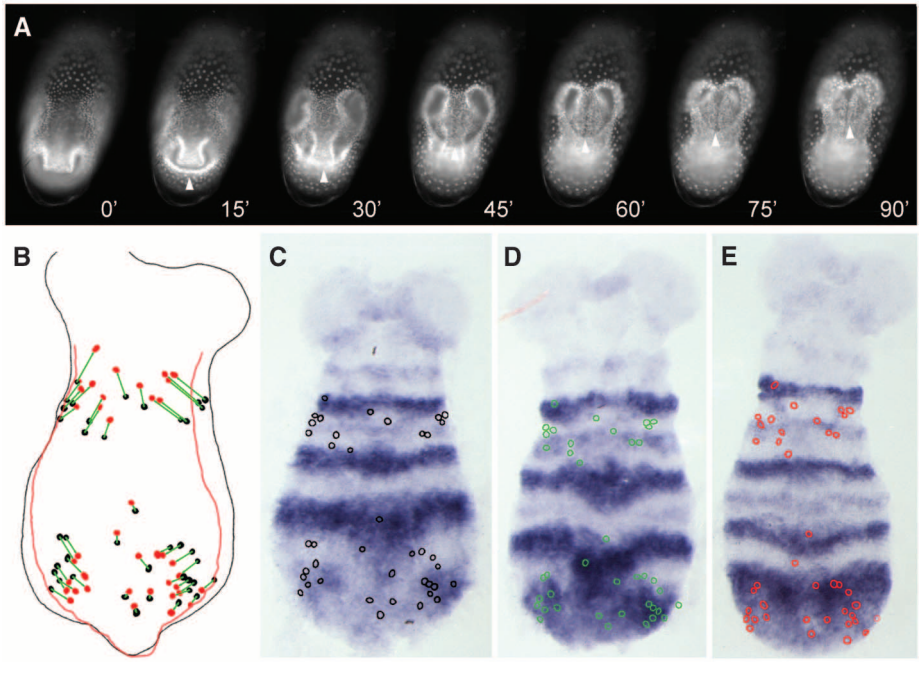


**Fig. 3.** Live imaging and tracking cell movements in *Tribolium* germbands. (**A**) Live imaging of *Tribolium* embryo expressing nuclear-localized GFP, during early stages of germband elongation. White arrowheads mark the posterior edge of the amniotic fold as it extends over the germband (compare to Fig. 1). The frames shown were taken at 15-min intervals at 30°C; the corresponding time-lapse movie is shown in movie S1. (**B**) Tracks of individual ectodermal cells over a 60-min period at 30°C; black circles mark the initial position of cells and red circles mark their final position. (**C** to **E**) Cell positions at 0, 30, and 60 min are superimposed on *Tc-odd* stained embryos at the corresponding developmental stages (4.I, 4.II, and 4.III) (see Fig. 1, C to E). Cell populations that initially express very low levels of *Tc-odd* subsequently lie in areas that express the gene at high levels, and then low levels. All panels show ventral views.

(Fig. 3, C to E). These changes must be due to changes in mRNA levels within cells.

We find that cells in the early extending germband tend to become separated along the anterior-posterior axis and converge toward the ventral midline, which indicates that they undergo convergent extension. This is likely to be a major force driving germband elongation. In contrast, mitosis does not appear to contribute significantly to early germband elongation (see fig. S6).

Overall, our analysis provides compelling evidence for a segmentation clock in the growth zone of arthropods. By exploiting methods for embryo culture, transgenic markers, live imaging, and cell tracking in *Tribolium*, we are able to demonstrate that oscillating expression is due to temporal changes in expression levels, proof of which was missing in previous studies. The clock involves *Tc-odd*, a pair-rule gene known to be essential for *Tribolium* germband elongation and segmentation (*19*). An *odd*-related gene is also expressed dynamically with a two-segment periodicity in the growth zone of a centipede (*4*), raising the possibility that a widely conserved segmentation clock may exist in the arthropods. These results are consistent with the hypothesis that pair-rule genes were ancestrally part of a segmentation clock and subsequently evolved regulation by gap genes, which underlies *Drosophila* segmentation (*20*).

In a wider context, our results support the idea that a clock-based mechanism underlies segmentation in animals as widely separated as arthropods and vertebrates. It will be interesting to discover whether this common feature reflects a common evolutionary origin of segmentation, or a design principle that was reinvented on separate occasions. In the latter case, the clock mechanism may have evolved independently but became integrated with a preexisting mechanism of posterior growth (*1*, *21*, *22*). Ultimately, this question might be resolved by comparing the gene regulatory networks underpinning the segmentation clock across phyla, as has already been attempted within the vertebrates (*16*). *Tribolium*, as an emerging model organism with an increasing array of genetic tools and resources (*23*), provides opportunities to investigate the arthropod clock mechanism by genetic means.

### References and Notes


1. B. L. Martin, D. Kimelman, *Curr. Biol.* **19**, R215 (2009).
2. V. Wilson, I. Olivera-Martinez, K. G. Storey, *Development* **136**, 1591 (2009).
3. A. Stollewerk, M. Schoppmeier, W. G. Damen, *Nature* **423**, 863 (2003).
4. A. D. Chipman, W. Arthur, M. Akam, *Curr. Biol.* **14**, 1250 (2004).
5. J. I. Pueyo, R. Lanfear, J. P. Couso, *Proc. Natl. Acad. Sci. U.S.A.* **105**, 16614 (2008).
6. N. Dray *et al.*, *Science* **329**, 339 (2010).
7. A. D. Chipman, *Bioessays* **32**, 60 (2010).
8. F. Kainz, B. Ewen-Campen, M. Akam, C. G. Extavour, *Development* **138**, 5015 (2011).
9. J. Cooke, E. C. Zeeman, *J. Theor. Biol.* **58**, 455 (1976).
10. I. Palmeirim, D. Henrique, D. Ish-Horowicz, O. Pourquié, *Cell* **91**, 639 (1997).
11. Y. Masamizu *et al.*, *Proc. Natl. Acad. Sci. U.S.A.* **103**, 1313 (2006).
12. M. L. Dequéant, O. Pourquié, *Nat. Rev. Genet.* **9**, 370 (2008).
13. A. C. Oates, L. G. Morelli, S. Ares, *Development* **139**, 625 (2012).
14. M. Schoppmeier, W. G. Damen, *Dev. Biol.* **280**, 211 (2005).
15. A. D. Chipman, M. Akam, *Dev. Biol.* **319**, 160 (2008).
16. A. J. Krol *et al.*, *Development* **138**, 2783 (2011).
17. H. Oda *et al.*, *Development* **134**, 2195 (2007).
18. T. Mito *et al.*, *Development* **138**, 3823 (2011).
19. C. P. Choe, S. C. Miller, S. J. Brown, *Proc. Natl. Acad. Sci. U.S.A.* **103**, 6560 (2006).
20. A. Peel, M. Akam, *Curr. Biol.* **13**, R708 (2003).
21. T. Copf, R. Schröder, M. Averof, *Proc. Natl. Acad. Sci. U.S.A.* **101**, 17711 (2004).
22. R. de Rosa, B. Prud'homme, G. Balavoine, *Evol. Dev.* **7**, 574 (2005).
23. S. J. Brown *et al.*, *Cold Spring Harbor Protocols* **2009**, pdb.emo126 (2009); http://dx.doi.org/10.1101/pdb.emo126.



**Acknowledgments:** We thank J. Schinko and G. Bucher for teaching us how to handle *Tribolium* and for help in generating the GFP-expressing transgenic line; J. P. Couso and S. Bishop for advice on embryo culture; D. Kosman, W. McGinnis, and C. Delidakis for advice on fluorescence in situ; and M. Strigini for critical comments on the manuscript. Our work was funded by the Marie Curie programs CELLIMAGE and ZOONET (FP6, European Union).


### Supporting Online Material

www.sciencemag.org/cgi/content/full/science.1218256/DC1
Materials and Methods
Figs. S1 to S6
Movies S1 to S3
References (*24*–*28*)


21 December 2011; accepted 27 February 2012
Published online 8 March 2012;
10.1126/science.1218256


# Synthetic Genetic Polymers Capable of Heredity and Evolution


**Vitor B. Pinheiro,[1] Alexander I. Taylor,[1] Christopher Cozens,[1] Mikhail Abramov,[2] Marleen Renders,[2]* Su Zhang,[3] John C. Chaput,[3] Jesper Wengel,[4] Sew-Yeu Peak-Chew,[1] Stephen H. McLaughlin,[1] Piet Herdewijn,[2] Philipp Holliger[1]†**



**Genetic information storage and processing rely on just two polymers, DNA and RNA, yet whether their role reflects evolutionary history or fundamental functional constraints is currently unknown. With the use of polymerase evolution and design, we show that genetic information can be stored in and recovered from six alternative genetic polymers based on simple nucleic acid architectures not found in nature [xeno-nucleic acids (XNAs)]. We also select XNA aptamers, which bind their targets with high affinity and specificity, demonstrating that beyond heredity, specific XNAs have the capacity for Darwinian evolution and folding into defined structures. Thus, heredity and evolution, two hallmarks of life, are not limited to DNA and RNA but are likely to be emergent properties of polymers capable of information storage.**


The nucleic acids DNA and RNA provide the molecular basis for all life through their unique ability to store and propagate information. To better understand these singular properties and discover relevant parameters for the chemical basis of molecular information encoding, nucleic acid structure has been dissected by systematic variation of nucleobase, sugar, and backbone moieties (*1*–*7*).

These studies have revealed the profound influence of backbone, sugar, and base chemistry on nucleic acid properties and function. Crucially, only a small subset of chemistries allows information transfer through base pairing with DNA or RNA, a prerequisite for cross-talk with extant biology. However, base pairing alone cannot conclusively determine the capacity of a given chemistry to serve as a genetic system, because hybridization need not preserve information content (*8*). A more thorough examination of candidate genetic polymers' potential for information storage, propagation, and evolution requires a system for replication that would allow a systematic exploration of the informational, evolutionary, and functional potential of synthetic genetic polymers and would open up applications ranging from biotechnology to materials science.

In principle, informational polymers can be synthesized and replicated chemically (*9*), with advances in the nonenzymatic polymerization of mononucleotides (*10*) and short oligomers (*11*, *12*) enabling model selection experiments (*13*). Nevertheless, chemical polymerization remains relatively inefficient. On the other hand, enzymatic polymerization has been hindered by the stringent substrate selectivity of polymerases. Despite progress in understanding the determinants of polymerase substrate specificity and in engineering polymerases with expanded substrate spectra (*7*), most unnatural nucleotide analogs are poor polymerase substrates at full substitution, as both nucleotides for polymer synthesis and templates for reverse transcription. Notable exceptions are 2'OMe-DNA and α-L-threofuranosyl nucleic acid (TNA). 2'OMe-DNA is present in eukaryotic ribosomal RNAs, is well tolerated by natural reverse transcriptases (RTs), and has been shown to support heredity and evolution at near full substitution (*14*). TNA allowed polymer synthesis and evolution in a three-letter system (*15*) but only limited reverse transcription (*16*).


[1]Medical Research Council (MRC) Laboratory of Molecular Biology, Hills Road, Cambridge CB2 0QH, UK. [2]Rega Institute, Katholieke Universiteit Leuven, Minderbroederstraat 10, B 3000, Leuven, Belgium. [3]Center for Evolutionary Medicine and Informatics, The Biodesign Institute at Arizona State University, 1001 South McAllister Avenue, Tempe, AZ 85287–5301, USA. [4]Nucleic Acid Center, Department of Physics and Chemistry, University of Southern Denmark, Campusvej 55, DK-5230 Odense M, Denmark.

*Present address: Department of Chemistry, University of British Columbia, Vancouver V6T 1Z1, Canada.
†To whom correspondence should be addressed. E-mail: ph1@mrc-lmb.cam.ac.uk

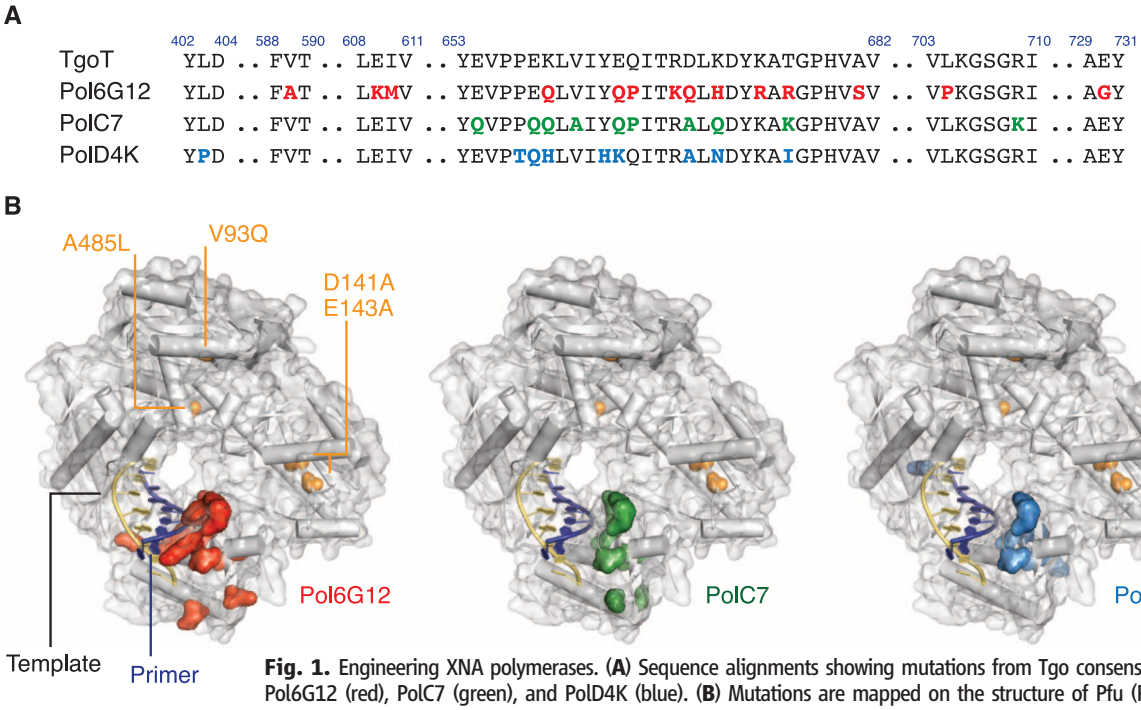


**Fig. 1.** Engineering XNA polymerases. (**A**) Sequence alignments showing mutations from Tgo consensus in polymerases Pol6G12 (red), PolC7 (green), and PolD4K (blue). (**B**) Mutations are mapped on the structure of Pfu (Protein Data Bank identification code: 4AIL). Yellow, template; dark blue, primer; orange, mutations present in the parent polymerase TgoT.

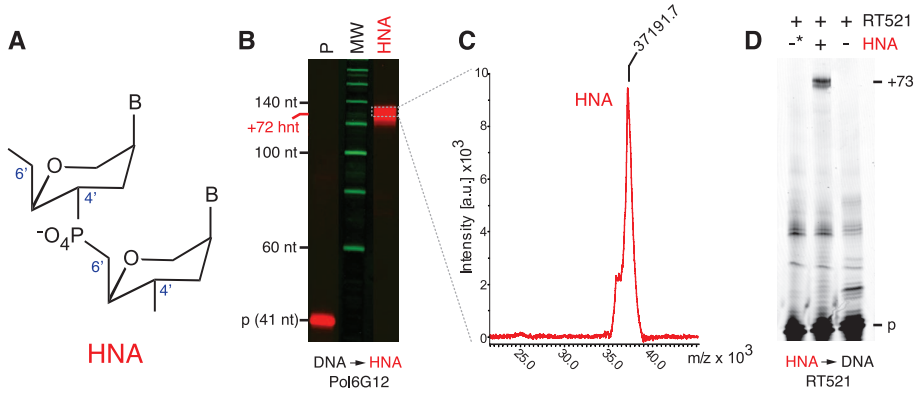


**Fig. 2.** HNA synthesis, MS analysis, and reverse transcription. (**A**) Structure of 1,5-anhydrohexitol (HNA) nucleic acids (B, nucleobase). (**B**) Pol6G12 extends the primer (p) incorporating 72 hNTPs against template T1 (table S3) to generate a full-length hybrid molecule with a 37,215-dalton expected molecular mass (*27*). MW, ILS 600 molecular weight marker. P, primer-only reactions. (**C**) Matrix-assisted laser desorption/ionization–time-of-flight spectrum of a full-length HNA molecule showing a measured HNA mass of 37,190 ± 15 daltons ($n$ = 3 measurements). a.u., arbitrary units; m/z, mass-to-charge ratio. (**D**) HNA reverse transcription (DNA synthesis from an HNA template). Polymerase-synthesized HNA (from template YtHNA4) (table S3) is used as template by RT521 for HNA-RT (-* denotes a no HNA synthesis control to rule out template contamination).

Here, we describe a general strategy to enable enzymatic replication and evolution of a broad range of synthetic genetic polymers based on: (i) a chemical framework [generically termed xeno-nucleic acid (XNA)] capable of specific base pairing with DNA, (ii) the engineering of polymerases that can synthesize XNA from a DNA template, and (iii) the engineering of polymerases that can reverse transcribe XNA back into DNA. We chose six different XNAs in which the canonical ribofuranose ring of DNA and RNA is replaced by five- or six-membered congeners comprising 1,5-anhydrohexitol nucleic acids (HNAs), cyclohexenyl nucleic acids (CeNAs), 2'-*O*,4'-*C*-methylene-β-D-ribonucleic acids [locked nucleic acids (LNAs)], arabinonucleic acids (ANAs), 2'-fluoro-arabino-nucleic acids (FANAs), and TNAs (*4*–*6*, *17*, *18*).

To enable discovery of polymerases capable of processive XNA synthesis, we developed a selection strategy called compartmentalized self-tagging (CST) (fig. S1). CST selections were performed on libraries of TgoT, a variant of the replicative polymerase of *Thermococcus gorgonarius* comprising mutations to the uracil-stalling [Val$^{93}$→Gln$^{93}$ (V93Q)] (*19*, *20*) and 3′-5′ exonuclease (D141A, E143A) functions, as well as the "Therminator" mutation (A485L) (*21*). TgoT libraries were created from both random and phylogenetic diversity targeted to 22 short sequence motifs within a 10 Å shell of the nascent strand (fig. S2).

CST selections with HNA and CeNA nucleotide triphosphates (hNTPs/ceNTPs) yielded rapid adaptation toward HNA and CeNA polymerase activity. One polymerase, Pol6G12 (TgoT: V589A, E609K, I610M, K659Q, E664Q, Q665P, R668K, D669Q, K671H, K674R, T676R, A681S, L704P, E730G) (Fig. 1A), displayed general DNA-templated HNA polymerase activity dependent on the presence of all four hNTPs (fig. S4) and enabled the synthesis of HNAs long enough to encode meaningful genetic information such as tRNA genes. HNA synthesis was further investigated by mass spectrometry (MS), confirming the expected molecular mass, composition, and sequence of HNA polymers (Fig. 2C and fig. S6).

Having established HNA synthesis, we sought to discover a reverse transcriptase for HNA (HNA-RT), capable of synthesizing complementary DNA from an HNA template, to retrieve the genetic information encoded in HNA and enable both analysis and evolution. As no available polymerase displayed this activity, we engineered an HNA-RT de novo. Because HNA adopts RNA-like A-form helical conformations (*5*), we hypothesized that an HNA-RT might be found in the structural neighborhood of an RNA-RT. Starting from TgoT, we used statistical correlation analysis (SCA) (*22*) of the polB family (fig. S7) to uncover potential allosteric interaction networks involved in template recognition. Random mutagenesis and screening by

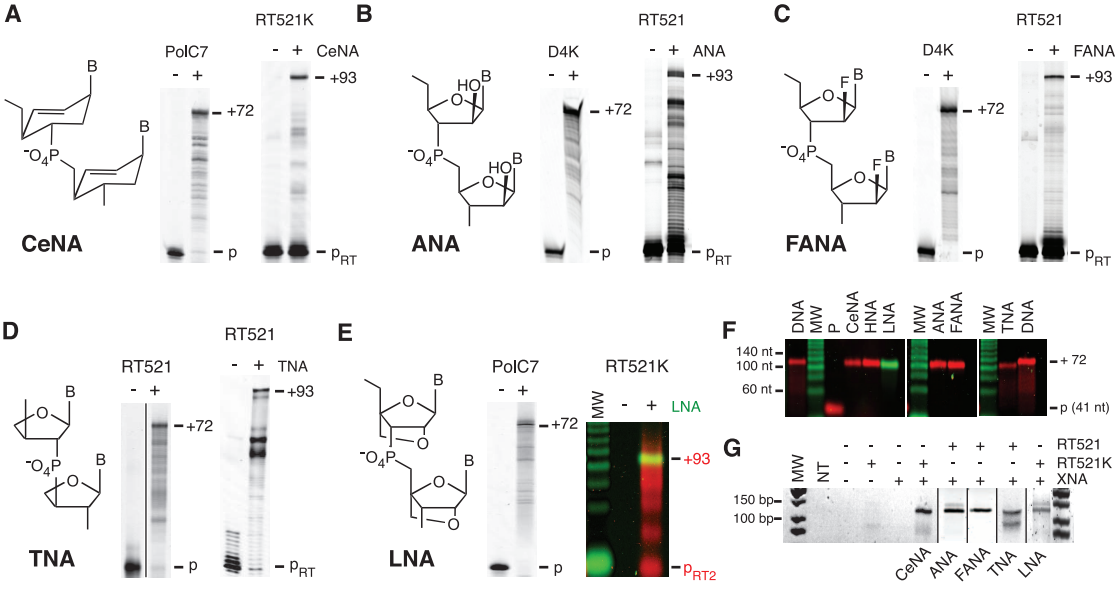


**Fig. 3.** XNA genetic polymers. Structures, polyacrylamide gel electrophoresis (PAGE) of synthesis (+72 xnt), and reverse transcription (+93 nt) of (**A**) CeNA, (**B**) ANA, (**C**) FANA, and (**D**) TNA. (**E**) PAGE of LNA synthesis [primer (41 nt) + 72 lnt] and LNA-RT (red) resolved by alkali agarose gel electrophoresis (AAGE). LNA synthesis (green) migrates at its expected size (113 nt) and comigrates with reverse transcribed DNA (red) synthesized from primer $P_{RT2}$ (20 nt) (fig. S8 and table S3). (**F**) AAGE of XNA and DNA polymers of identical sequence. MW, ILS 600 molecular weight markers. Equivalent PAGE is shown in fig. S5. (**G**) XNA RT–polymerase chain reaction (MW, New England Biolabs low molecular weight marker; NT, no template control). Amplification products of expected size (133 base pairs) are obtained only with both XNA forward synthesis and RT (RT521 or RT521K) (fig. S12).

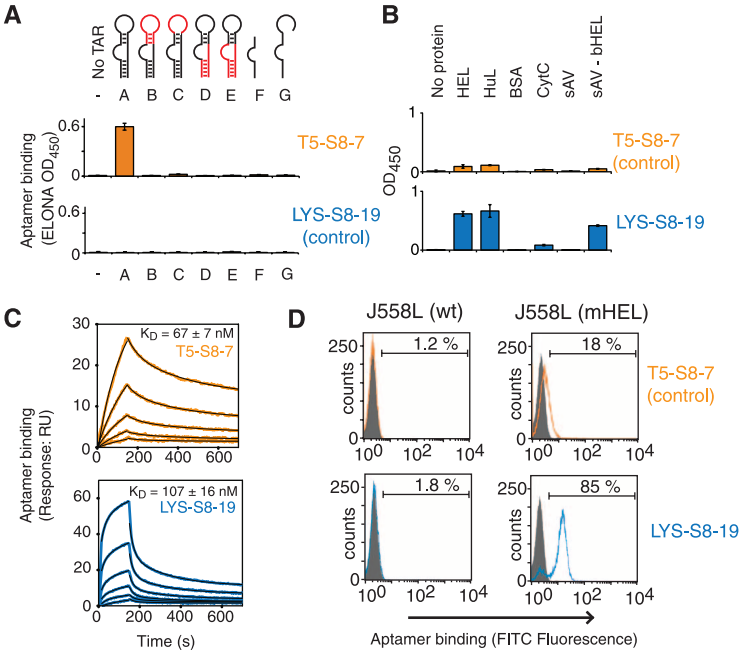


**Fig. 4.** Characterization of HNA aptamers. Anti-TAR aptamer T5-S8-7 (HNA: 6′-AGGTAGTGCTGTTCGTTCATCTCAAATCTAGTTCGCTATCCAGTTGGC-4′) and anti-HEL aptamer LYS-S8-19 (HNA: 6′-AGGTAGTGCTGTTCGTTTAAATGTGTGTCGTCGTTCGCTATCCAGTTGGC-4′) were characterized by ELONA (*27*). (**A** and **B**) Aptamer binding specificity against TAR variants (red, sequence randomized but with base-pairing patterns maintained) and different protein antigens (human lysozyme, HuL; cytochrome C, CytC; streptavidin, sAV; biotinylated-HEL bound to streptavidin, sAV-bHEL). OD, optical density. (**C**) Affinity measurements of aptamer binding by SPR. RU, response units. (**D**) FACS analysis of fluorescein isothiocyanate (FITC)–labeled aptamers binding to plasmacytoma line J558L with and without expression of membrane-bound HEL (mHEL) (*27*). wt, wild type.

a polymerase activity assay (fig. S3) of four SCA "hits" (F405, Y520, I521, L575) in the vicinity of L408 [a residue implicated in RNA-RT activity in the related Pfu DNA polymerase (*23*)] identified a mutant, TgoT: E429G, I521L, K726R (RT521), as a proficient HNA-RT (Fig. 2D). Together with Pol6G12, the evolved HNA polymerase, RT521 enables the transfer of genetic information from DNA to HNA and its retrieval back into DNA (fig. S11).

Next, we explored if other polymerases derived by CST and SCA might enable synthesis and reverse transcription of other synthetic genetic polymers. Screening identified PolC7 (TgoT: E654Q, E658Q, K659Q, V661A, E664Q, Q665P, D669A, K671Q, T676K, R709K) and PolD4K (TgoT: L403P, P657T, E658Q, K659H, Y663H, E664K, D669A, K671N, T676I) (Fig. 1) as efficient synthetases for CeNA (C7), LNA (C7), ANA (D4K), and FANA (D4K) (Fig. 3, A to C, E, and F). Therminator (9°N *exo*-: A485L) polymerase has previously been shown to support TNA synthesis (*16*), but TNA-RTs were lacking. RT521 proved capable of both efficient TNA synthesis and reverse transcription (Fig. 3D). In addition, RT521 is an efficient RT for both ANA and FANA (Fig. 3, B and C). Another polymerase variant, RT521K (RT521: A385V, F445L, E664K), was found to enhance CeNA-RT activity and enable reverse transcription of LNA (Fig. 3, A and E, and fig. S8). Together, these engineered polymerases support the synthesis and reverse transcription of six synthetic genetic polymers and thus enable replication of the information encoded therein (Fig. 3G).

Mutations enabling DNA-templated XNA synthesis were found to cluster at the periphery of the primer-template interaction interface in the polymerase thumb subdomain, >20 Å from the active site (Fig. 1B), and, in one case, allowed direct XNA-templated XNA replication (FANA, fig. S9). In contrast, broad XNA-RT activity was mostly effected by a mutation (I521L) in proximity to a catalytic aspartate (D542) and the polymerase active site. Its identification by SCA points to potential allosteric interaction networks involved in template recognition.

As previously observed for TNA (*16*), noncognate polymer synthesis can come at a cost of reduced fidelity as polymerase structures are poorly adapted to detect mismatches or aberrant geometry in the noncanonical XNA•DNA (or DNA•XNA) duplexes. We determined aggregate fidelities (as the probability of errors per position) of a full DNA → XNA → DNA replication cycle ranging from $4.3 \times 10^{-3}$ (CeNA) to $5.3 \times 10^{-2}$ (LNA), with HNA,

CeNA, ANA, and FANA superior to LNA and TNA (figs. S11 and S12 and table S8).

Synthesis and reverse transcription establish heredity (defined as the ability to encode and pass on genetic information) in all six XNAs. We next sought to explore the capacity of such genetic polymers for Darwinian evolution. As a stringent test for evolution and for acquisition of higher-order functions such as folding and specific ligand binding, we initiated aptamer selections directly from diverse HNA sequence repertoires. We used a modification of the standard aptamer selection protocol comprising magnetic beads for capture and isolation of all-HNA aptamers against two targets that had previously been used to generate both DNA and RNA aptamers (*24*, *25*): the HIV trans-activating response RNA (TAR) and hen egg lysozyme (HEL).

After eight rounds (R8) of selection with a biotinylated [27-nucleotide (nt)] version of the TAR RNA motif (sTAR) used as bait, clear consensus motifs emerged (fig. S13) from which we identified an HNA aptamer (T5–S8-7) that bound specifically to sTAR with a dissociation constant ($K_D$) between 28 and 67 nM, as determined by surface plasmon resonance (SPR), bio-layer interferometry (BLI), and enzyme-linked oligonucleotide assay (ELONA) titration (Fig. 4C, fig. S14, and table S6). Other anti-TAR HNA aptamers from the same selection experiment displayed similar affinities but distinctive fine specificities with regard to binding TAR loop or bulge regions (Fig. 4A and fig. S14). We initiated selection against HEL from an $N_{40}$ random sequence repertoire and again observed the emergence of consensus motifs after R8 (fig. S15). We identified specific HEL binders with $K_D$ of 107 to 141 nM, as determined by SPR, BLI, and fluorescence polarization (Fig. 4C, fig. S16, and table S7). Anti-HEL HNA aptamers cross-reacted with human lysozyme and, to a minor degree (<10%), with the highly positively charged cytochrome C (isoelectric point = 9.6), but did not show binding to unrelated proteins such as bovine serum albumin and streptavidin (Fig. 4B). Fluorescently labeled HNA aptamers allowed direct detection of surface HEL expression by flow cytometry [fluorescence-activated cell sorting (FACS)] in a transfected cell line, demonstrating specificity in a complex biological environment (Fig. 4D).

Our work establishes strategies for the replication and evolution of synthetic genetic polymers not found in nature, providing a route to novel sequence space. The capacity of synthetic polymers for both heredity and evolution also shows that DNA and RNA are not functionally unique as genetic materials. The methodologies developed herein are readily applied to other nucleic acid architectures and have the potential to enable the replication of genetic polymers of increasingly divergent chemistry, structural motifs, and physicochemical properties, as shown here by the acid resistance of HNA aptamers (fig. S17). Thus, aspects of the correlations between chemical structure, evolvability, and phenotypic diversity may become amenable to systematic study. Such "synthetic genetics" (*26*)—that is, the exploration of the informational, structural, and catalytic potential of synthetic genetic polymers—should advance our understanding of the parameters of chemical information encoding and provide a source of ligands, catalysts, and nanostructures with tailor-made chemistries for applications in biotechnology and medicine.

### References and Notes


1. A. Eschenmoser, *Science* **284**, 2118 (1999).
2. A. M. Leconte *et al.*, *J. Am. Chem. Soc.* **130**, 2336 (2008).
3. P. E. Nielsen, *Annu. Rev. Biophys. Biomol. Struct.* **24**, 167 (1995).
4. K.-U. Schöning *et al.*, *Science* **290**, 1347 (2000).
5. P. Herdewijn, *Chem. Biodivers.* **7**, 1 (2010).
6. M. A. Campbell, J. Wengel, *Chem. Soc. Rev.* **40**, 5680 (2011).
7. D. Loakes, P. Holliger, *Chem. Commun.* **2009**, 4619 (2009).
8. D. Loakes, *Nucleic Acids Res.* **29**, 2437 (2001).
9. C. Boiziau, J. J. Toulmé, *Antisense Nucleic Acid Drug Dev.* **11**, 379 (2001).
10. J. P. Schrum, A. Ricardo, M. Krishnamurthy, J. C. Blain, J. W. Szostak, *J. Am. Chem. Soc.* **131**, 14560 (2009).
11. X. Li, Z. Y. Zhan, R. Knipe, D. G. Lynn, *J. Am. Chem. Soc.* **124**, 746 (2002).
12. D. M. Rosenbaum, D. R. Liu, *J. Am. Chem. Soc.* **125**, 13924 (2003).
13. Y. Brudno, M. E. Birnbaum, R. E. Kleiner, D. R. Liu, *Nat. Chem. Biol.* **6**, 148 (2010).
14. P. E. Burmeister *et al.*, *Chem. Biol.* **12**, 25 (2005).
15. H. Yu, S. Zhang, J. C. Chaput, *Nat. Chem.* **4**, 183 (2012).
16. J. K. Ichida, A. Horhota, K. Zou, L. W. McLaughlin, J. W. Szostak, *Nucleic Acids Res.* **33**, 5219 (2005).
17. C. J. Wilds, M. J. Damha, *Nucleic Acids Res.* **28**, 3625 (2000).
18. A. M. Noronha *et al.*, *Biochemistry* **39**, 7050 (2000).
19. M. J. Fogg, L. H. Pearl, B. A. Connolly, *Nat. Struct. Biol.* **9**, 922 (2002).
20. Single-letter abbreviations for the amino acid residues are as follows: A, Ala; C, Cys; D, Asp; E, Glu; F, Phe; G, Gly; H, His; I, Ile; K, Lys; L, Leu; M, Met; N, Asn; P, Pro; Q, Gln; R, Arg; S, Ser; T, Thr; V, Val; W, Trp; and Y, Tyr.
21. A. F. Gardner, W. E. Jack, *Nucleic Acids Res.* **30**, 605 (2002).
22. S. W. Lockless, R. Ranganathan, *Science* **286**, 295 (1999).
23. B. Arezi, H. Hogrefe, J. A. Sorge, C. J. Hansen, U.S. Patent 2003/0228616 A1 (2003).
24. A. S. Potty, K. Kourentzi, H. Fang, P. Schuck, R. C. Willson, *Int. J. Biol. Macromol.* **48**, 392 (2011).
25. F. Ducongé, J. J. Toulmé, *RNA* **5**, 1605 (1999).
26. S. A. Benner, *Science* **306**, 625 (2004).
27. Materials and methods are available as supplementary materials on *Science* Online.



**Acknowledgments:** This work was supported by the MRC (U105178804) (P. Holliger, V.B.P., C.C.) and by grants from the European Union Framework [FP6-STREP-029092 NEST (P. Holliger, V.B.P., M.A., M.R., P. Herdewijn)], the European Science Foundation and the Biotechnology and Biological Sciences Research Council (BBSRC) UK (09-EuroSYNBIO-OP-013) (A.I.T.), the European Research Council (ERC-2010-AdG_20100317) (J.W.), and Katholieke Universiteit Leuven (GOA/IDO programs) (P. Herdewijn). MRC has filed a patent continuation in part (U.S. 2010/018407 A1) and a patent application (WO 2011/135280 A2) on the CST selection system and the polymerases for XNA synthesis and reverse transcription. Polymerases are available for noncommercial purposes from P. Holliger on request subject to a material transfer agreement.


### Supplementary Materials

www.sciencemag.org/cgi/content/full/336/6079/341/DC1
Materials and Methods
Figs. S1 to S17
Tables S1 to S7
References (*28*–*64*)


8 December 2011; accepted 6 March 2012
10.1126/science.1217622


# Nuclear Genomic Sequences Reveal that Polar Bears Are an Old and Distinct Bear Lineage


**Frank Hailer,[1]* Verena E. Kutschera,[1] Björn M. Hallström,[1] Denise Klassert,[1] Steven R. Fain,[2] Jennifer A. Leonard,[3] Ulfur Arnason,[4] Axel Janke[1,5]***



**Recent studies have shown that the polar bear matriline (mitochondrial DNA) evolved from a brown bear lineage since the late Pleistocene, potentially indicating rapid speciation and adaption to arctic conditions. Here, we present a high-resolution data set from multiple independent loci across the nuclear genomes of a broad sample of polar, brown, and black bears. Bayesian coalescent analyses place polar bears outside the brown bear clade and date the divergence much earlier, in the middle Pleistocene, about 600 (338 to 934) thousand years ago. This provides more time for polar bear evolution and confirms previous suggestions that polar bears carry introgressed brown bear mitochondrial DNA due to past hybridization. Our results highlight that multilocus genomic analyses are crucial for an accurate understanding of evolutionary history.**


Adaptation to novel environmental conditions is an important driver of niche specialization and speciation (*1*). Except for special cases such as hybrid speciation (*2*), the speciation process is generally considered to be rather slow in mammals: Paleontological and genetic evidence indicate that most species pairs or sister lineages of mammals diverged at least 1 million years ago (*3*, *4*). One notable exception seems to be the polar bear (*Ursus maritimus*), a uniquely adapted high-arctic specialist (*5*, *6*) for which recent studies have suggested a surprisingly modern matrilineal origin at less than 111 to 166 thousand years ago (ka) (*7*–*9*). These studies found extant polar bears rooted


[1]Biodiversity and Climate Research Centre (BiK-F), Senckenberg Gesellschaft für Naturforschung, Senckenberganlage 25, 60325 Frankfurt am Main, Germany. [2]National Fish and Wildlife Forensic Laboratory, 1490 East Main Street, Ashland, OR, USA. [3]Conservation and Evolutionary Genetics Group, Estación Biológica de Doñana (EBD-CSIC), Avenida Américo Vespucio, s/n, 41092 Seville, Spain. [4]Lund University Hospital, Box 117, 221 00 Lund, Sweden. [5]Goethe University Frankfurt, Institute for Ecology, Evolution and Diversity, 60438 Frankfurt am Main, Germany.

*To whom correspondence should be addressed. E-mail: frashai@gmx.net (F.H.); ajanke@senckenberg.de (A.J.)

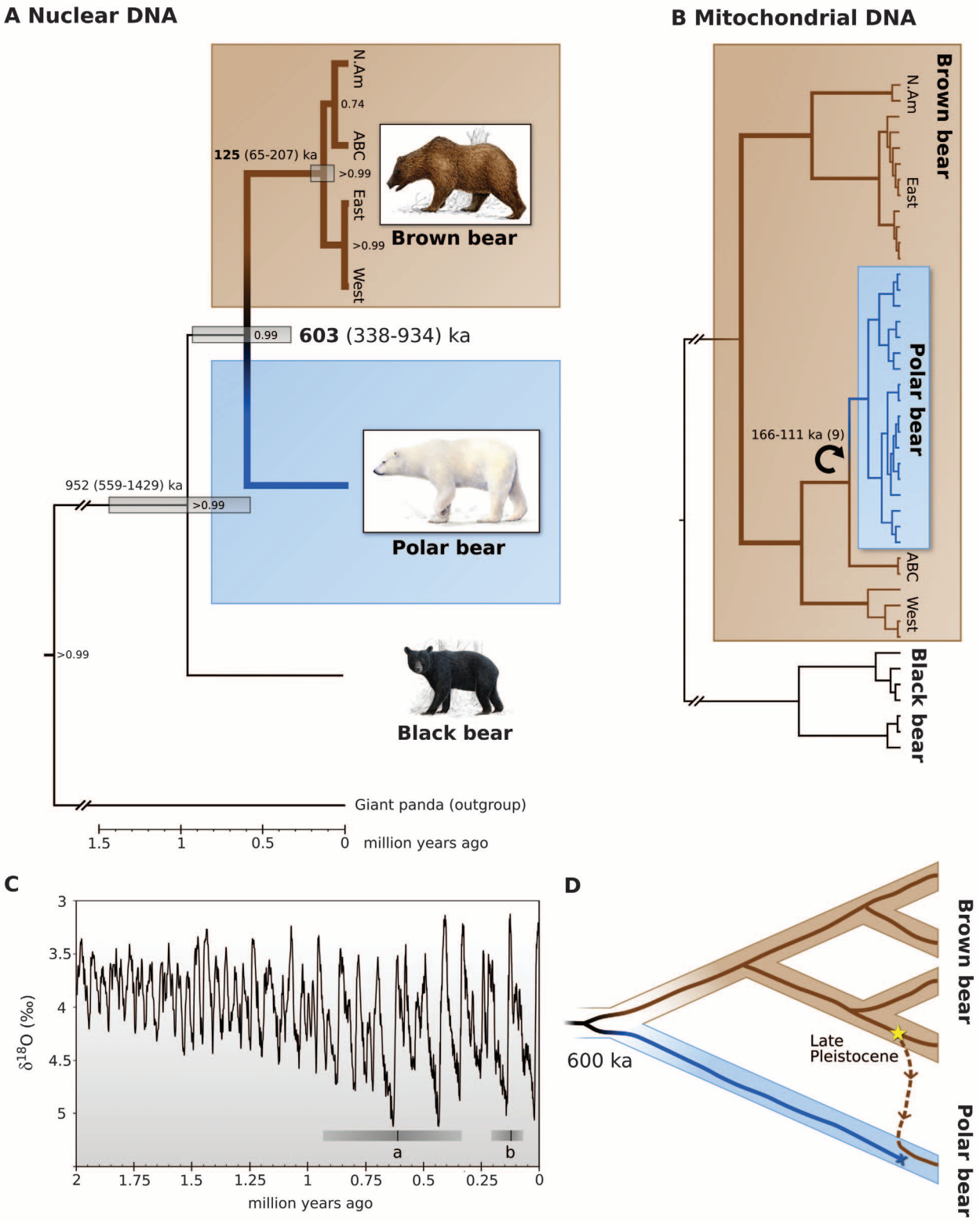


**Fig. 1.** Ancient origin of polar bears and subsequent introgressive replacement of their mitochondrial DNA with a brown bear haplotype. (**A**) Species tree of nuclear intron data. Polar and brown bears are sister groups, with their divergence time estimated at 603 (338 to 934) ka. Numbers next to nodes indicate statistical support, and gray bars are 95% highest credibility ranges for node ages. (**B**) MtDNA phylogeny. Polar bears are nested within the brown bear clade. The circular arrow denotes mtDNA replacement in polar bears before 166 to 111 ka [upper and lower 95% confidence limits from (*9*)]. Clades are named according to previously identified mtDNA lineages in brown bears (*8*, *18*). (**C**) Temperature curve since the Pleistocene [modified from (*32*)], and evolutionary events in bears. "a" denotes the origination of the polar bear lineage and "b" the diversification of extant brown bear lineages. Shaded gray bars are 95% credibility intervals; black lines denote median estimates. (**D**) Schematic scenario for mtDNA inheritance in bears. Speciation occurred in the middle Pleistocene, but hybridization during the late Pleistocene led to mtDNA similarity between extant polar bears and brown bears from the ABC islands (*7*, *8*) and Ireland (*9*). The star denotes the brown bear ancestor of extant polar bear mtDNA and the "X" a hypothesized disappearance of the ancestral matriline in polar bears. mtDNA data from ancient remains indicate additional instances of hybridization (*9*).

within brown bear (*U. arctos*) diversity, as a sister lineage to brown bears from the Alaskan Admiralty, Baranof, and Chichagof (ABC) islands or Ireland (*7*–*9*). Those results would render brown bears paraphyletic and are consistent with the absence of polar bear fossils before the late Pleistocene (*7*–*10*).

To date, the evolutionary history of polar and brown bears has primarily been studied using mitochondrial DNA (mtDNA) (*7*–*9*, *11*). The few studies that employed nuclear markers included only single representations per species, therefore lacking power to assess paraphyly (*9*, *12*–*14*). Although mtDNA analyses are routinely used in phylogenetics and phylogeography, they have well-known limitations, especially in cases of sex bias and/or introgressive hybridization (*15*). Its maternal inheritance renders mtDNA sensitive to random genetic drift but insensitive to male-biased gene flow. Moreover, its inheritance as a single linked molecule prevents the estimation of genome-wide population genetic parameters (*16*). To test the mtDNA-based observation of brown bear paraphyly (some brown bears being more closely related to polar bears than to some conspecifics), nuclear sequences from a diversity of brown and polar bears are required. Studies using multiple unlinked nuclear loci from a broad population sample allow the analysis of autonomously inherited genetic markers. These yield statistically independent information and are therefore essential for recovering an unbiased picture of evolutionary relationships (e.g., species trees) and for obtaining accurate estimates of divergence times (*16*).

**Table 1.** Mitochondrial and nuclear genetic diversity in bears. *n*, number of analyzed individuals; π, Tamura-Nei corrected nucleotide diversity.

| Species | *n* | π (mtDNA) ($\times 10^{-3}$) | π (nuclear DNA) ($\times 10^{-3}$) |
|---|---|---|---|
| Polar | 19 | 5.45 | 0.575 |
| Brown | 18 | 25.13 | 2.496 |
| Black | 7 | 17.75 | 1.437 |

We sequenced and analyzed 9116 nucleotides from 14 independent nuclear loci (introns) across the genome in 45 individuals of polar, brown, and black bears (tables S1 and S2) (*17*), using the giant panda as an outgroup (*17*). A species tree was reconstructed using a Bayesian multilocus coalescent approach (Fig. 1A) (*16*) that embeds the gene trees for each locus in a separately estimated species tree. With high statistical support ($P > 0.99$), polar bears were recovered as a sister lineage to all brown bears, and their divergence time was estimated at 603 ka (median estimate), with 95% credibility intervals (338 to 934 ka) that exclude the time frame determined for the extant matriline (111 to 166 ka) (*9*). A phylogenetic analysis of the concatenated data (fig. S2) and a neighbor-joining tree of pairwise differentiation estimates ($\Phi_{ST}$) (fig. S3) confirmed this multilocus analysis. Our results thus provide a fundamentally different picture of the polar bear's evolutionary history, compared with the "recent-origin" scenario suggested for its mtDNA (*7*, *8*).

Due to the contrasting evolutionary scenarios provided by our nuclear versus published mtDNA data, we analyzed (*17*) a 640–base pair section of the mitochondrial control region to verify that our samples represent the main lineages of extant brown and polar bears and that their evolutionary relationships reflect the current view of bear mtDNA phylogeny. Indeed, following the nomenclature of Leonard *et al*. (*18*), our sampling covers brown bear clades 1, 2, 3, and 4, encompassing individuals from northern and central Europe as well as the Alaskan ABC islands and across continental North America (Fig. 1B). Consistent with previous mtDNA studies (*7*–*9*, *11*), all polar bears clustered together with high posterior node support ($P > 0.99$) within the diversity of brown bears, sharing a most recent common ancestor with the ABC island lineage (clade 2a). Our sampling includes two of the most strongly differentiated microsatellite clusters in polar bears (*19*) (east versus west Greenland), as well as continental North America and Iceland (*17*). Therefore, this study represents a high-resolution data set that compares nuclear genomic variation in multiple polar and brown bear individuals, providing an independent view of their evolutionary history.

Recently diverged species still share many alleles in their nuclear genomes because of retained ancestral polymorphisms (*20*, *21*). Therefore, given the recent mtDNA divergence among extant polar and brown bears, one might expect the two species to share a majority of nuclear haplotypes. However, numerous nuclear haplotypes were unique to polar bears. Across all polar and brown bear samples, we encountered a total of 114 haplotypes at the 14 intron loci (table S3). Out of 35 haplotypes in polar bears and 79 in brown bears, only 6 were shared (table S3 and fig. S1), and most of these were rare in at least one taxon. For the majority of nuclear loci, polar bear sequences were distinct from those in brown bears (fig. S1), and at least 20 sites were fixed. Nucleotide diversity in polar bears was only about 20% of that in brown bears (Table 1), with 22 single-nucleotide polymorphisms in polar bears and 95 in brown bears. These analyses support that polar bears are a distinct and genetically differentiated species, rather than a lineage that evolved recently from a brown bear genotype. Although the polar bear genome thus harbors an unexpected abundance of unique genetic variation, effective population size is lower than that of its southern relative. This commonly observed biogeographic pattern likely reflects smaller long-term population sizes and stronger population bottlenecks in arctic than in temperate species (*22*).

Overall nuclear genomic differentiation (multilocus $\Phi_{ST}$) between polar and brown bears (0.692) was similar to that between each of these and black bears (brown-black 0.685, polar-black 0.893) (table S4), consistent with long-term genetic distinctiveness of polar bears. These findings agree with the nuclear species tree (Fig. 1A) but differ from the matrilineal scenario. A recent estimate of the polar/brown bear divergence time (0.4 to 2 million years)

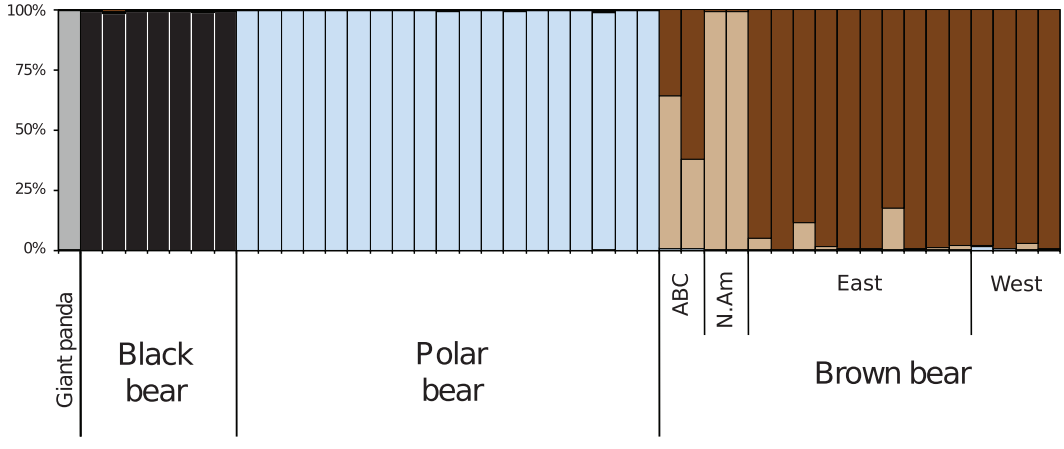


**Fig. 2.** Individual-based clustering results from nuclear variation in bears. Vertical bars show the cluster membership of each individual, for a clustering into five groups (indicated by separate colors). Polar bears (blue) appear to be genetically more homogeneous than brown bears, within which a subclustering is discernible (light and dark brown). Note the absence of multilocus introgression signals among brown and polar bears, indicating that much of the polar bear genome is unaffected by (recent) hybridization.

based on nuclear loci and single representations per species supports our results (*9*). Previous studies provided an older time frame for the black/brown bear divergence (*7*, *17*) than our data (Fig. 1A). Therefore, our dating of the polar/brown bear divergence could prove an underestimate, which would strengthen our main conclusions. Our nuclear dating closely resembles the time frame for speciation of another high-arctic specialist, the arctic fox, which diverged from its sister lineage about 900 ka (*23*). In accordance with matrilineal data (*9*), our nuclear gene analyses place the origin of extant brown bear diversity at approximately 125 (65 to 207) ka. The warm Eemian interglacial period at 125 ka and the ensuing onset of late Pleistocene glacial cycles (Fig. 1C) may explain the fragmentation and origin of modern brown bear lineages. Extant genetic diversity in the gray wolf also dates back to this time (*24*). Our dating of evolutionary events in bears therefore coincides with analogous events in other Eurasian and North American carnivores. Kurtén's allometry-based suggestion (*10*) that polar bears could have evolved during the middle Pleistocene supports our finding, although the oldest known polar bear fossils date to less than 110 to 130 ka (*7*–*10*). The life of polar bears on coastal ice, an ephemeral habitat shaped by multiple glacial advances and retreats, may explain why older fossils have not been found.

An earlier evolutionary origin of the polar bear lineage requires a reinterpretation of the established branching pattern of mtDNA lineages (*7*–*9*, *11*). In principle, all extant brown and polar bear mtDNA could be of polar bear origin, but this would require several events of hybridization and subsequent mtDNA replacement (*9*), which appears unlikely in a widespread generalist species like the brown bear. More parsimoniously, introgressed brown bear material may have replaced the original polar bear mtDNA (Fig. 1D). This would imply that female brown bears mated with male polar bears and that the offspring backcrossed into the polar bear population [consistent with recent observations of fertile hybrids in the wild (*25*)]. Polar and brown bears are not generally codistributed, but polar bears colonizing coastal land due to sea ice melting during the last interglacial could have been susceptible to introgression from resident brown bears (*25*, *26*). Regardless of the direction of mtDNA replacement, such a process has been described for other mammals (*27*, *28*).

A Bayesian multilocus genotype clustering analysis (*17*, *29*) revealed no detectable signal of recent or ongoing nuclear gene flow between the polar and brown bear individuals (Fig. 2 and fig. S5). Similarly, migration rates among polar and brown bear groups did not differ significantly from zero, as shown by coalescent-based multilocus simulations (table S5 and fig. S4) (*30*). This suggests that polar/brown bear hybridization is currently infrequent and/or limited to a few geographic regions (*25*). Nevertheless, mtDNA yields a signal of at least one or two hybridization events during the late Pleistocene (*9*), illustrating the usefulness of haploid, uniparentally inherited loci and ancient DNA studies to track reticulate evolutionary relationships (*7*–*9*). To obtain the overall species tree and associated timing estimates, however, the use of multiple independent loci is crucial. This study therefore highlights that mtDNA does not always reflect the species' overall (genome-wide) evolutionary history.

Despite the lack of average, multilocus signals of frequent or recent bear hybridization (Fig. 2 and fig. S4), indications of admixture are not limited to mtDNA. Some loci can remain informative about past hybridization events even when most of the genome is unaffected (*31*). We found a candidate locus for introgression by polar/brown bear hybridization. At the intron locus *11080*, bears clustered in species-specific haplogroups (fig. S1), with one notable outlier: ABC island brown bears carried the (fixed) polar bear haplotype. If this pattern reflects introgression, it could represent evidence of polar bear genetic material in brown bears, suggesting gene flow in the opposite direction relative to mtDNA (*9*). Because the process of lineage sorting is slow, spanning time scales relevant to speciation (*20*, *21*), linkage mapping studies like those in canids (*31*) will be necessary to pinpoint the phylogenetic origins of individual alleles in bears. Adaptive introgression not only may have helped polar bears to withstand interglacial warm phases (*9*) and potentially counteracted inbreeding but also may have facilitated the persistence of brown bear populations in subarctic landscapes.

In conclusion, our data suggest that polar bears are a genetically distinct lineage that is older than previously recognized. An evolutionary origin several hundred thousand years ago implies that polar bears as a species have experienced multiple glacial cycles and have had considerable time to adapt to arctic conditions. However, the low genetic diversity in polar bears suggests that changes in the environment, such as warm phases, caused population bottlenecks. Although polar bears have persisted through previous warm phases, multiple human-mediated stressors (e.g., habitat conversion, persecution, and accumulation of toxic substances in the food chain) could magnify the impact of current climate change, posing a novel and likely profound threat to polar bear survival.

### References and Notes


1. D. Schluter, *Science* **323**, 737 (2009).
2. P. A. Larsen, M. R. Marchán-Rivadeneira, R. J. Baker, *Proc. Natl. Acad. Sci. U.S.A.* **107**, 11447 (2010).
3. J. L. Blois, E. A. Hadly, *Annu. Rev. Earth Planet. Sci.* **37**, 181 (2009).
4. J. C. Uyeda, T. F. Hansen, S. J. Arnold, J. Pienaar, *Proc. Natl. Acad. Sci. U.S.A.* **108**, 15908 (2011).
5. G. J. Slater, B. Figueirido, L. Louis, P. Yang, B. Van Valkenburgh, *PLoS ONE* **5**, e13870 (2010).
6. S. C. Amstrup, in *Wild Mammals of North America: Biology, Management, and Conservation*, G. A. Feldhamer *et al.*, Eds. (Johns Hopkins Univ. Press, Baltimore, MD, 2003), pp. 587–610.
7. C. Lindqvist *et al.*, *Proc. Natl. Acad. Sci. U.S.A.* **107**, 5053 (2010).
8. J. Davison *et al.*, *Quat. Sci. Rev.* **30**, 418 (2011).
9. C. J. Edwards *et al.*, *Curr. Biol.* **21**, 1251 (2011).
10. B. Kurtén, *Acta Zool. Fenn.* **108**, 1 (1964).
11. G. F. Shields, T. D. Kocher, *Evolution* **45**, 218 (1991).
12. M. Pagès *et al.*, *Mol. Phylogenet. Evol.* **47**, 73 (2008).
13. S. Nakagome, J. Pecon-Slattery, R. Masuda, *Mol. Biol. Evol.* **25**, 1344 (2008).
14. L. Yu, Q. W. Li, O. A. Ryder, Y. P. Zhang, *Mol. Phylogenet. Evol.* **32**, 480 (2004).
15. D. J. Funk, K. E. Omland, *Annu. Rev. Ecol. Evol. Syst.* **34**, 397 (2003).
16. J. Heled, A. J. Drummond, *Mol. Biol. Evol.* **27**, 570 (2010).
17. Material and methods and BEAST and STRUCTURE input files are available as supplementary materials on *Science* Online.
18. J. A. Leonard, R. K. Wayne, A. Cooper, *Proc. Natl. Acad. Sci. U.S.A.* **97**, 1651 (2000).
19. D. Paetkau *et al.*, *Mol. Ecol.* **8**, 1571 (1999).
20. R. M. Zink, G. F. Barrowclough, *Mol. Ecol.* **17**, 2107 (2008).
21. A. J. Welch, A. A. Yoshida, R. C. Fleischer, *Mol. Ecol.* **20**, 1364 (2011).
22. G. Hewitt, *Nature* **405**, 907 (2000).
23. F. A. Perini, C. A. M. Russo, C. G. Schrago, *J. Evol. Biol.* **23**, 311 (2010).
24. M. Pilot *et al.*, *Mol. Ecol.* **15**, 4533 (2006).
25. B. P. Kelly, A. Whiteley, D. Tallmon, *Nature* **468**, 891 (2010).
26. M. Currat, M. Ruedi, R. J. Petit, L. Excoffier, *Evolution* **62**, 1908 (2008).
27. A. L. Roca, N. Georgiadis, S. J. O'Brien, *Nat. Genet.* **37**, 96 (2005).
28. J. M. Good *et al.*, *Mol. Ecol.* **17**, 1313 (2008).
29. J. K. Pritchard, M. Stephens, P. Donnelly, *Genetics* **155**, 945 (2000).
30. P. Beerli, *Bioinformatics* **22**, 341 (2006).
31. T. M. Anderson *et al.*, *Science* **323**, 1339 (2009).
32. L. E. Lisiecki, M. E. Raymo, *Paleoceanography* **20**, PA1003 (2005).



**Acknowledgments:** The study was supported by Hesse's LOEWE, Landes-Offensive zur Entwicklung Wissenschaftlich-ökonomischer Exzellenz. We thank E. W. Born, H.-G. Eiken, C. Frosch, S. Hagen, A. Kopatz, C. Nowak, M. Onucsán, M. Pfenninger, K. Skírnisson, F. Zachos, and P. Beerli for providing samples and for discussions. Obtained sequences have been deposited in the EMBL database (accession nos. HE657192 to HE657234 and HE657776 to HE658979). The authors declare no competing financial interests.


### Supplementary Materials

www.sciencemag.org/cgi/content/full/336/6079/344/DC1
Materials and Methods
Figs. S1 to S5
Tables S1 to S5
References (*33*–*61*)
Supplemental Files S1 and S2


9 November 2011; accepted 13 March 2012
10.1126/science.1216424

# A Common Pesticide Decreases Foraging Success and Survival in Honey Bees

Mickaël Henry,[1,2]* Maxime Béguin,[2,3] Fabrice Requier,[4,5] Orianne Rollin,[2,6] Jean-François Odoux,[5] Pierrick Aupinel,[5] Jean Aptel,[1,2] Sylvie Tchamitchian,[1,2] Axel Decourtye[2,6]

Nonlethal exposure of honey bees to thiamethoxam (neonicotinoid systemic pesticide) causes high mortality due to homing failure at levels that could put a colony at risk of collapse. Simulated exposure events on free-ranging foragers labeled with a radio-frequency identification tag suggest that homing is impaired by thiamethoxam intoxication. These experiments offer new insights into the consequences of common neonicotinoid pesticides used worldwide.

Colony collapse disorder (CCD) is a recent, pervasive syndrome affecting honey bee (*Apis mellifera*) colonies in the Northern hemisphere, which is characterized by a sudden disappearance of honey bees from the hive (*1*). Multiple causes of CCD have been proposed, such as pesticides, pathogens, parasites, and natural habitat degradation (*2*–*4*). However, the relative contribution of those stressors in CCD events remains unknown. Some scientists and beekeepers suspect pesticides to hold a central place in colony-weakening processes (*1*) or at least in interaction with other stressors (*5*, *6*). In modern cereal farming systems, honey bees are readily exposed to pesticides because they rely heavily on common blooming crops, such as oilseed rape (*Brassica napus*), maize (*Zea mays*), or sunflower (*Helianthus annuus*), that are now routinely treated against insect pests (*3*). Systemic pesticides in particular diffuse throughout all the tissues as plants grow up, eventually contaminating nectar and pollen (*7*). Foraging honey bees are therefore directly exposed, but so is the rest of the colony as returning foragers store or exchange contaminated material with hive conspecifics (*7*, *8*). Those exposure pathways are of important concern, and pesticide manufacturers pay special attention to reduce nonintentional intoxications in field conditions. Pesticide authorization procedures now require running mortality surveys to ensure that doses encountered in the field remain below lethal levels for honey bees.

However, a growing body of evidence shows that sublethal doses—doses that do not entail direct mortality—still have the potential to induce a variety of behavioral difficulties in foraging honey bees, such as memory and learning dysfunctions and alteration of navigational skills (*9*). Neonicotinoid pesticides used to protect crops against aphids and other sap-sucking insects are especially liable to provoke such behavioral troubles. They are highly potent and selective agonists of nicotinic acetylcholine receptors, which are important excitatory neurotransmitter receptors in insects (*10*, *11*). Effects of sublethal neonicotinoid exposures in honey bees may include abnormal foraging activity (*12*–*14*), reduced olfactory memory and learning performance (*15*–*17*), and possibly impaired orientation skills (*18*). Yet, the consequences of such behavioral difficulties on the fate of free-ranging foragers and on colony dynamics are extremely difficult to assess in the field and remain poorly investigated.

In this study, we tested the hypothesis that a sublethal exposure to a neonicotinoid indirectly increases hive death rate through homing failure in foraging honey bees. We focused our attention on thiamethoxam, a recently marketed neonicotinoid substance (*19*) currently being authorized in an increasing number of countries worldwide for the protection of oilseed rape, maize, and other blooming crops foraged by honey bees. We proceeded in two steps. First, we assessed mortality induced by homing failure ($m_{hf}$) in exposed foragers. This was achieved by monitoring free-ranging honey bees with radio-frequency identification (RFID) tagging technology (*14*, *20*). Second, we assessed the extent to which $m_{hf}$, in combination with natural forager mortality, may upset colony dynamics. For that purpose, $m_{hf}$ was introduced into a model of honey bee population dynamics (*21*).

We used a custom-made RFID device (*20*) to monitor the fate of 653 individual free-ranging foragers in the course of four separate treatment-versus-control homing experiments (*22*). The study was conducted in an intensive cereal farming system of western France, as a part of the ECOBEE monitoring facility (Zone Atelier Plaine et Val de Sèvre, Centre d'Études Biologiques de Chizé) and in a suburban area in Avignon, southern France. To simulate daily intoxication events, foragers received a field-realistic, sublethal dose of thiamethoxam (a real dose of 1.34 ng in a 20-µl sucrose solution) and were released away from their colony with a microchip glued on their thorax (Fig. 1A). RFID readers placed at the hive entrance (Fig. 1B) were set to detect on a continual basis tagged honey bees going through the entrance. Mortality due to postexposure homing failure, $m_{hf}$, was then derived from the proportion of nonreturning foragers. To further discriminate $m_{hf}$ from other causes of homing failure in treated foragers—such as natural mortality, predation, or handling stress—we simultaneously released equal numbers of control foragers fed with an untreated sucrose solution. Hence, $m_{hf}$ was calculated as the proportion of nonretuning treated foragers relative to expectations given by the proportion of returning control foragers. Depending on the experiment, tagged honey bees were released up to 1 km away from their respective colony, a distance usually covered by foragers during normal foraging flights (*23*). Experiments were conducted on individuals from three different colonies (*22*).

Our strategy was not to get an estimate of $m_{hf}$ per se. Instead, we assessed its upper and lower bounds, depending on whether foragers were familiar or not with the foraging site in which they might get intoxicated. Indeed, one might expect that foragers familiar with the pathway back to the colony are less prone to homing failure than are unfamiliar foragers. Under field conditions, many foragers are probably familiar with the pathway back to the colony because they repeatedly forage on the same

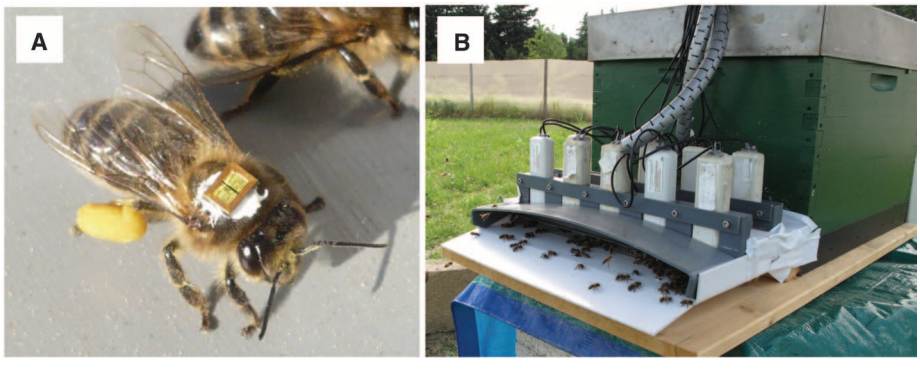


**Fig. 1.** Honey bee RFID monitoring equipment. (**A**) A pollen-forager honey bee fitted with a 3-mg RFID tag. (**B**) A hive entrance equipped with RFID readers for detecting returning marked foragers.

[1]INRA (Institut National de la Recherche Agronomique), UR406 Abeilles et Environnement, F-84914 Avignon, France. [2]UMT Protection des Abeilles dans l'Environnement, Site Agroparc, F-84914 Avignon, France. [3]Association pour le Développement de l'Apiculture Provençale, F-13626 Aix-en-Provence, France. [4]Centre d'Etudes Biologiques de Chizé, CNRS (USC-INRA 1339), UPR1934, F-79360 Beauvoir-sur-Niort, France. [5]INRA, UE1255, UE Entomologie, F-17700 Surgères, France. [6]Association de Coordination Technique Agricole, Site Agroparc, F-84914 Avignon, France.

*To whom correspondence should be addressed. E-mail: mickael.henry@avignon.inra.fr

site (*24*). However, many others are unfamiliar, too. Those include young honey bees at the onset of foraging, scouting honey bees that look for new food sources, and foragers newly recruited by scouting bees on the basis of the dance information (*25*). Most importantly, systemic pesticides such as thiamethoxam are readily present in the nectar and pollen when flowering starts and receive the first visits of honey bees, hitherto unfamiliar with this newly available food source.

To account for individuals' past foraging experience, we conducted two distinct homing experiments. Experiment 1 simulated intoxication at a familiar foraging site, and experiment 2 at a random site regarding past foraging experience. These experiments were assumed to return the lower and upper bounds of $m_{hf}$, respectively. In experiment 1, we referred to as "familiar" foragers those foragers for which we could make sure they covered at least once the pathway from the release site back to the colony. For that purpose, we selectively captured foragers returning to the colony with pollen loads from a known location and subsequently released them at that location. To ascertain pollen origin, we sowed beforehand a 1-ha field with scorpion weed *Phacelia tanacetifolia*, a highly attractive floral resource with bright blue pollen that is easily recognizable (*26*). Given that no other phacelia fields occurred in the area, we could ensure that phacelia-carrying honey bees came back from our experimental field. The colony was specifically placed 1 km away from the field for subsequent forager release (Fig. 2). In experiment 2, we used the non-phacelia pollen foragers. They were released in equal groups at six sites equally spaced on a 1-km circle around the colony (Fig. 2). Following that design, release sites were considered as random locations regarding the past experience of foragers.

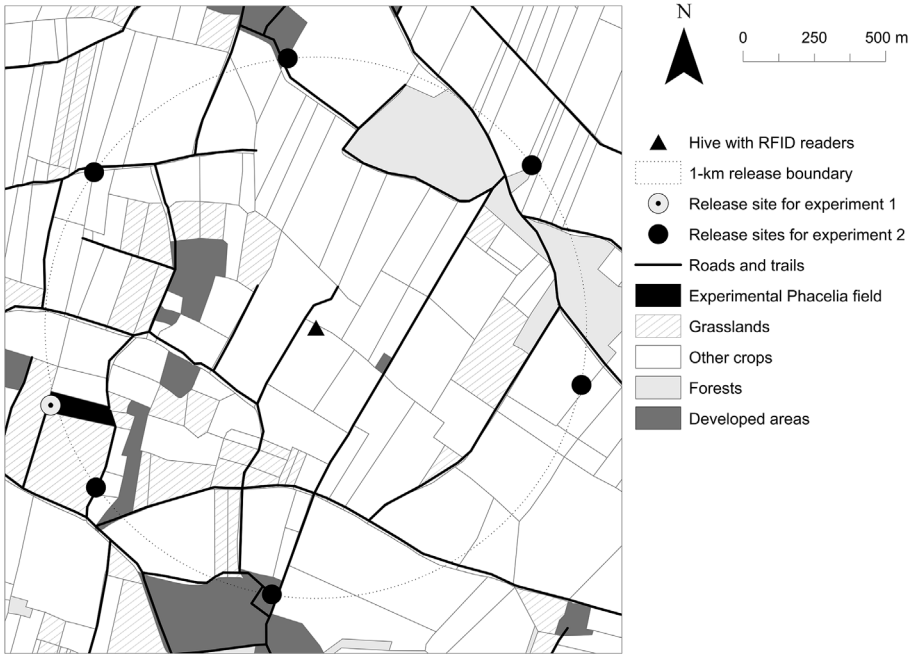


**Fig. 2.** Study area and location of honey bee release sites relative to the colony hive in experiments 1 and 2.

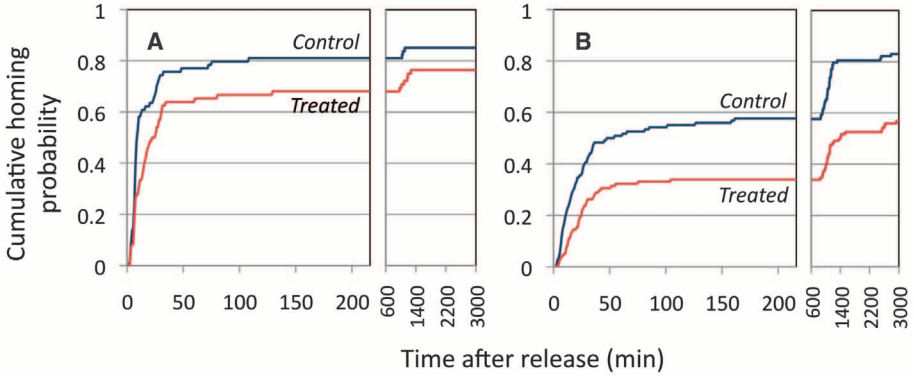


**Fig. 3.** Cumulative homing probability of foragers released 1 km away from the hive. Temporal gaps denote the nighttime between the first and second days of release. (**A**) Homing experiment 1 was carried out with foragers familiar with the release site, and (**B**) experiment 2 with foragers released at random sites regarding their past experience. In both cases, treated honey bees that received a nonlethal dose of thiamethoxam returned to the hive in significantly lower proportions than did control honey bees (table S1).

Both experiments 1 and 2 evidenced substantial mortality due to postexposure homing failure, $m_{hf}$, with the proportion of treated foragers returning to the colony being significantly lower than that of control foragers (exact binomial tests, $P = 0.033$ and $P < 0.001$, respectively) (Fig. 3 and table S1). Additionally, $m_{hf}$ was greater in treated foragers that tended to be unfamiliar with the foraging site, as indicated by their significantly lower homing proportions as compared with familiar foragers (exact binomial tests, $P < 0.001$). Experiments 1 and 2 returned $m_{hf}$ estimates of 0.102 and 0.316, respectively, potentially setting the lower and upper bounds for real $m_{hf}$ values. In other words, 10.2 to 31.6% of exposed honey bees would fail to return to their colony when foraging in treated crops on a daily basis. For the sake of comparison, foragers live ~6.5 days and therefore die at an average rate of $1/6.5 = 0.154$ individual day$^{-1}$ (*27*). Therefore, the probability that a forager would die because of homing failure during a day spent foraging on treated crops (up to 0.316) may attain twice the probability this same forager has to die naturally that day (~0.154).

Such an additional mortality might represent a heavy burden to bear for colonies exposed to treated crops in their environment. When implementing $m_{hf}$ into a honey bee population dynamics model (*21*), all the tested scenarios predicted a major deviation from the expected dynamic (Fig. 4). In our simulations, we considered the evolution of a typical colony during the first 3 months of a beekeeping season, encompassing the oilseed rape blooming period, which was April to May in our study area (*22*). At this time of the year, colonies emerge from the wintering period. Population size is rather low (<20,000 individuals) and gradually expands in order to rapidly increase food storage and ensure colony sustainability. The daily egg-laying rate of the queen is a critical parameter in this colony dynamic because it determines the daily egg-hatching rate and in turn the rate at which honey bees working in the hive will be replaced as they become themselves foragers. We simulated three scenarios with realistic levels of egg-laying rate (*28*), namely a rate allowing for a normal colony development (Fig. 4A), a rate ensuring equilibrium population (Fig. 4B), and a slightly deficient rate forcing the population to stabilize at a lower size (Fig. 4C). In each case, we also computed the expected trends if most foragers (90%) were exposed to nectar of treated oilseed rape each day and therefore had a natural mortality increased by a homing failure probability $m_{hf}$. Regardless of the queens' egg-laying rate, populations from colonies exposed to the treated nectar would follow a marked decline during the

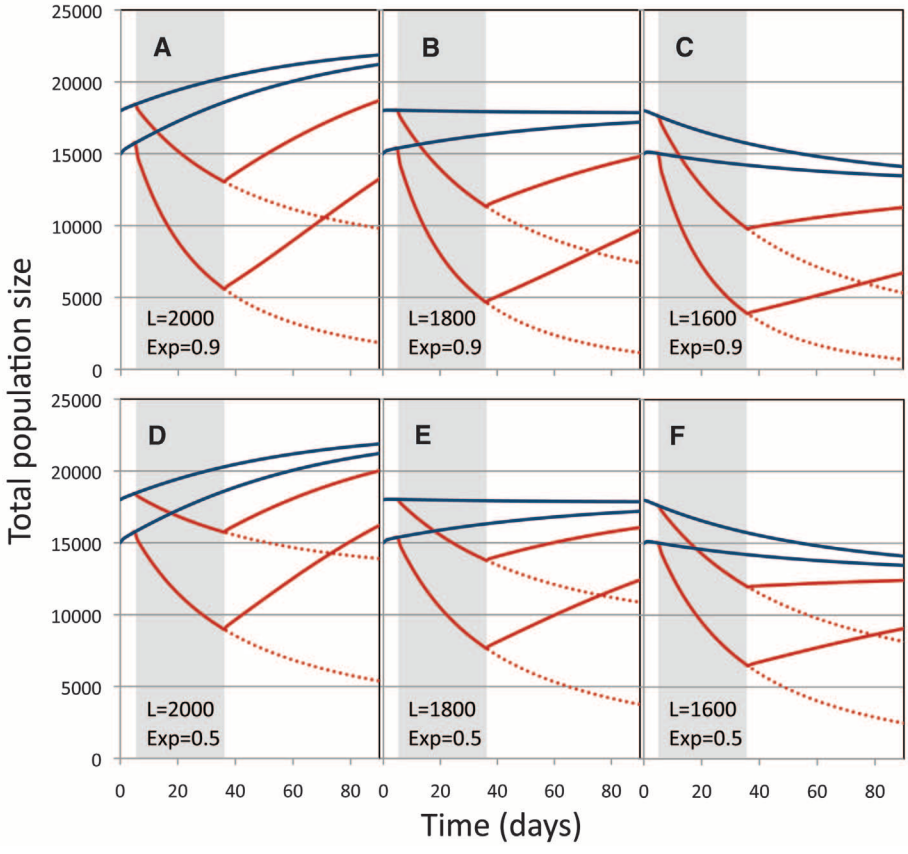


**Fig. 4.** Comparison of honey bee population dynamics between simulated colonies exposed to thiamethoxam (red lines) or not exposed (blue lines), following six demographic scenarios. *L* is the queen's daily laying rate (eggs per day). "Exp" is the proportion of foragers exposed to treated crops during the day. The nonexposed colony follows either (**A** and **D**) a normal development trajectory (at $L = 2000$), (**B** and **E**) an equilibrium dynamic ($L = 1800$), or (**C** and **F**) a slightly declining trajectory ($L = 1600$). Shaded areas delineate the exposure period (for example, oilseed rape). Pairs of trajectories in exposed colonies were obtained with the lower and upper bounds of homing failure mortality (0.102 and 0.316) in order to delineate the best and worst estimates for population dynamics, respectively. Dotted lines extend the declining trajectory expected for a sustained exposure. [Simulations derive from demographic models in (*21*)]

blooming period and would hardly recover afterward (Fig. 4, A to C). When combined with natural forager mortality, $m_{hf}$ raised total forager death rate up to a point that could hardly be compensated for by the rate at which new foragers are recruited. In the worse scenarios, populations would fall down to 5000 individuals, which is the lowest level one can usually observe in current beekeeping practices. With an exposure rate reduced to 50% of foragers exposed to treated nectar each day (Fig. 4, D to F), the model still predicts a major deviation from normal conditions.

In an attempt to verify the applicability of these results to other contexts, we repeated two additional experiments with two different colonies (fig. S2 and table S1). In experiment 3, we tested whether $m_{hf}$ was still significant when exposure occurred in the least challenging situation: in the direct vicinity of the colony and with honey bees familiar with the foraging site. We repeated experiment 1 with phacelia foragers captured from a beehive placed at the phacelia field margin and released from inside the phacelia field, only 70 m away. Homing failure ($m_{hf} = 0.061$) (fig. S2A and table S1) was much reduced as compared with that of experiment 1 ($m_{hf} = 0.102$) but was still significant (exact binomial test, $P = 0.003$). In experiment 4, we transposed experiment 2 into a different landscape. A beehive was placed in a suburban area in southern France, including a mosaic of mixed farming fields and orchards of moderate size. Foragers were released 1 km away at six equidistant sites. Homing failure ($m_{hf} = 0.098$) (fig. S2B and table S1) was significant as well (exact binomial test, $P = 0.029$) but much smaller than in experiment 2 ($m_{hf} = 0.316$).

Our study clearly demonstrates that exposure of foragers to nonlethal but commonly encountered doses of thiamethoxam can affect forager survival, with potential contributions to collapse risk. Furthermore, the extent to which exposures affect forager survival appears dependent on the landscape context and the prior knowledge of foragers about this landscape. Higher risks are observed when the homing task is more challenging. As a consequence, impact studies are likely to severely underestimate sublethal pesticide effects when they are conducted on honey bee colonies placed in the immediate proximity of treated crops. This study raises important issues concerning exposed solitary bee species, whose population dynamics are probably less resilient to forager disappearance than are honey bee colonies.

## References and Notes


1. B. P. Oldroyd, *PLoS Biol.* **5**, e168 (2007).
2. D. L. Cox-Foster *et al.*, *Science* **318**, 283 (2007).
3. C. A. Mullin *et al.*, *PLoS ONE* **5**, e9754 (2010).
4. D. Naug, *Biol. Conserv.* **142**, 2369 (2009).
5. C. Alaux *et al.*, *Environ. Microbiol.* **12**, 774 (2010).
6. C. Vidau *et al.*, *PLoS ONE* **6**, e21550 (2011).
7. A. Rortais, G. Arnold, M. P. Halm, F. Touffet-Briens, *Apidologie* **36**, 71 (2005).
8. C. H. Krupke, G. J. Hunt, B. D. Eitzer, G. Andino, K. Given, *PLoS ONE* **7**, e29268 (2012).
9. N. Desneux, A. Decourtye, J. M. Delpuech, *Annu. Rev. Entomol.* **52**, 81 (2007).
10. M. Tomizawa, J. E. Casida, *Annu. Rev. Entomol.* **48**, 339 (2003).
11. N. S. Millar, I. Denholm, *Invert. Neurosci.* **7**, 53 (2007).
12. E. C. Yang, Y. C. Chuang, Y. L. Chen, L. H. Chang, *J. Econ. Entomol.* **101**, 1743 (2008).
13. M. E. Colin *et al.*, *Arch. Environ. Contam. Toxicol.* **47**, 387 (2004).
14. C. W. Schneider, J. Tautz, B. Grünewald, S. Fuchs, *PLoS ONE* **7**, e30023 (2012).
15. A. Decourtye *et al.*, *Pestic. Biochem. Physiol.* **78**, 83 (2004).
16. A. Decourtye, E. Lacassie, M. H. Pham-Delègue, *Pest Manag. Sci.* **59**, 269 (2003).
17. A. Decourtye, J. Devillers, S. Cluzeau, M. Charreton, M. H. Pham-Delègue, *Ecotoxicol. Environ. Saf.* **57**, 410 (2004).
18. L. Bortolotti *et al.*, *Bull. Insectology* **56**, 63 (2003).
19. P. Maienfisch *et al.*, *Pest Manag. Sci.* **57**, 165 (2001).
20. A. Decourtye *et al.*, *Ecotoxicology* **20**, 429 (2011).
21. D. S. Khoury, M. R. Myerscough, A. B. Barron, *PLoS ONE* **6**, e18491 (2011).
22. Materials and methods are available as supporting online material on *Science* Online.
23. I. Steffan-Dewenter, A. Kuhn, *Proc. R. Soc. B Biol. Sci.* **270**, 569 (2003).
24. R. Menzel, R. J. De Marco, U. Greggers, *J. Comp. Physiol. A Neuroethol. Sens. Neural Behav. Physiol.* **192**, 889 (2006).
25. J. R. Riley, U. Greggers, A. D. Smith, D. R. Reynolds, R. Menzel, *Nature* **435**, 205 (2005).
26. M. Henry *et al.*, *Ecol. Modell.* **225**, 103 (2012).
27. R. Dukas, *Insectes Soc.* **55**, 252 (2008).
28. T. Schmickl, K. Crailsheim, *Ecol. Modell.* **204**, 219 (2007).


**Acknowledgments:** This study was funded by the European Community program (797/2004) for French beekeeping coordinated by the French Ministry of Agriculture (convention FranceAgriMer 11-45R). Special thanks go to L. Belzunces, J. L. Brunet, B. Vaissière, A. Maisonnasse, D. Fortini, Y. Le Conte, C. McDonnell, P. Jourdan, J. P. Vermandère, and V. Bretagnolle for valuable help and corrections, as well as three anonymous reviewers for useful comments on the manuscript. We are grateful to M. Grijolot for allowing experiments to take place in his fields. RFID devices were designed by Tag Tracing Solutions, Valence, France, and adapted to honey bees with the help of J. Fourrier, F. Brun, J. Devillers, M. Gauthier, and the ECOBEE monitoring facility. Data are in the supporting online material.

## Supporting Online Material

www.sciencemag.org/cgi/content/full/science.1215039/DC1
Materials and Methods
Figs. S1 and S2
Table S1
Reference (*29*)
Database S1

10 October 2011; accepted 5 March 2012
Published online 29 March 2012;
10.1126/science.1215039

# Neonicotinoid Pesticide Reduces Bumble Bee Colony Growth and Queen Production

Penelope R. Whitehorn,[1] Stephanie O'Connor,[1] Felix L. Wackers,[2] Dave Goulson[1]*

Growing evidence for declines in bee populations has caused great concern because of the valuable ecosystem services they provide. Neonicotinoid insecticides have been implicated in these declines because they occur at trace levels in the nectar and pollen of crop plants. We exposed colonies of the bumble bee *Bombus terrestris* in the laboratory to field-realistic levels of the neonicotinoid imidacloprid, then allowed them to develop naturally under field conditions. Treated colonies had a significantly reduced growth rate and suffered an 85% reduction in production of new queens compared with control colonies. Given the scale of use of neonicotinoids, we suggest that they may be having a considerable negative impact on wild bumble bee populations across the developed world.

Bees in agroecosystems survive by feeding on wildflowers growing in field margins and patches of seminatural habitat, supplemented by the brief gluts of flowers provided by mass flowering crops such as oilseed rape and sunflower (*1*, *2*). Many crops are now routinely treated with neonicotinoid insecticides as a seed dressing; these compounds are systemic, migrating in the sap to all parts of the plant and providing protection against insect herbivores. The most widely used of these compounds is imidacloprid, which is routinely used on most major crops, including cereals, oilseed rape, corn, cotton, sunflower, and sugar beets (*3*). Being systemic, imidacloprid spreads to the nectar and pollen of flowering crops, typically at concentrations ranging from 0.7 to 10 μg $kg^{-1}$ (*4*, *5*). Thus bee colonies in agroecosystems will be exposed to 2- to 4-week pulses of exposure to neonicotinoids during the flowering period of crops (*6*).

It is unclear what impact this exposure has on bee colonies under field conditions. A recent meta-analysis based on 13 studies of honey bees found that consumption of realistic doses of imidacloprid under laboratory and semifield conditions reduced their expected performance by 6 to 20% (*7*) but had no lethal effects. Fewer studies have been carried out on bumble bees, and results are conflicting (*8*–*11*). There is some evidence that low doses of neonicotinoids may reduce foraging ability (*12*), which is likely to have substantial impacts under natural conditions but little effect in cage studies. Although recent studies (*11*) have shown some evidence that neonicotinoids reduced forager success under field conditions, no studies have examined their impacts on colonies foraging naturally in the field. Here, we present an experiment, using 75 *Bombus terrestris* colonies, designed to simulate the likely effect of exposure of a wild bumble bee colony to neonicotinoids present on the flowers of a nearby crop. The colonies were randomly allocated to one of three treatments. Control colonies received ad libitum (ad lib) pollen and sugar water over a period of 14 days in the laboratory. Over the same period, colonies in the "low" treatment were fed pollen and sugar water containing 6 μg $kg^{-1}$ and 0.7 μg $kg^{-1}$ imidacloprid, respectively, representing the levels found in seed-treated rape (*13*). The "high"-treatment colonies received double these doses, still close to the field-realistic range. After 2 weeks, all colonies were then placed in the field, where they were left to forage independently for a period of 6 weeks while their performance was monitored.

All colonies experienced initial weight gain followed by a decline as they switched from their growth phase to producing new reproductives. Colonies in both low and high treatments gained less weight over the course of the experiment compared with the control colonies (Fig. 1) [linear mixed-effect model; $t(568) = -4.03$ (where the number in parentheses indicates the degrees of freedom), $P < 0.001$ and $t(568) = -5.39$, $P < 0.001$, respectively]. By the end of the experiment, the low- and high-treatment colonies were on average 8 and 12% smaller, respectively, than the control colonies. The weight change in the high-treatment colonies was not significantly different from that of the low-treatment colonies (Fig. 1) [linear mixed-effect model; $t(568) = -1.44$, $P = 0.151$]. The rate of colony growth was also dependent on the number of workers present

[1]School of Natural Sciences, University of Stirling, Stirling FK9 4LA, UK. [2]Lancaster Environment Centre (LEC), Lancaster University, Lancaster LA1 4YQ, UK.

*To whom correspondence should be addressed. E-mail: dave.goulson@stir.ac.uk

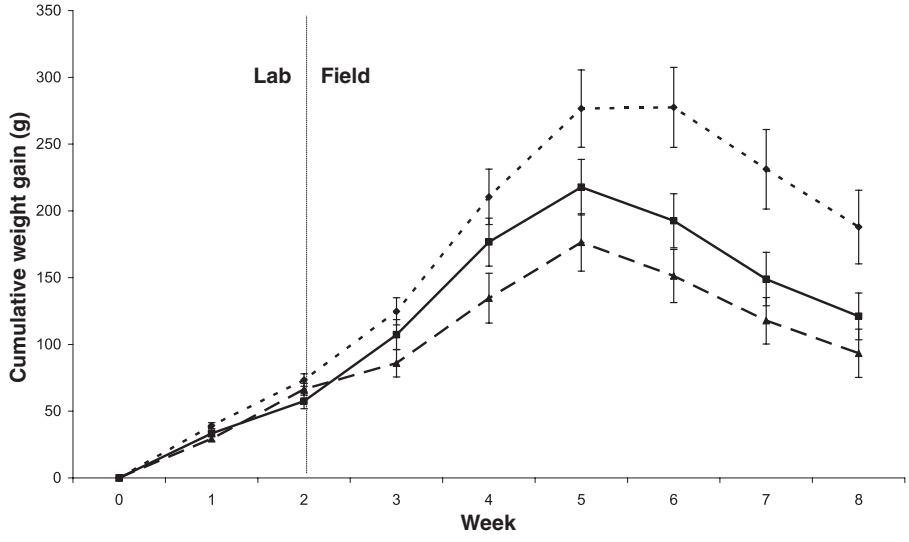


**Fig. 1.** Mean observed colony weight for control (short-dash line), low (solid line), and high (long-dash line) treatments at weekly intervals. The change in weight over time was significantly smaller ($P < 0.001$) in low- and high-treatment colonies compared with control colonies. The number of colonies per treatment was 25 in weeks 0 to 3. In the following weeks, the numbers of colonies in the control, low, and high treatments, respectively, were as follows: week 4 (25, 24, and 25), week 5 (25, 24, and 25), week 6 (23, 23, and 25), week 7 (22, 23, and 25), and week 8 (20, 18, and 21). Points represent cumulative weight increase since week 0 (and their standard errors); weight includes all accumulated biological material (wax, brood, food stores, and adult bees).

**Table 1.** Linear mixed-effect model for colony weight. Parameter estimates are with reference to the control treatment. Degrees of freedom are given in parentheses.

| Fixed effect | Parameter estimate | SE | *t* value | *P* |
|---|---|---|---|---|
| (Intercept) | 564.21 | 39.59 | 14.24 (568) | <0.001 |
| Treatment (high) | 13.62 | 27.80 | 0.490 (71) | 0.626 |
| Treatment (low) | 13.62 | 27.11 | 0.502 (71) | 0.617 |
| Week | 89.21 | 5.50 | 16.22 (568) | <0.001 |
| Week$^2$ | −6.68 | 0.430 | −15.51 (568) | <0.001 |
| No. workers at week = 0 | 0.759 | 1.92 | 0.396 (71) | 0.694 |
| Treatment (high)*Week | −13.42 | 2.49 | −5.39 (568) | <0.001 |
| Treatment (low)*Week | −9.95 | 2.47 | −4.03 (568) | <0.001 |
| Week*No. workers at week = 0 | 0.448 | 0.172 | 2.61 (568) | 0.009 |

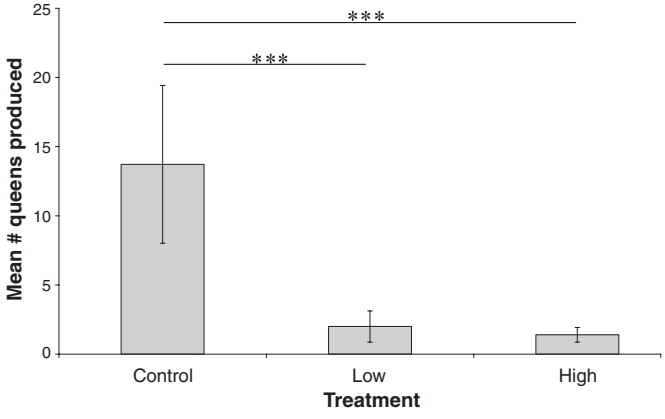


**Fig. 2.** The number of new queens produced by the control colonies was greater than the number produced in both low- and high-treatment colonies. Bars represent the mean number of queens and their standard errors. Asterisks indicate significant differences.

at week 0 (Table 1) [linear mixed-effect model; $t$ (568) = 2.61, $P$ = 0.009], reflecting the importance of a large workforce for optimal development. No significant differences between treatments were found in the numbers of males, workers, pupae, or empty pupal cells at the end of the experiment, although the number of empty pupal cells was 19% and 33% lower, respectively, in low and high treatments compared with controls.

The mean number of queens produced by colonies in the control treatment was 13.72 (SE = 5.70), whereas in low and high treatments it was only 2.00 (1.13) and 1.4 (0.53), respectively [Kruskall-Wallis test: $H$ (2) = 9.57, $P$ = 0.008] (Fig. 2). The drop in queen production is disproportionately large compared with the impact of imidacloprid on colony growth. However, there is evidence that only the very largest bumble bee colonies succeed in producing queens (*14*). For example, in field studies of reproduction of 36 colonies of the closely related *Bombus lucorum*, all queen production came from the largest six nests (*14*). Thus even a small drop in colony size may bring it below the threshold for queen production. Bumble bees have an annual life cycle, and it is only new queens that survive the winter to found colonies in the spring. Our results suggest that trace levels of neonicotinoid pesticides can have strong negative consequences for queen production by bumble bee colonies under realistic field conditions and that this is likely to have a substantial population-level impact.

Our colonies received ad lib treated food, which could result in them gathering more food and thus receiving higher exposure than they would in the wild. However, bumble bee colonies do not store substantial food reserves in the way that honey bees do, and the period of exposure (2 weeks) is substantially less than the flowering period of crops such as oilseed rape (3 to 4 weeks), so our experiment is conservative in this respect.

We did not study the mechanism underlying the observed effects, but previous lab studies suggested that workers treated with neonicotinoids have reduced foraging efficiency (*12*, *15*). Such effects are likely to be stronger when foragers have to navigate through a natural landscape and could readily explain reduced colony growth and queen production. Flowering crops such as oilseed rape attract numerous honey bees and a range of species of bumble bee (*16*). Bumble bee and honey bee workers travel a kilometer or more to collect food (*17*, *18*), and, in a recent study of a 10-km-by-20-km rectangle of lowland England, 100% of the land area in a 2007 snapshot was within 1 km of an oilseed rape crop, with rape providing the large majority of all floral resources in the landscape when flowering (*19*). Recent studies described levels of neonicotinoid up to 88 μg kg$^{-1}$ in pollen collected by honey bees foraging on treated corn (14 times our field-realistic dose) and also demonstrated the presence of up to 9 μg kg$^{-1}$ in wildflowers growing near treated crops, so exposure is not limited to bees feeding on the crop (*20*). Hence, we predict that impacts of imidacloprid on reproduction of wild bumble bee colonies are likely to be widespread and important, particularly because this chemical is registered for use on over 140 crops in over 120 countries (*3*). Because bumble bees are valuable pollinators of crops and wildflowers and vital components of ecosystems, we suggest that there is an urgent need to develop alternatives to the widespread use of neonicotinoid pesticides on flowering crops wherever possible.

## References and Notes


1. T. Diekötter, T. Kadoya, F. Peter, V. Wolters, F. Jauker, *J. Appl. Ecol.* **47**, 209 (2010).
2. R. D. Fell, *J. Kans. Entomol. Soc.* **59**, 72 (1986).
3. A. Elbert, M. Haas, B. Springer, W. Thielert, R. Nauen, *Pest Manag. Sci.* **64**, 1099 (2008).
4. C. Brittain, S. G. Potts, *Basic Appl. Ecol.* **12**, 321 (2011).
5. J. M. Bonmatin *et al.*, *Anal. Chem.* **75**, 2027 (2003).
6. R. Schmuck, R. Schöning, A. Stork, O. Schramel, *Pest Manag. Sci.* **57**, 225 (2001).
7. J. E. Cresswell, *Ecotoxicology* **20**, 149 (2011).
8. J. N. Tasei, J. Lerin, G. Ripault, *Pest Manag. Sci.* **56**, 784 (2000).
9. J. A. Gels, D. W. Held, D. A. Potter, *J. Econ. Entomol.* **95**, 722 (2002).
10. L. A. Morandin, M. L. Winston, *Environ. Entomol.* **32**, 555 (2003).
11. J. N. Tasei, G. Ripault, E. Rivault, *J. Econ. Entomol.* **94**, 623 (2001).
12. V. Mommaerts *et al.*, *Ecotoxicology* **19**, 207 (2010).
13. J. M. Bonmatin *et al.*, *J. Agric. Food Chem.* **53**, 5336 (2005).
14. C. B. Müller, P. Schmid-Hempel, *Ecol. Entomol.* **17**, 343 (1992).
15. R. Ramirez-Romero, J. Chaufaux, M. H. Pham-Delegue, *Apidologie (Celle)* **36**, 601 (2005).
16. K. E. Hayter, J. E. Cresswell, *J. Appl. Ecol.* **43**, 1196 (2006).
17. M. E. Knight *et al.*, *Mol. Ecol.* **14**, 1811 (2005).
18. J. L. Osborne *et al.*, *J. Anim. Ecol.* **77**, 406 (2008).
19. D. Goulson *et al.*, *J. Appl. Ecol.* **47**, 1207 (2010).
20. C. H. Krupke, G. J. Hunt, B. D. Eitzer, G. Andino, K. Given, *PLoS ONE* **7**, e29268 (2012).


**Acknowledgments:** We thank Agralan, UK for providing the bumble bee colonies, C. Brown for assisting with field work, and J. Minderman for statistical advice. Our data are available from the Dryad Repository: http://dx.doi.org/10.5061/dryad.1805c973.

## Supporting Online Material

www.sciencemag.org/cgi/content/full/science.1215025/DC1
Materials and Methods
SOM Text

10 October 2011; accepted 7 March 2012
Published online 29 March 2012;
10.1126/science.1215025

# Recent Plant Diversity Changes on Europe's Mountain Summits

Harald Pauli,[1]* Michael Gottfried,[2]† Stefan Dullinger,[2,3]* Otari Abdaladze,[4] Maia Akhalkatsi,[4] José Luis Benito Alonso,[5] Gheorghe Coldea,[6] Jan Dick,[7] Brigitta Erschbamer,[8] Rosa Fernández Calzado,[9] Dany Ghosn,[10] Jarle I. Holten,[11] Robert Kanka,[12] George Kazakis,[10] Jozef Kollár,[12] Per Larsson,[13] Pavel Moiseev,[14] Dmitry Moiseev,[14] Ulf Molau,[13] Joaquín Molero Mesa,[9] Laszlo Nagy,[15,16] Giovanni Pelino,[17] Mihai Puşcaş,[18] Graziano Rossi,[19] Angela Stanisci,[17] Anne O. Syverhuset,[11] Jean-Paul Theurillat,[20,21] Marcello Tomaselli,[22] Peter Unterluggauer,[8] Luis Villar,[5] Pascal Vittoz,[23] Georg Grabherr[1]

In mountainous regions, climate warming is expected to shift species' ranges to higher altitudes. Evidence for such shifts is still mostly from revisitations of historical sites. We present recent (2001 to 2008) changes in vascular plant species richness observed in a standardized monitoring network across Europe's major mountain ranges. Species have moved upslope on average. However, these shifts had opposite effects on the summit floras' species richness in boreal-temperate mountain regions (+3.9 species on average) and Mediterranean mountain regions (−1.4 species), probably because recent climatic trends have decreased the availability of water in the European south. Because Mediterranean mountains are particularly rich in endemic species, a continuation of these trends might shrink the European mountain flora, despite an average increase in summit species richness across the region.

Biodiversity scenarios for the 21st century consistently forecast the reduction of alpine habitat and, ultimately, the regional loss of many European high-mountain plants (*1*, *2*). This process is supposedly driven by a general upward shift of plant species under a warming climate (*3*), resulting in a concurrent increase of species numbers at higher altitudes and local extinctions of those plants that already live near the upper margins of elevation gradients (*4*, *5*). However, empirical evidence on recent plant diversity trends in mountain systems is still scarce and is mostly based on resurveys of historical sites (*6*–*9*) [but see (*10*, *11*)].

A worldwide observation network (*12*, *13*) was initiated in the year 2000 as a standardized system to monitor changes in high-mountain biodiversity. As part of this network, vascular plant species occurrence was recorded first in 2001 on 66 mountain summits distributed across 17 study regions, which span all major mountain systems of Europe (Fig. 1). These summits were resurveyed in 2008. Here we compare the data from all summits from both years of observations to show changes in vascular plant species numbers.

Summits were grouped in a set of four within each region, spanning an altitudinal range from the treeline to the alpine/nival ecotone (*13*, *14*), or to the uppermost peaks on lower mountain ranges. The sampling areas covered the summits from their tops down to the 10-m contour line and were divided into eight sections (fig. S1) (*13*). For each section, a complete list of vascular plants was collected in 2001 and again in 2008. To avoid drawing conclusions from spurious species turnover caused by observation errors, we filtered the data to remove singleton records and potentially misidentified species from the list before analysis (*12*). Differences in number of species (i.e., the pooled species richness per summit and per region, respectively, between the two sampling dates) were then compared by means of linear mixed-effects models (*12*).

Between 2001 and 2008, vascular plant species numbers have increased on 45 mountain summits, decreased on 10 summits, and remained unchanged on 11 summits (Fig. 2A and table S1). Across all 66 summits, the average numbers of

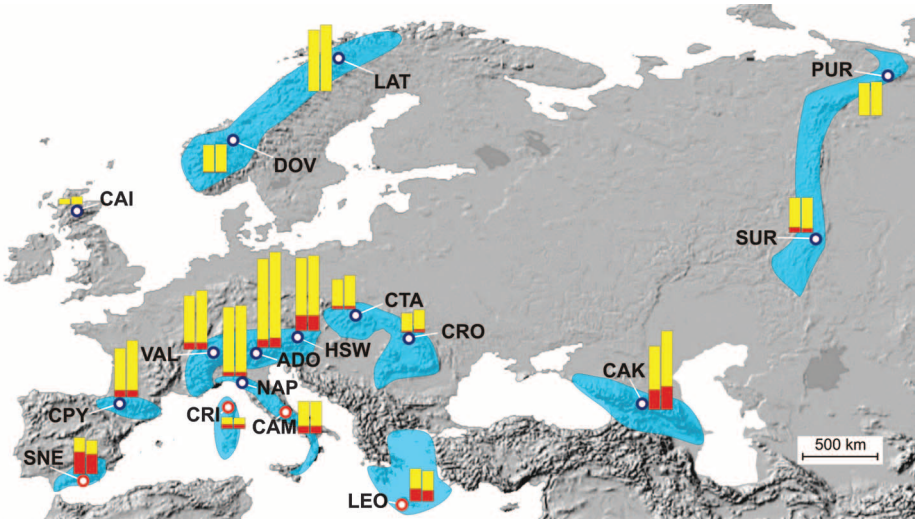


**Fig. 1.** Vascular plant species numbers in the 17 study regions. Blue circles indicate boreal and temperate, red circles indicate Mediterranean regions. Bars show the number of species found in 2001 (left bar) and 2008 (right bar); the proportion of endemic species is shown in red. Species number (endemic number) per region in 2001/in 2008: LAT (N-Scandes/Sweden, 109(0)/118(0); PUR (Polar Urals/Russia), 58(0)/60(0); DOV (S-Scandes/Norway), 49(1)/50(1); CAI (Cairngorms/UK), 10(0)/14(0); SUR (S-Urals/Russia), 62(9)/62(7); CTA (High Tatra/Slovakia), 53(5)/60(5); HSW (NE-Alps/Austria), 130(27)/134(27); CRO (E-Carpathians/Romania), 33(2)/40(5); ADO (S-Alps/Italy), 158(14)/170(17); VAL (W-Alps/Switzerland), 96(12)/105(12); NAP (N-Apennines/Italy), 123(7)/126(7); CPY (Central Pyrenees/Spain), 87(12)/101(12); CAK (Central Caucasus/Georgia), 113(35)/140(41); CRI (Corsica/France), 20(7)/19(7); CAM (Central Apennines/Italy), 57(13)/57(13); SNE (Sierra Nevada/Spain), 65(39)/60(35); LEO (Lefka Ori-Crete/Greece), 58(22)/54(19). Blue shaded areas indicate the respective maximum distribution of species defined as endemic (*12*); most endemics have a far more narrow distribution area.

[1]Institute of Mountain Research, Austrian Academy of Sciences, c/o University of Vienna, 1030 Wien, Austria. [2]Faculty Centre of Biodiversity, University of Vienna, 1030 Wien, Austria. [3]Vienna Institute for Nature Conservation and Analyses, 1090 Wien, Austria. [4]Institute of Ecology, Ilia State University, 0162 Tbilisi, Georgia. [5]Instituto Pirenaico de Ecología, Consejo Superior de Investigaciones Científicas, 22700 Jaca, Spain. [6]Department of Taxonomy and Plant Ecology, Institute of Biological Research, 400015 Cluj-Napoca, Romania. [7]Centre for Ecology and Hydrology, EH26 0QB Midlothian, Scotland, UK. [8]University of Innsbruck, 6020 Innsbruck, Austria. [9]Department of Botany, Faculty of Pharmacy, University of Granada, 18071 Granada, Spain. [10]Department of Environmental Management, Mediterranean Agronomic Institute of Chania, 73100 Chania, Greece. [11]Department of Biology, Norwegian University of Science and Technology, 7491 Trondheim, Norway. [12]Institute of Landscape Ecology of the Slovak Academy of Sciences, 81499 Bratislava, Slovakia. [13]Department of Plant and Environmental Sciences, University of Göteborg, 40530 Göteborg, Sweden. [14]Institute of Plant and Animal Ecology, Russian Academy of Sciences, 620144 Ekaterinburg, Russia. [15]EcoScience Scotland, G41 4QP Glasgow, Scotland, UK. [16]Instituto Nacional de Pequisa da Amazonia, Avenida André Araújo, 2936, Manaus, Brazil. [17]Laboratory of Environmetrics, University of Molise, 86090 Pesche (Isernia), Italy. [18]Alexandru Borza Botanical Garden, Babes-Bolyai University, 400015 Cluj-Napoca, Romania. [19]Department of Earth and Environmental Sciences, University of Pavia, 27100 Pavia, Italy. [20]Centre Alpien de Phytogéographie, Fondation J.-M. Aubert, 1938 Champex-Lac, Switzerland. [21]Section of Biology, University of Geneva, 1292 Chambésy, Switzerland. [22]Department of Evolutionary and Functional Biology, University of Parma, 43100 Parma, Italy. [23]Department of Ecology and Evolution, University of Lausanne, 1015 Lausanne, Switzerland.

*These authors contributed equally to this work.
†To whom correspondence should be addressed. E-mail: michael.gottfried@univie.ac.at

species per summit increased from 34.9 to 37.7; that is, by ~8%, a change that was significantly different from the null hypothesis of constant species richness ($t$ = 2.9, df = 49, $P$ = 0.006). Changes were, however, strikingly divergent among biomes: Most summits in boreal and temperate regions have gained additional species (43 out of 52; average increase from 38.0 to 41.9, $t$ = 4.0, df = 39, $P$ = 0.0004), and only two have lost one species each. In contrast, from the 14 summits in Mediterranean regions, the majority (8) had lower species counts in 2008 than in 2001, and only 2 have gained additional species (average decrease from 23.6 to 22.2, $t$ = –2.9, df = 10, $P$ = 0.018; Fig. 2A).

At the regional scale, observed changes were congruent with summit-level trends: Species richness increased in 12, decreased in 3, and remained constant in 2 regions (Figs. 1 and 2A). On average, species numbers per region were rising from 75.4 to 80.6 ($t$ = 2.8, df = 16, $P$ = 0.013). All 12 regions with higher species richness in the second survey were located in the boreal or temperate zone (mean increase in species numbers from 83.2 to 90.8, $t$ = 3.82, df = 12, $P$ = 0.001), whereas species counts were decreasing in three out of four Mediterranean regions, although this was not statistically significant because of the low sample size (average decrease from 50.0 to 47.5 species, $t$ = –2.1, df = 3, $P$ = 0.12; Fig. 2A).

To evaluate whether these changes in summit species richness might be related to a possible upward or downward move of species ranges, we calculated an altitudinal index for each species within each region in both 2001 and 2008. To compute this index, we first defined the relative altitude of each summit as the altitude above the lowest summit within the region it belongs to. Next, we weighted these relative altitudes by the species' frequencies on the respective summits in either 2001 or 2008. Finally, we calculated the species' altitudinal index for a particular region and monitoring campaign as the weighted average altitude of its distribution observed in the respective region and year (*12*). For all species recorded in both years, we then compared these altitudinal indices between 2001 and 2008 using linear mixed-effects models. The results suggest that species were indeed shifting their distributions to higher altitudes, by 2.7 m on average (Table 1). This is in line with a recent related study that found evidence that the more–warm-adapted species increase and the cold-adapted ones decline in European alpine summit vegetation (*15*). A general upward shift, as indicated in our study, is consistent across the continent's biomes (Table 1). An overall upward move of species hence seems to be compatible with both an average increase and a decrease of summit plant richness.

Parallel relationships between the magnitude of the observed changes and the relative altitude of the summits within one region (that is, its altitudinal difference from the region's lowest summit site) offer a clue for interpreting this unexpected finding: Both gains (in the boreal-temperate regions) and losses (in the Mediterranean regions) were more pronounced on the lower summits (Fig. 2B). This suggests that upward shifts of plants are mostly driven by leading-edge expansions on boreal-to-temperate mountains, with the higher number of new arrivals on the lower peaks probably resulting from larger nearby pools of potential invaders. In contrast, rear-edge retractions seem to make an important contribution to altitudinal species shifts in the Mediterranean.

We hypothesize that the range expansion in the boreal-to-temperate mountains is a result of warmer conditions, such as previously observed (*7, 9, 16*), whereas range retractions in the Mediterranean mountain ranges result from a combination of rising summer temperatures and stable-to-decreasing precipitation sums, such as was recently documented for southern Europe for the past decades (*17–19*). As a corollary, a possible attenuation of low-temperature constraints on Europe's Mediterranean mountains is probably foiled by rising water stress, and particularly so at the lowest summits, because aridity generally decreases with altitude in the Mediterranean basin (*20*). In line with this interpretation, Crimmins *et al.* (*21*) have recently suggested rapid responses of Californian Mediterranean-type mountain plants to changing climatic water balance, although in the opposite direction; i.e., a downward shift of species' optimum elevations through increasing water availability. Yet McCain and Colwell (*22*) suggested in a global study, albeit on vertebrates, that population extirpation risks in mountain areas due to climate warming would increase 10-fold, on average, when decreases in precipitation were also considered.

Species losses on Mediterranean summits are worrying because southern European mountain floras have high proportions of endemic plants (*12*, *23*) (Fig. 1). Indeed, there were 31% endemics among the species not redetected on those summits where they were recorded in 2001 (17 out of 55 species), but only 13%

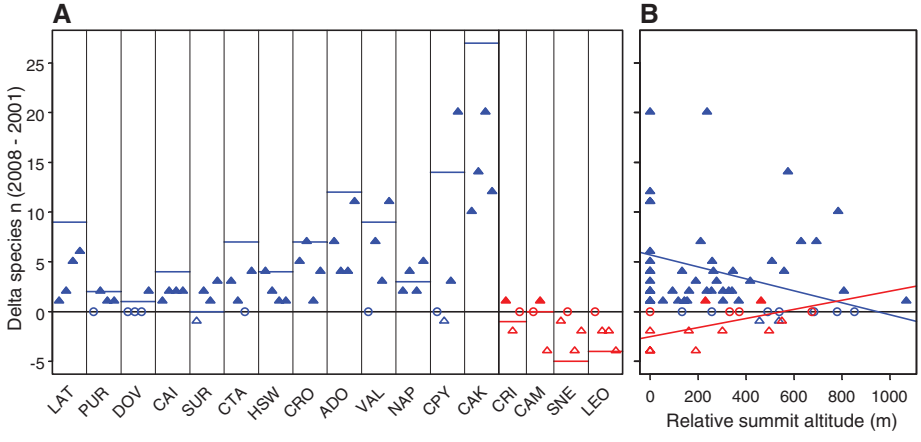


**Fig. 2.** Changes in vascular plant species numbers on 66 European summits between the years 2001 and 2008. (**A**) Summits within 13 boreal-temperate (blue) and 4 Mediterranean (red) mountain regions are arranged from north to south, and from high to low altitude within regions. Triangles represent the increase (solid symbols) or decrease (open symbols) of observed species numbers per summit; horizontal lines represent the changes in species numbers per region. Summits where species numbers did not change are symbolized by open circles. Region-scale changes were calculated after pooling species lists of all the summits surveyed within the respective region; that is, each species was counted only once per region and observation year. For full region names, see Fig. 1. (**B**) Summits are arranged along the $x$ axis according to their relative altitudes within regions, with a value of zero for the lowest summit in the respective region. Lines are drawn based on the fixed-effect coefficients of linear mixed-effects models, regressing the change in species number per summit on this summit's relative altitude. The slope coefficients are significantly different from zero in both cases (boreal-temperate summits: −0.006, $t$ = −3.3, df = 38, $P$ = 0.002; Mediterranean summits: 0.005, $t$ = 2.5, df = 9, $P$ = 0.034).

**Table 1.** Change in the species' altitudinal distribution between 2001 and 2008. Coefficients measure the average shift of the species' altitudinal index between 2001 and 2008 (in meters). SE, df, $t$, and $P$ are the standard errors of the coefficients, the degrees of freedom, the $t$ values of the coefficient given the specified degrees of freedom, and the associated two-sided $P$ values.

| | Coefficient (m) | SE | df | $t$ | $P$ |
|---|---|---|---|---|---|
| All summits | 2.7 | 1.10 | 1246 | 2.5 | **0.012** |
| Boreal and temperate and boreal | 2.7 | 1.23 | 1060 | 2.2 | **0.028** |
| Mediterranean | 2.5 | 1.1 | 185 | 2.3 | **0.024** |

among the species first detected on a particular summit in 2008 (32 out of 239; test on proportional equality: $X^2 = 8.7$, df = 1, $P = 0.003$). This does not imply that mountain endemics are intrinsically more threatened by a warming climate, but follows from simultaneous species loss in areas rich in endemics (the Mediterranean) and species gains in areas where endemics are rarer (boreal and temperate mountains). In total, the number of species recorded across all 66 summits increased from 821 to 869 species (by ~6%), whereas the number of endemics increased at a much lower rate, from 201 to 203 species (by ~1%). Overall, the proportion of endemics within our sample of Europe's summit flora decreased from 24.5 to 23.4%. Although this decrease is not significant yet (test on proportional equality: $X^2 = 0.24$, df = 1, $P = 0.63$), it would become so after 25 years if average annual rates of species gains remain constant for both endemic plants (~0.25 species/year) and nonendemic plants (~5.75 species/year). In the long run, such a decrease in the share of endemics will tend to homogenize the species composition of mountaintop communities across regions.

Our observations match the general expectation of a climate warming–driven upward shift of species distributions (*2*, *3*, *14*, *15*, *24*). However, they show that these upward shifts do not necessarily result in higher species richness on mountaintops. If rising aridity is actually the driver of observed species loss on many Mediterranean summits, this trend is likely to continue during the coming decades, because climate models predict increasing temperatures, decreasing annual precipitation, and an extension of the dry summer season in southern Europe (*25*–*27*). Owing to the high degree of endemism in these regions, the species pool of the continent's mountain flora might shrink even if local diversity on the majority of boreal and temperate mountaintops increases.

### References and Notes


1. W. Thuiller, S. Lavorel, M. B. Araújo, M. T. Sykes, I. C. Prentice, *Proc. Natl. Acad. Sci. U.S.A.* **102**, 8245 (2005).
2. R. Engler *et al.*, *Glob. Change Biol.* **17**, 2330 (2011).
3. I. C. Chen, J. K. Hill, R. Ohlemüller, D. B. Roy, C. D. Thomas, *Science* **333**, 1024 (2011).
4. J.-P. Theurillat, A. Guisan, *Clim. Change* **50**, 77 (2001).
5. R. K. Colwell, G. Brehm, C. L. Cardelús, A. C. Gilman, J. T. Longino, *Science* **322**, 258 (2008).
6. G. Grabherr, M. Gottfried, H. Pauli, *Nature* **369**, 448 (1994).
7. K. Klanderud, H. J. B. Birks, *Holocene* **13**, 1 (2003).
8. A. E. Kelly, M. L. Goulden, *Proc. Natl. Acad. Sci. U.S.A.* **105**, 11823 (2008).
9. P. Vittoz, J. Bodin, S. Ungricht, C. Burga, G. R. Walther, *J. Veg. Sci.* **19**, 671 (2008).
10. H. Pauli, M. Gottfried, K. Reiter, C. Klettner, G. Grabherr, *Glob. Change Biol.* **13**, 147 (2007).
11. K. J. Feeley *et al.*, *J. Biogeogr.* **38**, 783 (2011).
12. Materials and methods are available as supplementary materials on *Science* Online.
13. H. Pauli *et al.*, *The GLORIA Field Manual—Multi-Summit Approach* (Office for Official Publications of the European Communities, Luxembourg, 2004).
14. M. Gottfried *et al.*, *Environ. Res. Lett.* **6**, 014013 (2011).
15. M. Gottfried *et al.*, *Nat. Clim. Change* **2**, 111 (2012).
16. G.-R. Walther, S. Beißner, C. A. Burga, *J. Veg. Sci.* **16**, 541 (2005).
17. A. Mariotti *et al.*, *Environ. Res. Lett.* **3**, 044001 (2008).
18. S. del Río, L. Herrero, R. Fraile, A. Penas, *Int. J. Climatol.* **31**, 656 (2011).
19. A. Toreti, G. Fioravanti, W. Perconti, F. Desiato, *Int. J. Climatol.* **29**, 1976 (2009).
20. H. Walter, S. W. Breckle, *Spezielle Ökologie der Gemäßigten und Arktischen Zonen Ausserhalb Euro-Nordasiens* (Gustav Fischer Verlag, Stuttgart, Germany, 1991).
21. S. M. Crimmins, S. Z. Dobrowski, J. A. Greenberg, J. T. Abatzoglou, A. R. Mynsberge, *Science* **331**, 324 (2011).
22. C. M. McCain, R. K. Colwell, *Ecol. Lett.* **14**, 1236 (2011).
23. L. Nagy, G. Grabherr, C. Körner, D. B. A. Thompson, *Alpine Biodiversity in Europe* (Springer, Berlin, 2003), vol. 167.
24. C. M. Van de Ven, S. B. Weiss, W. G. Ernst, *Earth Interact.* **11**, 1 (2007).
25. J. H. Christensen *et al.*, in *Climate Change 2007: The Physical Science Basis. Contribution of Working Group I to the Fourth Assessment Report of the Intergovernmental Panel on Climate Change*, S. Solomon *et al.*, Eds. (Cambridge Univ. Press, Cambridge, 2007), pp. 847–940.
26. D. Nogués Bravo, M. B. Araújo, T. Lasanta, J. I. López Moreno, *Ambio* **37**, 280 (2008).
27. B. Benito, J. Lorite, J. Penas, *Clim. Change* **108**, 471 (2011).


**Acknowledgments:** Baseline data were collected within the European Union FP-5 project GLORIA-Europe (EVK2-CT-2000–0006) and with the support of Switzerland (OFES 00.0184-1). Resurvey was supported by the Swiss MAVA Foundation for Nature Conservation and by a number of national funding agencies, and analysis was supported by the Austrian Federal Ministry of Science and Research; the Austrian Academy of Sciences (Institute of Mountain Research); and the University of Vienna, where data are archived in the central GLORIA database and are available from the authors upon request. We thank the European Topic Centre on Biological Diversity for ambituos discussions in the early stage, C. Klettner for data compilation, S. Laimer for administration assistance, 17 GLORIA-Europe field teams with more than 80 fieldworkers for species recording, and protected-area authorities for logistic support. We also thank three anonymous referees for their valuable comments and suggestions.

### Supplementary Materials

www.sciencemag.org/cgi/content/full/336/6079/353/DC1
Materials and Methods
Figs. S1 and S2
Tables S1 to S4
References (*28*–*32*)

12 January 2012; accepted 15 March 2012
10.1126/science.1219033



# A Yeast Prion, Mod5, Promotes Acquired Drug Resistance and Cell Survival Under Environmental Stress

**Genjiro Suzuki, Naoyuki Shimazu, Motomasa Tanaka***

**Prion conversion from a soluble protein to an aggregated state may be involved in the cellular adaptation of yeast to the environment. However, it remains unclear whether and how cells actively use prion conversion to acquire a fitness advantage in response to environmental stress. We identified Mod5, a yeast transfer RNA isopentenyltransferase lacking glutamine/asparagine-rich domains, as a yeast prion protein and found that its prion conversion in yeast regulated the sterol biosynthetic pathway for acquired cellular resistance against antifungal agents. Furthermore, selective pressure by antifungal drugs on yeast facilitated the de novo appearance of Mod5 prion states for cell survival. Thus, phenotypic changes caused by active prion conversion under environmental selection may contribute to cellular adaptation in living organisms.**

Prion phenomena have been observed in yeast and filamentous fungi (*1*, *2*), and fungal prion proteins share common characteristics with mammalian prion protein. Prion inheritance is caused by the propagation of self-perpetuating and infectious prion particles composed of β sheet–rich fibrillar aggregates called amyloid (*3*–*5*). All of the yeast prion proteins identified thus far contain aggregation-prone Gln/Asn-rich domains that are critical for the formation of self-propagating amyloid. A number of Gln/Asn-rich proteins in yeast have the potential to behave as prions (*6*), implying that yeast might use prion conversion to regulate some cellular functions in vivo. Prion states acquire previously unrecognized genetic traits (*7*, *8*) and affect cellular functions such as transcriptional regulation (*3*, *9*), though they may represent disease states (*4*). Induction of the prion state [*PSI*$^+$] resulting from aggregation of Sup35 may be linked to a survival advantage under the selective pressure of environmental stressors (*10*), suggesting that prion conversion might help an organism adapt to environmental stress (*11*).

Laboratory for Protein Conformation Diseases, RIKEN Brain Science Institute, 2-1 Hirosawa, Wako, Saitama 351-0198, Japan.

*To whom correspondence should be addressed. E-mail: motomasa@brain.riken.jp

However, our understanding of whether and how prion conversion responds to environmental stress for cell survival and if specific mechanisms exist that mediate such adaptive processes is limited.

To address these questions, we attempted to identify yeast prions. We performed a genome-wide screen for PIN (inducible to [$PSI^+$]) factors whose aggregation facilitates the de novo appearance of [$PSI^+$] (*12*). Among the known PIN factors (*12*), several proteins behave as yeast prions (*13*–*16*). We used a [$q^-$] yeast strain, a non-prion form of yeast expressing a Q62-Sup35 chimera in which a Gln/Asn-rich domain (residues 1 to 40) in Sup35 was replaced with 62 glutamine repeats (Q62) (*17*), and searched for QIN (inducible to the [$Q^+$] prion state) factors (*18*). Because expanded polyglutamine readily forms amyloids, we reasoned that both Gln/Asn-rich and non–Gln/Asn-rich proteins might represent QIN factors. Among the QIN factors we identified (fig. S1 and table S1), we focused on Mod5, a tRNA isopentenyltransferase that catalyzes the transfer of an isopentenyl group to $A_{37}$ in the anticodon loop (*19*), because Mod5 did not contain Gln/Asn-rich or repeat domains but acted as both a QIN and PIN factor (fig. S1).

Prion aggregates demonstrate infectivity through their self-propagating amyloid forms (*20*, *21*). We first investigated whether Mod5 forms amyloid fibers in vitro. By multiple criteria, Mod5 aggregates formed amyloid-like fibrillar aggregates (Fig. 1, A to D, and fig. S2). Because Mod5 does not contain Gln/Asn-rich domains, we searched for a core aggregation region in Mod5 amyloids. Limited proteolysis of Mod5 amyloids with proteinase K and following mass analysis allowed us to identify the core of Mod5 amyloids (Fig. 1E), which was predicted to be aggregation-prone by the TANGO algorithm (fig. S3) (*22*). Soluble Mod5 was fully digested under the same conditions. Furthermore, deletion of the amyloid core region abolished the ability of Mod5 to act as a PIN factor (fig. S1C) and greatly decreased the reactivity of Mod5 amyloids to thioflavin T (Fig. 1B). The aggregates of Mod5 were self-propagating, as the addition of preformed Mod5 fibers to soluble Mod5 substantially accelerated the aggregation of soluble Mod5 (Fig. 1F). Furthermore, Mod5 amyloid seeds facilitated polymerization of soluble Sup35NM in vitro (Fig. 1G), indicating cross-seeding between Mod5 and Sup35NM. This result is consistent with the ability of Mod5 as a PIN factor (fig. S1) and sequestration of intrinsically disordered proteins into cross–β sheets (*23*). Thus, Mod5 forms self-propagating amyloids in vitro, despite the lack of Gln/Asn-rich domains.

Next, we employed a range of assays based on color phenotypes using the [$PSI^+$] system (*18*) and found that Mod5 has the potential to undergo a heritable conformational switch to the prion state by forming aggregates (fig. S4). Thus, we investigated whether a prion state could be induced by the aggregation of endogenous Mod5.

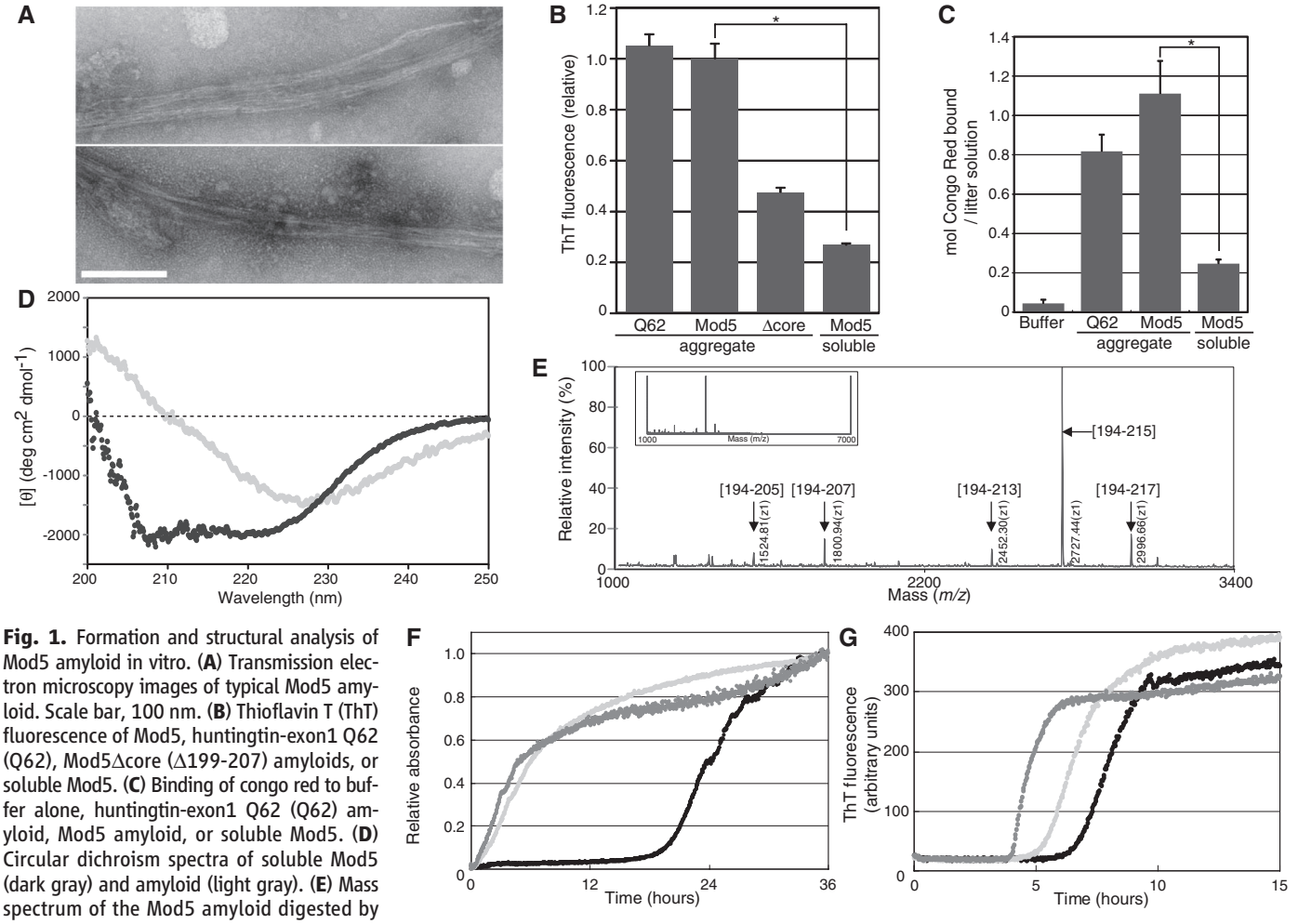


**Fig. 1.** Formation and structural analysis of Mod5 amyloid in vitro. (**A**) Transmission electron microscopy images of typical Mod5 amyloid. Scale bar, 100 nm. (**B**) Thioflavin T (ThT) fluorescence of Mod5, huntingtin-exon1 Q62 (Q62), Mod5Δcore (Δ199-207) amyloids, or soluble Mod5. (**C**) Binding of congo red to buffer alone, huntingtin-exon1 Q62 (Q62) amyloid, Mod5 amyloid, or soluble Mod5. (**D**) Circular dichroism spectra of soluble Mod5 (dark gray) and amyloid (light gray). (**E**) Mass spectrum of the Mod5 amyloid digested by proteinase K. Peptide regions corresponding to mass peaks are shown (arrows). (Inset) A full spectrum and no obvious peak was observed at >3400 mass/charge ratio (*m*/*z*). (**F**) Aggregation of Mod5 in the absence (black) or presence of Mod5 amyloid seeds [10% (light gray), 20% (dark gray) (mol/mol)] was monitored at 25°C. (**G**) Mod5 amyloid cross-seeds Sup35NM. Amyloid formation of Sup35NM in the absence (black) or presence of Mod5 amyloid seeds [10% (light gray), 20% (dark gray) (mol/mol)] was monitored by ThT fluorescence at 37°C. Error bars denote SD. *$P < 0.01$, based on an independent *t* test ($n = 3$ experiments) in comparison with soluble Mod5.

Because a double knockout of Mod5 and Trm1, which encodes tRNA methyltransferase, shows sensitivity to 5-fluorouracil (5-FU) (*24*), we used Δ*trm1* strains throughout this study unless otherwise indicated and introduced pure Mod5 amyloids (fig. S5) into Δ*trm1* strains by a protein infection protocol (*25*). We used a Δ*trm1* diploid strain with homozygous deletion of *TRM1* to avoid the accidental isolation of recessive chromosomal mutants. We examined 480 infectants for their sensitivity to 5-FU, and 10 colonies showed such sensitivity. The sensitivity of 6 out of the 10 colonies was reversed by the transient treatment with 3 mM guanidine hydrochloride (GdnHCl) (Fig. 2A), an inhibitor of the Hsp104 chaperone (*26*). Disruption of the *HSP104* gene also reversed it (Fig. 2B). This phenotypic reversal by elimination of Hsp104 is a common characteristic of yeast prions (*9*); we hereafter refer to this state as [*MOD*$^+$]. Overexpression of Hsp104 in [*MOD*$^+$] yeast also partially restored its sensitivity to 5-FU (fig. S6). These results established that the [*MOD*$^+$] prion state propagated in an Hsp104-dependent manner. In addition, the [*MOD*$^+$] state was mitotically stable because [*MOD*$^+$] yeast showed sensitivity to 5-FU after many passages. Next, we investigated whether endogenous Mod5 undergoes conformational changes in [*MOD*$^+$] yeast. We prepared cell lysates and separated them into supernatant and pellet fractions by centrifugation (*27*). In contrast to soluble Mod5 in [*mod*$^-$] and [*MOD*$^+$]Δ*hsp104* yeast, Mod5 in [*MOD*$^+$] yeast was observed in the pellet fraction (Fig. 2C). We examined the cellular localization of Mod5–green fluorescent protein (GFP) with or without mild overexpression of Mod5-GFP (*18*). In both cases, [*mod*$^-$] and [*MOD*$^+$]Δ*hsp104* cells displayed diffusible Mod5-GFP throughout the cytoplasm, whereas [*MOD*$^+$] cells exhibited multicytoplasmic Mod5-GFP aggregates that were not colocalized to either mitochondria or nucleus (Fig. 2D and fig. S7). Like other yeast prions, Mod5 aggregates from [*MOD*$^+$] yeast were resistant to SDS (Fig. 2E) (*28*). Thus, Mod5 is in an altered, aggregated conformational state in [*MOD*$^+$] yeast, compared with the soluble and diffusible Mod5 in [*mod*$^-$] yeast. The ectopic expression of Mod5 in Δ*mod5* but not [*MOD*$^+$] yeast restored the sensitivity to 5-FU, probably because ectopically expressed Mod5 was sequestered into preexisting Mod5 aggregates (Fig. 2F). [*MOD*$^+$] cells expressing ectopic Trm1 could grow on 5-FU plates (Fig. 2F), indicating specific recruitment of Mod5 monomer into Mod5 aggregates. Thus, the [*MOD*$^+$] state is caused by self-propagating Mod5 aggregates in vivo.

We investigated dominant inheritance of [*MOD*$^+$] yeast upon mating. To isolate [*MOD*$^+$] haploids, we introduced lysates of [*MOD*$^+$] diploids into [*mod*$^-$] haploid cells by protein infection and assayed infectants for both their sensitivity to 5-FU and phenotypic reversion

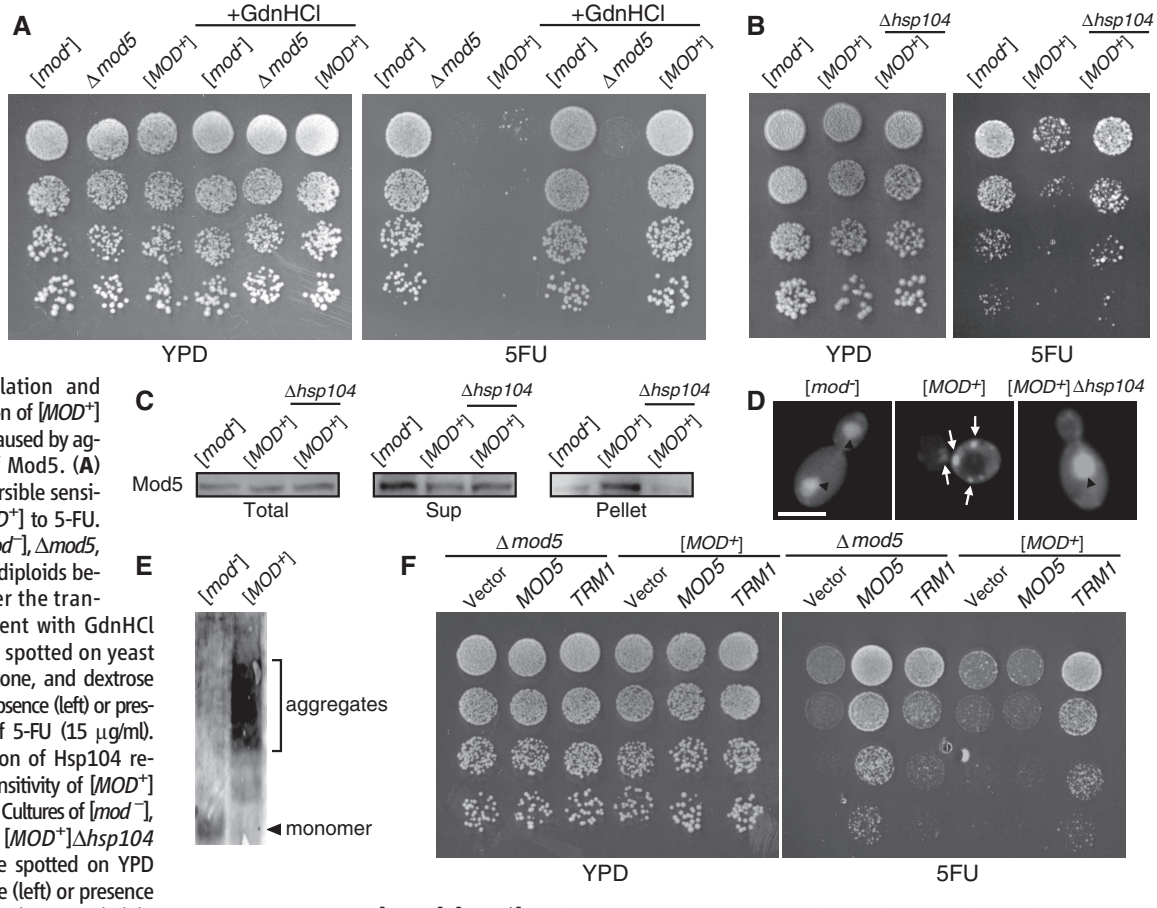


**Fig. 2.** Isolation and characterization of [*MOD*$^+$] prion states caused by aggregation of Mod5. (**A**) GdnHCl-reversible sensitivity of [*MOD*$^+$] to 5-FU. Cultures of [*mod*$^-$], Δ*mod5*, and [*MOD*$^+$] diploids before and after the transient treatment with GdnHCl (3 mM) were spotted on yeast extract, peptone, and dextrose (YPD) in the absence (left) or presence (right) of 5-FU (15 μg/ml). (**B**) Elimination of Hsp104 restored the sensitivity of [*MOD*$^+$] yeast to 5-FU. Cultures of [*mod*$^-$], [*MOD*$^+$], and [*MOD*$^+$]Δ*hsp104* diploids were spotted on YPD in the absence (left) or presence (right) of 5-FU (15 μg/ml). (**C**) Sedimentation analysis of [*mod*$^-$], [*MOD*$^+$], and [*MOD*$^+$]Δ*hsp104* yeast. Lysates of the yeast strains were separated into supernatant (Sup) and pellet fractions, and endogenous Mod5-GFP was detected by immunoblotting with an antibody to GFP. (**D**) Localization of Mod5 in [*mod*$^-$], [*MOD*$^+$], and [*MOD*$^+$]Δ*hsp104* yeast cells. Fluorescence images of [*mod*$^-$] (left), [*MOD*$^+$] (center), and [*MOD*$^+$]Δ*hsp104* (right) cells mildly overexpressing Mod5-GFP are shown. Fluorescent foci appeared in the cytoplasm of 55% of [*MOD*$^+$] cells, 12% of [*mod*$^-$] cells, and 9% of [*MOD*$^+$]Δ*hsp104* cells ($n$ > 100 cells). Arrows and arrowheads show Mod5 aggregates and nuclei, respectively. Similar results were obtained in the yeast strains without overexpression of Mod5-GFP [68% of [*MOD*$^+$] cells, 12% of [*mod*$^-$] cells and 10% of [*MOD*$^+$]Δ*hsp104* cells ($n$ > 100 cells)] (fig. S7). Scale bar, 5 μm. (**E**) Detection of SDS-resistant Mod5 aggregates by semi-denaturating detergent agarose gel electrophoresis in the lysates of [*mod*$^-$] and [*MOD*$^+$] cells that overexpress Mod5-GFP. (**F**) Ectopic overexpression of Mod5 in [*MOD*$^+$] yeast did not restore the sensitivity to 5-FU, whereas that of Trm1 recovered it. Fivefold serial dilutions of yeast cells were spotted in the sensitivity assay.

by GdnHCl (Fig. 3A). Five colonies out of 360 infectants were sensitive to 5-FU in a GdnHCl-reversible manner and were mitotically stable, indicating that they represent [*MOD*$^+$] states, whereas such colonies were not isolated from the same number of cells infected by [*mod*$^-$] yeast lysates (Fig. 3A and table S2). A [*MOD*$^+$] haploid was crossed with a [*mod*$^-$] haploid, and the resulting diploid showed sensitivity to 5-FU (Fig. 3B), indicating that the [*MOD*$^+$] state is dominantly inherited. Next, we disrupted the *MOD5* gene in a [*MOD*$^+$] haploid, crossed it with [*mod*$^-$] yeast and examined the sensitivity to 5-FU. The diploid recovered the ability to grow on 5-FU plates, indicating that the transient loss of Mod5 in [*MOD*$^+$] yeast eliminated the [*MOD*$^+$] state (Fig. 3B). Thus, the continuous expression of Mod5 is necessary for propagation of [*MOD*$^+$], and Mod5 is the protein determinant of [*MOD*$^+$]. Next, we explored non-Mendelian inheritance of [*MOD*$^+$], but the tetrad analysis of [*MOD*$^+$] diploids was unsuccessful (*18*). Thus, we examined cytoplasmic inheritance of [*MOD*$^+$] by cytoduction. We crossed a *kar1-1* Δ*trm1* yeast with the [*MOD*$^+$] or [*mod*$^-$] diploids that had been converted to *Mat* a/a diploids (*18*) and tested cytoductants for growth on 5-FU plates to identify [*MOD*$^+$] colonies. About half of the cytoductants from [*MOD*$^+$] showed sensitivity to 5-FU (47%), whereas those from [*mod*$^-$] did not (0%) (Fig. 3C). Thus, [*MOD*$^+$] is a cytoplasmically inherited genetic trait.

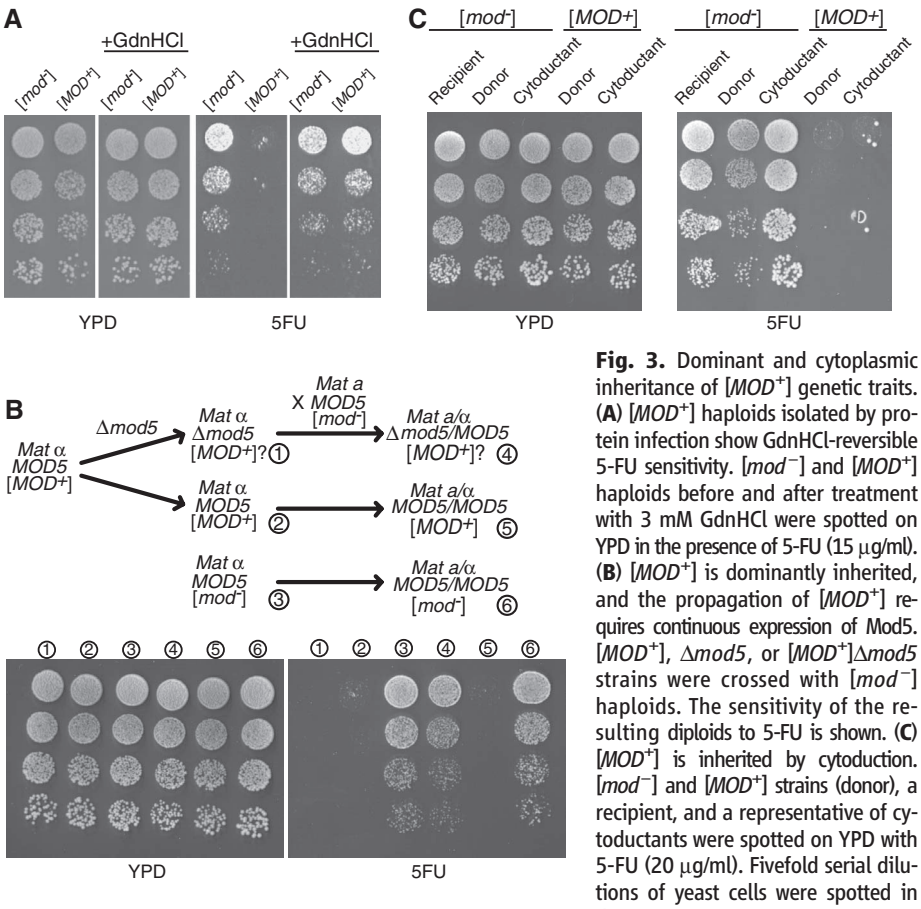


**Fig. 3.** Dominant and cytoplasmic inheritance of [*MOD*$^+$] genetic traits. (**A**) [*MOD*$^+$] haploids isolated by protein infection show GdnHCl-reversible 5-FU sensitivity. [*mod*$^-$] and [*MOD*$^+$] haploids before and after treatment with 3 mM GdnHCl were spotted on YPD in the presence of 5-FU (15 μg/ml). (**B**) [*MOD*$^+$] is dominantly inherited, and the propagation of [*MOD*$^+$] requires continuous expression of Mod5. [*MOD*$^+$], Δ*mod5*, or [*MOD*$^+$]Δ*mod5* strains were crossed with [*mod*$^-$] haploids. The sensitivity of the resulting diploids to 5-FU is shown. (**C**) [*MOD*$^+$] is inherited by cytoduction. [*mod*$^-$] and [*MOD*$^+$] strains (donor), a recipient, and a representative of cytoductants were spotted on YPD with 5-FU (20 μg/ml). Fivefold serial dilutions of yeast cells were spotted in the sensitivity assay.

Finally, we investigated physiological consequences of the prion conversion of Mod5. Mod5 catalyzes isopentenylation of tRNA by transferring dimethylallyl pyrophosphate (DMAPP) to tRNA $A_{37}$; DMAPP is also a substrate for Erg20 in the sterol biosynthetic pathway (*29*). Thus, a decrease in the tRNA modification by less soluble (functional) Mod5 should boost the sterol synthesis. We found that [*MOD*$^+$] cells contain lower levels of the tRNA modification [isopentenyladenosine ($^{i6}$A)] and higher ergosterol levels than [*mod*$^-$] cells (Fig. 4, A and B, and fig. S8) (*30*, *31*). [*MOD*$^+$] yeast showed resistance to a microtubule inhibitor, nocodazole (Fig. 4C), as in the case of overexpression of Erg20 in [*mod*$^-$] yeast (fig. S9). Thus, the prion conversion to [*MOD*$^+$] states stabilized microtubule structures. [*MOD*$^+$] yeast also acquired resistance against antifungal agents such as fluconazole, ketoconazole, and clotrimazole that inhibit ergosterol biosynthesis (Fig. 4D), presumably because of the increased ergosterol levels. Δ*trm1* was not responsible for the acquired antifungal resistance of [*MOD*$^+$] because the rescue of Trm1 in [*MOD*$^+$] yeast did not alter the antifungal resistance (Fig. 4D). To address whether the antifungal resistance of [*MOD*$^+$] is linked to positive selection under environmental stress, we examined if the de novo appearance of [*MOD*$^+$] prion states could be detected by culturing nonprion [*mod*$^-$] yeast with antifungal drugs. The [*MOD*$^+$] prion state appeared in culture in the presence of antifungal agents, but not sodium chloride that causes general stress conditions (Fig. 4E) (*10*). The de novo appearance of [*MOD*$^+$] states was also seen in a wild-type [*mod*$^-$] strain that expresses intact Mod5 and Trm1 (fig. S10), indicating that the GFP tag in Mod5 or the deletion of Trm1 was not responsible to the selective advantage of [*MOD*$^+$]. The de novo appearance of prion states was selective for [*MOD*$^+$] because the color of [*MOD*$^+$] yeast remained red; hence [*PSI*$^+$] states did not appear. Thus, whereas prions are known to be unstable when they first appear, antifungal drugs selectively allowed newly appearing [*MOD*$^+$] prions to grow and stabilize. Next, we performed competition experiments to examine which [*MOD*$^+$] or [*mod*$^-$] yeast grows preferentially in the absence or presence of antifungal drugs. In the presence of fluconazole, [*MOD*$^+$] yeast showed a growth advantage (Fig. 4F), indicating positive selection of [*MOD*$^+$] under the pressure of antifungal agents. In contrast, the fraction of [*MOD*$^+$] cells was decreased in cultures without fluconazole. This reduction was not due to prion loss (*18*) but rather to differences in the doubling time of yeast between [*MOD*$^+$] (150 min) and [*mod*$^-$] (124 min) because the distinct doubling time predicted the decrease in the fraction of [*MOD*$^+$] (Fig. 4F). Furthermore, Δ*trm1* did not contribute to the competitive growth of [*MOD*$^+$] and [*mod*$^-$] strains (fig. S11). Thus, the [*mod*$^-$] nonprion yeast became dominant when both [*MOD*$^+$] and [*mod*$^-$] yeasts were released from the pressure of antifungal agents. These results uncover a cellular mechanism in which a conformational switch of non–Gln/Asn-rich Mod5 from a soluble state to an aggregated form allows the yeast to adapt to the harmful environment of antifungal drugs by up-regulating ergosterol biosynthesis at the expense of tRNA modification (fig. S12). The dominance of the [*MOD*$^+$] yeast due to its growth advantage was eventually lost when the cells were released from the selective pressure of antifungal drugs. Thus, yeast cells employ prion conversion only when necessary for cell survival.

Acquisition of resistance to drugs including antifungal agents is a historical problem in medicine and agriculture. Recently, it has been shown that Hsp90 regulates the phenotype of antifungal resistance in pathogenic yeasts (*32*). This study suggests that active prion conversion in response to environmental selection may also be responsible for a wide spectrum of cellular adaptation and that cells may have evolved epigenetic prion conversion for fast on-demand adaptation in stressful environments to complement slower genetic adaptation processes and without the risk of generating deleterious mutations. In summary, our findings

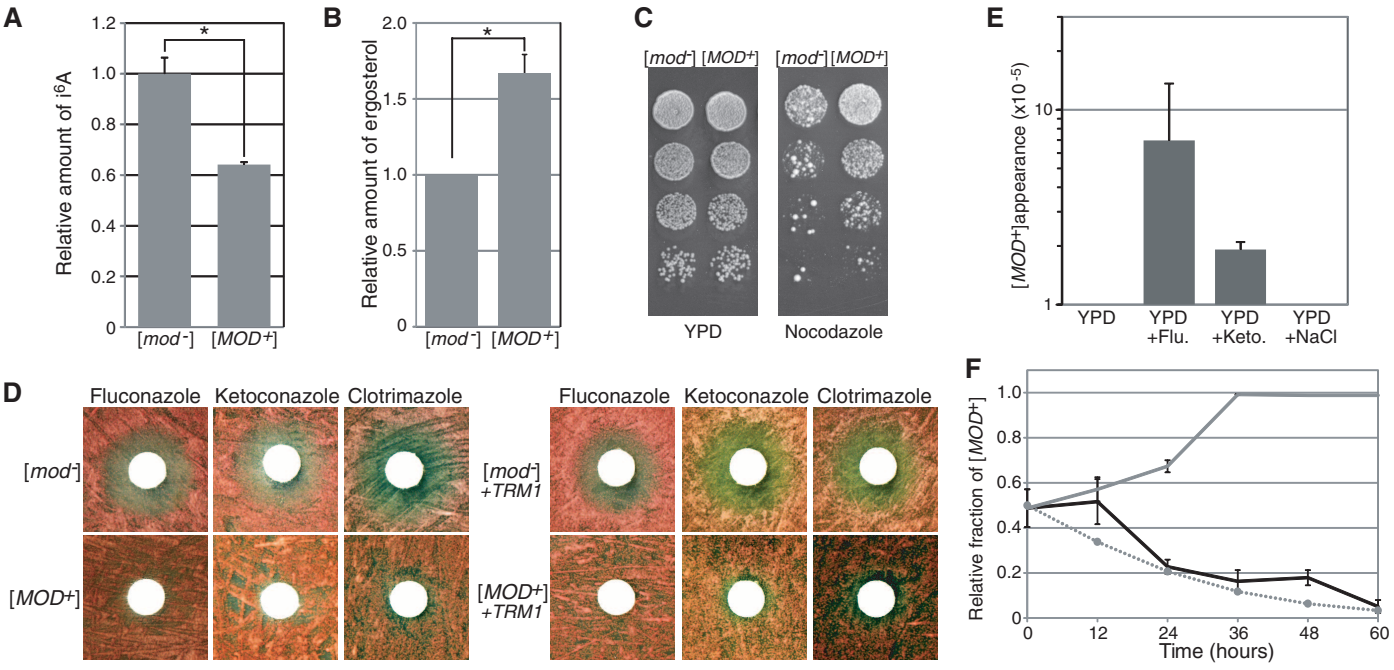


**Fig. 4.** Physiological roles of [*MOD*$^+$] genetic traits. (**A**) Relative amounts of isopentenyladenosine ($^{i6}$A) in tRNA of [*mod* $^-$] and [*MOD*$^+$] yeasts. (**B**) Relative ergosterol levels in [*mod* $^-$] and [*MOD*$^+$] yeasts. (**C**) The resistance of [*MOD*$^+$] to nocodazole, a microtubule inhibitor. Fivefold serial dilutions of yeast cells were spotted on YPD plates with or without nocodazole (3 μg/ml). (**D**) Resistance of [*MOD*$^+$] to antifungal agents was examined by a halo assay. [*MOD*$^+$] and [*mod* $^-$] cells (left panels) or those cells in which Trm1 is supplemented from a low-copy plasmid (right panels) were plated onto YPD plates. 10 μl of fluconazole (2 mg/ml), ketoconazole (100 μg/ml), and clotrimazole (50 μg/ml) were spotted onto a round paper filter. (**E**) Frequency of de novo appearance of [*MOD*$^+$] by YPD culture with fluconazole (50 μg/ml), ketoconazole (10 μg/ml), or sodium chloride (0.5 M). (**F**) Growth advantage of [*MOD*$^+$] in YPD culture with fluconazole. Yeast cells of [*mod* $^-$] and [*MOD*$^+$] strains were mixed at the 1:1 ratio and grown in YPD (black) or YPD containing fluconazole (50 μg/ml) (gray). A fraction of [*MOD*$^+$] yeast was determined at each time point. Theoretical relative ratios of [*MOD*$^+$] in YPD calculated from doubling times of [*mod* $^-$] (124 min) and [*MOD*$^+$] (150 min) strains are shown by a dotted line. Error bars denote SD. *$P < 0.01$, based on an independent *t* test ($n = 3$ experiments).

expand the definition of prion conversion beyond the disease state to a normal control mechanism for cellular fitness adaptation during environmental selection.

### References and Notes


1. R. B. Wickner, *Science* **264**, 566 (1994).
2. M. L. Maddelein, S. Dos Reis, S. Duvezin-Caubet, B. Coulary-Salin, S. J. Saupe, *Proc. Natl. Acad. Sci. U.S.A.* **99**, 7402 (2002).
3. M. F. Tuite, T. R. Serio, *Nat. Rev. Mol. Cell Biol.* **11**, 823 (2010).
4. T. Nakayashiki, C. P. Kurtzman, H. K. Edskes, R. B. Wickner, *Proc. Natl. Acad. Sci. U.S.A.* **102**, 10575 (2005).
5. Y. O. Chernoff, *Curr. Opin. Chem. Biol.* **8**, 665 (2004).
6. S. Alberti, R. Halfmann, O. King, A. Kapila, S. Lindquist, *Cell* **137**, 146 (2009).
7. H. L. True, S. L. Lindquist, *Nature* **407**, 477 (2000).
8. H. L. True, I. Berlin, S. L. Lindquist, *Nature* **431**, 184 (2004).
9. R. B. Wickner, H. K. Edskes, F. Shewmaker, T. Nakayashiki, *Nat. Rev. Microbiol.* **5**, 611 (2007).
10. J. Tyedmers, M. L. Madariaga, S. Lindquist, *PLoS Biol.* **6**, e294 (2008).
11. R. Halfmann, S. Lindquist, *Science* **330**, 629 (2010).
12. I. L. Derkatch, M. E. Bradley, J. Y. Hong, S. W. Liebman, *Cell* **106**, 171 (2001).
13. Z. Du, K. W. Park, H. Yu, Q. Fan, L. Li, *Nat. Genet.* **40**, 460 (2008).
14. B. K. Patel, J. Gavin-Smyth, S. W. Liebman, *Nat. Cell Biol.* **11**, 344 (2009).
15. B. K. Patel, S. W. Liebman, *J. Mol. Biol.* **365**, 773 (2007).
16. A. Brachmann, U. Baxa, R. B. Wickner, *EMBO J.* **24**, 3082 (2005).
17. L. Z. Osherovich, B. S. Cox, M. F. Tuite, J. S. Weissman, *PLoS Biol.* **2**, e86 (2004).
18. Materials, methods, and additional data are available as supplementary materials on *Science* Online.
19. M. E. Dihanich *et al.*, *Mol. Cell. Biol.* **7**, 177 (1987).
20. F. Chiti, C. M. Dobson, *Annu. Rev. Biochem.* **75**, 333 (2006).
21. R. Nelson, D. Eisenberg, *Curr. Opin. Struct. Biol.* **16**, 260 (2006).
22. A. M. Fernandez-Escamilla, F. Rousseau, J. Schymkowitz, L. Serrano, *Nat. Biotechnol.* **22**, 1302 (2004).
23. H. Olzscha *et al.*, *Cell* **144**, 67 (2011).
24. M. Gustavsson, H. Ronne, *RNA* **14**, 666 (2008).
25. M. Tanaka, P. Chien, N. Naber, R. Cooke, J. S. Weissman, *Nature* **428**, 323 (2004).
26. M. F. Tuite, C. R. Mundy, B. S. Cox, *Genetics* **98**, 691 (1981).
27. F. Ness, P. Ferreira, B. S. Cox, M. F. Tuite, *Mol. Cell. Biol.* **22**, 5593 (2002).
28. D. S. Kryndushkin, I. M. Alexandrov, M. D. Ter-Avanesyan, V. V. Kushnirov, *J. Biol. Chem.* **278**, 49636 (2003).
29. A. L. Benko, G. Vaduva, N. C. Martin, A. K. Hopper, *Proc. Natl. Acad. Sci. U.S.A.* **97**, 61 (2000).
30. T. Suzuki, Y. Ikeuchi, A. Noma, T. Suzuki, Y. Sakaguchi, *Methods Enzymol.* **425**, 211 (2007).
31. O. N. Breivik, J. L. Owades, *J. Agric. Food Chem.* **5**, 360 (1957).
32. N. Robbins *et al.*, *PLoS Pathog.* **7**, e1002257 (2011).



**Acknowledgments:** We thank J. Weissman (Univ. of California, San Francisco) for providing plasmids and yeast stains, C. Yokoyama for critical reading of the manuscript, Y. Komi and M. Yoshizawa for help with the construction of plasmids and yeast strains and drug-sensitivity assays, Y. Ohhashi for advice on structural analyses of amyloids, Y. Nekooki for providing huntingtin-exon1 Q62 protein, N. Takahashi for help with the screen for QIN, and Y. Sakamaki for transmission electron microscopy analysis. DNA sequencing and mass spectrometry were performed at the RIKEN Brain Science Institute Research Resources Center facility. Funding was provided by Japan Science and Technology Agency PRESTO; grants from the Ministry of Education, Culture, Sports, Science and Technology of Japan (Priority Area on Protein Society); the Next Program; and the Sumitomo Foundation and the Novartis Foundation (Japan) for the Promotion of Science (M.T.).


### Supplementary Materials

www.sciencemag.org/cgi/content/full/336/6079/355/DC1
Materials and Methods
Supplementary Text
Figs. S1 to S13
Tables S1 and S2
References (*33*–*43*)


23 January 2012; accepted 13 March 2012
10.1126/science.1219491

# When Are Two Heads Better than One and Why?

Asher Koriat[1]*

A recent study, using a perceptual task, indicated that two heads were better than one provided that the members could communicate freely, presumably sharing their confidence in their judgments. Capitalizing on recent work on subjective confidence, I replicated this effect in the absence of any dyadic interaction by selecting on each trial the decision of the more confident member of a virtual dyad. However, because subjective confidence monitors the consensuality rather than the accuracy of a decision, when most participants were in error, reliance on the more confident member yielded worse decisions than those of the better individual. Assuming that for each issue group decisions are dominated by the more confident member, these results help specify when groups will be more or less accurate than individuals.

Many everyday decisions are made jointly by two or more people. Studies that compared the accuracy of individual and group decisions have yielded somewhat inconsistent results. The groupthink phenomenon, which refers to a mode of decision-making that occurs within a cohesive group, has been claimed to underlie some of the disastrous decisions made in U.S. history (*1*–*3*). However, several studies have indicated that cooperative groups perform better than independent individuals on a wide range of tasks (*4*, *5*).

The immediate motivation for the present work comes from a recent study that delivers encouraging news. In the article *Optimally Interacting Minds* (*6*), Bahrami *et al*. compared individual and dyadic performance in a simple visual task. They asked, "[H]ow [can] signals from the same sensory modality (vision) in the brains of two different individuals ... be combined through social interaction?" In their experiments, participants judged which of two briefly presented stimuli contained an oddball target. Participants worked in dyads; they first made their decision individually, then shared their decisions, and if they disagreed, they discussed the matter until they reached a joint decision. The results led to the conclusion that "for two observers of nearly equal visual sensitivity, two heads were definitely better than one provided they were given the opportunity to communicate freely." In discussing the mechanism responsible for the two-heads-better-than-one (2HBT1) effect, the authors assumed that each individual can monitor the accuracy of his or her performance and can communicate his or her confidence accurately to the other member.

The present proposal, which capitalizes on recent work on the bases of subjective confidence (*7*–*9*), can account for the 2HBT1 effect in the absence of any communication between the members. On the one hand, this work, along with the results of (*6*), suggests a useful algorithm for combining judgments across two people who operate individually. In this algorithm—maximum-confidence slating (MCS)—for each trial, the decision that is made with higher confidence by one member of a virtual dyad is selected, circumventing dyadic interaction altogether. According to the self-consistency model (SCM) of subjective confidence (*7*), the MCS algorithm should yield a 2HBT1 effect, allowing a decision-maker to reach better decisions by combining information across a group of noninteracting participants. On the other hand, SCM implies boundary conditions to the group benefit so that under some conditions, two heads should be substantially worse than one.

SCM addressed the question of when confidence judgments are diagnostic of accuracy and why. In many two-alternative forced-choice (2AFC) tasks, a relatively high within-person confidence-accuracy (C/A) correlation is typically observed across items, suggesting that participants can monitor the accuracy of their choices. In attempting to clarify how people know that they know (*10*), it was noted (*11*) that in all previous studies of the C/A correlation, participants were more often correct than wrong, so that the correct answer was also the consensual or popular answer. When correctness and consensuality were dissociated by including a large number of items for which most participants chose the wrong answer, confidence was clearly correlated with the consensuality of the answer rather than with its correctness: For consensually correct (CC) items, the C/A correlation was positive, whereas for consensually wrong (CW) items, it was consistently negative. This consensuality principle has now been confirmed for word-matching, feeling-of-knowing judgments, general-information questions, memory of studied sentences, and perceptual judgments (*7*, *8*, *11*–*14*). Although in none of these studies were participants informed about others' choices, their confidence correlated strongly with the proportion of other participants who made that choice, not with the correctness of the choice.

SCM attempted to account for these and other findings. The model is described elsewhere (*7*). It assumes that people's responses to a 2AFC item are based on the random sampling of cues and representations associated with the item. An individual's subjective confidence, much like statistical level of confidence, is based on the consistency with which the decision reached is favored across the sampled representations. Assuming that the population of potential representations associated with each item is commonly shared across individuals, it was shown that a random sampling of representations is bound to yield higher confidence for consensual than for nonconsensual decisions (*7*–*9*).

The implications for the 2HBT1 effect are twofold. First, in many situations the knowledge that is shared by all participants corresponds by and large to the truth, so that the MCS algorithm as well as social interaction are expected to yield decisions that are more accurate than those of each individual alone. Thus, MCS is expected to yield a 2HBT1 effect for many perceptual and general-knowledge tasks in which the items are representative of their domain. Indeed, the wisdom-of-crowds phenomenon suggests that information that is aggregated across participants is generally closer to the truth than is the information provided by each individual participant (*15*–*18*).

The second implication, however, is that if confidence is tuned to the "common knowledge" rather than to the truth, reliance on confidence can be misleading when the shared knowledge departs from the truth. The psychological literature is replete with documentations of situations in which participants' perceptions, judgments, and beliefs deviate consistently from the truth (*19*, *20*). Examples include perceptual and memory illusions, deceptive general-knowledge questions, reconstructive memory errors, illusory truth judgments, and various judgmental biases. Assuming that collec-

**Table 1.** Percentage of correct decisions. In study 1, participants decided which of two displays contained an oddball target. In study 3, participants decided which of two lines was longer (Lines) or which of two shapes had a larger area (Area).

| | | *HP* (%) | *LP* (%) | *D-HC* (%) | *D-LC* (%) |
|---|---|---|---|---|---|
| | | *Study 1* | | | |
| Oddball target | | 67.82 | 66.98 | 69.88 | 64.93 |
| | | *Study 3* | | | |
| Lines | CC | 81.58 | 80.59 | 85.03 | 77.14 |
| | CW | 25.00 | 26.31 | 17.10 | 34.21 |
| Shapes | CC | 83.33 | 84.58 | 86.67 | 81.25 |
| | CW | 28.13 | 24.06 | 22.50 | 29.69 |

[1]Department of Psychology and Institute of Information Processing and Decision Making, University of Haifa, Haifa 31905, Israel.

*To whom correspondence should be addressed. E-mail: akoriat@research.haifa.ac.il

tive decisions are dominated by the most confident members (*6*, *21*, *22*), these decisions (and the MCS algorithm) should yield performance in these cases inferior to the performance of the individual members. For example, the results of (*11*) suggest that when two participants decide whether the capital of Norway is Copenhagen or Oslo, the more confident participant is the more likely to be correct, but when they decide whether the capital of Ausralia is Canberra or Sydney, the more confident member is more likely to be wrong.

In studies 1 to 4, participants responded individually to 2AFC questions and indicated their confidence in each response. To nullify chronic individual differences in confidence (*23*), the confidence judgments were first standardized so that the mean and SD of all participants were equal to the mean and SD of the raw scores. Participants were then paired ad hoc to form virtual dyads. The member with higher percent correct was designated as high performing (*HP*), and the other as low performing (*LP*). In addition, two dummy participants were created as follows: For each item, the response of the member with higher confidence was slated to the dummy high-confidence (*D-HC*) participant, and the other to the dummy low-confidence (*D-LC*) participant. Percent accuracy was then calculated for the four "participants." The performance of the *D-HC* participant represents the MCS algorithm (*24*).

In studies 1 and 2, the 2AFC items were selected to be representative of their domains. Hence, participants' decisions are more likely to be correct than wrong, and the MCS algorithm is expected to yield better decisions than those of the better individual.

Study 1 used the same task as in (*6*), but participants performed the entire experiment individually and indicated their confidence in each response on a 50-to-100% scale. The stimuli were selected randomly from all possible combinations, but the same pairs were presented to all participants in the same random order. 38 participants were paired ad hoc on the basis of their percent correct to form 19 virtual dyads. Mean percentage of correct answers was calculated for each of the four "participants" (Table 1).

First, accuracy was higher for *D-HC* than for *D-LC* [$t(18) = 7.52$, $P < 0.0001$], indicating a positive C/A correlation in a between-individual comparison. Second, performance was more accurate for *D-HC* than for *HP* [$t(18) = 6.69$, $P < 0.0001$], supporting the 2HBT1 effect. The superiority of *D-HC* performance was observed for 18 out of the 19 dyads ($P < 0.0001$) by a binomial test. Last, percent correct was significantly lower for *D-LC* than for *LP* [$t(18) = 6.69$, $P < 0.0001$]. The same pattern was observed when the raw (rather than standardized) confidence judgments were used.

I also examined whether three heads are better than two by adding one participant to each dyad and selecting the response of the most confident participant in the triplet. The performance of the triplet *D-HC* (71.88%) was better than that of the dyadic *D-HC* (69.88%) [$t(18) = 5.05$, $P < 0.0001$].

Study 2 (*24*) replicated the results of study 1 by using a general-knowledge task in which participants judged which of two European countries has a larger area or a larger population. The stimuli were constructed to be representative of their domain (*25*). The results indicated that performance was more accurate for *D-HC* than for *HP* for both the area task and the population task. For both tasks, the results also indicated that three heads were better than two.

The results of studies 1 and 2 yielded a 2HBT1 effect in the absence of interaction between the members of the dyad. This effect derived from confidence being diagnostic of accuracy even in a between-individual analysis: When the members of a dyad disagreed, the decision associated with higher confidence was the more likely to be correct.

I then turned to tasks for which "common knowledge" did not always correspond to the truth. SCM predicts that when participants' decisions are incorrect by and large, the selection of the high-confidence decisions should yield inferior accuracy than that of each individual alone.

Study 3 was based on a reanalysis of the data from two experiments that tested basic predictions of SCM for perceptual judgments (*8*). In experiment 1, participants decided which of two irregular lines was longer (Lines), and in experiment 2, participants decided which of two shapes (Shapes) had a larger area. A deliberate attempt was made to include a sufficiently large number of CW pairs—pairs for which the majority of participants are likely to choose the wrong answer.

The items were classified as CC or CW according to whether most participants chose the correct or the wrong answer (Fig. 1). Nineteen and 20 virtual dyads were formed for the Lines and Shapes tasks, respectively. The results (Table 1) indicated a different pattern for the CC and CW items. For the CC items, *D-HC* exhibited the best performance, which is consistent with the 2HBT1 effect. For the CW items, in contrast, *D-HC* exhibited the worst performance of all "participants." This pattern was observed for each of the two tasks.

A two-way analysis of variance (ANOVA) across the two tasks, which compared *D-HC* with *HP* for CC and CW items, yielded $F_{1,38} = 10.49$, mean squared error (MSE) = 95.26, $P < 0.005$ for the interaction. For the CC items, performance was better for *D-HC* (85.87%) than for *HP* (82.48%) [$t(38) = 2.82$, $P < 0.01$]. In contrast, for the CW items percent correct was lower for *D-HC* (19.87%) than for *HP* (26.60%) [$t(38) = 2.86$, $P < 0.01$].

For the CW items, *D-HC* performance was worse than that of the worst participant (*LP*) (25.16%) [$t(38) = 2.20$, $P < 0.05$]. For these items, the best accuracy was achieved by *D-LC* (31.89%), so that a 2HBT1 effect can be obtained if the responses of the participant with lower confidence are selected.

Study 4 was based on a reanalysis of the results of (*11*), which included CC and CW 2AFC general-knowledge items. For the CC items, *D-HC* exhibited the best performance, whereas for the CW items, it exhibited the worst performance (*24*).

For an external observer who cannot tell CW from CC items (cannot tell whether the consensual or high-confidence answer is right or wrong), applying the same heuristic across the board (for example, "take the high-confidence response"), or relying on dyadic decisions, can generally be beneficial. However, if the "crowd" is in error, reliance on confidence is bound to be misleading.

Study 5 extended the MCS algorithm to a within-individual design. This extension can allow

**Table 2.** Percentage of correct decisions in study 5. The study was similar to study 3, but participants performed the tasks twice with a 1-week interval.

| | | *AP* (%) | *D-HC* (%) | *D-LC* (%) |
|---|---|---|---|---|
| Lines | CC | 81.16 | 82.75 | 79.56 |
| | CW | 22.63 | 21.00 | 24.25 |
| Shapes | CC | 81.33 | 82.33 | 80.33 |
| | CW | 27.38 | 27.13 | 27.63 |

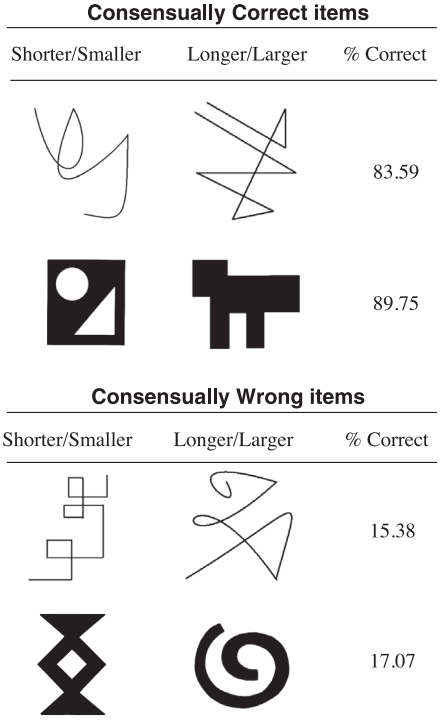


**Fig. 1.** Examples of the stimuli used in studies 3 and 5, divided into those for which the consensual answer was the correct answer (consensually correct) and those for which the consensual answer was the wrong answer (consensually wrong). The percentage of correct responses in study 3 is indicated.

generalizing the findings beyond the theoretical context of (*6*), which focused on the benefits of social interaction. Indeed, predictions from SCM were confirmed for a within-individual design: When participants responded to 2AFC items on several occasions, they were more confident when they made their more frequent decision than when they made their less frequent decision (*7*–*9*). The tasks used in study 3 were presented twice with a 1-week interval. The hypothesis tested is that a compilation of the high-confidence choices across the two presentations should yield the same pattern of results as that observed for a between-person compilation.

The extension of the wisdom-of-crowds idea to a within-person context (*26*–*28*) indicated that when participants estimated a quantity on two occasions, their average estimate was closer to the truth than their individual estimates. Therefore, in Study 5 *D-HC* performance was compared with average performance (*AP*) across the two sessions. The items were classified as CC or CW by using the same classification as in (*8*) and in study 3. Between-session differences in confidence were first nullified by setting the mean and SD of confidence judgments in session 2 as those of session 1 for each task and participant. For each item, the response associated with higher confidence across the two sessions was slated to *D-HC* and the other to *D-LC*. Mean percent correct for *D-HC*, *D-LC*, and *AP* is presented in Table 2 for the CC and CW items in each task.

A three-way ANOVA, task (Shapes versus Lines) × measure (*D-HC* versus *AP*) × item type (CC versus CW) yielded $F_{1,49} = 5.03$, MSE = 24.83, $P < 0.05$ for the measure × item type interaction. For the CC items, *D-HC* accuracy (82.54%) was higher than *AP* accuracy (81.24%) [$t(49) = 2.67$, $P < 0.05$]. For the CW items, *D-HC* accuracy (24.06%) tended to be somewhat lower than *AP* accuracy (25.00%) [$t(49) = 1.05$, $P < 0.31$]. In addition, across the CC items, confidence was higher when the correct choice was made than when the wrong choice was made, whereas the opposite was true for the CW items.

A comparison of *D-HC* with *D-LC* suggests that the benefit from the MCS algorithm in the case of CC items was more limited for the within-person confidence-based slating (study 5; 2.68 percentage points) than for the cross-person slating (study 3; 6.62 percentage points). The reason derives from the greater independence between decisions of two members of a dyad (study 3; a correlation of 0.02) than between the two decisions of the same person (study 5; a correlation of 0.63) (*28*).

The present work delivers three messages. First, under many conditions in which participants' decisions are correct by and large, a 2HBT1 effect should be observed. The results of the present study are consistent with Bahrami *et al.*'s (*6*) proposition that the benefit from dyadic interaction derives from individuals communicating their level of confidence accurately to each other. Here, however, a 2HBT1 effect was observed (studies 1 and 2) in the absence of social interaction. The selection of responses on the basis of confidence improved accuracy beyond the improvement achieved by the aggregation of responses across individuals (*15*).

Second, however, in situations in which most participants tend to make the wrong decisions, the MCS algorithm, as well as social interaction, is expected to yield group decisions that are even less accurate than those of each individual alone. In such cases, it is the low-confidence individuals who are more likely to be correct, and reliance on the more confident members should lead the group astray.

Last, the within-individual results (study 5) highlight a general perspective for the analysis of decision accuracy that goes beyond the effects of social interaction (*6*). This perspective, as captured by SCM, involves the variations in confidence that occur both within individuals and between individuals when choice and confidence are based on the sampling of clues from a common database (*7*, *27*).

### References and Notes


1. R. S. Baron, in *Advances in Experimental Social Psychology*, M. P. Zanna, Ed. (Elsevier Academic Press, San Diego, CA, 2005), pp. 219–253.
2. J. K. Esser, *Organ. Behav. Hum. Decis. Process.* **73**, 116 (1998).
3. I. Janis, Ed., *Groupthink: A Psychological Study of Policy Decisions and Fiascos* (Houghton Mifflin, Boston, 1982).
4. G. W. Hill, *Psychol. Bull.* **91**, 517 (1982).
5. P. R. Laughlin, E. C. Hatch, J. S. Silver, L. Boh, *J. Pers. Soc. Psychol.* **90**, 644 (2006).
6. B. Bahrami *et al.*, *Science* **329**, 1081 (2010).
7. A. Koriat, *Psychol. Rev.* **119**, 80 (2012).
8. A. Koriat, *J. Exp. Psychol. Gen.* **140**, 117 (2011).
9. A. Koriat, S. Adiv, *Soc. Cogn.* **29**, 577 (2011).
10. J. Dunlosky, J. Metcalfe, *Metacognition* (Sage, Thousand Oaks, CA, 2009)
11. A. Koriat, *J. Exp. Psychol. Learn. Mem. Cogn.* **34**, 945 (2008).
12. W. F. Brewer, C. Sampaio, *Memory* **14**, 540 (2006).
13. A. Koriat, *Mem. Cognit.* **4**, 244 (1976).
14. A. Koriat, *J. Exp. Psychol. Gen.* **124**, 311 (1995).
15. D. Ariely *et al.*, *J. Exp. Psychol. Appl.* **6**, 130 (2000).
16. R. Clemen, *Int. J. Forecast.* **5**, 559 (1989).
17. J. Surowiecki, *The Wisdom of Crowds* (Anchor Books, New York, 2005).
18. T. S. Wallsten, A. Diederich, *Math. Soc. Sci.* **41**, 1 (2001).
19. For a popular presentation, see (*29*).
20. D. Kahneman, *Thinking Fast and Slow* (Farrar, Straus & Giroux, New York, 2011).
21. B. L. Cutler, S. D. Penrod, T. E. Stuve, *Law Hum. Behav.* **12**, 41 (1988).
22. Z. L. Tormala, D. D. Rucker, *Soc. Personal. Psychol. Compa.* **1**, 469 (2007).
23. K. Kleitman, L. Stankov, *Appl. Cogn. Psychol.* **15**, 321 (2001).
24. Materials and methods, and additional analyses, are available as supplementary materials on *Science* Online.
25. M. K. Dhami, R. Hertwig, U. Hoffrage, *Psychol. Bull.* **130**, 959 (2004).
26. S. M. Herzog, R. Hertwig, *Psychol. Sci.* **20**, 231 (2009).
27. K. L. Hourihan, A. S. Benjamin, *J. Exp. Psychol. Learn. Mem. Cogn.* **36**, 1068 (2010).
28. E. Vul, H. Pashler, *Psychol. Sci.* **19**, 645 (2008).
29. R. Burton, *On Being Certain: Believing You Are Right Even When You're Not* (St. Martin's Press, New York, 2008).



**Acknowledgments:** I am grateful to R. Gil and D. Klein for their help in the analyses of the results, and to S. Adiv for her assistance in the preparation of the article. Support for this project was received from the Max Wertheimer Minerva Center for Cognitive Processes and Human Performance, University of Haifa.


### Suppplementary Materials

www.sciencemag.org/cgi/content/full/336/6079/360/DC1
Materials and Methods
SOM Text
Table S1
References


14 November 2011; accepted 29 February 2012
10.1126/science.1216549


# Structure of an Intermediate State in Protein Folding and Aggregation


**Philipp Neudecker,[1,2,3,4,5] Paul Robustelli,[6] Andrea Cavalli,[6] Patrick Walsh,[1,7] Patrik Lundström,[1,2,3] Arash Zarrine-Afsar,[1,2] Simon Sharpe,[1,7] Michele Vendruscolo,[6] Lewis E. Kay[1,2,3,7]***



Protein-folding intermediates have been implicated in amyloid fibril formation involved in neurodegenerative disorders. However, the structural mechanisms by which intermediates initiate fibrillar aggregation have remained largely elusive. To gain insight, we used relaxation dispersion nuclear magnetic resonance spectroscopy to determine the structure of a low-populated, on-pathway folding intermediate of the A39V/N53P/V55L (A, Ala; V, Val; N, Asn; P, Pro; L, Leu) Fyn SH3 domain. The carboxyl terminus remains disordered in this intermediate, thereby exposing the aggregation-prone amino-terminal β strand. Accordingly, mutants lacking the carboxyl terminus and thus mimicking the intermediate fail to safeguard the folding route and spontaneously form fibrillar aggregates. The structure provides a detailed characterization of the non-native interactions stabilizing an aggregation-prone intermediate under native conditions and insight into how such an intermediate can derail folding and initiate fibrillation.


Insoluble β sheet–rich fibrillar aggregates, called amyloid fibrils, form conspicuous deposits in tissue associated with a wide range of human pathologies, including Alzheimer's and Parkinson's diseases and type 2 diabetes (*1*–*4*). Fibril formation has been reported for many

proteins, and aggregates are often highly cytotoxic, even for proteins not linked directly to a clinical condition, as in the case of SH3 domains (*5*).

Although experimentally determined atomic-resolution models have started to appear for amyloid fibrils (*6*), the detailed structural mechanisms of aggregation, generally believed to follow nucleation-and-growth schemes (*3*), are still largely unclear. Initial observations that amyloid formation often occurs for disordered or destabilized polypeptide chains suggested that aggregation requires extensive unfolding (*7*). However, fibril formation is also observed for globular proteins under native conditions, and theoretical considerations as well as experimental evidence indicate that aggregation proceeds via native-like intermediates that are formed after the major folding barrier in many of these systems (*4*). Reports that pre- and protofibrillar oligomers are often as or even more cytotoxic than the fibrils themselves (*3*, *5*, *8*–*10*) have increasingly shifted focus toward early stages of aggregation and fibril formation. Recently, an intermediate with a non-native *trans*-proline conformation was identified as the direct precursor of β-2-microglobulin fibril elongation under native conditions (*11*). The structure of this intermediate, although not known in detail, is close to the native state (*11*). A mutant enforcing the trans conformation crystallized directly as a crystallographic dimer, suggesting a straightforward model for monomer arrangement within a fibril (*12*).

Because the experimental detection and characterization of low-populated, transiently formed intermediates in protein folding and aggregation is challenging (*13*, *14*), their atomic-resolution structures, aggregation propensities, and roles in aggregation are not understood in detail. With the development of Carr-Purcell-Meiboom-Gill (CPMG) relaxation dispersion nuclear magnetic resonance (RD NMR) spectroscopy (fig. S1) (*15*), however, protein-folding exchange reactions on the millisecond time scale can be studied at atomic resolution and under native equilibrium conditions (*16*). In addition to quantifying the kinetics and thermodynamics of the exchange process, backbone chemical shifts and bond vector orientations of low-populated (excited) states can be obtained, which are key to the atomic-resolution structure determination of these transient conformers (*17*, *18*).

In previous $^{15}$N CPMG RD NMR studies (*16*, *19*), we demonstrated that the A39V/N53P/V55L (A, Ala; V, Val; N, Asn; P, Pro; L, Leu) Fyn SH3 domain folds from the unfolded state (U) via an on-pathway, low-populated (≈2%) intermediate (I) to a native β-sandwich fold (N). The stability and folding kinetics of this mutant are well within the window of the CPMG method (fig. S1). In the structure of the A39V/N53P/

[1]Department of Biochemistry, University of Toronto, Toronto, Ontario M5S 1A8, Canada. [2]Department of Chemistry, University of Toronto, Toronto, Ontario M5S 3H6, Canada. [3]Department of Molecular Genetics, University of Toronto, Toronto, Ontario M5S 1A8, Canada. [4]Institut für Physikalische Biologie, Heinrich-Heine-Universität, 40225 Düsseldorf, Germany. [5]ICS-6 (Strukturbiochemie), Forschungszentrum Jülich, 52425 Jülich, Germany. [6]Department of Chemistry, University of Cambridge, Cambridge, CB2 1EW, UK. [7]Program in Molecular Structure and Function, Hospital for Sick Children, Toronto, Ontario M5G 1X8, Canada.

*To whom correspondence should be addressed. E-mail: kay@pound.med.utoronto.ca

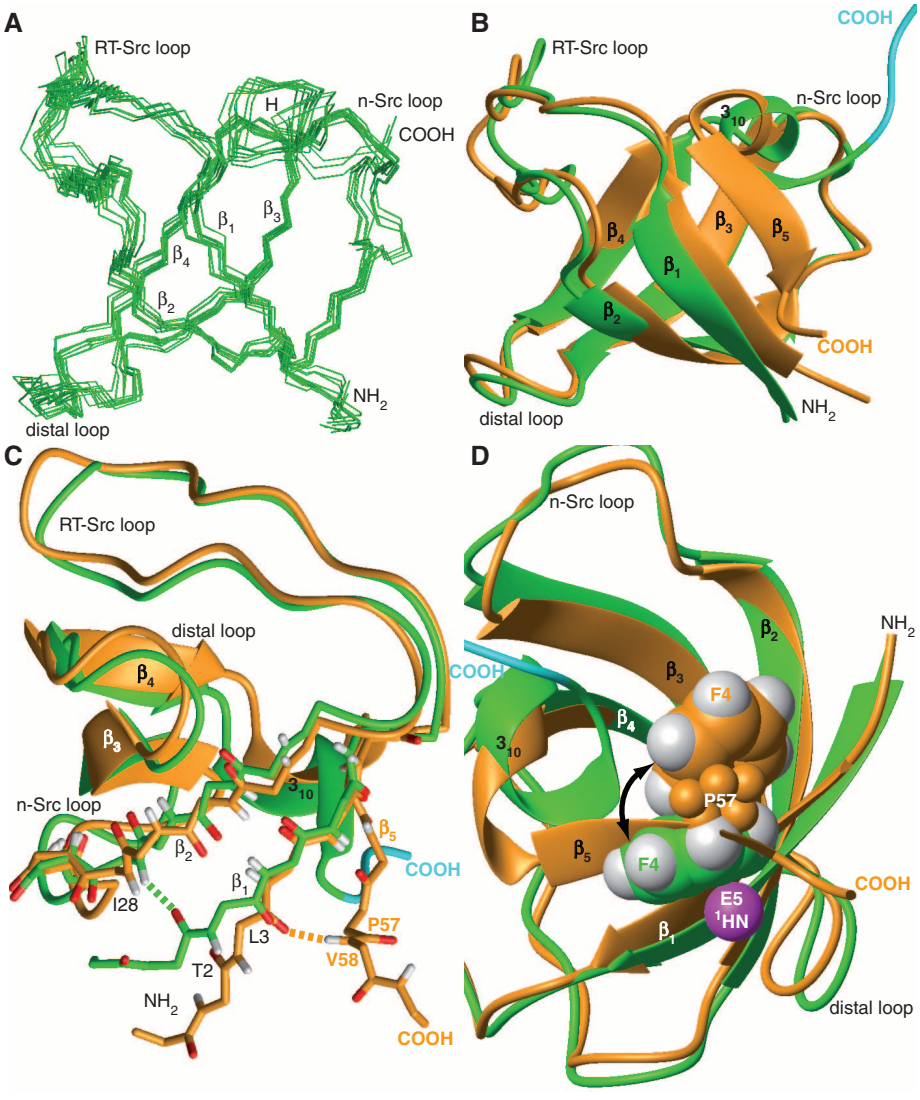


**Fig. 1.** Structure of the low-populated intermediate. (**A**) Backbone overlay of the 10 lowest-energy structures of the intermediate of A39V/N53P/V55L Fyn SH3 from Ser[1] to Ala[56]. (**B**) Backbone overlay in schematic representation of the lowest-energy solution structure of the native state (orange) (fig. S2 and table S1) with the lowest-energy solution structure of the intermediate state (green). Residues Pro[57] to Asp[59], which are completely flexible as established by random-coil chemical shifts (fig. S5B), have been added in an extended conformation for illustrative purposes only and are highlighted in light blue. (**C**) Same overlay as in (B) illustrating the differences in hydrogen bonding (dashed lines) between strands $\beta_5$, $\beta_1$, and $\beta_2$. (**D**) Overlay as in (B) and (C) illustrating how the side chain of Phe[4] (F4) (space-filling representation) stacks with Pro[57] (P57) (ball-and-stick representation) in the native state but fills the gap left by the missing strand $\beta_5$ in the intermediate. The amide proton of Glu[5] (E5) is shown in magenta.

V55L Fyn SH3 domain native state, determined from NMR data starting from the crystal structure of the N53I/V55L Fyn SH3 domain (*20*) (fig. S2 and table S1), the terminal (strands $\beta_1$ and $\beta_5$) and central (strands $\beta_2$, $\beta_3$, and $\beta_4$) β sheets are connected at one edge by hydrogen bonds between $\beta_1$ and $\beta_2$ to form a five-stranded incomplete antiparallel β barrel (Fig. 1). The I state is a compact near-native intermediate formed after the major folding barrier (*19*), with the central three-stranded β sheet already intact in the rate-limiting transition state between U and I (*19*, *21*, *22*). Interestingly, the $^{15}$N chemical shifts of the intermediate revealed pronounced non-native interactions (fig. S3) (*19*, *22*). Contrary to the notion that such interactions cause kinetic traps that evolution has largely selected against, there is increasing evidence that they play an important role in the folding and misfolding of many proteins (*4*, *14*, *20*, *23*), including the Fyn SH3 domain (*20*). To gain further insight into how non-native interactions influence both folding and misfolding, we used CPMG RD NMR spectroscopy under solution conditions that favor the native state to determine the three-dimensional structure of the transient intermediate of the A39V/N53P/V55L Fyn SH3 domain (see supplementary materials and methods).

To this end, we recorded and analyzed a variety of CPMG RD experiments (fig. S4) on several suitably isotope-labeled A39V/N53P/V55L Fyn SH3 samples at 20°C. $^{15}$N, $^{1}$HN, $^{13}$CO, $^{13}$Cα, and $^{1}$Hα backbone chemical shifts of the intermediate (fig. S3B), $^{15}$N-$^{1}$HN backbone amide residual dipolar couplings, and $^{13}$CO residual chemical shift anisotropies were obtained from fits of the resulting RD profiles from sites showing chemical exchange (fig. S4). The extracted chemical shifts corroborate our earlier observations (*19*, *22*) that much of the native backbone fold is already formed in I, except for the N- and C-terminal regions (fig. S5A), but provide substantially more data on which to base a structural analysis so that the conformational changes to the N and C termini can be elucidated. Most notably, the C terminus from Pro$^{57}$ to Asp$^{59}$ is disordered in I (fig. S5B), which implies that strand $\beta_5$ is not formed. We used the CamShift chemical shift restrained molecular dynamics structure calculation protocol (figs. S6 to S8) (*24*), which makes use of RD-derived backbone chemical shifts, $^{15}$N-$^{1}$HN residual dipolar couplings, and $^{13}$CO residual chemical shift anisotropies, to obtain more quantitative structural information about the well-ordered part of the domain.

Superposition of the 10 resulting lowest-energy structures of the folding intermediate (Fig. 1A) reveals that the topology of strands $\beta_1$ to $\beta_4$ followed by the helical turn is native-like (Fig. 1B; see table S2 for structural statistics), in agreement with backbone amide H/D exchange experiments (fig. S9). The tertiary interactions missing in the absence of strand $\beta_5$ are partially compensated for by non-native contacts within this residual native-like backbone topology. In particular, strand $\beta_1$ compensates for the loss of hydrogen bonding to $\beta_5$ by associating more tightly with strand $\beta_2$ through the formation of a non-native hydrogen bond between Ile$^{28}$ HN and Thr$^{2}$ CO (Fig. 1C), with a much shorter HN-O distance in the intermediate (1.92 ± 0.08 Å) relative to the native structure (4.39 ± 0.28 Å). In addition, the four-stranded β sheet of I is stabilized by non-native hydrophobic core packing with the bulky aromatic ring of Phe$^{4}$ filling the space occupied by the backbone of strand $\beta_5$ in the native state (Fig. 1D). An advantage of the chemical shift restrained structure calculation is the possibility to determine side-chain conformations by exploiting aromatic-ring current effects on nearby backbone atom chemical shifts. The difference in aromatic packing between states N and I is associated with large chemical shift changes affecting the amide proton of Glu$^{5}$ (Fig. 1D and fig. S3) and other backbone resonances; this enables reliable placement of the aromatic side chain of Phe$^{4}$ in a position that is consistent with backbone amide H/D exchange measurements (fig. S9).

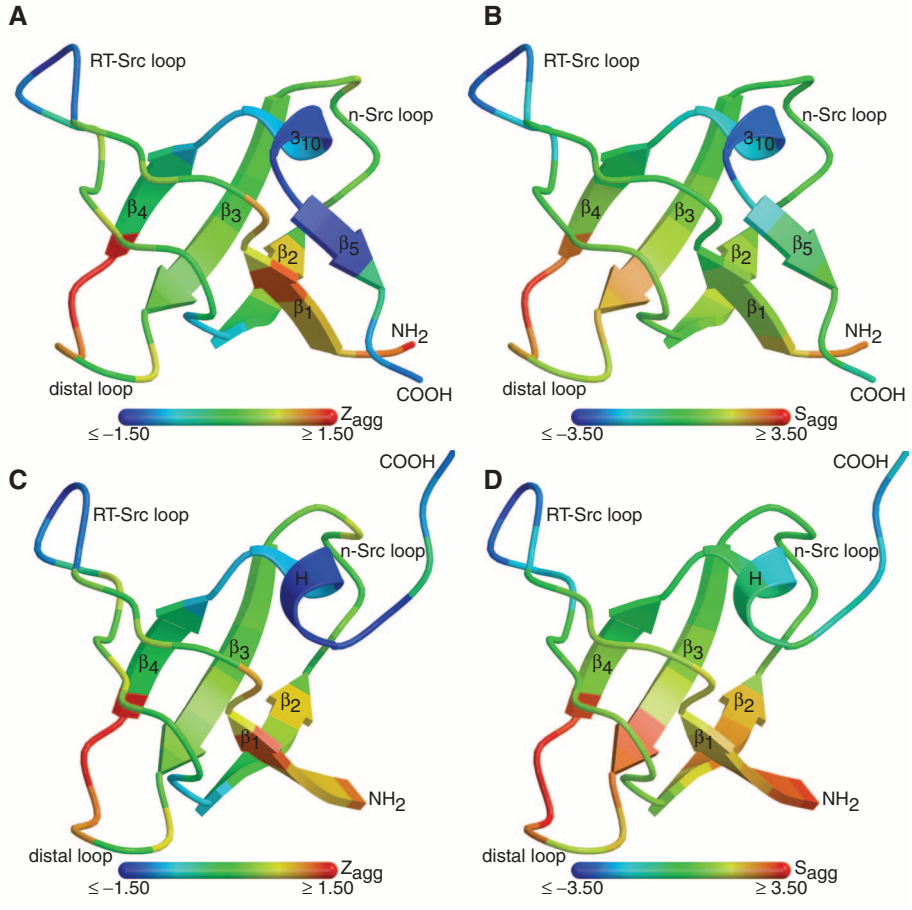


**Fig. 2.** Aggregation propensities of the native and intermediate states of A39V/N53P/V55L Fyn SH3. Sequence-based aggregation propensity score, $Z_{agg}$ (*25*), color-coded onto the lowest-energy solution structure of (**A**) the native state and (**C**) the intermediate. $Z_{agg}$ is normalized with respect to random sequences; $Z_{agg} > 1$ (orange to red) indicates significant propensity to aggregate. (**B**) Surface aggregation propensity score, $S_{agg}$ (*32*), for the lowest-energy solution structure of the native state and (**D**) the intermediate.

Our structure thus explains why the four-stranded β sheet constitutes a metastable folding intermediate. It also reveals how this state can lead to aggregation, as it exposes strand $\beta_1$, which has an unusually hydrophobic amino acid sequence that is predicted (*25*) to be aggregation-prone (Fig. 2, A and C). β sheets require nonideal edge strands to avoid aggregation (*26*), such as the bulge at $Pro^{57}$ in strand $\beta_5$ of the native Fyn SH3 (Fig. 1C), a conserved structural feature at this position in SH3 domains. Accordingly, the native state is protected from aggregation (Fig. 2B), whereas the intermediate is highly aggregation-prone (Fig. 2D). Because the extent of aggregation of I is limited by its low population (≈2% of the total concentration), we have experimentally studied its aggregation propensity by engineering the truncation mutant, A39V/N53P/V55L/Δ(57-60) Fyn SH3. The truncated domain has the same temperature midpoint and enthalpy of folding (fig. S10) as predicted for I based on the thermodynamics of the A39V/N53P/V55L Fyn SH3 domain (*19*) and is a structural mimic of I, as verified by backbone chemical shifts (Fig. 3A, inset, and fig. S11).

As expected, A39V/N53P/V55L/Δ(57-60) Fyn SH3 spontaneously forms aggregates at room temperature under NMR conditions, associated with a significant resonance intensity loss on the time scale of days (Fig. 3A, top). This process can be slowed down dramatically by lowering the temperature (Fig. 3A, top), indicating a sizable rate-limiting energy barrier. This suggests that formation of stable aggregates after an initial oligomerization step may require extensive structural rearrangements. The resulting aggregates have a curly fibrillar shape with a diameter of several nanometers in negative-stain transmission electron micrographs (Fig. 3, B and C, and fig. S12, A to C). They exhibit characteristic amyloid-like properties: For example, they have a high β-strand content, as established by circular dichroism (CD) spectra that feature a very negative minimum at 214 nm in contrast with CD spectra of the native state (Fig. 3D), and they bind to Congo red dye (Fig. 3E and fig. S13A), a stain commonly used to identify amyloid deposits (*1*–*3*). Similar fibrillar aggregates are also formed by the truncation mutants Δ(56-60) and Δ(57-60) Fyn SH3 in the wild-type background (figs. S12, D to H, and S13, C and D). The aggregation observed here is specific only to the truncation mutants that were rationally designed on the basis of the intermediate-state structure (Fig. 3A, top). None of the other mutants we have studied previously (*22*) show any evidence for spontaneous aggregation under similar conditions (Fig. 3A, bottom), not even when the unfolded state populations are as high or higher than for the truncated domains examined above. These results provide strong evidence that aggregation does not proceed via global unfolding, but rather involves a locally unfolded state accessed through thermal fluctuations.

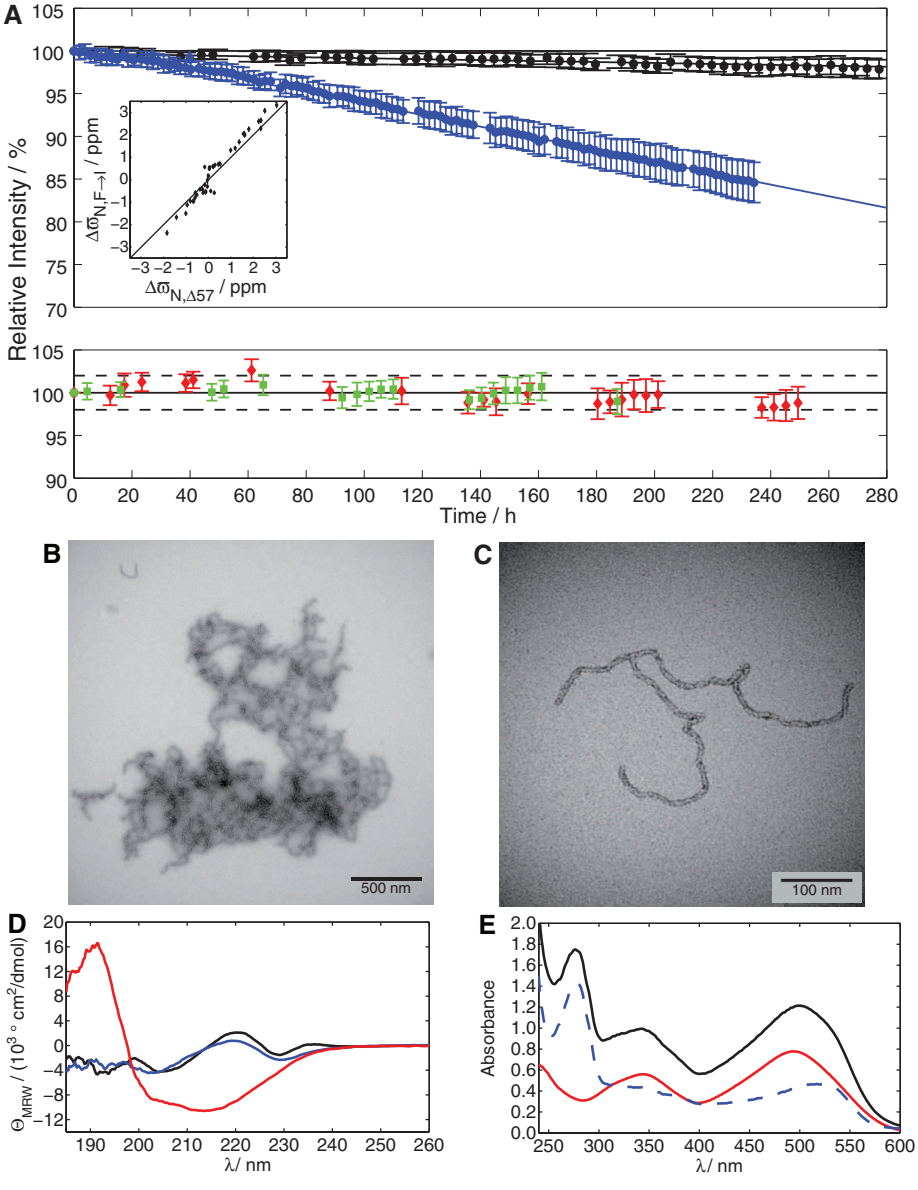


**Fig. 3.** Aggregation of the structural mimic of the folding intermediate. (**A**) Intensity loss of backbone amide resonances in a series of [$^1$H,$^{15}$N]–heteronuclear single quantum coherence spectroscopy experiments recorded on 1.0 mM [U-$^{13}$C,$^{15}$N] A39V/N53P/V55L/Δ(57-60) Fyn SH3 (top panel). Signal decreases of 0.16% per day at 15°C (black) and 1.6% per day at 20°C (blue) are quantified. The initial intensity (100%) is marked with a thick continuous horizontal line; sloped continuous lines are the result of linear regression. Monomeric A39V/N53P/V55L/Δ(57-60) Fyn SH3 predominantly adopts a structure mimicking the folding intermediate of the A39V/N53P/V55L Fyn SH3 domain [inset shows correlation between $^{15}$N chemical shifts of I (*y* axis) and A39V/N53P/V55L/Δ(57-60) Fyn SH3 (*x* axis); fig. S11], with populations of the unfolded state estimated to be 5.7% at 15°C or 8.3% at 20°C (fig. S10). ppm, parts per million. In contrast, no significant systematic intensity loss could be detected for other destabilizing mutants (bottom panel) such as 0.9 mM L3A/A39V/N53P/V55L Fyn SH3 (red diamonds) (*22*) or 0.9 mM F20L/A39V/N53P/V55L Fyn SH3 (green squares) (*22*) at 35°C, even though the relative and absolute populations of the unfolded state under these conditions are similar (*22*) to those in the top panel. A threshold of 2% (dashed horizontal lines) was estimated to indicate a statistically significant change under the experimental conditions. Intensities are plotted as mean ± SD (error bars) over all backbone amide resonances that could be quantified accurately. (**B** and **C**) Negative stain transmission electron micrographs of A39V/N53P/V55L/Δ(57-60) Fyn SH3 showing aggregates at two different magnifications, as indicated by the scale bars. (**D**) Overlay of the CD spectra of A39V/N53P/V55L (black), A39V/N53P/V55L/Δ(57-60) Fyn SH3 monomers (blue), and aggregates (red). λ, wavelength; $\Theta_{MRW}$, mean residue molar ellipticity. (**E**) Overlay of the absorption spectra of 20 μM Congo red in the absence (red) and presence (black) of A39V/N53P/V55L/Δ(57-60) Fyn SH3 aggregates. The difference spectrum (dashed blue curve) shows a clear hyperchromicity and red shift of the absorbance band around 500 nm.

Locally unfolded states that are separated from the N state by only low free-energy barriers play important roles in aggregation (*4*). In vivo or under physiological conditions, the structural fluctuations that access these locally destabilized conformers can be accelerated in a variety of ways, including by mutation, subunit dissociation, or cis-trans prolyl peptide bond isomerization (*4*, *11*, *12*). In vitro, fibril formation is often facilitated by destabilization through denaturants or acidic conditions, as in the case of the PI3K (*5*, *27*, *28*), α-spectrin (*29*, *30*), and Yes (*31*) SH3 domains. Interestingly, even under acidic conditions the aggregation propensity of an α-spectrin SH3 mutant was shown not to be correlated with overall stability (*29*), and thermodynamic measurements indicated that aggregation involved only partial unfolding (*30*), as observed for the Fyn SH3 domain studied here. In fact, many of the key residues and structural features that stabilize the A39V/N53P/V55L Fyn SH3 intermediate are also found in these other SH3 domains, suggesting that the mechanism of aggregation reported here is likely to be conserved. For example, Yes, N47A ($Asn^{47}$→$Ala^{47}$), α-spectrin, and PI3K SH3 domains all contain a hydrophobic side chain at the position corresponding to $Phe^4$ in Fyn SH3 (Fig. 1D), as well as a hydrogen bond corresponding to the one between $Ile^{28}$ HN and $Thr^2$ CO (fig. S14) in the I state of the A39V/N53P/V55L Fyn SH3 domain, which compensates for the loss of interactions involving $\beta_5$ (Fig. 1C). Furthermore, the carboxyl-terminal region of strand $\beta_5$ is unfolded in amyloid-like PI3K SH3 fibrils (*27*, *28*), providing strong evidence in support of the conclusion that the formation of native strand $\beta_5$ is critical in preventing aggregation during folding.

Our study demonstrates that key processes leading to amyloid fibril formation can be understood through detailed structural studies of the monomeric precursors populated under close to physiological conditions. The three-dimensional structure of the SH3 domain intermediate reported here, obtained under native equilibrium conditions, provides a compelling illustration of how incomplete folding can trigger misfolding and aggregation. In this process, key non-native interactions that normally lead to folding also cause transient exposure of an aggregation-prone region subject to aberrant intermolecular association. These results highlight the promise of RD NMR for increasing our understanding of the link between thermally accessible, low-populated folding intermediates and fibril formation, as well as for the identification of specific structural elements that can be targeted through rational design of therapeutics against protein misfolding diseases.

### References and Notes


1. C. M. Dobson, *Nature* **426**, 884 (2003).
2. D. J. Selkoe, *Nature* **426**, 900 (2003).
3. F. Chiti, C. M. Dobson, *Annu. Rev. Biochem.* **75**, 333 (2006).
4. F. Chiti, C. M. Dobson, *Nat. Chem. Biol.* **5**, 15 (2009).
5. M. Bucciantini *et al.*, *Nature* **416**, 507 (2002).
6. R. Tycko, *Annu. Rev. Phys. Chem.* **62**, 279 (2011).
7. V. N. Uversky, A. L. Fink, *Biochim. Biophys. Acta* **1698**, 131 (2004).
8. R. Kayed *et al.*, *Science* **300**, 486 (2003).
9. C. Haass, D. J. Selkoe, *Nat. Rev. Mol. Cell Biol.* **8**, 101 (2007).
10. R. Roychaudhuri, M. Yang, M. M. Hoshi, D. B. Teplow, *J. Biol. Chem.* **284**, 4749 (2009).
11. T. R. Jahn, M. J. Parker, S. W. Homans, S. E. Radford, *Nat. Struct. Mol. Biol.* **13**, 195 (2006).
12. C. M. Eakin, A. J. Berman, A. D. Miranker, *Nat. Struct. Mol. Biol.* **13**, 202 (2006).
13. A. Fersht, *Structure and Mechanism in Protein Science* (Freeman, New York, 1999).
14. A. P. Capaldi, S. E. Radford, *Curr. Opin. Struct. Biol.* **8**, 86 (1998).
15. A. G. Palmer 3rd, *Chem. Rev.* **104**, 3623 (2004).
16. P. Neudecker, P. Lundström, L. E. Kay, *Biophys. J.* **96**, 2045 (2009).
17. P. Vallurupalli, D. F. Hansen, L. E. Kay, *Proc. Natl. Acad. Sci. U.S.A.* **105**, 11766 (2008).
18. D. M. Korzhnev, T. L. Religa, W. Banachewicz, A. R. Fersht, L. E. Kay, *Science* **329**, 1312 (2010).
19. P. Neudecker *et al.*, *J. Mol. Biol.* **363**, 958 (2006).
20. A. Zarrine-Afsar *et al.*, *Proc. Natl. Acad. Sci. U.S.A.* **105**, 9999 (2008).
21. D. S. Riddle *et al.*, *Nat. Struct. Biol.* **6**, 1016 (1999).
22. P. Neudecker, A. Zarrine-Afsar, A. R. Davidson, L. E. Kay, *Proc. Natl. Acad. Sci. U.S.A.* **104**, 15717 (2007).
23. Y. Bai, *Chem. Rev.* **106**, 1757 (2006).
24. P. Robustelli, K. Kohlhoff, A. Cavalli, M. Vendruscolo, *Structure* **18**, 923 (2010).
25. G. G. Tartaglia *et al.*, *J. Mol. Biol.* **380**, 425 (2008).
26. J. S. Richardson, D. C. Richardson, *Proc. Natl. Acad. Sci. U.S.A.* **99**, 2754 (2002).
27. N. Carulla *et al.*, *Proc. Natl. Acad. Sci. U.S.A.* **106**, 7828 (2009).
28. M. J. Bayro *et al.*, *Biochemistry* **49**, 7474 (2010).
29. L. Varela, B. Morel, A. I. Azuaga, F. Conejero-Lara, *FEBS Lett.* **583**, 801 (2009).
30. B. Morel, L. Varela, A. I. Azuaga, F. Conejero-Lara, *Biophys. J.* **99**, 3801 (2010).
31. J. M. Martín-García, I. Luque, P. L. Mateo, J. Ruiz-Sanz, A. Cámara-Artigas, *FEBS Lett.* **581**, 1701 (2007).
32. S. Pechmann, E. D. Levy, G. G. Tartaglia, M. Vendruscolo, *Proc. Natl. Acad. Sci. U.S.A.* **106**, 10159 (2009).


**Acknowledgments:** We thank J. Forman-Kay and A. Davidson for providing laboratory space. S.S. and L.E.K. hold Canada Research Chairs in Biochemistry. P.R. was funded by a Gates Cambridge Scholarship and an NSF Graduate Research Fellowship, and P.W. is funded by a Natural Sciences and Engineering Research Council of Canada (NSERC) Canada Graduate Scholarship. This work was supported by grants from the NSERC and the Canadian Institutes of Health Research (L.E.K). The ensembles of 10 structures each representing the A39V/N53P/V55L Fyn SH3 domain native state from $Ser^1$ to $Asp^{59}$ and the folding intermediate from $Ser^1$ to $Ala^{56}$ have been deposited with the Protein Data Bank (accession codes 2LP5 and 2L2P, respectively).

### Supplementary Materials

www.sciencemag.org/cgi/content/full/336/6079/362/DC1
Materials and Methods
Figs. S1 to S14
Tables S1 and S2
References (*33*–*111*)

20 September 2011; accepted 9 February 2012
10.1126/science.1214203

# New Products: Mass Spectrometry

## ICP-MS SYSTEM

The new iCAP Q is an ICP-MS system featuring world-class performance and increased throughput to help laboratories cut analysis times by up to 50% when compared to the XSERIES 2 ICP-MS, the model it replaces. The unique ion-focusing system in the iCAP Q delivers best-in-class signal-to-noise performance, and the proprietary QCell with flatapole technology for low mass cut-off offers unparalleled interference removal for complete confidence in results. New Qtegra software fully automates the system for one-click setup, which enables users to go from standby to performance-qualified analysis with the push of a button. To ensure nearly continuous uptime, the iCAP Q is designed to be easy to service. Access to the skimmer and sampler cones, the extraction lenses, and the torch assembly make routine maintenance fast and easy. The iCAP Q is ideal for environmental, metals, clinical research, food safety, semiconductor, and geochemical laboratories conducting both routine and complex elemental analyses.

**Thermo Fisher Scientific**

**For info: 800-532-4752 | www.thermoscientific.com/dramatic**

## MASS SPECTROMETER

The TripleQuad 4500 System is a new triple quadrupole system that delivers 10x better sensitivity over competitive triple quadrupole systems in the same mid-level class. The new 4500 system is designed to be the new 'workhorse' mass spectrometer with industry-leading ruggedness. The 4500 system has the option of QTRAP technology, which is recognized as delivering the world's leading solution for simultaneous quantitation and library searching. The proprietary QTRAP increases full-scan sensitivity by 100x over basic triple quadrupoles by incorporating the world's most sensitive Linear Accelerator Trap, providing unmatched levels of confidence in results for screening applications. To simplify the adoption of this next generation of LC/MS/MS technology, new bundled solution packages called Accelerated Lab Integration Packages are offered. These packages consist of not only the mass spectrometer, but also the standards, software, training, validation services, and a liquid chromatography (LC) system, including the new Eksigent ekspert ultra 100 and 100-XL systems.

**AB Sciex**

**For info: 877-740-2129 | www.absciex.com**

## HIGH-SENSITIVITY ION SOURCE

The high-sensitivity ionBooster is an ion source designed to meet the increasing demands for sensitivity enhancements in environmental analysis, food testing, and forensics. Sensitivity gains of 5x to 100x for many compounds extend the quantitative capability of modern accurate-mass MS systems to the sensitivity range of high-end triple-quadrupole instruments. The ion source enhances sensitivity and lowers detection limits by delivering more efficient ionization across a wide range of applications. Inside the ionBooster, an electrospray is maintained at an elevated vaporizing temperature to enable enhanced desolvation of the analyte ions, even at high eluent flow rates in UHPLC separations with sharp chromatographic peaks. The exact response with the ionBooster depends upon the type of compound and its specific chemical characteristics and thermal properties. In combination with a maXis impact, a UHR-TOF system, accurate-mass data is obtained across the full mass range, enabling qualitative analysis of unknowns, analysis of multiple other drugs or target compounds, and retrospective screening of data for any target formula.

**Bruker**

**For info: 510-683-4300 | www.bdal.com**

## ECONOMY GC-MS SYSTEM

The GCMSQP2010 SE is an advanced standard gas chromatograph mass spectrometer that combines the benefits of economy, simple operation, and enhanced performance. The GCMS-QP2010 SE features stable mass spectra that achieve high sensitivity and stability. The ion optical system is optimized with a high-performance quadrupole mass filter and Optdesign simulation program to provide high-quality mass spectra. Fully automated MS tuning allows users to optimize parameters easily and constantly to ensure stable mass spectra can always be obtained. Enhanced maximum column flow up to 4 mL/minute gives users the ability to select from a variety of columns so that productivity and sample throughput can be dramatically increased. An optional direct injection probe lets users easily obtain a mass spectrum when analyzing materials that don't lend themselves to chromatography. It can also offer easy qualitative analysis without setting analytical parameters of the gas chromatograph.

**Shimadzu Scientific Instruments**

**For info: 800-477-1227 | www.ssi.shimadzu.com**

## COMPACT MASS SPECTROMETER

The Expression Compact Mass Spectrometer (CMS) is designed for the discovery research and process development synthetic organic chemistry market. Compact enough to operate in fume hoods and space-restricted laboratories, chemists can have direct access to identify, monitor, and confirm compounds rapidly as they are created in the reactor. Moreover, the personal single quadrupole mass spectrometer allows for rapid compound confirmation in normal phase chromatography fractions. Traditionally, chemists initiate a multihour reaction and periodically withdraw samples for analysis in an open access mass spectrometry lab. The remote analysis takes hours, decreasing the usefulness of the information and building workflow inefficiencies. Additionally, large numbers of normal phase purification fractions are generated and add to the central lab burden, further slowing vital feedback. The combination of a small footprint, critical design features, and an intuitive software package permits operation within a fume hood or next to existing bench instrumentation, allowing users access to fast answers.

**Advion**

**For info: 607-379-4565 | www.advion.com**

Electronically submit your new product description or product literature information! Go to **www.sciencemag.org/products/newproducts.dtl** for more information.

Newly offered instrumentation, apparatus, and laboratory materials of interest to researchers in all disciplines in academic, industrial, and governmental organizations are featured in this space. Emphasis is given to purpose, chief characteristics, and availability of products and materials. Endorsement by *Science* or AAAS of any products or materials mentioned is not implied. Additional information may be obtained from the manufacturer or supplier.

NEW ENGLAND BioLabs® Inc.
*enabling technologies in the life sciences*

# Mix it up.

## RE-Mix™ Restriction Enzyme Master Mixes

Restriction enzyme digests are now even easier! The same high quality restriction enzymes that you have come to trust from New England Biolabs are now available in master mix format, including enzyme, buffer and loading dye; simply add your DNA and digest.

With RE-Mix Master Mixes take advantage of:

- Simplified and shortened protocols
- Fast digestion in 15 minutes (Time-Saver qualified)
- High product quality with reproducible results

RE-Mix Master Mixes – just add your DNA and mix

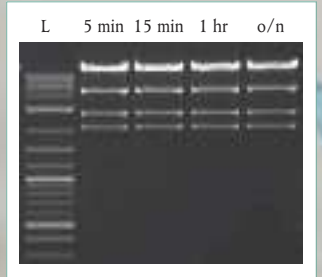


*pXba DNA was digested with EcoRV-HF™ RE-Mix™ according to the recommended protocol. Lane L is the TriDye™ 2-Log DNA Ladder (NEB #N3270). The same results are obtained whether incubated for 5–15 minutes, 1 hour or overnight.*

GTAGC CTT
TCUTGA ATT
AGTIT G C
TTT
GTTOUT T
TAC TACG

To experience the new restriction enzyme challenge from NEB, visit **www.NEBcutitout.com**

For more information, visit **www.NEBREMIX.com**

*Blue-footed Booby (Sula nebouxii)*
*© Tui De Roy*

# Else Kröner Fresenius Immunology Award
## Call for Candidates

In commemoration of the 25th anniversary of the early death of Else Kröner, June 5, 2013, the Else Kröner-Fresenius-Stiftung (Foundation) intends to award world-wide pioneering discoveries in the field of medical immunology and to facilitate future research by the winning individual or team.

The award - At least 500,000 € will be awarded to the winner(s) in person. Up to 3,500,000 € will be awarded for future research.

The candidates must be fully active researchers, who have made groundbreaking discoveries in medical immunology. They need to be in the position to accomplish the research intended in the next 3-5 years.

Candidate nomination - Candidates will be proposed by IUIS member associations. Self-nominations need to be accompanied by two letters of recommendation from at least two internationally leading researchers in immunology from two different countries.

Deadline for nominations: July 4, 2012. For further details please see www.ekfs.de and www.iuis-online.org.

ELSE KRÖNER-FRESENIUS-STIFTUNG

IUIS

Be the next winner!

**2011 Winner**
Dr. Tiago Branco
Postdoctoral
Research Fellow
University College
London

Get recognized!
**US$ 25,000 Prize**

Deadline for entries:
**June 15, 2012**

It´s easy to apply! Learn more at:
**www.eppendorf.com/prize**

eppendorf & Science PRIZE FOR NEUROBIOLOGY

# Eppendorf & Science Prize for Neurobiology

Congratulations to Dr. Tiago Branco on winning the 2011 Eppendorf & *Science* Prize for his studies on how dendrites discriminate temporal input sequences and apply different integration rules depending on input location. The results of Dr. Branco's research provide insight on how the brain performs computations, and suggest that even single neurons can solve complex computational tasks.

**You could be the 11th winner of this award.**
The annual Eppendorf & *Science* Prize for Neurobiology honors young scientists for their outstanding contributions to neurobiological research based on methods of molecular and cell biology. The winner and finalists are selected by a committee of independent scientists, chaired by *Science's* Senior Editor, Dr. Peter Stern.

To be eligible, you must be 35 years of age or younger. If you're selected as this year's winner, you will receive US$ 25,000, have your work published in *Science* and be invited to visit Eppendorf in Hamburg, Germany. Past winners and finalists have come from as far a field as China, Chile, India and New Zealand.

**Yes, it can happen to you. Enter your research now!**

eppendorf
*In touch with life*

Science
AAAS

Kurstin Roe Photography

**LOCATION:** Jackson Park Health Club
**ARTICLE:** *An Electronic Second Skin*
**DATE:** Sep 21, 7:43am

**LOCATION:** University Faculty Lounge
**ARTICLE:** *The Visual Impact of Gossip*
**DATE:** Sep 21, 4:22pm

**LOCATION:** Gyro King
**ARTICLE:** *Cavemen Craved Carbs, Too*
**DATE:** Sep 21, 1:13pm

**LOCATION:** Hemlock Bar
**ARTICLE:** *Quantum Simulation of Frustrated Classical Magnetism in Triangular Optical Lattices*
**DATE:** Sep 21, 9:21pm

**LOCATION:** Bed
**ARTICLE:** *Consciousness: What, How and Why*
**DATE:** Sep 21, 10:56pm

# A new way to look at science

The new *Science* Reader app for iPad® from AAAS puts *Science* in your hands, wherever you go. Read abstracts, career advice, and highlights from our newest journals, *Science Signaling* and *Science Translational Medicine*. Plus, AAAS members can access full text articles from *Science*. Visit iTunes App Store℠ or content.aaas.org/ipad for details.

Available on the App Store

Science
AAAS

# New Products: Mass Spectrometry

## ICP-MS SYSTEM

The new iCAP Q is an ICP-MS system featuring world-class performance and increased throughput to help laboratories cut analysis times by up to 50% when compared to the XSERIES 2 ICP-MS, the model it replaces. The unique ion-focusing system in the iCAP Q delivers best-in-class signal-to-noise performance, and the proprietary QCell with flatapole technology for low mass cut-off offers unparalleled interference removal for complete confidence in results. New Qtegra software fully automates the system for one-click setup, which enables users to go from standby to performance-qualified analysis with the push of a button. To ensure nearly continuous uptime, the iCAP Q is designed to be easy to service. Access to the skimmer and sampler cones, the extraction lenses, and the torch assembly make routine maintenance fast and easy. The iCAP Q is ideal for environmental, metals, clinical research, food safety, semiconductor, and geochemical laboratories conducting both routine and complex elemental analyses.

**Thermo Fisher Scientific**

**For info: 800-532-4752 | www.thermoscientific.com/dramatic**

## MASS SPECTROMETER

The TripleQuad 4500 System is a new triple quadrupole system that delivers 10x better sensitivity over competitive triple quadrupole systems in the same mid-level class. The new 4500 system is designed to be the new 'workhorse' mass spectrometer with industry-leading ruggedness. The 4500 system has the option of QTRAP technology, which is recognized as delivering the world's leading solution for simultaneous quantitation and library searching. The proprietary QTRAP increases full-scan sensitivity by 100x over basic triple quadrupoles by incorporating the world's most sensitive Linear Accelerator Trap, providing unmatched levels of confidence in results for screening applications. To simplify the adoption of this next generation of LC/MS/MS technology, new bundled solution packages called Accelerated Lab Integration Packages are offered. These packages consist of not only the mass spectrometer, but also the standards, software, training, validation services, and a liquid chromatography (LC) system, including the new Eksigent ekspert ultra 100 and 100-XL systems.

**AB Sciex**

**For info: 877-740-2129 | www.absciex.com**

## HIGH-SENSITIVITY ION SOURCE

The high-sensitivity ionBooster is an ion source designed to meet the increasing demands for sensitivity enhancements in environmental analysis, food testing, and forensics. Sensitivity gains of 5x to 100x for many compounds extend the quantitative capability of modern accurate-mass MS systems to the sensitivity range of high-end triple-quadrupole instruments. The ion source enhances sensitivity and lowers detection limits by delivering more efficient ionization across a wide range of applications. Inside the ionBooster, an electrospray is maintained at an elevated vaporizing temperature to enable enhanced desolvation of the analyte ions, even at high eluent flow rates in UHPLC separations with sharp chromatographic peaks. The exact response with the ionBooster depends upon the type of compound and its specific chemical characteristics and thermal properties. In combination with a maXis impact, a UHR-TOF system, accurate-mass data is obtained across the full mass range, enabling qualitative analysis of unknowns, analysis of multiple other drugs or target compounds, and retrospective screening of data for any target formula.

**Bruker**

**For info: 510-683-4300 | www.bdal.com**

## ECONOMY GC-MS SYSTEM

The GCMSQP2010 SE is an advanced standard gas chromatograph mass spectrometer that combines the benefits of economy, simple operation, and enhanced performance. The GCMS-QP2010 SE features stable mass spectra that achieve high sensitivity and stability. The ion optical system is optimized with a high-performance quadrupole mass filter and Optdesign simulation program to provide high-quality mass spectra. Fully automated MS tuning allows users to optimize parameters easily and constantly to ensure stable mass spectra can always be obtained. Enhanced maximum column flow up to 4 mL/minute gives users the ability to select from a variety of columns so that productivity and sample throughput can be dramatically increased. An optional direct injection probe lets users easily obtain a mass spectrum when analyzing materials that don't lend themselves to chromatography. It can also offer easy qualitative analysis without setting analytical parameters of the gas chromatograph.

**Shimadzu Scientific Instruments**

**For info: 800-477-1227 | www.ssi.shimadzu.com**

## COMPACT MASS SPECTROMETER

The Expression Compact Mass Spectrometer (CMS) is designed for the discovery research and process development synthetic organic chemistry market. Compact enough to operate in fume hoods and space-restricted laboratories, chemists can have direct access to identify, monitor, and confirm compounds rapidly as they are created in the reactor. Moreover, the personal single quadrupole mass spectrometer allows for rapid compound confirmation in normal phase chromatography fractions. Traditionally, chemists initiate a multihour reaction and periodically withdraw samples for analysis in an open access mass spectrometry lab. The remote analysis takes hours, decreasing the usefulness of the information and building workflow inefficiencies. Additionally, large numbers of normal phase purification fractions are generated and add to the central lab burden, further slowing vital feedback. The combination of a small footprint, critical design features, and an intuitive software package permits operation within a fume hood or next to existing bench instrumentation, allowing users access to fast answers.

**Advion**

**For info: 607-379-4565 | www.advion.com**

Electronically submit your new product description or product literature information! Go to **www.sciencemag.org/products/newproducts.dtl** for more information.

Newly offered instrumentation, apparatus, and laboratory materials of interest to researchers in all disciplines in academic, industrial, and governmental organizations are featured in this space. Emphasis is given to purpose, chief characteristics, and availability of products and materials. Endorsement by *Science* or AAAS of any products or materials mentioned is not implied. Additional information may be obtained from the manufacturer or supplier.

# 44

## best practices for overcoming skepticism post-Climategate.

One more data point on why you should spend more time at membercentral.aaas.org. There you can enjoy webinars, videos, blogs, discounts, and downloads geared for people who prefer content based on empirical evidence.

membercentral.aaas.org

AAAS MEMBERCENTRAL

# FROM DISCOVERY TO RECOVERY

## Step up your career at Queen's

At Queen's, we are building on our substantial reputation with a focussed and ambitious plan to create an internationally recognised School and Institute of Health Sciences that will have a global impact on medical, dental and biomedical research and education.

The School's aim is to drive discovery, innovation, the development of novel targeted therapies and to create a unique fusion of clinical and basic science research, underpinned by clinical and scientific leaders of national and international repute. Over the last eighteen months our on-going campaign has already demonstrated success with the appointment of a significant number of international Chairs in a range of clinical and scientific disciplines and we have also recently launched a separate campaign to recruit up to 20 clinical academic staff in a range of disciplines.

To further support this vision we are now seeking to appoint up to 15 outstanding and committed non-clinical academic staff at Lecturer, Senior Lecturer, Reader/ Professor level who have the expertise, motivation and know-how to contribute to the development of a global School of Medicine, Dentistry and Biomedical Sciences. We are seeking candidates in the following disciplines but will also consider applicants in other scientific disciplines that align with the School's strategic priorities.

- **Statistics and Bioinformatics**
- **Medical and Bio Imaging**
- **Microbiology**
- **Genetics/Epigenetics**
- **Immunology/Inflammation**
- **Pharmacology**
- **Stem Cell Biology**
- **DNA Damage**
- **Angiogenesis**
- **Health Economics**
- **Protein Modification**
- **Health Care Education Research** (encompassing all aspects of education-related research)

Discover a career for yourself at Queen's and visit **qub.ac.uk/jobs**

Queen's University Belfast

SCHOOL OF
**Medicine, Dentistry and Biomedical Sciences**

WE ARE QUEEN'S UNIVERSITY BELFAST
We are exceptional

RUSSELL INTERNATIONAL EXCELLENCE GROUP

## Cancer Genetics and Genomics Senior Faculty Position NCI Designated Cancer Center

The Hollings Cancer Center and The Medical University of South Carolina (MUSC) announce an exciting recruitment opportunity for faculty at the Associate Professor or Professor level to carry out independent research in Cancer Genetics or Genomics. Candidates should have a national reputation in studying cancer genetics or genomics, demonstrated ability to carry out translational and/or basic research, and a solid record of collaborative, peer-reviewed publications and research funding. Faculty will be located in state-of-the-art laboratories in a new building with outstanding resources and research support available.

A National Cancer Institute designated cancer center, the Hollings Cancer Center has a strong culture of promoting basic and translational research. MUSC holds an NIH-funded Clinical and Translational Science Award. There are multiple complementary shared resources in place, including a Drug Discovery Screening Core, a Drug Metabolism and Clinical Pharmacology Core, Translational Research Laboratory, and a Proteomics facility.

Located on the Atlantic coast of South Carolina, Charleston boasts one of the nation's most historic and picturesque downtown areas, beautiful beaches, outstanding cuisine, and international cultural events such as the Spoleto Festival USA.

Interested researchers should send their CV and a summary of future research plans to:

**Dr. Andrew Kraft or Dr. Stephen Ethier**
**Hollings Cancer Center**
**Medical University of South Carolina**
**PO Box 250955**
**Charleston, SC 29425**
**campbetb@musc.edu**

And/or apply on-line at:
**www.jobs.musc.edu/applicants/Central?quickFind=189282**

*MUSC is an Equal Opportunity Employer, promoting workplace diversity.*

## NORTHWESTERN UNIVERSITY

The Department of Cell and Molecular Biology at the Feinberg School of Medicine, Northwestern University, seeks to recruit full-time tenure-track positions at the rank of Assistant Professor, Associate Professor, or Professor to conduct research in the areas of high resolution cellular imaging including optical and electron microscopy. Technical expertise can include single molecule detection, quantitative analysis of cellular dynamics and electron tomography. Scientific areas of interest to the Department include the structure and molecular dynamics of the cytoskeleton, signal transduction, cell adhesion, nuclear architecture, and the development of novel biosensors. PhD or MD/PhD is required. Start date is open and salary will be commensurate with experience.

Applications, including curriculum vitae, a statement of research interests, and three letters of recommendation should be sent electronically to the **CMB Search Committee,** care of **cmbsearch@northwestern.edu**.

**Dr. Vladimir Gelfand**
**Professor, Department of Cell and Molecular Biology**
**Northwestern University**
**Feinberg School of Medicine**
**Ward 8-140**
**303 E. Chicago Avenue**
**Chicago, IL 60611**

The Application Review process begins May 15, 2012 and the closing date is **July 15, 2012**.

*Northwestern University is an Affirmative Action/Equal Opportunity Employer. Hiring is contingent upon eligibility to work in the United States. Women and minorities are encouraged to apply.*

## UC DAVIS

### TENURE TRACK POSITION – ASSISTANT PROFESSOR Energy Efficiency Department of Food Science and Technology and Energy Efficiency Center

The Department of Food Science and Technology, in collaboration with the Energy Efficiency Center is seeking to fill a faculty position. We are interested in individuals who have or can establish a strong extramurally funded research program in an advanced contemporary area of energy efficiency in food processing. The areas of expertise we seek are in the broad area of food processing, and include physical chemistry, chemistry, biochemistry, or engineering, processing or microbiology used to investigate (i) minimizing water usage; (ii) decreasing energy usage; or (iii) applying technologies central to improving energy efficiency. Candidates are expected to have a PhD (or equivalent) and demonstrated ability in engineering, food processing, chemistry, biochemistry, food science or a related discipline. Postdoctoral experience is highly desirable. Selection will be based in part on a record of research publications in peer-reviewed journals, and the ability to obtain extramural funding. The specific research program will depend upon the expertise and interests of the candidate. The successful applicant will be expected to develop an independent, internationally recognized research, teach at the undergraduate and graduate level, and supervise graduate student research.

Applicants should submit online at **https://secure.caes.ucdavis.edu/Recruitment** a letter of application, curriculum vitae (including list of publications), a statement of research, a separate statement describing teaching interests and background; reprints of three publications; academic transcripts and names, addresses including e-mail, and telephone numbers of three references. The position is open until filled; but to assure full consideration, completed online applications should be submitted no later than **June 1, 2012**, for a targeted start date of September 1, 2012.

*UC Davis is an Affirmative Action/Equal Employment Opportunity Employer and is dedicated to recruiting a diverse faculty community. We welcome all qualified applicants to apply, including women, minorities, individuals with disabilities and veterans.*

## Homeland Security

### KEEP AMERICA SAFE THROUGH SCIENCE AND TECHNOLOGY!

### Director, Chemical/Biological Defense Division

The Department of Homeland Security seeks an Executive who influences and develops policy regarding chemical or biological programs, and countermeasures that protect against biological and chemical attacks for the position of Director, Chemical/Biological Defense Division (CBD). This is a Senior Executive Service (SES) position, located in the Science and Technology Directorate (S&T), in the Homeland Security Advanced Research Projects Agency (HSARPA).

The CBD Director administers a $100M Research & Development (R&D) portfolio to provide novel solutions aimed towards protecting the country from a Weapons of Mass Destruction attack. The Director is responsible for the management and leadership of the Chemical and Biological program, stewardship of assigned resources, and execution of the Division's programs including the cost, schedule, technical performance and deliverables associated with those programs.

The successful candidate will creatively leverage resources and partnerships to develop the next-generation architecture for chemical and biological defense, including bio-surveillance, point-of-care diagnostics, and real-time detection. In close cooperation with the White House and Executive branch agencies, the Director actively shapes policies and plans for detection, response and mitigation from a chemical or biological attack. You will find additional qualifications and responsibilities at **www.usajobs.gov**. The vacancy announcement number is **CHCO-12-016-DHS-645716**. Submit your application by **May 21, 2012**.

### Technical Program Managers needed in all Disciplines!

HSARPA is also seeking Program Managers and subject matter experts in the following areas of expertise: Cyber Security, Borders and Maritime Security, Explosives, Human Factors and Infrastructure Protection & Disaster Management. If interested in a career opportunity in one of these areas of expertise, please send your resume/qualifications to **STExecutiveResource@dhs.gov**.

For more information about S&T can be found here: **http://www.dhs.gov/scienceandtechnology**.

ETH

Eidgenössische Technische Hochschule Zürich
Swiss Federal Institute of Technology Zurich

# Professor of Multicellular Systems Bioengineering

The Department of Biosystems Science and Engineering (www.bsse.ethz.ch) at ETH Zurich invites applications for the above-mentioned professorship. The Department is located in Basel, in the heart of the BioValley area, providing excellent opportunities for collaboration within this strong life science research community at the academic, clinical and industrial levels. Its main research focus is the understanding and engineering of biological systems for medical or chemical purposes, which generates numerous opportunities for interaction. Collaborations with the SystemsX.ch community (www.systemsx.ch), the Swiss initiative in Systems Biology, are encouraged. The educational goal of the Department is to teach at the undergraduate and graduate level by integrating expertise and knowledge from biologists, chemists, physicists, engineers, computer scientists and mathematicians along with industrial collaborators.

The Department is looking for an outstanding candidate experimentally working on the biology and control of multicellular systems. He or she should have a strong background in molecular cell biology, genetics, tissue development and regeneration and be interested in molecular bioengineering, preferably with cells in a context of complex cell biological systems. The ideal candidate should have demonstrated success in obtaining support for independent research projects and a strong publication record reflecting innovative, interdisciplinary and collaborative approaches to identify and solve important problems of multicellular systems. The new professor will be expected to teach undergraduate level courses (German or English) and graduate level courses (English).

Please apply online at **www.facultyaffairs.ethz.ch**. Your application should include your curriculum vitae, a list of publications, and statements on future teaching and research activities. The letter of application should be addressed **to the President of ETH Zurich, Prof. Dr. Ralph Eichler. The closing date for applications is 30 June 2012**. ETH Zurich is an equal opportunity and affirmative action employer. In order to increase the number of women in leading academic positions, we specifically encourage women to apply. ETH Zurich is further responsive to the needs of dual career couples and qualifies as a family friendly employer.

ETH

Eidgenössische Technische Hochschule Zürich
Swiss Federal Institute of Technology Zurich

# Professor of Biological Systems Theory (Optimisation)

The Department of Biosystems Science and Engineering (www.bsse.ethz.ch) at ETH Zurich invites applications for the above-mentioned professorship at the Associate or Full Professor level. The Department is located in Basel, in the heart of the BioValley area, providing excellent opportunities for collaboration within this strong life science research community at the academic, clinical, and pharmaceutical industry level. The new Professor is required to develop a strong and visible research programme in the area of optimisation for the analysis, design and control of biological systems. Research topics include, but are not limited to, mathematical and computational optimisation techniques for experimental design, model building, systems identification, and rational design of biological systems at multiple scales.

The successful candidate holds a PhD in Mathematics, Engineering, Computer Science, or related disciplines and has an excellent track record in the theory of biological systems and the development of optimisation methods for the analysis and design of biological systems. The ideal applicant should have demonstrated success in obtaining support for independent research projects and a strong publication record reflecting innovative, interdisciplinary, and collaborative approaches to important problems in biology or medicine. Commitment to teaching and a demonstrated ability to lead a research group are required. The new Professor will be expected to teach undergraduate level courses (German or English) and graduate level courses (English).

Please apply online at **www.facultyaffairs.ethz.ch**. Your application should include your curriculum vitae, a list of publications, and statements on future teaching and research activities. The letter of application should be addressed **to the President of ETH Zurich, Prof. Dr. Ralph Eichler. The closing date for applications is 30 June 2012**. ETH Zurich is an equal opportunity and affirmative action employer. In order to increase the number of women in leading academic positions, we specifically encourage women to apply. ETH Zurich is further responsive to the needs of dual career couples and qualifies as a family friendly employer.

# Science

# Biotech & Pharma

**Special Career Feature: June 8**

Reserve your ad by May 22 to guarantee space.*

*Ads accepted until June 4 if space is still available.



ScienceCareers.org

The industry landscape is constantly evolving. Mergers and acquisitions can mean big changes for companies and their employees. *Science*'s June 8 career feature examines the opportunities and challenges that come along with the merging of company cultures and workforces.

Whether you need to recruit technicians or a chief scientist, your *Science* sales representative can customize a solution for advertising in this issue that helps you benefit from:

- 700,000 readers worldwide who rely on *Science* to keep them informed about industry changes and related career issues
- Bonus distribution to the American Society for Microbiology Meeting in San Francisco, CA
- Bonus distribution to the BIO International Convention as well as the BIO Career Fair, in Boston, MA.

Customized packages to correspond with this special feature are available

**To Book Your Ad:**

E-mail:
advertise@sciencecareers.org

Or telephone us:

**US:** 202-326-6582

**Europe/RoW:** +44 (0) 1223 326500

**Japan:** +81-6-6627-9250

**China/Korea/Singapore/Taiwan/Thailand:** +86-1367-1015-294

For recruitment in science, there's only one Science

Produced by the *Science*/AAAS Custom Publishing Office

Yolande **OBADIA**, Présidente

Didier **RAOULT**, Directeur

**Membres Fondateurs:**

Assistance Publique-Hôpitaux de Marseille
C.N.R.S.
Établissement Français du Sang
INSERM
Institut Mérieux
IRD
Université de la Méditerranée, Aix-Marseille 2

**Partenaires:**

CERBA European Lab
CHU de Montpellier
CHU de Nice
CHU Nîmes
Crédit Coopératif
Consortium Médi-Handtrace
EHESP
GALDERMA
I2a
IRT Lyon
Qiagen
Sanofi
Université de Montpellier 1
Université de Montpellier 2
Université de Sophia Antipolis

# University Hospital Institute

## For Infectious and Tropical Diseases

Marseille, France

MÉDITERRANÉE INFECTION

**SEEKING INVESTIGATORS**
**OFFERING STUDENT POSITIONS**
**PROVIDING GRANTS**

The University Hospital Institute (IHU) "Méditerranée Infection" in Marseille is a 600-personnel medical institute (MD, PhD, pharmacists, biology researchers, engineers and technicians, and HCW) working on infectious diseases. It includes the largest diagnostic and research microbiology laboratory in France. Providing one of the largest genomic, transcriptomic and proteomic platform, it is one leader within the fields of microbiology, infectious diseases and emerging infections; it is also a key organ within the European surveillance network for imported infectious diseases. *See additional information on* **www.ifr48.com**

1. We are seeking three outstanding tenure-track investigators to work in the areas of **TROPICAL PARASITOLOGY, MEDICAL MYCOLOGY and EPIDEMIOLOGY OF CHRONIC INFECTIOUS DISEASES** (associated to full level professors). 4-year contracts will be signed with the possibility to integrate permanent positions within the IHU (involving both University and Hospital responsibilities). *To apply please send a curriculum vitae, along with a bibliography and an outline of your proposed research program (no more than two pages) via email to* **didier.raoult@gmail.com**.
2. We are also providing **10** 2-year **POST-DOC** positions and **10** 3-year **PHD** positions for students. Applicants **COMING FROM THE SOUTH** are particularly welcome. *To apply please connect to* **www.infectiopolesud.com**, *choose your topic and follow the instructions.*
3. The IHU is also providing **GRANTS FOR SCIENTISTS** with French tenure (IRD, INSERM, CNRS) in the field of infectious diseases to move and join us. *To apply please send a curriculum vitae along with a covering letter to* **jean-louis.mege@univ-amu.fr**.

# Get a Career Plan that Works.

An exceptional career requires insightful planning and management. That's where *Science* Careers comes in. From job search to career enhancement, *Science* Careers has the tools and resources to help you achieve your goals. Get yourself on the right track today and get a real career plan that works. Visit **ScienceCareers.org**.

Science Careers
From the journal *Science* AAAS

ScienceCareers.org

# Royal Society Research Professorship

The Royal Society's most prestigious senior funding scheme is now open for applications. The Royal Society Research Professorships provide long term support to world-class scientists, releasing them from teaching and administration to enable them to focus on research.

The scheme provides a substantial contribution to salary, which can be supplemented at the discretion of the host organisation; a one-off start-up grant of up to £35,000; and research expenses of up to £16,000 per academic year. Funding is available for five years, with the opportunity for renewal for a further five years.

These prestigious posts enable individuals of proven ability and achievement to undertake independent, original research at a UK institution. Former Research Professors include Presidents of the Royal Society and Nobel Laureates.

Several Royal Society Research Professorships are available. The number of awards made will be determined by the quality of applications received. The Professorships may be awarded in any field across the natural sciences but the following are restricted to specific areas:

- The Royal Society Wolfson Research Professorship in Physics or Chemistry at the interface with Biology
- The Royal Society GSK Research Professorship in Molecular aspects of Medicine
- The Royal Society Noreen Murray Research Professorship in Neurobiology

The Professorships are available to scientists of any nationality and applications are particularly welcomed from scientists currently resident outside the UK.

**Closing date: 26 June 2012**

To find out more about this prestigious scheme visit: **royalsociety.org/grants/schemes**
or email **seniorfellowships@royalsociety.org**

Registered Charity No 207043

THE ROYAL SOCIETY


# FACTS & FICTION

## Careers in Industry and Academia

Trying to figure out the next step in your career? Join us for a roundtable discussion that will look at facts and fiction surrounding academic and industry career options for PhD-level scientists. Get some nuts and bolts advice on how to research career options, what questions to ask, and how to best prepare for various careers.

- Do industry and academic careers require different skill sets?
- Do industry jobs have better compensation? Less autonomy?
- Do academic scientists have less work/life balance?

For answers view our roundtable discussion for free at:

**ScienceCareers.org/webinar**

Science Careers
From the journal *Science* AAAS

Produced by the *Science*/AAAS Business Office.

# Learn how current events are impacting your work.

***Science*Insider, the new policy blog from the journal *Science*,** is your source for breaking news and instant analysis from the nexus of politics and science.

Produced by an international team of science journalists, *Science*Insider offers hard-hitting coverage on a range of issues including climate change, bioterrorism, research funding, and more.

Before research happens at the bench, science policy is formulated in the halls of government. Make sure you understand how current events are impacting your work. Read *Science*Insider today.

**www.ScienceInsider.org**

*Science*Insider
**Breaking news and analysis from the world of science policy**

Science
AAAS

## POSITIONS OPEN

### FACULTY POSITION IN PHYSIOLOGY

The Department of Anatomy, Physiology and Pharmacology, within the College of Veterinary Medicine at Auburn University, invites applications for a full-time, 12-month, tenure-track position in physiology at the **ASSISTANT/ASSOCIATE PROFESSOR** level. Minimum qualifications include a Ph.D. in physiology or an allied field, postdoctoral experience, and excellent communication skills. Responsibilities include teaching physiology in the veterinary curriculum and participation in graduate instruction. A D.V.M. (or equivalent), teaching experience, and research interests and skills that complement the Department and College are considered beneficial for this position. The successful candidate will be expected to develop an externally funded research program. The candidate selected for this position must be able to meet eligibility requirements to work in the United States at the time the appointment is scheduled to begin and to continue working legally for the proposed term of employment. Applicants should submit: (1) a letter describing their teaching philosophy and research goals, (2) curriculum vitae, and (3) names, mailing and e-mail addresses, and telephone numbers of three references to: **Ms. Hattie Alvis, Department of Anatomy, Physiology and Pharmacology, 109 Greene Hall, College of Veterinary Medicine, Auburn University, AL 36849, e-mail: alvishm@auburn.edu.** Inquiries can be directed to **Dr. Robert Kemppainen,** Chairman, Search Committee: **e-mail: kempprj@auburn.edu; telephone: 334-844-5403.** Interested persons can also visit our **website: http://www.vetmed.auburn.edu/employment.** Review of applications will begin June 1, 2012 and continue until a candidate is recommended for hire. *Auburn University is an Affirmative Action/Equal Opportunity Employer. Women and minorities are encouraged to apply.*

### ASSOCIATE OR FULL PROFESSOR
**Department of Anesthesiology**
**University of Florida**

The Department of Anesthesiology at the University of Florida is recruiting for a prominent Ph.D. neuroscientist for a tenure or non-tenure-track Associate or Full Professor. Applicants should currently have significant federal funding, including being Principal Investigator on one or more NIH grants of the R01, P or U series that complement existing clinical interests in chronic pain. Focus areas may include changes in ion channels leading to congenital analgesia, channel mutations resulting in extreme pain disorders, other electrophysiological disorders, etc. Via these skill sets, the successful applicants will directly participate and foster neuro-related basic and clinical research, a strategic area of interest to the College of Medicine and University. In addition, the applicant should be integrated into the national network of pain researchers studying these phenomena. The anticipated start date of this position is July 1, 2012. Interested individuals should respond by April 29, 2012, please send your curriculum vitae to: **Mary Ann Hoyt, Office Manager, Department of Anesthesiology, PO Box 100254, Gainesville FL 32610-0254** or to **e-mail: mhoyt@anest.ufl.edu.** *An Equal Opportunity Institution.*

### POSTDOCTORAL POSITION
**University of California, Berkeley**

Postdoctoral research training position in genetic and biochemical experimental approaches toward discovery of bacterial and mammalian cell interactions. Focus of research targets a diverse spectrum of obligate intracellular Chlamydia organisms, including their cellular and molecular mechanisms of infection of host cells and tissues. Candidates should send curriculum vitae to: **Dr. R.S. Stephens, 1 Barker Hall, University of California, Berkeley, CA 94720** or **e-mail: rss@berkeley.edu.**

## POSITIONS OPEN

### SENIOR RESEARCH SCIENTIST
**GrassRoots Biotechnology**
**Plant Biology**

GrassRoots Biotechnology is seeking a highly motivated Ph.D.-level plant biologist to join a research team developing the C4 monocot *Setaria viridis* as a model for expression element and agronomic trait discovery. Our expression element discovery program utilizes high resolution expression datasets and genome wide chromatin maps to identify regulatory elements for synthetic biology applications. Our trait discovery program integrates forward and reverse genetics to correlate genes with their biological functions for crop improvement. The successful applicant will have a Ph.D. in an appropriate discipline and 0–3 years of relevant postdoctoral experience. Expertise in monocot physiology, development, genomics, and/or genetics is a plus. GrassRoots is located in downtown Durham, North Carolina. We offer a vibrant scientific environment and a competitive compensation package. Candidates must be authorized to work in the U.S. To apply, please send curriculum vitae and names of three references to **e-mail: careers@grassrootsbio.com.** *GrassRoots is an Equal Opportunity Employer.*

### BIOMEDICAL FACULTY POSITION
**University of Wisconsin-Madison**

The Department of Comparative Biosciences, School of Veterinary Medicine invites applications for a tenure-track faculty position (**ASSISTANT, ASSOCIATE, FULL PROFESSOR**). Qualifications include Ph.D. or equivalent, postdoctoral experience, ability to develop extramurally funded research program and commitment to excellent teaching. Research area is open, but preference given to neural, respiratory, developmental, or cancer biology. Teaching responsibilities based on expertise. Send curriculum vitae, brief statements of research interests and teaching philosophies, and three letters of reference to: **Gordon S. Mitchell, Chair, Department of Comparative Biosciences, University of Wisconsin, 2015 Linden Dr., Madison, WI, 53706.** Apply by June 4, 2012. For additional information, **see website: http://www.vetmed.wisc.edu/cbs.** *Equal Opportunity/Affirmative Action Employer.*

### POSTDOCTORAL FELLOW

Two postdoctoral positions are available at NYU Langone Medical Center. Qualified applicants must hold an M.D. or Ph.D. and will investigate the roles of growth factor, cytokine, and metalloproteinase in regulating musculoskeletal development and disorders. Preference will be given to those who have experience in inflammatory arthritis and other autoimmune diseases. Interested applicants should send a cover letter, CV, and three letters of recommendation to **Dr. Chuanju Liu, e-mail: chuanju.liu@med.nyu.edu.**